ALFRED-WEGENER-INSTITUT
HELMHOLTZ-ZENTRUM FÜR POLAR- UND MEERESFORSCHUNG

793
2025

Berichte
zur Polar- und Meeresforschung
Reports on Polar and Marine Research

The Expedition PS141 of the Research Vessel POLARSTERN to the Davis Sea and Mawson Sea in 2024

Edited by

Sebastian Krastel
with contributions of the participants

HELMHOLTZ

Die Berichte zur Polar- und Meeresforschung werden vom Alfred-Wegener-Institut, Helmholtz-Zentrum für Polar- und Meeresforschung (AWI) in Bremerhaven, Deutschland, in Fortsetzung der vormaligen Berichte zur Polarforschung herausgegeben. Sie erscheinen in unregelmäßiger Abfolge.

Die Berichte zur Polar- und Meeresforschung enthalten Darstellungen und Ergebnisse der vom AWI selbst oder mit seiner Unterstützung durchgeführten Forschungsarbeiten in den Polargebieten und in den Meeren.

Die Publikationen umfassen Expeditionsberichte der vom AWI betriebenen Schiffe, Flugzeuge und Stationen, Forschungsergebnisse (inkl. Dissertationen) des Instituts und des Archivs für deutsche Polarforschung, sowie Abstracts und Proceedings von nationalen und internationalen Tagungen und Workshops des AWI.

Die Beiträge geben nicht notwendigerweise die Auffassung des AWI wider.

Herausgeber
Dr. Horst Bornemann

Redaktionelle Bearbeitung und Layout
Susan Amir Sawadkuhi

Alfred-Wegener-Institut
Helmholtz-Zentrum für Polar- und Meeresforschung
Am Handelshafen 12
27570 Bremerhaven
Germany

www.awi.de
www.awi.de/reports

Erstautor:innen bzw. herausgebende Autor:innen eines Bandes der Berichte zur Polar- und Meeresforschung versichern, dass sie über alle Rechte am Werk verfügen und übertragen sämtliche Rechte auch im Namen der Koautor:innen an das AWI. Ein einfaches Nutzungsrecht verbleibt, wenn nicht anders angegeben, bei den Autor:innen. Das AWI beansprucht die Publikation der eingereichten Manuskripte über sein Repositorium ePIC (electronic Publication Information Center, s. Innenseite am Rückdeckel) mit optionalem print-on-demand.

The Reports on Polar and Marine Research are issued by the Alfred Wegener Institute, Helmholtz Centre for Polar and Marine Research (AWI) in Bremerhaven, Germany, succeeding the former Reports on Polar Research. They are published at irregular intervals.

The Reports on Polar and Marine Research contain presentations and results of research activities in polar regions and in the seas either carried out by the AWI or with its support.

Publications comprise expedition reports of the ships, aircrafts, and stations operated by the AWI, research results (incl. dissertations) of the Institute and the Archiv für deutsche Polarforschung, as well as abstracts and proceedings of national and international conferences and workshops of the AWI.

The papers contained in the Reports do not necessarily reflect the opinion of the AWI.

Editor
Dr. Horst Bornemann

Editorial editing and layout
Susan Amir Sawadkuhi

Alfred-Wegener-Institut
Helmholtz-Zentrum für Polar- und Meeresforschung
Am Handelshafen 12
27570 Bremerhaven
Germany

www.awi.de
www.awi.de/en/reports

The first or editing author of an issue of Reports on Polar and Marine Research ensures that he possesses all rights of the opus, and transfers all rights to the AWI, including those associated with the co-authors. The non-exclusive right of use (einfaches Nutzungsrecht) remains with the author unless stated otherwise. The AWI reserves the right to publish the submitted articles in its repository ePIC (electronic Publication Information Center, see inside page of verso) with the option to "print-on-demand".

Titel: Polarstern bei Probenahmearbeiten in der Vincennes Bay vor Nelly Island, der östlichen Insel des Frazier Archipels, Ostantarktis (Foto: Katharina Hochmuth, University of Tasmania)

Cover: Polarsten during sampling work in Vincennes Bay, off Nelly Island, the eastern island of the Frazier archipelago, East Antarctica (Photo: Katharina Hochmuth, University of Tasmania)

The Expedition PS141 of the Research Vessel POLARSTERN to the Davis Sea and Mawson Sea (East Antarctica) in 2024

Edited by

Sebastian Krastel

with contributions of the participants

Please cite or link this publication using the identifiers

https://epic.awi.de/id/eprint/60017/
https://doi.org/10.57738/BzPM_0793_2025

ISSN 1866-3192

PS141

6 February 2024 – 14 April 2024

Hobart – Walvis Bay

EASI 3
East Antarctic Ice Sheet Instability and its interaction with changes in Southern Ocean circulation – Part 3

Chief scientist
Sebastian Krastel

Coordinator
Ingo Schewe

Contents

1. ÜBERBLICK UND EXPEDITIONSVERLAUF

Sebastian Krastel[1], Lester Lembke-Jene[2]

[1]DE.CAU
[2]DE.AWI

Die Expedition PS141 unter dem Titel „East Antarctic Ice Sheet Instability and its interaction with changes in Southern Ocean circulation – Part 3“ war die dritte der EASI Expeditionen, die das Ziel haben, Eisschildveränderungen der Ostantarktis in verschiedenen Zeiten der Vergangenheit zu untersuchen. Eisschildfluktuationen in der Ostantarktis haben direkten Einfluss auf den globalen Meeresspiegel und wirken sich auf die globale Energiebilanz sowie die Umweltbedingungen im und über dem Südozean aus. Untersuchungen zur Variabilität von Eisschilden auf verschiedenen Zeitskalen haben sich bisher auf den Westantarktischen Eisschild (WAIS) konzentriert. Im Gegensatz zum WAIS ist nur wenig über die Reaktion des Ostantarktischen Eisschilds (EAIS) auf Klimaänderungen bekannt, insbesondere an der Grenze Kontinent-Ozean. Während der Fahrt wurden neue geologische und geophysikalische Daten und Proben gewonnen, um zum verbesserten Verständnis der Wechselwirkungen zwischen dem EAIS und den Klimabedingungen während des Neogens beizutragen, einerseits mit einem Schwerpunkt der Paläoumweltrekonstruktionen auf dem letzten Glazial-Interglazial-Übergang und andererseits über Zeitskalen, die die relevanten Warmzeiten des Pliozäns, Miozäns und Oligozäns umfassen. Zielregion war der kontinentale Schelf zwischen 85°E und 115°E, vor dem Eisrand von Wilhelm II bis Wilkes Land. Unser Forschungsansatz ist multidisziplinär und beinhaltet sowohl marine als auch landbasierte Untersuchungen. Auf der Grundlage von bathymetrischen und flachseismischen Messungen wurden Sedimentarchive vom kontinentalen Schelf sowie aus Seen gewonnen. Daraus soll die laterale und zeitliche Ausdehnung von Eisschildvorstößen und -rückzügen im Kontext mit gleichzeitig ablaufenden Veränderungen der Ozeanographie, der Meereis- und Seeeisbedeckung sowie der Limnologie rekonstruiert werden. Aus GPS-Messungen und Daten über lokale relative Meeresspiegelstände werden Massenänderungen des EAIS während des Spätpleistozäns abgeleitet. Seismische Vermessungen der tieferen Sedimentfolgen und deren glazialtektonischen Strukturen über den Schelf und oberen Kontinentalhang werden die EAIS Variabilität seit dem Beginn der Eozän-/Oligozän-Vereisung bis in das Spätquartär erfassen. Trotz teilweise schwieriger Wetter- und Eisbedingungen konnten die wesentlichen Ziele der Expedition erreicht werden. Eine erste Sichtung der Daten zeigt eine Vielzahl von Indikatoren für die vergangene Lage der Eisschilde. Geophysikalische und geologische Daten konnten in allen postulierten Arbeitsgebieten gesammelt werden.

Die Expedition begann am 06. 02. 2024 in Hobart, wo wir um 18:00 Uhr lokaler Zeit ausgelaufen sind. Ursprünglich war es geplant, auf direktem Kurs in die Ostantarktis zu fahren; entlang des Kurses waren neun Tiefwasserstationen geplant, um ein Profil über verschiedene ozeanische Fronten zu sammeln. Leider verhinderte ein Orkan-Tief, dass wir direkten Kurs auf die Antarktis nehmen konnten. So fuhren wir vorerst nach Westen, bis das Tief südlich an uns vorbeigezogen war. Am 08.02. begannen wir nach Verlassen der australischen ausschließlichen Wirtschaftszone das wissenschaftliche Programm mit dem Anschalten der hydroakustischen und weiterer profilierender Systeme. Die Anzahl der Tiefwasserstationen auf dem Transit musste allerdings aufgrund schlechter Wetterbedingungen und Mangel an ungestörten Sedimentabfolgen auf vier Stationen reduziert werden. An diesen sowie drei

zusätzlichen Stationen wurden ebenfalls CTDs und Multinetze gefahren. Am 17.04. um 02:00 Uhr Bordzeit haben wir dabei den 60. Breitengrad überquert.

Das erste Ziel auf dem Ostantarktischen Schelf war das Ausfliegen der Kölner Landgruppe in die Bunger Oase. In einem kleinen Zeitfenster mit Flugwetter konnte die Truppe am 19.02. ausgeflogen werden. Die Arbeiten des Kölner Teams umfassten die Entnahme von Sedimentkernen in Seen und Meeresbuchten sowie die Beprobung von Strandterrassen und glazialen Erratika. Anhand des Materials sollten der Zeitpunkt des Eisrückgangs, die Entwicklung des relativen Meereisspiegels und das Paläoklima des Holozäns in der Region rekonstruiert werden. In der anschließenden Nacht wurden bathymetrische Vermessungen in der Bucht vor der Bunger Oase durchgeführt, in der es zahlreiche glaziale Tröge gibt. Am 20.02. wurde ein erster Test des Kieler Seismik-Systems erfolgreich durchgeführt. Dabei handelt es sich um ein System für hochauflösende Messungen. Das zweite Streamer-System – ein 600 m-langer Streamer von CSIRO Australien – wurde am Nachmittag nach Passieren einer Eisbarriere ausgesetzt. Die seismischen Vermessungen führten uns entlang des Shackleton-Schelfeis über den Bruce Rise in Richtung des Gaußberges. Bis auf kleinere Unterbrechungen aufgrund von Meeressäugern verliefen die Messungen ohne Probleme. Am frühen Nachmittag des 24.02. wurde der Streamer in der Nähe des Gaußberges geborgen. Nach einem Eiserkundungsflug begann bereits am Abend des 24.02. das Ausfliegen von Ausrüstungsgegenständen für die Landgruppe zum Gaußberg. Die Nacht wurde für hydroakustische Messungen genutzt bevor dann am 25.02. das restliche Material und fünf Personen zum Gaußberg geflogen wurden. Der Gaußberg ist ein erloschener Vulkan, der 1902 erstmalig von Erich von Drygalski, dem Leiter der ersten deutschen Südpolarexpedition, gesichtet wurde. Das Team der TU Dresden führte mit Unterstützung von Kolleg:innen der University of Tasmania insbesondere geodätische Messungen durch, um so Bewegungen der Erdkruste als Folge von vergangenen und heutigen Eismassenveränderungen vermessen zu können. Ein weiteres Ziel war die geologische Beprobung des Vulkans und glazialer Erratika.

Nach Beendigung der Flugoperationen wurde am Nachmittag ein Schwerelot und ein MUC in dem davor kartierten Gebiet genommen. Auf einem kurzen Transit wurde ein Float ausgesetzt bevor am 26.02. CTDs und ein Schwerelot nördlich des Shackleton-Schelfeis genommen wurden, um mögliche Schmelzwassserflüsse zu detektieren. In diesem Gebiet wurden zwei weitere Floats ausgesetzt. Auf dem Weg zurück Richtung Denman Gletscher sollten Lücken in den zuvor aufgezeichneten seismischen Daten geschlossen werden. Allerdings kam es aufgrund von niedrigen Lufttemperaturen zu einer Fehlfunktion der seismischen Quellen. Am 28.02. begannen wir eine Region mit zahlreichen glazialen Strukturen auf dem mittleren Schelf vor dem Denman Gletscher mit den hydroakustischen Systemen zu vermessen. Aufgrund einer extrem schlechten Wettervorhersage mit Orkanböen für das folgende Wochenende wurde jedoch beschlossen, das Landteam aus der Bunger Oase wieder an Bord zu holen. Dazu wurden die hydroakustischen Messungen am Abend des 28.02. unterbrochen, um mit der *Polarstern* möglichst dicht an der Bunger Oase zu sein. Am 29.02. morgens war jedoch noch kein Flugwetter, so dass im Laufe des Vormittages basierend auf neuen hydroakustischen Daten eine Geologie-Station in der Bucht vor der Bunger Oase erfolgreich (5 m Kern plus MUC und CTD) durchgeführt werden konnte. Die Flugoperationen konnten dann um 15:30 Uhr begonnen werden. Bis zur Dämmerung konnten fünf Flüge durchgeführt werden, so dass alle Personen sowie ein Großteil der Ausrüstung an Bord gebracht werden konnten. Aufgrund der Wettervorhersage ging es dann zurück in das Gebiet, in dem die hydroakustischen Arbeiten in Folge der Rückholaktion abgebrochen worden waren. Auf dem Transit wurden zwei weitere Floats ausgesetzt. Nach wenigen zusätzlichen hydroakustischen Profilen wurde die hochauflösende Seismik am Morgen des 01.03. ausgesetzt, um den Datensatz in dieser Gegend zu komplementieren. Die seismischen Messungen wurden bis Mitternacht mit einigen Walsichtungsunterbrechungen ohne technische Probleme fortgesetzt. Anschließend begann der Transit Richtung Windmill Islands und Vanderford Gletscher.

Hydroakustische Kartierung des glazialen Troges vor dem Vanderford Gletscher begannen am Abend des 02.03. und wurden bis zum Mittag des 03.03. fortgesetzt. Die Daten zeigen einen tief eingeschnittenen Trog mit Wassertiefen von mehr als 2300 m direkt vor der Gletscherzunge. Auf Grund eines Sturms in Orkanstärke wurde bis zum 04.03. morgens in einer geschützten Lage vor den Frazier Islands abgewettert. In den beiden drauffolgenden Tagen wurden geologische Stationen in unterschiedlichen Bereichen des Troges vor dem Vanderford Gletscher durchgeführt. Die Tage wurden auch genutzt, um an Land eine permanente GNSS-Station am Ivanoff Head aufzubauen, sowie die Browning Halbinsel geologisch zu beproben. Am Abend des 05.03. wurde die Seismik mit dem langen Streamer ausgesetzt, um ein Profil von der Schelfeiskante zum oberen Hang entlang eines Troges vor dem Vanderford- und Adams-Gletschern aufzuzeichnen. Dabei wurde eine Grounding Zone Wedge (GWZ) gekreuzt, die vom 08.03. mit der hochauflösenden Seismik der Uni Kiel kartiert werden sollte. Leider blieb der Streamer kurz nach dem Aussetzen an einem Growler hängen und riss. Aufgrund der Endboje konnte der gerissene Teil des Streamers jedoch geborgen werden. Die GWZ wurde dann mit hochauflösender Quelle und dem 600 m-Streamer bis um 23:00 Uhr am 09.03. kartiert. Die Daten zeigen eindrucksvoll, dass es sich um eine sehr große gestapelte GZW handelt. Am 10. und 11.03. wurde ein Kernprofil über den Schelf vor dem Adams-Gletscher gefahren. Einzelne Strukturen wie ein möglicher subglazialer See, Gletscher-Lineationen und die GWZ wurden gezielt vor allem mit dem Schwerelot beprobt. Am 12.03. gegen Mittag erreichten wir Nelly Island, eine Insel der Frazier Islands Gruppe. Von dort wurde ein Teil der Kölner Landgruppe mit einem Boot auf die Insel gebracht, um Proben zu nehmen, während ein zweiter Teil der Landgruppe Holl Island beprobt hat. Die Nacht zum 13.03. wurde genutzt, um im Bereich vor der australischen *Casey Station* zu kartieren, um dann dort am 13.03. ein Kernprogramm durchzuführen. Am Abend des 13.03. wurde ein kurzes seismisches Profil über den tiefen Trog vor dem Vanderford-Gletscher aufgezeichnet. Das Kernprogramm sollte am 14.03. vor dem Adams-Gletscher fortgesetzt werden, aber Winde mit bis zu 11 Beaufort machten Stationsarbeiten unmöglich. Mit einem letzten hydroakustischen Profil entlang der Schelfeiskante begann unser Transit zum Gaußberg, um dort die Dresdener Landgruppe wieder einzusammeln.

Am 16.03. erreichten wir die Gaußberg Region und begannen am frühen Nachmittag bei besten Wetterbedingungen das Zurückfliegen der Landtruppe. Die Nacht wurde für hydroakustische Vermessungen eines Troges verwendet, in dem wir bei der Anfahrt gut geschichtete Sedimente identifizieren konnten. Nachdem am 17.03. mit zwei Außenlastflügen auch alle Ausrüstung an Bord war, haben wir in dem zuvor vermessenden Trog eine vollständige Station mit MUC, Schwerelot, CTD und Multinetzen durchgeführt. Dort wurde auch ein weiterer Float ausgesetzt. Ein 12 Stunden Transit brachte uns weiter nach Osten, wo wir am 18.03. erfolgreich ein seismisches Profil über die Schelfkante komplementierten. Der 19.03. wurde genutzt, um eine Lokation auf dem westlichen Bruce-Rise in ca. 1900 m Wassertiefe zu beproben. In der drauffolgenden Nacht wurde eine GWZ auf dem äußeren Schelf hydroakustisch vermessen. Die GWZ liegt in der Verlängerung des Denman-Gletschers und reicht meist bis an die Schelfkante. Basierend auf den hydroakustischen Daten wurden am 20.03. Kerne an unterschiedlichen Lokationen der GZW genommen.

In der Nacht zum 21.03. fuhren wir erneut in den Bereich der Bunger-Oase, um die dort verbliebene Ausrüstung von dem Feldcamp zurück zu holen. Dies konnte erfolgreich bewerkstelligt werden. Parallel wurde an Land eine neue GNSS-Station (Watson-Bluff) aufgebaut und auf See ein Bereich bathymetrisch vermessen, in dem vor wenigen Tagen ein großes Stück des Schelfeises abgebrochen waren. An zwei Positionen wurden auf den neuen Daten basierend Stationen gefahren. Nach einem kurzen Transit auf den mittleren Schelf und dem Aussetzen eines weiteren Floats wurden am 22.03. bei stürmischen Wetterbedingungen an fünf Stationen geologische Proben genommen. Am 23.03. wurde mit der hochauflösenden Seismik eine potentielle GWZ direkt am äußeren Schelf vermessen, die in der Verlängerung

des Denman-Gletschers liegt. Am 24.03. wurde ein letztes tiefes Seismik-Profil vom mittleren Schelf vor der Bunger Oase nach Nordosten vermessen, um dort einen Anschluss an seismische Daten am Kontinentalhang herzustellen. Am folgenden Tag sollten dann Kerne auf den Flanken von zwei Canyons am oberen Kontinentalhang genommen werden, da die Parasounddaten dort lange ungestörte Sedimentabfolgen abgebildet haben. Nach einem MUC an der ersten Lokation musste die Station aufgrund der Wetterbedingungen (Windstärken von 10 Beaufort und mehr) abgebrochen werden. Am 26.04. um 04:30 Uhr hatten sich die Bedingungen dann soweit beruhigt, dass ein Transit zum westlichen Bruce Rise möglich war, wo wir im Laufe des Abends eine letzte sehr erfolgreiche Station mit Schwerelot, MUC und CTD durchführten. Nach einem weiteren Tag Transit wurde am 28.04. in der Nähe des Gaußberges eine australische GNSS-Stationen (Carey Ntk.) gewartet bevor der lange Transit Richtung Namibia begann. Während der gesamten Zeit auf dem Schelf wurden bei günstigen Wetterbedingungen Krabbenfresser-Robben besendert, indem zwei Kolleginnen des CNRS/ Laboratoire d'Océanographie et du Climat, Paris; auf Eisströme geflogen wurden. Insgesamt konnten wie geplant 15 Robben besendert werden.

Am 02.04. um die Mittagszeit überquerten wir den 60. südlichen Breitengrad; der Eintritt in die Südafrikanische AWZ und damit das Ende unserer Forschungshandlungen war am 10.04. um 07:00 Uhr. Die Expedition endete am 14.04.2024 um 08:00 Uhr in Walvis Bay.

Die Expedition trägt zu den Zielen des Forschungsprogramms „Erde im Wandel – Unsere Zukunft sichern" bei. Sie ist Teil der programmorientierten Förderung (PoF IV) der Helmholtz-Gemeinschaft. Die meisten Forschungsaktivitäten beziehen sich direkt auf die Ziele von Thema 2 (Ozean und Kryosphäre im Klimawandel) mit einem Fokus auf die Unterthemen 2.1 (Erwärmung des Klimas) und 2.3 (Meeresspiegeländerung). Für die CAU liefert die Expedition wichtige Impulse für die Forschung innerhalb des universitären Forschungsschwerpunktes Kiel Marine Science (KMS).

SUMMARY AND ITINERARY

Expedition PS141, entitled “East Antarctic Ice Sheet Instability and its interaction with changes in Southern Ocean circulation – Part 3”, was the third of the EASI expeditions that aim to investigate ice sheet changes in East Antarctica at different times in history. Ice sheet fluctuations in East Antarctica have a direct impact on global sea level, and affect the global energy balance and environmental conditions both in and north of the Southern Ocean. Studies on the variability of ice sheets over different time scales have so far concentrated on the West Antarctic Ice Sheet (WAIS). In contrast to the WAIS, little is known about the response of the East Antarctic Ice Sheet (EAIS) to climate change, especially at the continent-ocean boundary. We acquired new geophysical data and geological samples to contribute to an improved understanding of the behaviour of the EAIS in response to climate conditions during the Neogene. Our work focussed on paleoenvironmental reconstructions of the last glacial-interglacial transition, as well as timescales spanning warmer-than-present periods during the Pliocene, Miocene and Oligocene. The target region was the continental shelf between 85°E and 115°E, off the ice margin from Wilhelm II to Wilkes Land. Our research approach is multidisciplinary, and includes both marine and land-based investigations. Sediment archives from the continental shelf as well as from lakes were sampled based on preceding bathymetric and shallow seismic measurements. These archives will be used to reconstruct the lateral and temporal extent of ice sheet advances and retreats in the context of concurrent changes in oceanography, sea ice and lake ice cover, and limnology. Changes in the mass of the EAIS during the Late Pleistocene will be derived from the acquired GPS measurements and data on local relative sea levels. Seismic surveys of deeper sedimentary sequences and their glacial-tectonic structures across the shelf and upper continental slope record EAIS variability from the beginning of the Eocene/Oligocene glaciation to the Late Quaternary. Preliminary analysis of the data shows a variety of indicators for the past position of the ice sheet. Geophysical and geological data were collected in all the intended working areas.

The expedition began on 6 February 2024 in Hobart, where we departed at 18:00 local time. The original plan was to sail a direct course to East Antarctica, and collect nine deep-water stations along the transit to record a profile across various oceanic fronts. Unfortunately, a deep low-pressure system prevented us from setting a direct course for Antarctica, and we headed west until the low had passed southward of us. On 8 February, after leaving the Australian Exclusive Economic Zone, we switched on the hydroacoustic and other underway profiling devices, thereby starting the scientific programme. The number of deep-water stations on the transit had to be reduced to four due to poor weather conditions and a lack of undisturbed sediment sequences. CTDs and multinets were also run at these four (and three additional) stations. On 17 February at 02:00 shipboard time, we crossed 60°S.

Once we arrived on the East Antarctic Shelf, the first objective was to fly out the Cologne land group to Bunger Oasis. The team were flown out on 19 February during a small window of good flying conditions. While there, the Cologne team took sediment cores from lakes, and sampled beach terraces and glacial erratics. The material will be used to reconstruct the time of ice retreat, the development of relative sea level, and the palaeoclimate of the Holocene in the region. The following night, bathymetric surveys were carried out in the bay off the Bunger Oasis, where numerous glacial troughs were mapped. On 20 February, the Kiel seismic system, which is optimised for high-resolution measurements, was successfully tested in the water.

The second streamer system – a 600 m-long streamer loaned from the CSIRO in Hobart – was deployed in the afternoon after passing an ice barrier. This first seismic survey took us along the Shackleton Ice Shelf, across the Bruce Rise, and towards Gaussberg. Apart from some interruptions caused by marine mammals, the data were collected without any problems. In the early afternoon of 24 February, the streamer was recovered near Gaussberg. Following an ice reconnaissance flight, transport of equipment to Gaussberg started on the evening of 24 February. The night was used for hydroacoustic measurements, before the remaining equipment and 5 people were flown to Gaussberg on 25 February. Gaussberg is an extinct volcano that was first sighted in 1902 by Erich von Drygalski, the leader of the first German South Polar expedition. With the support of colleagues from the University of Tasmania, the TU Dresden team carried out geodetic measurements in order to measure movements of the Earth's crust as a result of past and present ice mass changes. Volcanic rocks and glacial erratics were also sampled during the Gaussberg field campaign.

In the afternoon, after the completion of flight operations, a gravity corer and a MUC were taken in the previously mapped area. An Argo float was deployed during a short transit, before CTDs and a gravity corer were taken on 26 February to detect possible meltwater fluxes north of the Shackleton Ice Shelf. Two more floats were deployed in this area. On the way back towards Denman Glacier, we planned to close gaps in the previously recorded seismic data, but the seismic sources malfunctioned due to extreme air temperatures over the days preceding deployment, and we were not able to acquire the data. On 28 February, we began a detailed hydroacoustic survey of an area of the mid-shelf off the Denman Glacier with numerous glacial structures. Due to an extremely bad weather forecast that indicated gale-force winds for the coming weekend, we decided to pre-emptively collect the land team from Bunger Oasis. The planned hydroacoustic measurements were thus interrupted on the evening of 28 February in order to transit as close as possible to Bunger Oasis. Weather conditions on the morning of 29 February were not suitable for flying, so we used the time to carry out geological station work in the bay off Bunger Oasis (5 m core plus MUC and CTD) based on the new hydroacoustic data. Flight operations were able to begin at 15:30, and five flights were completed by dusk; so that all the people (and most of the equipment) were back on board. Due to the weather forecast, we then returned to the area where hydroacoustic work had been interrupted prior to the flight operations. Two more floats were deployed on the transit. After collecting a few additional hydroacoustic profiles, we began a high-resolution seismic survey in the morning of 1 March to complement the dataset in this area. Seismic measurements continued until midnight with some interruptions due to whale sightings but without further technical problems. Afterwards, we started the transit towards Windmill Islands and the Vanderford Glacier.

Hydroacoustic mapping of the glacial trough off the Vanderford Glacier began on the evening of 2 March and continued until midday on 3 March. The data show a deeply incised trough with water depths of more than 2,300 m directly in front of the glacier tongue. Due to a gale-force storm, we waited in a sheltered position off the Frazier Islands until the morning of 4 March. In the following two days, geological stations were taken in different areas of the trough in front of the Vanderford Glacier. During these days, we were also able to set up a permanent GNSS station on land at Ivanoff Head and geologically sample the Browning Peninsula. On the evening of 5 March, the seismic system was deployed with the long streamer to record a profile from the ice shelf edge to the upper slope along a trough in front of the Vanderford and Adams Glaciers. During this survey, we crossed a grounding-zone wedge (GZW), and intended to map it using the high-resolution seismic system of Kiel University from 8 March. However, the streamer unfortunately got caught in a growler shortly after deployment and broke. The end buoy, however, remained attached to the torn part of the streamer, enabling its recovery. The GZW was then mapped with a single high-resolution source and the 600 m streamer until 23:00 on 9 March. The data are impressive and show that this is a very large stacked GZW. On 10 and 11 March, a profile of geological stations was collected across the shelf in front of Adams

Glacier. Individual structures, including a possible subglacial lake, glacial lineations, and the GZW were specifically targeted, primarily with the gravity corer. Around midday on 12 March, we reached Nelly Island, part of the Frazier Islands group. Members of the Cologne land group were taken to the island by zodiak to collect samples, while a second part of the Cologne group sampled Holl Island. The night was used to map the area in front of the Australian *Casey Station* to verify locations for coring on 13 March. A short seismic profile was collected across the trough off the Vanderford glacier in the evening of 13 March. We intended to carry out geological station work in front of Adams Glacier on 14 March, but winds of up to 11 Beaufort made this impossible. We thus started a transit to Gaussberg to pick up the Dresden land group; collecting a hydroacoustic profile along the edge of the shelf ice during the transit.

We reached the Gaussberg region on 16 March, and flight operations started in the early afternoon in perfect weather conditions. The night was used for a hydroacoustic survey of a glacial trough, which we passed on the transit to Gaussberg. This trough is partly filled with well-stratified sediments. Two additional flights with swing loads in the morning of 17 March concluded the Gaussberg flight operations. Following their completion, we carried out a full station with MUC, gravity corer, CTD and multinets in a well-stratified part of the trough we had previously surveyed. Another float was also deployed at the station. A 12-hour transit took us further east, where we successfully completed a seismic profile over the shelf edge on 18 March. The 19 March was used to sample a location on the western Bruce Rise at a water depth of about 1,900 m. The following night, we surveyed a possible GZW on the outer shelf using the onboard hydroacoustic systems. The GZW is part of the prolongation of the Denman Glacier, and extends to the shelf edge. Cores were taken on 20 March at different locations on the GZW based on the hydroacoustic data.

On the night of 21 March, we travelled back to the Bunger Oasis to retrieve the remaining equipment from the field camp. This was successfully accomplished on 22 March. In parallel, a new GNSS station (Watson Bluff) was set up on land, and an area was bathymetrically surveyed at sea where a large piece of the shelf ice had broken off a few days prior. Station work based on the new data was undertaken at two locations. After a short transit to the middle shelf and the deployment of another float, geological samples were taken at five stations on 22 March in stormy weather conditions. On 23 March, the high-resolution seismic system was deployed to image the possible GZW linked to the Denman Glacier and located on the outer shelf. On 24 March, a final deep seismic profile was collected from the mid-shelf off Denman Glacier towards the north-east to establish a connection to available seismic data on the continental slope. We planned to take cores on the flanks of two canyons on the upper continental slope the next day, because Parasound data there had imaged long undisturbed sediment sequences. However, after a MUC at the first location, the station had to be terminated due to bad weather conditions (wind forces exceeding 10 Beaufort). At 04:30 on 26 April, the conditions had calmed down enough to allow a transit to the western Bruce Rise, where we conducted a last, very successful station with gravity corer, MUC and CTD in the evening. After another day of transit, an Australian GNSS station (Carey Ntk.) was serviced near Gaussberg on 28 April before the long transit towards Namibia began. Additionally, during our time on the continental shelf, two scientists from the CNRS/Laboratoire d'Océanographie et du Climat, Paris, tagged crabeater seals during favourable weather conditions. A total of 15 seals were tagged as planned.

We crossed 60°S latitude on 2 April around noon and arrived in the South African EEZ on 10 April at 07:00, marking the end of scientific activities. The expedition ended on 14 April 2024 at 08:00 in Walvis Bay.

The expedition contributes to the objectives of the research programme "Changing Earth – Sustaining our Future". It is part of the Helmholtz Association's programme-oriented funding

(PoF IV). Most of the research activities are directly related to the objectives of Topic 2 (Ocean and Cryosphere in Climate) with a focus on Subtopics 2.1 (Warming Climate) and 2.3 (Sea Level Change). For the CAU, the expedition integrates important themes for research within the university's research focus Kiel Marine Science (KMS).

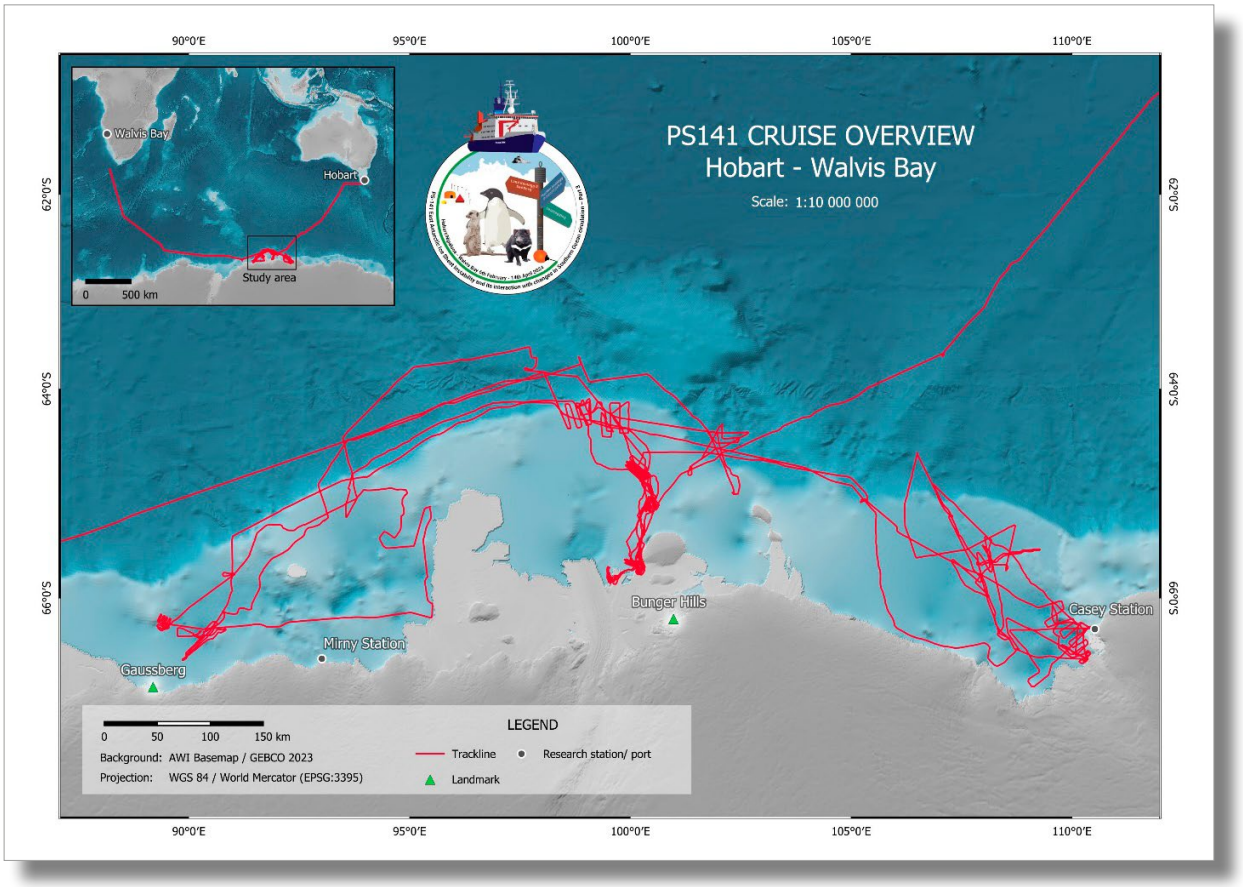

Abb. 1.1: Fahrtroute (rote Linie) der Polarstern-Expedition PS141

Fig. 1.1 Ship track (red lines) of Polarstern expedition PS141

WEATHER CONDITIONS DURING PS141

Julia Wenzel DE.DWD

Right at the beginning of the expedition, the planned route from Hobart to the research area between 89°E and 110°E in the Australian sector of Antarctica had to be adjusted due to the weather conditions. A deep lower pressure system moving eastwards between Australia and Antarctica would have caused a significant wave height of 11 m on the planned route. Thus, after leaving the port of Hobart on 6 February, instead of taking the direct route, *Polarstern* first headed west and on 9 February turned at the backside of the low towards Antarctica. During the first part of this route, the significant wave height therefore only reached 3 to 4 m with a westerly wind of temporarily up to 7 Bft (on 7 February south of Tasmania due to the corner effect and on the night to 9 February in the area of the cold front of the low). On 9 February, there was a significant drop in winds on the back of the cold front in the area of a high south of Australia, but at the same time a 5 m swell reached *Polarstern* from the southwest, which was produced by the deep low and then slowly dissipated.

On the way to the southwest, *Polarstern* passed through the famous latitudes of the “Roaring Forties”, “Furious Fifties” and “Screaming Sixties”, the often stormy westerly wind area between 40° South and Antarctica, which is caused by several consecutive deep lows moving eastwards off the coast of East Antarctica. Therefore, in the period from 10 February to 13 February, westerly winds of often 7 to 8 Bft and a sea state of temporarily just below 6 m occurred. When *Polarstern* was crossed by the cold front of the second low on 10 February, the wind increased to 8 Bft prefrontally and there was a significant jump of the wind direction from northwest to southwest. On 12 February the cold front of a third low followed. Starting on 13 February, the fourth low moved from the Prydz Bay to the northeast and weakened, while the previous low moved eastwards. As *Polarstern* was travelling southwest between these two pressure systems, the wind and sea state dropped significantly from 13 February in the afternoon (to 3 Bft and 3 m). When *Polarstern* was crossed by the occlusion of the fourth low in the night to 15 February, there was a temporary increase in wind and wave height to 8 Bft and 4 m until the afternoon of 15 February, which afterwards rapidly decreased again. In the area between the filling low and a remaining trough off the coast of the Australian sector of Antarctica, a mostly moderate to weak westerly wind occurred from 16 to 18 February, which turned to the east on the outer area of a low moving to the southeast on 18 February.

In the morning of 19 February, *Polarstern* reached the Antarctic ice shelf edge northwest of the first target in the main research area: the Bunger Oasis at 66° South 101° East. A very small-scale low reduced the flying conditions, but all transport flights of the research team of the University of Cologne to the camp, which was planning to spend several weeks in the Bunger Oasis, were nevertheless able to be carried out, before the snow began to fall and the visibility was significantly reduced. In the shelter of the ice shelf, for a while weak variable winds occurred, which shifted to the east in the afternoon and increased to 6 Bft. The small-scale low subsequently filled up, with the wind easing to 2 Bft by the evening of 20 February.

Continuing the journey towards the Gaussberg (at 67° South 89° East) on 20 February, from the night to 21 February on *Polarstern* came under the influence of a new deep low pressure system that had formed north of the Prydz Bay and was moving southeastwards, building up

stormy to hurricane-force easterly winds along the nearby Antarctic coast. During the night to 21 February, the wind therefore shifted to the east and increased rapidly to 8 Bft by the morning of 21 February. After crossing the southward moving occluding front, the wind shifted to the north on the evening of 21 February and dropped to 5 Bft. At the same time, a minimum air pressure of 959 hPa was measured on board. The low itself had a core pressure of 946 hPa. The deep low was located far northnorthwest of the Gaussberg on the evening of 21 February, was first moving to the southeast, then to the southwest while slowly weakening and filled up northeast of the Prydz Bay by 24 February. After travelling around the Shackleton Ice Shelf and then heading southwest, from 23 February on *Polarstern* reached again the area of strong winds close to the coast, with easterly winds of up to 8 Bft until end of 24 February, which calmed to 1 Bft by 25 February. On the evening of 24 February and on 25 February, the short window with better wind and weather conditions was used to fly the second land team, the research group from the Technical University of Dresden, together with their equipment to the Gaussberg, where they spent the next three weeks.

With the approach of a new deep low pressure system from the west, the wind increased steadily during the night to 26 February, while *Polarstern* continued its journey eastwards and sampled several stations in the southeast of the Davis Sea on 26 February. Thereby, an easterly wind of 9 Bft was measured throughout the whole day with a resulting wind sea of at times up to 3 m, while the deep low moved north of the Davis Sea rapidly to the east. On the back side of the low, the wind dropped to 1 Bft on 27 February. A trough line off the coast with embedded small-scale lows moving eastwards repeatedly caused unsteady weather over the next few days, with wind speeds between 1 and 6 Bft.

In the meanwhile, a low that had formed east of the Kerguelen Islands on 1 March moved southeastwards. By the time it reached the Davis Sea on 3 March, the low had deepened into a very deep low with a core pressure of 930 hPa and, from the night of 3 March, caused a storm with average wind speeds of up to 12 Bft in some areas along the coastal region of the Australian sector of Antarctica. The camp of the Cologne research team at the Bunger Hills was therefore cleared earlier as planned on 29 February and *Polarstern* reached the Frazier Islands west of the Australian *Casey station* on 3 March, where, despite of the violent storm (11 Bft), a sea state of only 3 m was built up due to the proximity to the coast and the ice shelf. For a short time gusts of even force 12 were encountered. The deep low moved southwest on 4 March while slowly weakening and at the same time the wind dropped significantly over the working area in the Vincennes Bay near *Casey Station*.

On 5 March, the effect of the katabatic wind above the glacier ice could be observed in the prevailing southeasterly wind. In the shelter directly in front of the ice shelf edge, an average wind speed of mostly 5 Bft was measured on board of *Polarstern*, while a local wind overshoot of 10 Bft was observed during a flight over the Vanderford Glacier.

In the following days, a trough line with embedded small-scale, shallow, eastward moving lows was extending just off the coast (mostly weak to moderate winds), temporarily interrupted by an eastward moving deep low, which caused a southeast wind of 7 Bft at the position of *Polarstern* on 9 and 10 March.

From 13 March to 14 March, a deep low pressure system moved from the northwest to just northeast of the Shackleton Ice Shelf and weakened there subsequently. On 13 March, wind speeds in the range of 1 to 10 Bft were measured due to very regional differences, as the southeasterly wind was accelerated over the Vanderford Glacier for catabatic reasons and could not develop in the land protection near *Casey*. On 14 March, the average wind speed was mostly 9 to 10 Bft. Despite of a layer of new ice on the water, a significant wave height of 3 m could at times build up. On 14 March, *Polarstern* finally left the working area in the

Vincennes Bay and returned to the Gaussberg, where the Dresden land team was picked up on 16 and 17 March during sunny and calm intermediate high pressure weather.

From 17 March to 20 March, *Polarstern* travelled east, back to the working area near the Bunger Oasis and was influenced by a weakening deep low moving eastwards. The wind shifted to the east in front of the occlusion front on 18 March and increased to 7 Bft. In the night to 19 March, when crossing the front the wind abruptly shifted to west and dropped to 5 Bft. During the day on 19 March, the wind continued to shift to the north and dropped to 3 Bft. At the same time, the sea state rose to 3 m in the areas unprotected by the ice due to a swell from the northwest. In the moist ground layer temporary very dense fog occurred on 20 March during moderate winds.

After a slight weather improvement on 21 March that was used to pick up the rest of the Cologne team's equipment from the Bunger Oasis, a deep low that was moving just north of the Shackleton Ice Shelf to the east during the night to 22 March caused a southeastern wind of 9 to 10 Bft at the stations north of Mill Island from 21 March in the evening until 22 March noon. Behind the low, the wind in the trough line that was remaining just off the coast decreased to at times 3 Bft by 23 March.

Another deep low pressure system moved on 23 March while further deepening from the Prydz Bay to the Davis Sea, where it slowly weakened from 25 March evening and had filled up by 28 March. In the vicinity of *Polarstern* north of the Mill Island and north of the Bowman Island, the wind therefore shifted to the east on the evening of 24 March and increased to on average 10 to 11 Bft with gusts of 12 Bft by the evening of 25 March. At the same time, the sea state in the open water rose to 5 m. As *Polarstern* was heading north on 26 March and crossed the front, the visibility improved significantly in the afternoon by leaving the area of the continuous snow fall area and the wind finally dropped significantly and shifted to the northeast. During the night to 27 March, *Polarstern* continued its voyage to the southwest with a significant wave height of 3 m, whereby the wind shifted to the east in the vicinity of the filling low on 27 March and temporarily increased to 7 to 8 Bft. On 28 March, north of the West Ice Shelf, the weather improvement on the back side of the low was used to carry out a final scientific helicopter flight to the ice shelf.

Afterwards, the transit to Africa started. *Polarstern* first travelled westwards, whereby the significant wave height rose to 2 to 3 m when leaving the ice area and reaching open water during the night to 29 March. Based on a deep low that moved on 27 March northeast of the Shackleton Ice Shelf to the southeast while further deepening, a trough extended on 28 March westwards along the coast to the Prydz Bay. As a result, a southeasterly wind, untypical for the coastal regions, occurred in the night to 29 March. On 29 March, a low moved north of the Prydz Bay just north of *Polarstern* to the east, whereas only the wind direction shift was remarkable but not the moderate wind speed. North of the Mawson coast, a small-scale low that was embedded in a trough line off the coast moved eastwards just south of *Polarstern* during the night to 30 March, accompanied by a large wind direction shift from south via east to west and a brief increase to 7 Bft. In the morning of 30 March, in the unstable stratified air mass isolated cumulonimbi, which are atypical for polar regions, also occurred in between the snow showers.

During the night to 31 March,*Polarstern* came under the influence of a deep low pressure system approaching from the northwest and deepening to 954 hPa north of the Enderby Land. To avoid stormy winds from ahead and too high waves, the route and speed were adjusted so that *Polarstern* continued travelling west instead of taking the direct route to Namibia. By the morning of 31 March, the westerly wind shifted to the northeast on the front side of the low and increased to 7 Bft by noon. *Polarstern* then travelled just south of the low's core further west, so that a minimum air pressure of 954.8 hPa was measured in the afternoon (09 UTC).

Close to the core, the wind shifted to the east and dropped to 5 to 6 Bft, while the significant wave height remained at only 3 m. Further south and further north of the low, the conditions were much more unfavorable with winds of up to 10 Bft and wave heights of up to 7 m. In the evening, the wind shifted south behind the low pressure system and *Polarstern* finally started heading to the northwest.

Immediately afterwards, a less deep low moved off the coast to the east, so that in the night to 1 April the wind shifted further to the northwest and increased to 7 Bft. North of the low, *Polarstern* was getting into a wide band of westerly winds. During the 1 April, the westerly winds increased to 8 Bft and the sea state rose to 6 m. These conditions remained until the end of the following day.

On 3 April, the sea state had finally dropped to 3 m and the wind also abated for a while. During the night to 4 April, a low pressure system moving to the southeast crossed the research vessel's route. Due to another course change, which had already been set a few days earlier, unfavourable weather conditions were avoided by aiming for a slightly more westerly waypoint, so that *Polarstern* travelled on the back side instead of the front side of the low. Therefore, by the evening of 3 April, the wind shifted to the east and increased to 8 Bft. Close to the low pressure core, the wind temporarily dropped to 3 Bft in the night to 4 April and turned to the northwest. After the low pressure core had crossed *Polarstern* in the night to 4 April, the wind turned abruptly south and increased to 8 Bft. Additionally, the sea state rose to 5 m. During the course of the day, the wind continued to shift west and decreased to 7 Bft.

The strong pressure gradient that occurred between the departing deep low and an intensive high pressure system southwest of South Africa intensified temporarily in the night to 5 April when a small-scale deep low moved just south of *Polarstern* to the eastnortheast, causing a brief wind speed increase to 8 to 9 Bft. On its back side, the wind shifted southwest, slowly decreased as it approached the high in the following days and shifted again west on 6 April. The high slowly moved to the west on 7 April while weakening, so that the wind and sea state had finally dropped to 4 Bft (southwest) and 2.5 m on 8 April.

South of the high, a last deep low moved eastwards on 8 and 9 April, while at the same time its northward-reaching frontal system touched *Polarstern*. On the back side, the high intensified again and approached South Africa. When *Polarstern* reached southwest of Cape Town, the northeastern flank of the high during the night to 10 April, the wind turned southeast and, additionally intensified by a trough extending southwards along the Namibian and South African coasts, temporarily increased to 9 Bft by 11 April. At the same time, the significant wave height temporarily rose to 5 m (including 3 m swell from southwest to south caused by the eastwards moving deep low).

As *Polarstern* travelled north, the pressure gradient in the area of the trough, which remained off the coast until the end of the voyage, decreased, so that the wind and wave height also decreased. Due to the cold coastal ocean current (Benguela Current) and the resulting stable stratified air mass, sunny weather dominated from 11 April. From 12 to 14 April, directly off the coast of Namibia where the warm Namibian desert air met the cold Benguela current, fog occurred, which was most dense at night and in the mornings and which is very typical for this region. In the morning of 14 April 2024, *Polarstern* finally arrived in the harbour of Walvis Bay (Namibia).

2. MARINE GEOPHYSICS

Sebastian Krastel[1], Karsten Gohl[2], [1]DE.CAU
Rachel Barrett[1], Patrick Schwarzbach[2], [2]DE.AWI
Estella Weigelt[2]

Grant-No. AWI_PS141_01, AWI_PS141_03

Objectives and outline

The ice sheets of Antarctica have been losing ice mass over the last several decades. This is mainly driven by warm ocean deep-water coming into contact with the ice-water interface of ice shelves and grounding zones, which results in acceleration of glacier flows depending on the bed topography. The long-standing perception that – in addition to the Greenland Ice Sheet – only the marine-based West Antarctic Ice Sheet (WAIS) is vulnerable to ongoing climate change for the next centuries to come, while the East Antarctic Ice Sheet (EAIS) will remain relatively stable, has turned into a controversial debate. Recently improved data on sub-glacial topography along the margins of Antarctica show deep glacial troughs adjacent to stabilizing ridges below current sea-level at several locations. These deep glacial troughs potentially connect warm ocean deep-water with grounding zones and the bed-ice interface on bed slopes that are inclined towards deep-seated basins of the continental interior. The Denman, Vanderford and Totten glaciers of the Davis Sea and Mawson Sea sectors of East Antarctica are three such ice-stream systems that drain ice from the large marine-based Wilkes and Aurora basins. Detailed stratigraphy of the continental shelf and slope sediments, as well as glacial morphology of this region, however, remains poorly constrained. Such glacial sedimentary features can be imaged using geophysical methods, which then enables reconstruction of advance and retreat dynamics of the past regional ice sheet. During PS141, we collected high-resolution seismic profiles, deep-penetrating seismic profiles, sediment echo-sounder and multibeam bathymetric data on the continental shelves, slopes and continental rise in the vicinity of the outflow of the Denman and Vanderford, as well as neighbouring glaciers of the eastern Davis Sea and western Mawson Sea. Details of each of these methods and their preliminary results are described in Subchapters 2.1 to 2.3.

2.1 Seismic Profiling

Rachel Barrett[1], Karsten Gohl[2], Sebastian Krastel[1], Adalbert Pfeiffer[2], Chiara Tobisch[1], Timo Krause[2], Lenya Baumann[1], Katharina Hochmuth[3], Alejandro Cammareri[4], Ursula Pena Gonzalez[4], Andres Alejandro Scrigna[4]

[1]DE.CAU
[2]DE.AWI
[3]AUS.UTAS
[4]AR.MARYBIO

Grant-No. AWI_PS141_01

Objectives

The behaviour of polar ice sheets in relation to climatic changes and their contribution to global sea-level change is poorly understood. Reports of the Intergovernmental Panel for Climate Change (IPCC) (e.g., IPCC 2021) explicitly flag this deficiency in knowledge. In contrast to most of the West Antarctic Ice Sheet and the Antarctic Peninsula Ice sheet, which have been shown to exhibit very dynamic activity both at present and during their history, the East Antarctic Ice Sheet (EAIS) has long been assumed for being relatively dormant during past and present initial phases of climate change. However, this paradigm has been challenged by recent data that show that ice mass loss due to incursions of warm deep-water onto the continental shelves and into sub-ice shelf cavities occurs in parts of the East Antarctic margin, such as off Wilkes Land Subglacial Basin, at Sabrina Coast off Totten Glacier and – in its earlier stage – off Denman Glacier and Vanderford Glacier. This led to Hypothesis 1 in the ship-time proposal for Expedition PS141 (EASI 3): "*The marine-based EAIS sectors have reacted with rapid and extended phases of retreat to climatic conditions in all relevant warm phases since early glaciation.*"

The Shackleton Ice Shelf off Princess Elisabeth, Wilhelm II and Queen Mary Lands (eastern Davis Sea sector) and the continental shelf near Petersen Bank (western Mawson Sea sector) are fed by two major glacier systems: Denman Glacier and Vanderford Glacier, which, together with Totten Glacier further to the east, form one of the largest ice catchment and drainage areas of East Antarctica (Fig. 2.1.1). Denman and Vanderford glaciers, as well as most of the coastal glaciers in the Davis Sea and Mawson Sea, are marine-based, making them inherently unstable and thus vulnerable to potential warm-water incursions. The deep submarine basin beneath Denman Glacier is currently protected against potential warm-water incursions only by a very narrow coastal basement ridge (Morlighem et al. 2020). In the hinterland, both glaciers connect to the vast submarine Wilkes Land and Aurora Subglacial Basins. Earlier studies suggested that the EAIS has been relatively stable since early glaciation, but recent results from the shelf off Totten Glacier show that at least the marine-based sectors of the EAIS behaved dynamically throughout the Oligocene to Pliocene. Ice advanced across the coast and retreated at least 11 times during the Oligocene and Miocene (e.g., Gulick et al. 2017). In particular, conditions during the Mid-Miocene Climatic Optimum and warm periods of the Pliocene are analogous to the present and the near future, necessitating quantification of ice sheet behaviour during these time periods.

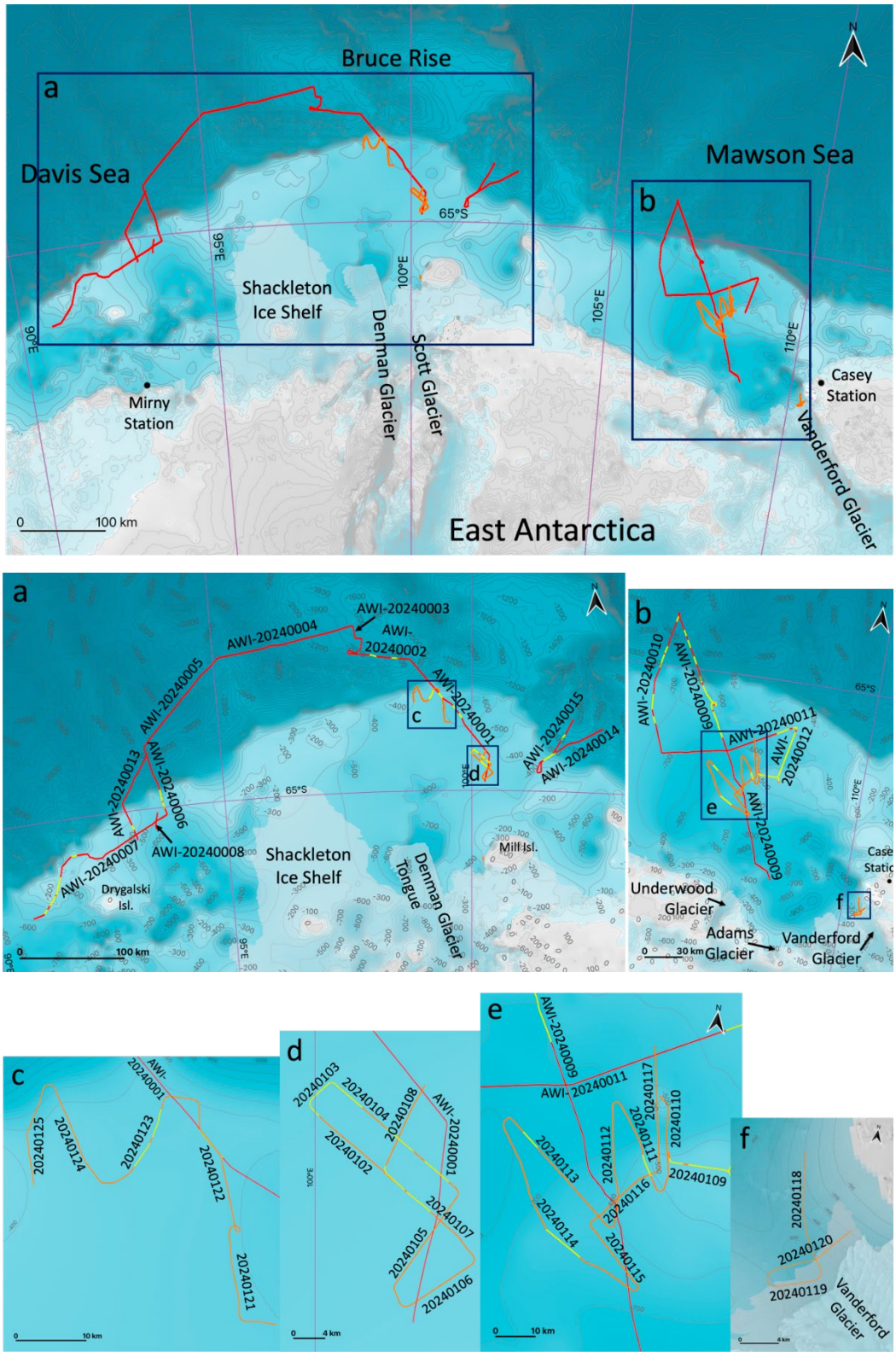

Fig. 2.1.1: Bathymetric overview map and inset maps (a-f) of the working areas for seismic surveys in Davis Sea and Mawson Sea offshore East Antarctica showing collected seismic profiles on the continental shelf and rise. Red lines show deep-penetration profiles, orange lines mark high-resolution profiles. Shutdown data gaps due to the presence of marine mammals in the safety zone are marked with yellow lines in the inset maps. Bathymetry is from the International Bathymetric Chart of the Southern Ocean, Version 2 (IBCSO v2; Dorschel et al. 2022).

Seismic reflection surveying (Fig. 2.1.2) of shelf areas and adjacent slopes, combined with multibeam bathymetric mapping, sediment echosounding and coring of outcropping older strata at appropriate locations, provides data for assessing EAIS dynamics in terms of advance/retreat behaviour and extent in warmer-than-present time periods, from early Antarctic glaciations in the Eocene-Oligocene to the Pleistocene. Detailed seismic reflection imaging reveals the sedimentary architecture of the shelves and illustrates periods of major progradation during glacier advances, as well as aggradation deposition during prolonged warmer-than-present periods, such as the mid to late Eocene, middle Oligocene, early to middle Miocene, and early/middle Pliocene. Glacial maxima are characterized by major advances of grounded ice onto and across the shelf, and are indicated by truncational unconformities on the inner to middle shelf, as well as progradational sequences on the outer shelf to slope (e.g., Hochmuth and Gohl 2019). Such seismic characteristics have been successfully investigated on both the Ross Sea shelf (De Santis et al. 1999) and the Amundsen Sea shelf (Gohl et al. 2013, 2021). Integrating the scientific drill records from the East Antarctic margin with a stratigraphic model of the continental rise along that margin (Leitchenkov et al. 2007) will enable correlation of seismic horizons and units with shelf sequences, and provide age control for major seismic units and unconformities. In addition, recently dated sediment core and seismic records of outcropping Eocene to Pliocene strata on the steep flanks of glacial troughs off Totten Glacier (Gulick et al. 2017) provide another link to our seismic network.

The mismatch between model results and field evidence of EAIS behaviour in the Late Quaternary requires investigations of past ice-sheet configurations in East Antarctica. Knowledge of paleo-ice sheet geometries can support future projections of ice sheet behaviour, either through direct evidence or by providing past examples that can be used to test ice-sheet models. Accordingly, we applied an integrated approach to evaluate Late Quaternary dynamics of vulnerable marine-based EAIS portions on the continental shelf; incorporating swath bathymetric mapping, shallow seismic surveying, sediment echosounding, and sediment coring to test Hypothesis 2: "*The palaeo-Denman and Totten Glaciers extended towards the shelf edge during the LGM and reacted very sensitively to past warm-water incursions and sea-level fluctuations*". Integrating seismic profiling and hydroacoustic mapping with sediment coring provides new evidence for ice expansion, paleo-flow pathways and stillstands in grounding-line retreats. In combining these datasets, we can decipher past ice-flow trajectories and ice-retreat patterns by mapping sub- and proglacial landforms such as mega-scale glacial lineations (MSGLs), grounding-zone wedges (GZWs), drumlin and moraine features, as well as subsurface depositional systems and glaciogenic fault tectonics.

Seismic Equipment

Seismic sources, activation and timing

We used an airgun cluster of 4 GI-Guns to resolve sedimentary layers for the deep-penetrating seismic profiles, and a single GI-Gun from the cluster for high-resolution seismic acquisition (Fig. 2.1.3). Each GI-Gun™ consists of two independent airguns within the same body. The first airgun ("Generator") produces the primary pulse, while the second airgun ("Injector") is used to control oscillation of the bubble produced by the "Generator". The "Injector", which has a volume of 1.68 liters (105 in^3), was fired 40 ms after the "Generator" (0.72 liters = 45 in^3). This leads to an almost bubble-free signal. The GI-Gun cluster was towed 10-20 m behind the vessel at 2 m water-depth, and fired every 10 s for the deep-penetrating seismic profiles and every 5 s for the high-resolution seismic profiles. Air pressure was generated by the onboard compressors and fed to the umbilical at 170 bar. An AWI-made airgun trigger unit sent the signal to activate the solenoid valves of the airguns. The trigger unit received a TTL time pulse every second from a time pulse generator called "SchwaBox" from the University of Kiel.

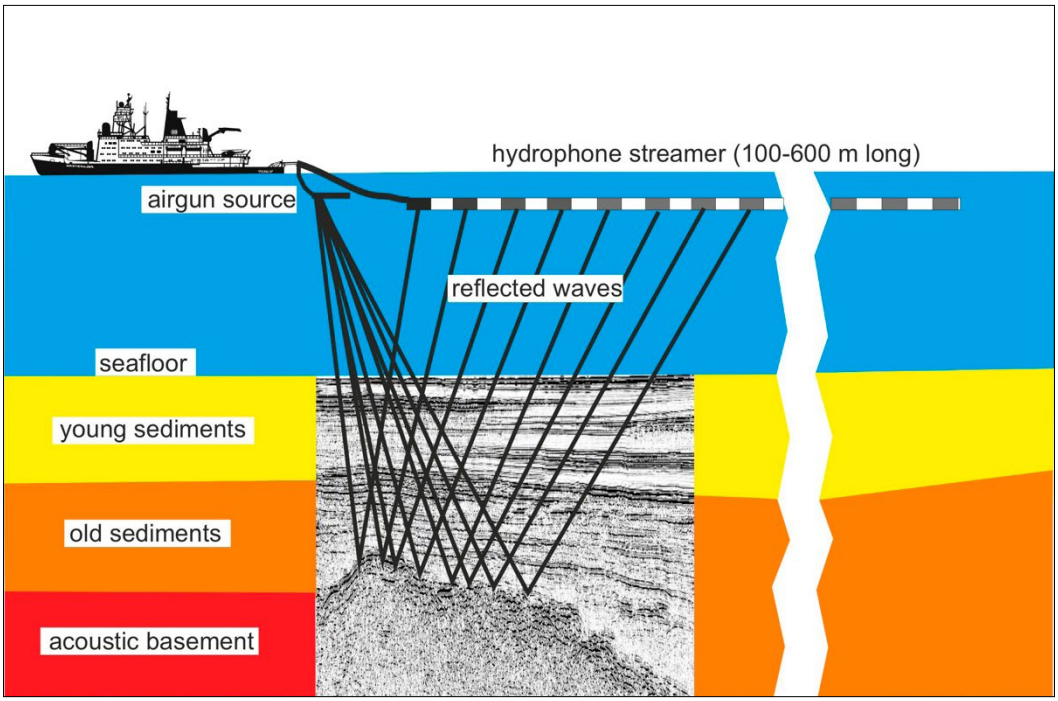

Fig. 2.1.2: Principle of marine seismic reflection surveying

Seismic recording systems

We used two digital solid-state streamers (Geometrics GeoEel) with different configurations to acquire multi-channel seismic reflection data (Fig. 2.1.3, Fig. 2.1.4): (i) a 600 m long streamer for the deeper-penetrating seismic surveying (loaned to AWI from CSIRO-MNF, Hobart, Australia); and (ii) a 60-100 m long streamer for the high-resolution seismic surveying (University of Kiel).

1. The CSIRO system consists (in sequence) of a tow cable (40 m in water), a vibration isolation section (10 m long), a stretch section (10 m long), and six active sections (100 m each) (Fig. 2.1.4a). An active section of the streamer consists of eight channels spaced at 12.5 m, each of which contains six hydrophones.

2. The Uni Kiel system consists of a tow cable (34 m in water), five to seven active sections (12.5 m each), and two vibration isolation sections (one preceding and one following the active sections: 10 m each) (Fig. 2.1.4b). An active section consists of eight channels spaced at 1,5625 m, each containing four hydrophones. Configuration of the Uni Kiel streamer was changed between different surveys due to equipment malfunctions (detailed under the section "*Problems encountered during seismic data acquisition*" below).

For both systems, each active section is preceded by an AD digitizer module (a small Linux computer that transfers data through the streamer via Ethernet). The AD digitizer modules and the recording system in the lab communicate via TCP/IP. A repeater module was located between the deck cable and the tow cable (lead-in) to amplify the signal. The Streamer Power Supply Unit (SPSU) manages power supply and communication between the recording system and the AD digitizer modules. Data were recorded as multiplexed SEG-D using Geometrics acquisition software. The analogue signal was digitized with a sample rate of 500 microseconds for the streamer of the University Kiel, and 1000 microseconds for the CSIRO streamer.

One SEG-D file was generated per shot and the recording length was set between 3 and 4.6 s for the high-resolution profiles, and at 9 s for the deep penetrating profiles. Shot gathers, single channel plots, and noise content of each shot were monitored to enable on-profile quality control. The cycle time of the shots and recording log messages were also displayed. On-profile ship navigation was recorded and saved to log-files using Franson GPSGate (v2.6).

A summary of the seismic profiles collected during PS141 can be found in Appendix A.4.

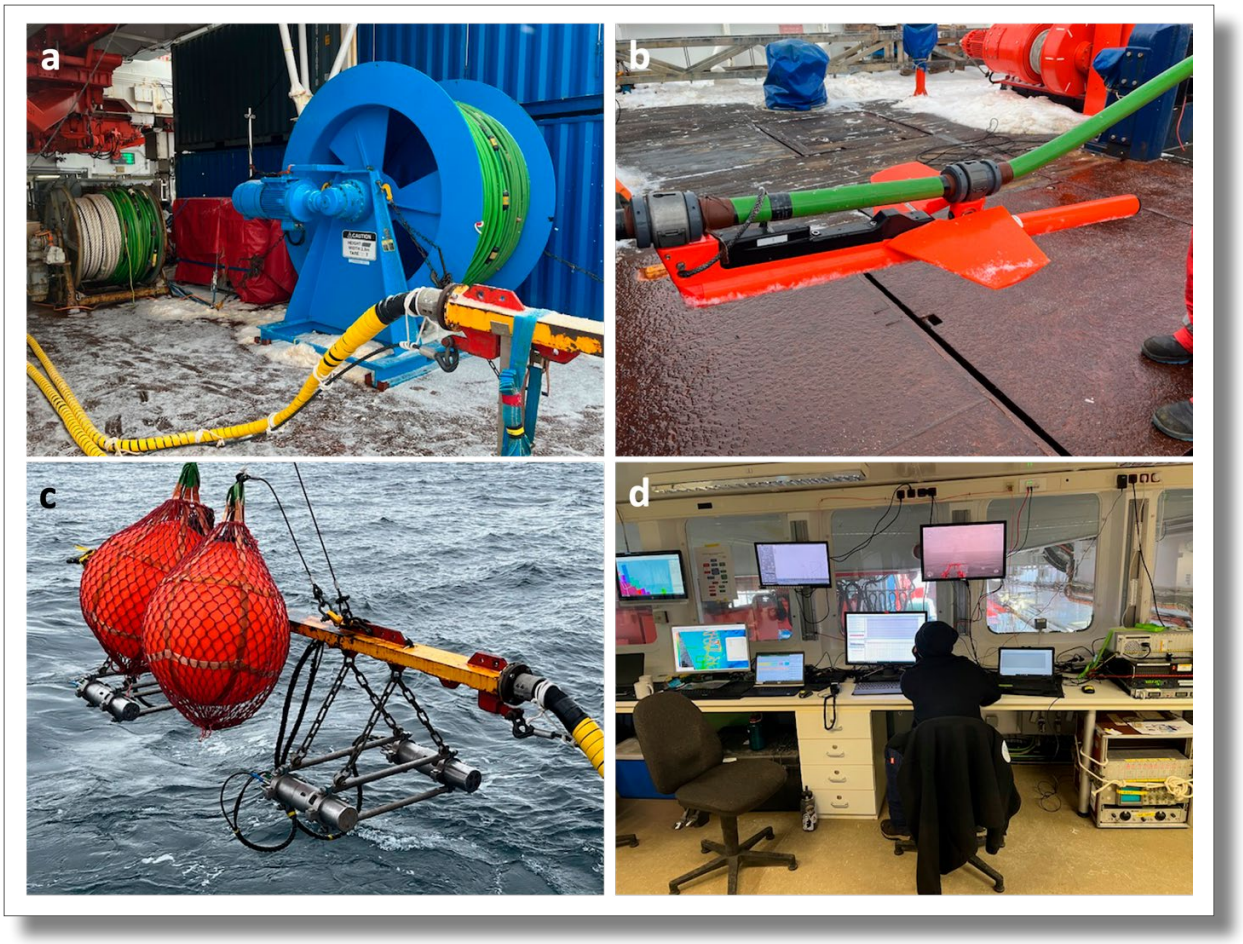

Fig. 2.1.3: Photos show (a) the Uni Kiel (left) and 600 m long CSIRO (right) streamers on their winches, (b) a depth-control "bird" mounted on a streamer, (c) the seismic source (GI-Gun) configuration during deployment, and (d) seismic recording and trigger systems monitored in the seismic lab.

Depth control and positioning

Water depth of both streamer systems was controlled using ION Model 5010/5011 DigiBIRD™ and CompassBIRD™ II birds/remote units (Fig. 2.1.3). The birds have adjustable wings and were controlled using Digicourse™ software. The depth can be changed during operation by setting new target depths for each bird through the controller software. The CSIRO streamer had either four or five birds and a recovery device (SRD) (Fig. 2.1.4a), and was set to a depth of 6 m. The Uni Kiel streamer had a single bird, which was attached to the vibration isolation section preceding the active sections (Fig. 2.1.4b) and was set to a nominal depth of 4 m.

Problems encountered during seismic data acquisition

Seismic data acquisition during PS141 occurred generally without problems, apart from two issues that require further documentation and are described in the following:

1. The first significant technical problem occurred on 27 February 2024 following several days of extreme temperatures (-14°C air temperature, -28°C wind chill) west of the Shackleton Ice Shelf. Internal components of all four GI-Guns froze and the GI-Guns could not seal when under pressure, even after being triggered individually during ~1,5 hours in the water. The GI-Guns were then retrieved, and we re- and dis-assembled them before and after every subsequent deployment; storing them in the working corridor for warmth between surveys.

2. The second significant problem was encountered on 8 March 2024 during acquisition of profile AWI-20240109, north of the Adams and Vanderford Glaciers. The buoy at the end of the Uni Kiel streamer caught on a small iceberg, and the resulting high tension ripped the streamer in two after the AD digitizer module between the third and fourth streamer sections. The streamer sections that were still attached to *Polarstern* were recovered and the ship turned around to search for the damaged sections. The end buoy was sighted, and the second half of the streamer – still attached to the buoy and swimming vertically in the water column – was able to be recovered. The Uni Kiel streamer sections and AD digitizers were tested thoroughly following the accident to determine the extent of the damage, and a shortened streamer was able to be deployed on 13 March 2024.

Seismic data processing

Preliminary seismic data processing was performed on the shot records of both streamer systems during the expedition.

The SEG-D raw data of the deep-penetrating profiles were imported to the ECHOS processing software (by AspenTech-Paradigm) of AWI for quality control, geometry definition, sorting to CDP gathers, and first preliminary processing with velocity analysis, multiple suppression, filtering and stacking.

Preliminary processing of the high-resolution SEG-D raw data was conducted with Schlumberger's VISTA software. Data was imported and geometry defined before the data were sorted into CDP gathers, filtered and stacked. Velocity analysis was conducted prior to stacking for the survey collected with the CSIRO streamer. After defining the geometry, each complete profile was exported in SEG-Y format for archiving.

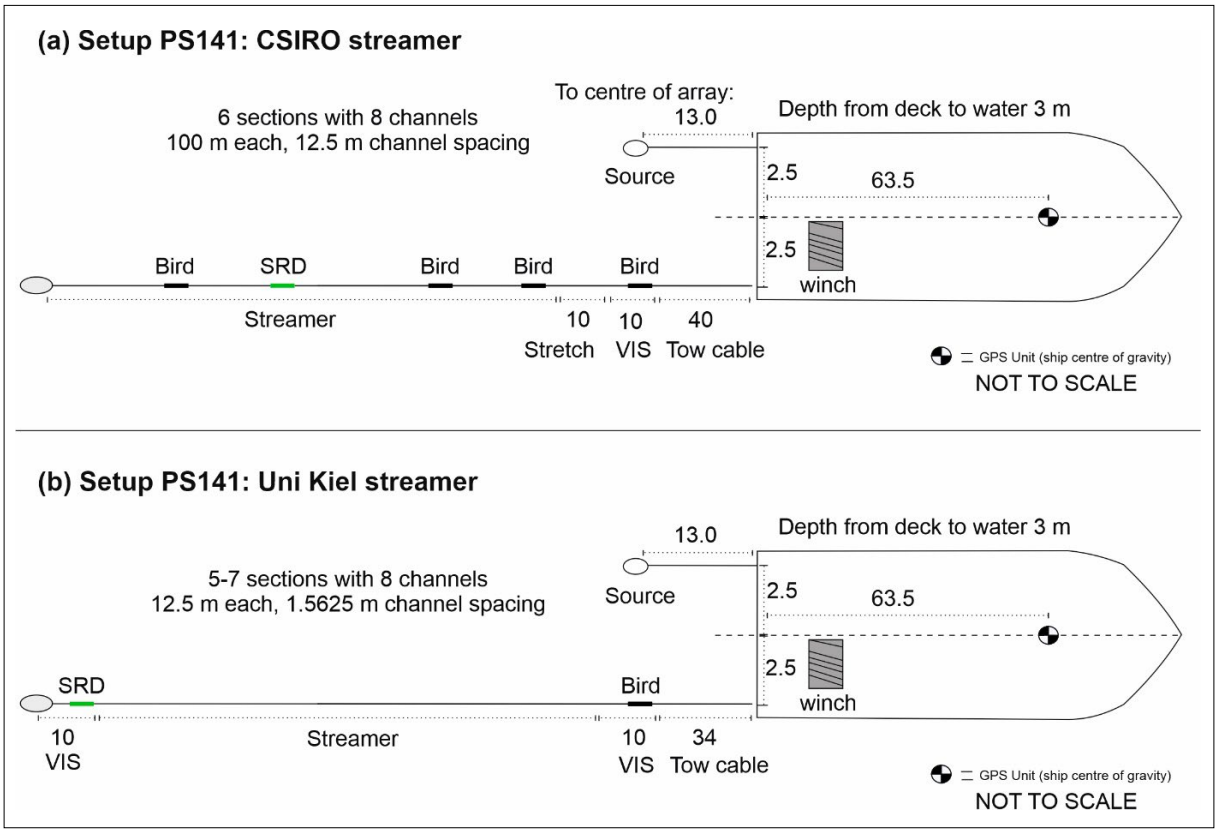

Fig. 2.1.4: Deck layout of the two seismic systems used during PS141 showing (a) the CSIRO streamer and (b) the Uni Kiel streamer.

Mitigation for Marine Mammals

Mitigation regulations for seismic operations in Antarctic waters require that visual observation for marine mammals within a predefined safety zone is carried out by marine mammal observers (MMOs). The MMOs of PS141 followed the mitigation protocol according to the permit issued by Germany's Federal Environment Agency (Umweltbundesamt – UBA).

Marine mammal observation was coordinated and conducted by three professional, experienced and qualified MMOs – Alejandro Cammareri, Ursula Pena and Andres Scrigna (from Marybio Foundation) – with support of additional observers drafted from the various science teams of PS141 and trained by the professional MMOs during the expedition. During seismic operations, a constant visual watch for marine mammals was conducted by three marine mammal observers per shift to detect any marine mammals within the predefined safety zone around the ship (1,000 m for whales; 500 m for seals; and no defined maximum distance for beaked whales and southern elephant seals). Visual observations were conducted by two MMOs at the port and starboard sides of the bridge, and the third MMO monitored the shipboard infrared (IR) camera system and high-resolution optical camera (FLIR) installed to observe the area behind the ship's stern. Observers shifted watch positions every 40 minutes and changed every two hours, with one professional MMO always on watch.

The primary observation technique for spotting marine mammals was to continuously scan the sea around the vessel and within the safety zone using both the naked eye and reticulated binoculars (Fujinon 7x50). Areas of interest on the water (breaking wave crests, splashes, blows, footprints, dark shapes, bird activity, etc.) were used as visual cues for further investigation. An

IR thermal imaging sensor (FIRST Navy), installed in the crow's nest of *Polarstern* (Zitterbart et al. 2013), was used to ensure that most of the perimeter of the seismic sources was observed continuously. The IR sensor constantly monitors its environment within a field of view of 360° horizontally (approximately 100° to the stern obstructed by the crow's nest) by 28.8° vertically. The recorded image shows the thermographic signatures of marine mammals (e.g. blow) and provides the observer in the IR observation room with detected cues on the monitor to help the MMOs decide whether a shut-down is necessary.

Pre-watch observations started at least 60 minutes before scheduled seismic operations were to begin to ensure that no marine mammal was present within the safety zone when seismic operations were due to start. Clearance for the 30 minute soft-start procedure (a gradual increase of energy and number of the air pulsers) was given when no marine mammals were detected within the mitigation area during the defined safety period (30 min for whales and seals, and 60 min for beaked whales and southern elephant seals). Airgun shutdown occurred when a marine mammal was detected in the water within the corresponding mitigation zone.

During seismic operations, MMOs performed continuous watch during all seismic surveys, totalling 237 hours (10 days) of visual and IR monitoring efforts. During that period, 159 detections of marine mammals were recorded, of which 43 were within the safety zone (Tab. 2.1.1). In all 43 of these encounters, shut-downs (SD) of airguns were conducted. The sum of the shut-down periods resulted in 177.1 nmi (327.9 km) of data loss, which is 16.7 % of the total seismic data acquisition of 1961.3 km.

Tab. 2.1.1: Summary of airgun shut-downs due to detection of marine mammals within the safety zone during seismic surveys.

Date	Time [UTC]	Sighting number	Visual or IR	Species	Mitigation action
20.02.2024	20:37	6	IR	Whale no ID	Shut-down
20.02.2024	21:44	7	visual	Humpback Whale	Shut-down
20.02.2024	23:45	10	both	Humpback Whale	Shut-down
21.02.2024	07:10	13	IR	Whale no ID	Shut-down
21.02.2024	09:40	14	visual	Humpback Whale	Shut-down
23.02.2024	03:19	22	both	Humpback Whale	Shut-down
23.02.2024	03:59	23	visual	Humpback Whale	Shut-down
23.02.2024	04:49	25	visual	Humpback Whale	Shut-down
23.02.2024	18:14	26	IR	Whale no ID	Shut-down
23.02.2024	21:37	29	both	Humpback Whale	Shut-down
23.02.2024	23:57	37	both	Humpback Whale	Shut-down
24.02.2024	01:47	39	visual	Whale no ID	Shut-down
01.03.2024	05:09	43	visual	Humpback Whale	Shut-down
01.03.2024	07:13	45	visual	Humpback Whale	Shut-down
01.03.2024	08:02	46	visual	Humpback Whale	Shut-down
01.03.2024	14:07	48	IR	Whale no ID	Shut-down
01.03.2024	14:44	49	IR	Whale no ID	Shut-down
06.03.2024	04:21	51	both	Minke Whale	Shut-down
06.03.2024	06:08	55	visual	Whale no ID	Shut-down
06.03.2024	07:10	58	visual	Humpback Whale	Shut-down
06.03.2024	09:04	62	visual	Humpback Whale	Shut-down

Date	Time [UTC]	Sighting number	Visual or IR	Species	Mitigation action
06.03.2024	11:14	68	visual	Humpback Whale	Shut-down
06.03.2024	13:04	71	both	Humpback Whale	Shut-down
06.03.2024	14:48	72	IR	Whale no ID	Shut-down
06.03.2024	16:01	77	IR	Whale no ID	Shut-down
06.03.2024	18:44	78	IR	Whale no ID	Shut-down
06.03.2024	22:00	82	both	Humpback Whale	Shut-down
06.03.2024	22:49	83	IR	Seal no ID	Shut-down
07.03.2024	02:37	87	visual	Humpback Whale	Shut-down
07.03.2024	04:51	90	visual	Humpback Whale	Shut-down
07.03.2024	18:58	92	IR	Whale no ID	Shut-down
07.03.2024	20:33	98	IR	Whale no ID	Shut-down
07.03.2024	21:20	101	both	Humpback Whale	Shut-down
08.03.2024	03:03	127	visual	Humpback Whale	Shut-down
08.03.2024	04:50	129	visual	Minke Whale	Shut-down
08.03.2024	14:04	135	IR	Whale no ID	Shut-down
08.03.2024	23:20	138	visual	Minke Whale	Shut-down
09.03.2024	03:58	139	visual	Minke Whale	Shut-down
18.03.2024	05:57	141	visual	Leopard Seal	Shut-down
23.03.2024	09:48	146	visual	Humpback Whale	Shut-down
23.03.2024	10:30	147	visual	Minke Whale	Shut-down
24.03.2024	09:15	153	visual	Humpback Whale	Shut-down
24.03.2024	17:00	159	IR	Whale no ID	Shut-down

Preliminary results

Deep-penetrating seismic reflection data

A total of 809.7 nmi (1499.5 km) of high-quality deep-penetrating seismic reflection profiles was collected (Appendix A.4). The profiles cover the middle to outer shelves (Fig. 2.1.1). Some profiles connect with pre-existing Japanese and Russian seismic lines on the continental shelf, rise and Bruce Rise to form a network for seismic stratigraphic mapping. Quality-control plots (Fig. 2.1.5) and results from initial data processing on board provide images of preglacial sedimentary strata as well as glacially-transported and deposited sequences on the shelf and slope of the Davis Sea and Mawson Sea sectors. Through connecting these new seismic data with pre-existing profiles and – through long-distance correlation – with scientific drill sites of ODP Legs 119 and 188 in Prydz Bay, DSDP Leg 28 (Site 268) in the northern Mawson Sea, and IODP Expedition 318 offshore western Wilkes Land, we expect to decipher dominant phases of early Oligocene to Pleistocene ice sheet development in these sectors, in particular in ice-proximal settings of the shelf offshore Denman Glacier and Shackleton Ice Shelf as well as Vanderford and Adams glaciers. An observation of particular interest was made with a gigantic stacked grounding-zone wedge (GZW) in the past outflow sector of Vanderford, Adams and neighbouring glaciers. The results of the deep-penetrating seismic acquisition forms for the first time the necessary data base for a thorough analysis of the preglacial to glacially dominated sedimentation processes of this central part of the East Antarctic Ice Sheet with particular focus on major extended ice sheet expansion and retreat periods.

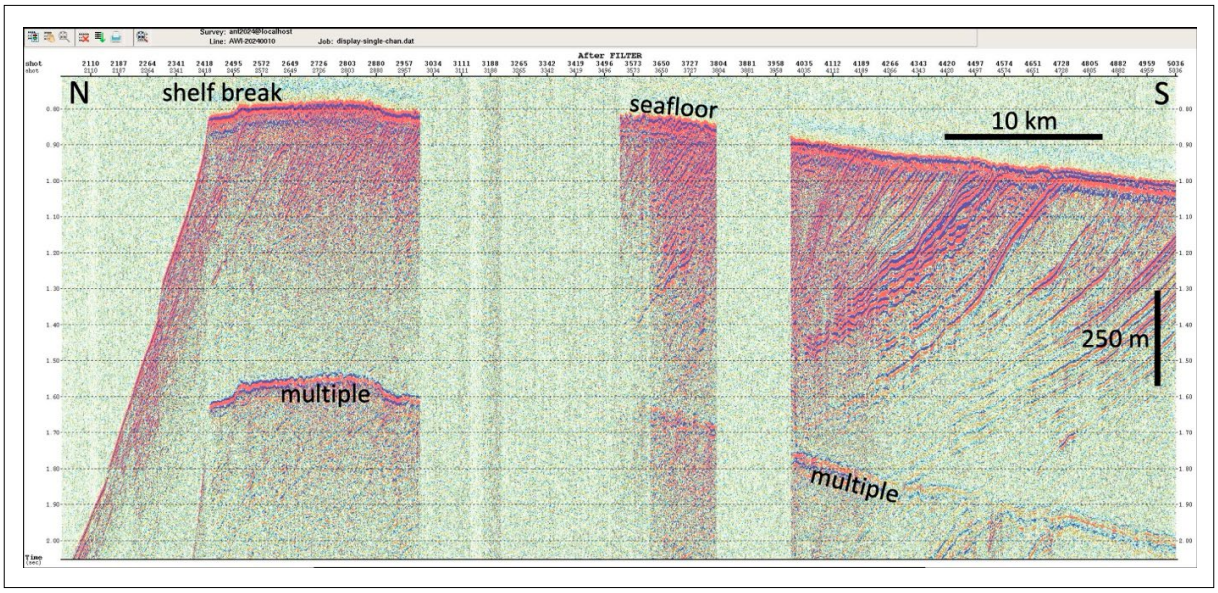

Fig. 2.1.5: Quality-control display example of a segment of an unprocessed deep-penetration seismic profile AWI-20240010 (single-channel plot) showing northward dipping sedimentary sequences of the middle to the outer continental shelf. Strong-amplitude seafloor multiples will be partly suppressed after complete data processing. The data gaps are due to the presence of marine mammals in the safety zone, which necessitated the shut-down of airgun operations.

High-resolution seismic reflection data on the continental shelf

We collected a total of 249.4 nmi (461.8 km) of high-resolution seismic reflection profiles within four main areas on the continental shelf (Appendix A.4). The profiles within these areas are short (an average of ~19 km long), and form a grid, crossing each other as well as profiles collected with the deep penetrating seismic system (Fig. 2.1.1). This survey geometry will enable us to correlate the different datasets. Collection of the high-resolution seismic data was preceded by hydroacoustic mapping to determine the best location for seismic surveying, and focussed particularly on the shelf in front of the Vanderford and Denman Glaciers. Preliminary results reveal a broad range of glacial geomorphology, including a grounding zone wedge in front of the Vanderford glacier, iceberg striations and mega-scale glacial lineations across the width of the shelf (Fig. 2.1.6). These data will help us to resolve glacial processes active across multiple temporal and spatial scales, providing important insights into past glacial movement.

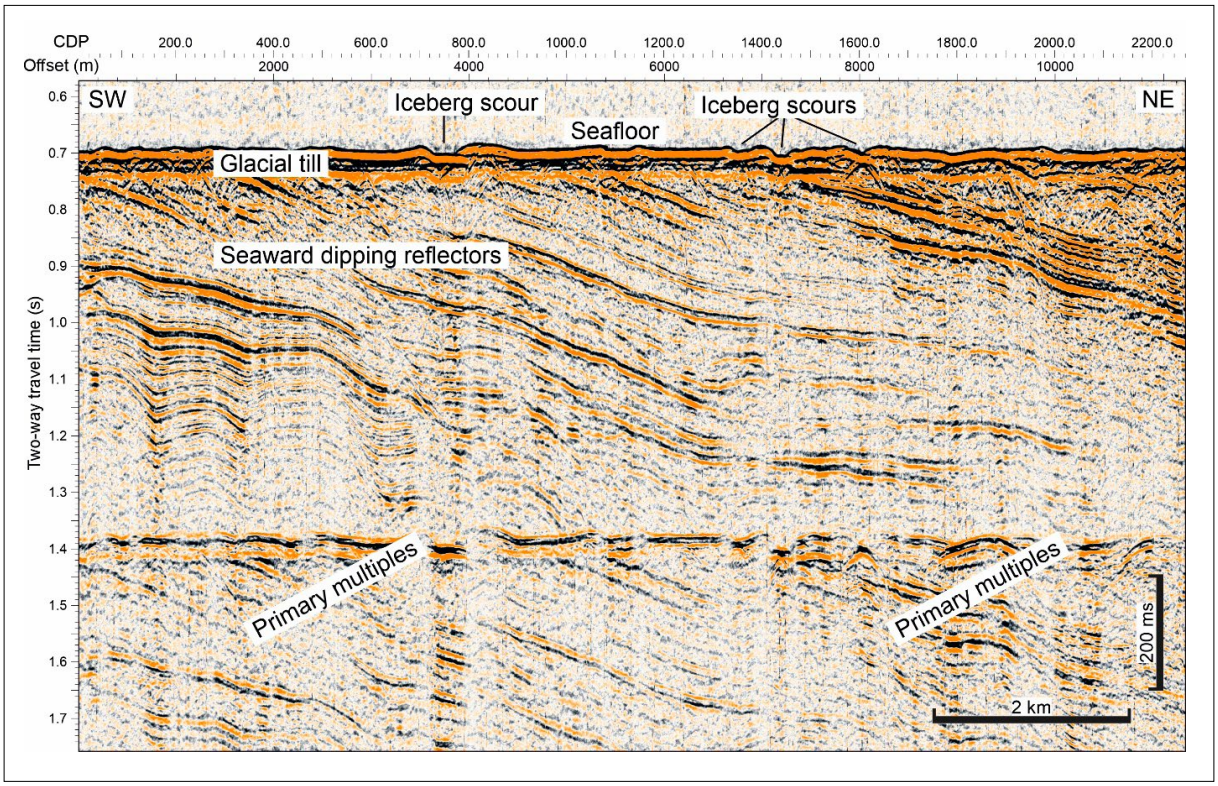

Fig. 2.1.6: Preliminary CMP stack of the seismic profile AWI-20240108 showing northward-dipping sedimentary sequences on the mid-continental shelf east of the Shackleton Ice Shelf. The data have been filtered (band pass and a basic FK filter), corrected for normal moveout (at a constant velocity of 1,500 m/s), and stacked. Further data processing to improve the signal-to-noise ratio will continue onshore.

Data management

Metadata and a short report will be submitted to DOD and PANGAEA. Seismic data will be submitted to the SCAR Antarctic Seismic Data Library System (SDLS; https://sdls.ogs.trieste.it), which will make them available to interested collaboration partners two years after data acquisition and as open access four years after acquisition according to the SDLS guidelines.

Moratorium extension may be possible if necessary. Access for the science community will also be provided according to international standards by the World Data Center PANGAEA Data Publisher for Earth & Environmental Science (https://www.pangaea.de) within two years after the end of the expedition or after an extended moratorium period. Moratorium extension may also be possible if necessary. By default, the CC-BY license will be applied.

The research activities are directly related to the objectives the Helmholtz Research Programme POF-IV “Changing Earth – Sustaining our Future” in Topic 2 (Ocean and Cryosphere in Climate) with a focus on Subtopics 2.1 (Warming Climate) and 2.3 (Sea Level Change).

In all publications based on this expedition, the **Grant No. AWI_PS141_01** will be quoted and the following publication will be cited: Alfred-Wegener-Institut Helmholtz-Zentrum für Polar- und Meeresforschung (2017), Polar Research and Supply Vessel POLARSTERN Operated by the Alfred Wegener Institute. Journal of Large-Scale Research Facilities, 3, A119. http://dx.doi.org/10.17815/jlsrf-3-163.

References

De Santis L, Prato S, Brancolini G, Lovo M, Torelli L (1999) The Eastern Ross Sea continental shelf during the Cenozoic: implications for the West Antarctic ice sheet development. Glob. Planet. Change 23:173–196. https://doi.org/10.1016/S0921-8181(99)00056-9

Dorschel B et al (2022) The International Bathymetric Chart of the Southern Ocean Version 2. Scientific Data 9(1). https://doi.org/10.1038/s41597-022-01366-7

Gohl K, Uenzelmann-Neben G, Gille-Petzold J, Hillenbrand C-D, Klages J, Bohaty SM, Passchier S, Frederichs T, Wellner J, Lamb R, Leitchenkov G, IODP Expedition 379 Scientists (2021) Evidence for a highly dynamic West Antarctic Ice Sheet during the Pliocene. Geophysical Research Letters 48:e2021GL093103. https://doi.org/10.1029/2021GL093103

Gohl K, Uenzelmann-Neben G, Larter RD, Hillenbrand C-D, Hochmuth K, Kalberg T, Weigelt E, Davy B, Kuhn G, Nitsche FO (2013) Seismic stratigraphic record of the Amundsen Sea Embayment shelf from pre-glacial to recent times: Evidence for a dynamic West Antarctic ice sheet. Marine Geology 344:115–131. https://doi.org/10.1016/j.margeo.2013.06.011

Gulick SPS, Shevenell AE, Montelli A, Fernandez R, Smith C, Warny S, Bohaty SM, Sjunneskog C, Leventer A, Frederick B, Blankenship DD (2017) Initiation and long-term instability of the East Antarctic Ice Sheet. Nature 552:225–229. https://doi.org/10.1038/nature25026

Hochmuth K, Gohl K (2019) Seaward growth of Antarctic continental shelves since establishment of a continentwide ice sheet: Patterns and mechanisms. Palaeogeogr., Palaeoclim., Palaeoecol. 520:44–54. https://doi.org/10.1016/j.palaeo.2019.01.025

Intergovernmental Panel on Climate Change – IPCC (2021) Climate Change 2021 - The Physical Science Basis, IPCC AR6 WG1, https://www.ipcc.ch/report/ar6/wg1/

Leitchenkov GL, Guseva YB, Gandyukhin VV (2007) Cenozoic environmental changes along the East Antarctic continental margin inferred from regional seismic stratigraphy. In A. K. Cooper and C. R. Raymond et al., USGS Open-File Report 2007–1047, Short Research Paper 005. https://doi.org/10.3133/of2007-1047.srp005

Morlighem M, Rignot E, Binder T et al (2020) Deep glacial troughs and stabilizing ridges unveiled beneath the margins of the Antarctic ice sheet. Nature Geoscience 13:132–137. https://doi.org/10.1038/s41561-019-0510-8

2.2 Bathymetry of the East Antarctic Sea

Patrick Schwarzbach[1], Natalie Cornish[1], [1]DE.AWI
Laura Höppner[2] [2]DE.TUM
not on board: Boris Dorschel[1], Simon Dreutter[1]

Grant-No. AWI_PS141_03

Objectives

Accurate knowledge of the seafloor topography, hence high-resolution bathymetry data, is key basic information necessary to understand many marine processes. It is of particular importance for the interpretation of scientific data in a spatial context. Bathymetry, hence geomorphology, is furthermore a basic parameter for the understanding of the general geological setting of an area and geological processes such as erosion, sediment transport and deposition. Even information on tectonic processes can be inferred from bathymetry.

While world bathymetric maps give the impression of a detailed knowledge of worldwide seafloor topography, most of the world's ocean floor remains unmapped by hydroacoustic systems. In these areas, bathymetry is modelled from satellite altimetry with a corresponding low resolution. Satellite-altimetry derived bathymetry therefore lack the resolution necessary to resolve small- to meso-scale geomorphological features (e.g. sediment waves, glaciogenic features and small seamounts). Ship-borne multibeam data provide bathymetry information in a resolution sufficient to resolve those features and for site selection for the other scientific working groups on board.

Glaciogenic landforms preserved at the seafloor can form the basis for the reconstruction of the dynamic history of Antarctic Ice Sheets. In particular, these landforms can shed light on its retreat since its maximum extent during the Last Glacial Maximum. Understanding the processes that led to this ice sheet retreat in the past can provide important information for predicting future responses of Antarctic ice sheets to changing climate conditions and oceanographic settings. Glaciogenic landforms can only be determined in high-resolution bathymetric data sets. These data are, however, sparse for the study areas of the PS141 (EASI3) expedition. Therefore, detailed bathymetric data of these areas were acquired with the ships hydroacoustic instruments.

Furthermore, the collection of underway data during PS141 contributes to the bathymetry data archive at the AWI and thus to bathymetric world datasets such as GEBCO (General Bathymetric Chart of the Ocean).

Work at sea

Bathymetric data were recorded with the hull-mounted multibeam echosounder Atlas Hydrosweep DS3. The main task of the bathymetry group was to plan and run bathymetric surveys in the study areas and during transit. The raw bathymetric data were corrected for sound velocity changes in the water column, and were further processed and cleaned for erroneous soundings and artefacts. Detailed seabed maps derived from the data provide information on the general and local topographic setting in the study areas. High-resolution seabed data recorded during the survey were made available for site selection and cruise planning. During the survey, the acoustic measurement were carried out by three operators in a 24/7 shift mode (except for periods of stationary work).

Technical description

During expedition PS141, bathymetric surveys were conducted with the hull-mounted multibeam echosounder (MBES) Teledyne Reson HYDROSWEEP DS3 (HSDS3). The HYDROSWEEP

is a deep water system for continuous mapping with the full swath potential. It operates on a frequency of ~14 kHz with chirped pulses. On *Polarstern*, the MBES transducer arrays are arranged in a Mills cross configuration of three m (transmit unit) by three m (receive unit). Combined motion, position (Trimble GNSS), and time information is provided by an iXBlue Hydrins motion reference unit (MRU). MRU data is directly transferred into the Processing Unit (PU) of the MBES for real-time motion compensation (Pitch, Roll and Yaw). With a combination of phase and amplitude detection algorithms the PU computes the water depth from the returning backscatter signal. The system can cover a sector of up to 140° with 70° per side. In the deep sea, an angle of ~50° to both sides could be achieved. In shallower shelf areas, the angle could be opened up to ~60° from nadir on both sides to get an overall swath width of approximately 3.5 times the water depth.

Data acquisition and processing

Bathymetric data acquisition was carried out throughout the entire expedition, as long as the ship was sailing in international waters or the Southern Ocean (south of 60°S). There the surveying was conducted in accordance to the Antarctic Treaty regulation set by the German Environmental Agency (Umweltbundesamt).

The HYDROSWEEP was operated with the software Sonar UI and for online data visualization, Teledyne PDS was used. Data was stored in S7K raw files in the shipboard file system for later transfer into the long-term data archive PANGAEA. Subsequent data processing was done with Caris HIPS and SIPS. For generating maps onboard, the data were exported to QGIS in the GeoTIFF raster format.

Sound velocity profiles

For best survey results and to correct HYDROSWEEP depths for changes of the sound velocity (SV) in the water column, SV profiles were generated from CTD data that were collected and provided by the oceanographic group. SV correlates with the density of a water mass and is thus depending on pressure, temperature and salinity of the seawater in a given location at a given depth. Wrong or outdated SV profiles lead to refraction errors, reduced data quality and faulty depth measurements.

When the CTD rosette (CTD_SBE9plus_485) was not operated, SV profiles were obtained by the bathymetry group using a Valeport MIDAS Sound Velocity Profiler (MIDAS_SVP). In these cases, the Valeport was attached to the winch cable of the multi corer (MUC_PS).

During PS141, a total of 66SV profiles were applied to the MBES. They include 24 SV profiles from the CTD data and five SV profiles recorded with the Valeport. The remaining 37 profiles were generated using the World Ocean Atlas 2018 (WOA18).

Stations

Data collection with the HYDROSWEEP received the number PS141_0_Underway-28 throughout the expedition but dedicated bathymetric surveys received a separate station number. Examples for bathymetry related stations are listed in Table 2.2.1. For CTD only station starts of the first stations are listed. For a complete station list see Appendix A.4.

Tab. 2.2.1: List of bathymetric stations during PS141

Device Operation	Device	Action	Event Time	Latitude South [°]	Longitude East [°]
PS141_0_ Underway-28	Hydrosweep DS3	station start	2024-02-07T20:33	44.13991	140.95367
PS141_0_ Underway-28	Hydrosweep DS3	profile start	2024-02-07T20:33	44.13991	140.95172
PS141_0_ Underway-28	Hydrosweep DS3	profile end	2024-04-10T05:00	36.20335	14.99760
PS141_0_ Underway-28	Hydrosweep DS3	station end	2024-04-10T05:00	36.20335	14.99760
PS141_1-2	CTD_SBE9plus_485	station start	2024-02-07T22:57	44.13777	140.890992
PS141_3-3	CTD_SBE9plus_485	station start	2024-02-10T0 8:19	46.95134	134.756879
PS141_9-1	Hydrosweep DS3	station start	2024-02-19T08:48	65.71221	100.3171
PS141_9-1	Hydrosweep DS3	profile start	2024-02-19T08:48	65.71221	100.3171
PS141_9-1	Hydrosweep DS3	profile end	2024-02-20T01:58	65.60583	100.17636
PS141_9-1	Hydrosweep DS3	station end	2024-02-20T01:58	65.60583	100.17636

Preliminary results

During 62 days of survey, a track length of 10,995 nmi (20,363 km) was surveyed with the HYDROSWEEP. The raw data volume of bathymetric data (S7K) was 251 GB broken up in 1,292 separated survey track lines. Figure 2.2.1 shows the coverage of the bathymetric data collected during transit and dedicated surveys in the research areas.

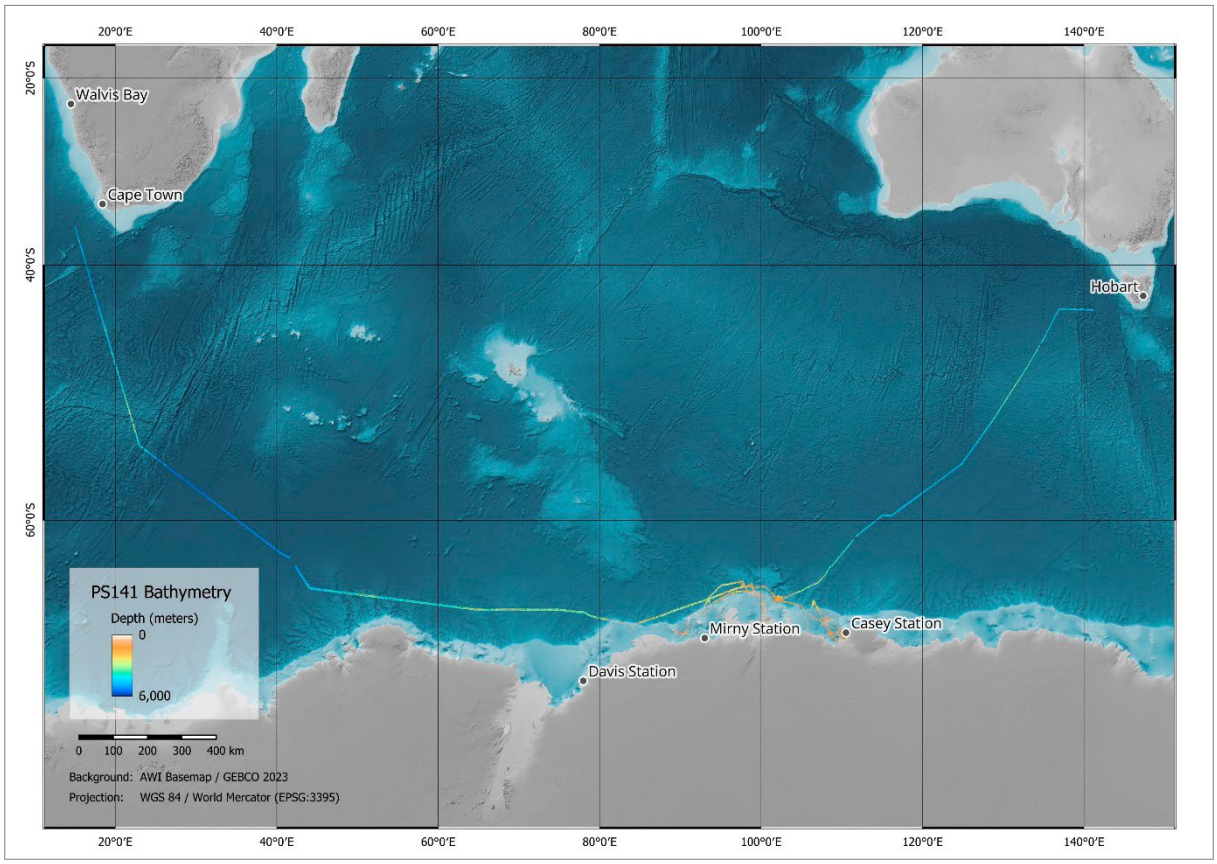

Fig 2.2.1: Overview on the bathymetric data acquired during PS141; background data used are GEBCO (GEBCO Bathymetric Compilation Group 2023).

Offshore Gaussberg, Mirny western Shackleton Ice Shelf

Systematic surveys were conducted in areas offshore Gaussberg (see white box 'A' in Fig. 2.2.2). Effectively an area of ~10,412 km² was covered. The depth in the survey area ranges from ~150 m down to ~3,000 m in the north.

Offshore BungerHills, Denman Glacier and eastern Shackleton Iceshelf

Other surveys were conducted north and east of Denman Glacier tongue (see white box 'B' in Fig. 2.2.2), again for geological and oceanographic site selections and for palaeo-glaciological interpretation of the obtained information on seabed topography. An area of ~11,362 km² was covered. The depth in the survey area ranges from ~170 m down to ~2,800 m.

Vincennes Bay

For geological and oceanographic site selection and to obtain comprehensive information on the seabed topography for palaeo-glaciological interpretation, bathymetric data were collected, covering areas in front of the Vanderford Glacier and Adams Glacier (see white box 'C' in Fig. 2.2.2), a potential grounding-zone wedge to the north of Vincennes Bay, and the continental slope. An area of ~9,921 km² was mapped. The depth in the survey area ranges from ~50 m down to ~3,500 m in the North.

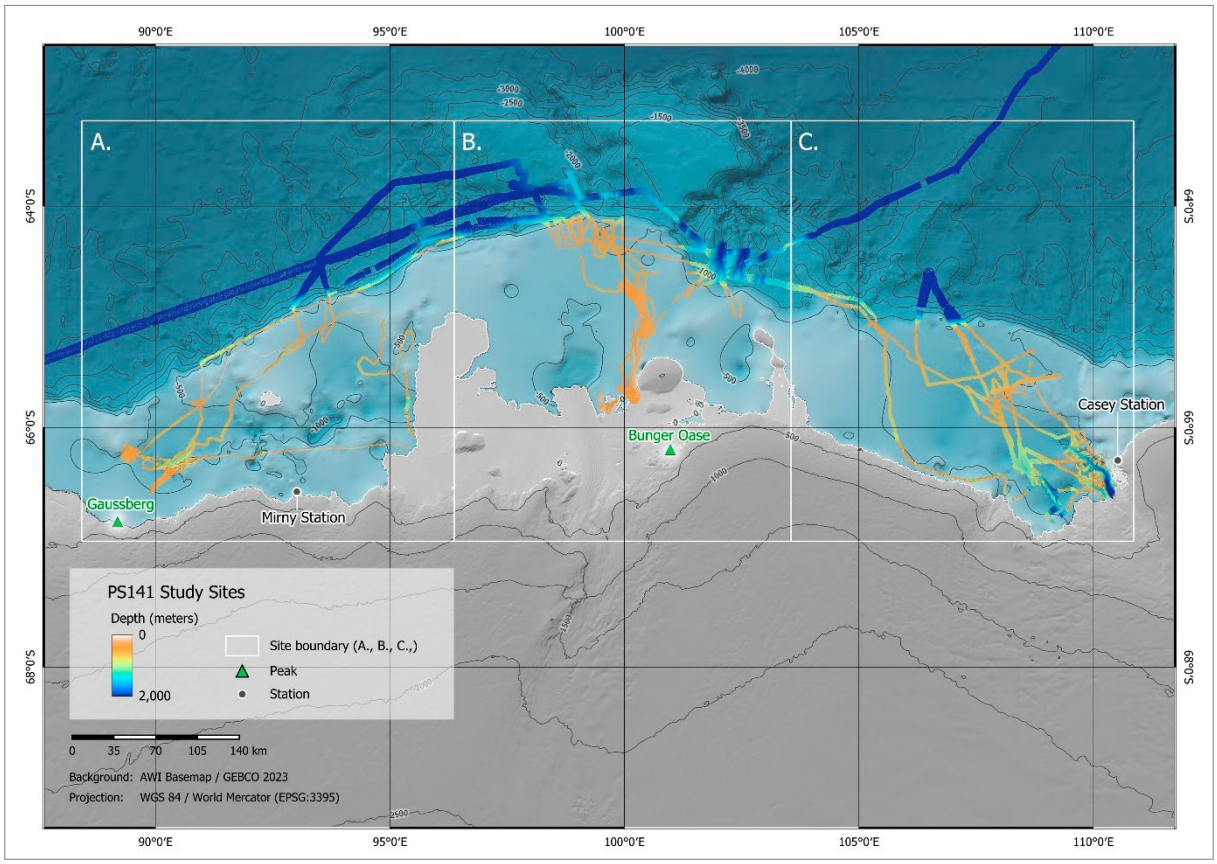

Fig 2.2.2: Bathymetric working areas (background data used are IBCSO (Dorschel et al. 2022), GEBCO (GEBCO Bathymetric Compilation Group 2024))

Data management

Environmental data will be archived, published and disseminated according to international standards by the World Data Center PANGAEA Data Publisher for Earth & Environmental Science (https://www.pangaea.de) within two years after the end of the expedition at the latest. By default, the CC-BY license will be applied. Furthermore, bathymetric data will be provided to the Nippon Foundation – GEBCO Seabed 2030 Project.

This expedition was supported by the Helmholtz Research Programme “Changing Earth – Sustaining our Future” Topic 2, Subtopic 2.3 "Sea Level Change".

In all publications based on this expedition, the **Grant No. AWI_PS141_03** will be quoted and the following publication will be cited:

Alfred-Wegener-Institut Helmholtz-Zentrum für Polar- und Meeresforschung (2017) Polar Research and Supply Vessel POLARSTERN Operated by the Alfred-Wegener-Institute. Journal of large-scale research facilities, 3, A119. http://dx.doi.org/10.17815/jlsrf-3-163.

References

Dorschel B, Hehemann L, Viquerat S et al. (2022) The International Bathymetric Chart of the Southern Ocean Version 2. Scientific Data 9:275. https://doi.org/10.1038/s41597-022-01366-7

GEBCO Bathymetric Compilation Group 2023 (2023) The GEBCO_2023 Grid – a continuous terrain model of the global oceans and land. https://doi.org/10.5285/F98B053B-0CBC-6C23-E053-6C86ABC0AF7B

2.3 Sediment echosounding (Parasound)

Estella Weigelt[1], Mardi McNeil[2]
and 33 voluntary PARASOUND Watchkeepers:
Rachel Barrett[3], Lenya Baumann[3], Karsten Gohl[1], Sebastian Krastel[3], Timo Krause[1], Chiara Tobisch[3], Katharina Hochmuth[4], Julia Gottschalk[3], Lester Lembke-Jene[1], Juliane Müller[1], Ole Jasper Ferber[3], Lena Jebasinski[3], Gernot Nehrke[1], Tim Stobbe[3], Anna Völkert[3], Sonja Berg[5], Bernd Wagner[5], Damian Gore[6], Daniela Dägele[5], Amber Howard[8] Timo Lange[5], Stephanie Scheidt[5], Marie Weber[1], Mirko Scheinert[7], Lutz Eberlein[7], Erik Loebel[7], Xabier Gorriz[7], Jodi Fox[4], Jack Beardsley[4], Georgios Xydis[3], Lisa Rüther[1], Sara Labrousse[9], Laurène Trudelle[9]
not on board: Catalina Gebhardt[1]

[1]DE.AWI
[2]AU.GA
[3]DE.CAU
[4]AU.UTAS
[5]DE.UNI-KÖLN
[6]AU.MACQUARIE
[7]DE.TU-DRESDEN
[8]AU.UC
[9]FR.CNRS

Grant-No. AWI_PS141_01

Objectives

For the PS141 study area, the sub-bottom profiling or sediment echosounding system Teledyne Parasound P70 was used to image the upper tens of meters of the ocean floor's subsurface, to understand glacial and geological processes such as erosion, sediment transport and deposition, and tectonic processes of the recent past. Especially, the identification of glacially formed structures is essential to reconstruct the advance, extension and retreat pattern of ice sheets e.g. by mapping the distribution of megascale glacial lineations, moraines, or grounding zone wedges (e.g. Evans et al. 2005; Ó Cofaigh et al. 2008; Jakobsson et al. 2011; Livingstone et al. 2012). In turn, understanding the processes of past ice sheet dynamics can provide important information for predictions of future responses of the East Antarctic Ice Sheet (EASI) to changing climate conditions and oceanographic settings. The correct identification and interpretation of subglacial bedforms crucially depends on the detailed recording of its internal architecture, which can be achieved by acoustic sub-bottom profiling.

By imaging the upper few tens of meters of the subsurface, sediment echography provides an important link between bathymetry (mapping the surface morphology) and reflection seismics (imaging deeper structures down to several km depth). The integration of these three data sets is of particular importance for interpreting geological data in a wider spatial context, whereas coring results provide crucial information about chronology as well as structural and lithological components of the imaged features. Generally, sediment echography surveys are essential to define ideal geological coring locations (see Chapter 3).

Work at Sea

Instruments

Sub-bottom profiles were recorded with the hull-mounted Deep-Sea Sediment Echosounder PARASOUND (Teledyne Reson, Bremen, Germany), system PS3-P70. This system generates two primary, high-frequency acoustic signals with slightly differing frequencies selectable in a range of 18-24 kHz (PLF, PHF). Due to the non-linear acoustic behaviour of water, the so-called "Parametric Effect", two secondary harmonic frequencies (SLF, SHF) are generated in the water column of which one is the difference (SLF) and the other the sum (SHF), respectively. As a result of the longer wavelength, the secondary low frequency signal (SLF) is able to penetrate the sediment column as deep as for example a 4 kHz signal (up to 100 m depending

on sediment conditions), with a vertical resolution of about some decimeters in sediments. With the primary high frequency-signal (PHF), a higher lateral resolution can be achieved, and imaging of small-scale structures on the seafloor is superior to conventional systems. (The secondary high frequency (SHF) can be used for detection of bubbles in the water column, but was not applied on this cruise.)

The primary signals are emitted in a narrow beam of 4.5°, but at high power. That has the advantage that the sediment-penetrating SLF pulse is generated within the narrow beam of the primary frequencies, and thereby providing a very high lateral resolution.

The system, however, has limitations in imaging rough sea floor topographies or submarine ridges with slopes steeper than 4°. Here, the signal energy reflected from the small inclined footprint on the seafloor is scattered out of the lateral range of the receiving transducers in the hull of the vessel. As a consequence, only few reflections from the seafloor are recorded, i.e., even fewer from the sub-bottom.

Survey settings

During expedition PS141, a 22 kHz setting was used as the Primary High Frequency (PHF), to avoid interferences with the Hydrosweep (Bathymetry) echosounder system (see Chapter 2.2). The Secondary Low Frequency (SLF) was set to 4 kHz. Depending on the properties of the sea-floor surface and sediments, our settings enabled an imaging of the sub-bottom down to more than 100 m, and with a vertical resolution of about 30 cm. The combined signal has a beam width of ~4.5°. The resulting beam's footprint on the sea bottom is about 7 % of the water depth.

The system was controlled using the programme Hydromap Control. Live data visualisation and data storage was performed with the Parastore software. Every hour, screenshots of the profiles were stored and made directly accessible on a public directory.

Sub-bottom profiling

During expedition PS141, digital data acquisition and storage were switched on after *Polarstern* left the EEZ of Australia on 7 February 2024 at 19:34 UTC, and was switched off on 10 April 2024 at 05:00 UTC when the ship reached the EEZ of South Africa and Namibia at the end of the expedition.

During all times on transit and while surveying in the main study area to provide information for station planning and sediment coring sites, data acquisition took place. For some specific surveys, and throughout seismic reflection measurements, the ship's speed was reduced from 10 kn on average to only 5 kn, to achieve undisturbed and high-resolution profiles. Parasound profiling was carried out in a 24-hour/7-day shift mode, and recorded data were promptly made available for site selection and cruise planning. All actions and reasons concerning switching on and off the system, system parameters, actions on stations, sea state conditions, and events concerning MMO calls are documented in Appendix A.6.

Four times system failures occurred. In three cases the system (HYDROMAP server) had to be closed and restarted completely after the error message "FTP Transfer from Server 10.197.124.95 with user ftp and password ftp failed. Source file ASD_data/SLF/PS3SLF…". One time it was sufficient to close and restart PARASTORE for proper data acquisition.

The daily routine included the subsequent processing steps that are established as a standardised workflow consisting of (a) acquisition of data in the internal PARASOUND ASD and PS3 formats, (b) conversion of PS3 to standard SGY format, (c) extraction of navigation data and conversion to standard UKOOA format, (d) preparation for storage in Pangaea,

and (e) performance of a preliminary processing of data and visualisation with the Kingdom software (Version 2020, IHS Markit Ltd) (Appendix A.7). For the PS3 data collected in the main sampling area, frequency conversion to standard SGY format was applied which enabled a better resolution of reflectors at the site locations. For the transit, conversion to envelopes was applied which provide a better overview on regional reflection structures.

Mitigation for marine mammals

The mitigation regulations for profiling operations consisted of visual observations for marine mammals (MMs) by observers (MMO), following the mitigation protocol predefined by Germany's Federal Environment Agency (Umweltbundesamt – UBA).

In detail, the mitigation actions comprised:

1. Start of sounding only after at least 15 minutes MMO watch without sightings of MMs.

2. After interruptions of more than 30 min the Parasound P70 sediment echosounder was restarted with reduced pulse rate ("Whale Warning Mode") after 15 min MMO watch before without sightings of MMs.

3. When sounding is needed **on station**, continuous MMO watches by two persons was performed. Sounding was stopped whenever marine mammals were sighted in the water closer than 100 m to the ship. Restart only after 15 min without sightings of MMs.

4. Pulse rate and sounding operations were reduced appropriate to a scientifically necessary level and water depth. Pulse rate never exceeded 500 ms.

5. During the operation of the sediment echosounder **on stations** closer than 500 m to icebergs, ice-shelf edges, and coasts, and whales were observed in between, sounding was stopped. Sounding was restarted after 15 min without sightings.

6. If opportunistic sightings of whales between ship's course and icebergs, ice-shelf edges, and coasts, the ship maintained a distance of > 500 m.

7. Every exception of following the mitigation regulations were documented in a report.

All actions and reasons concerning switching on and off the system, and events concerning MMO calls are documented in Appendix A.6.

Preliminary results

In total ~20,362.63 km (~10,994.94 nmi) of sub-bottom profiles were acquired during 62.35 days of operation. South of 60° our working comprised 14,469.07 km (~7812 nmi) of sub-bottom profiling (see Fig. 1.1). The profile names, sub-bottom penetration range, sub-seafloor characterisation for geological sampling, and other notes are listed in (Appendix A.7).

The acquired dataset provides both subsurface and geomorphological information of the upper ~50 m of the substrate of the research area. The Parasound records serve as a compilation of high-resolution sub-bottom profiles along the cruise track, and at the target sites for coring measurements (Fig. 2.3.1). These sub-bottom profiles image the surfaces and internal architecture of glacial-geomorphological features (e.g. iceberg plough marks and grounding zone wedges (Fig. 2.3.2)), erosional structures, and depositional features (e.g. slumps, slides, fans). Linked to the results from multibeam mapping and sediment coring, the network of sub-bottom profiles offers an important tool for the interpretation of geological data in a spatial context. Expected outcomes aim towards a better understanding of ice-sheet dynamics and geological processes in the research area.

For the selection of target coring site locations, the sub-bottom profiles enabled the identification of areas of high and low sedimentation rates, outcrops, and to avoid areas of sediment re-deposition or erosion.

Preliminary results show numerous glacial-geomorphological features on the continental shelf and slope of the Davis Sea and Mawson Sea. Abundant presence of subglacial lineations, iceberg plough marks and grounding zone wedge ridges indicate the former presence of grounded ice sheets and icebergs extending across the continental shelf off West Ice Shelf, Shackleton Ice Shelf, and Vanderford Glacier, and furrowing deep through the seabed surface (Fig. 2.3.2).

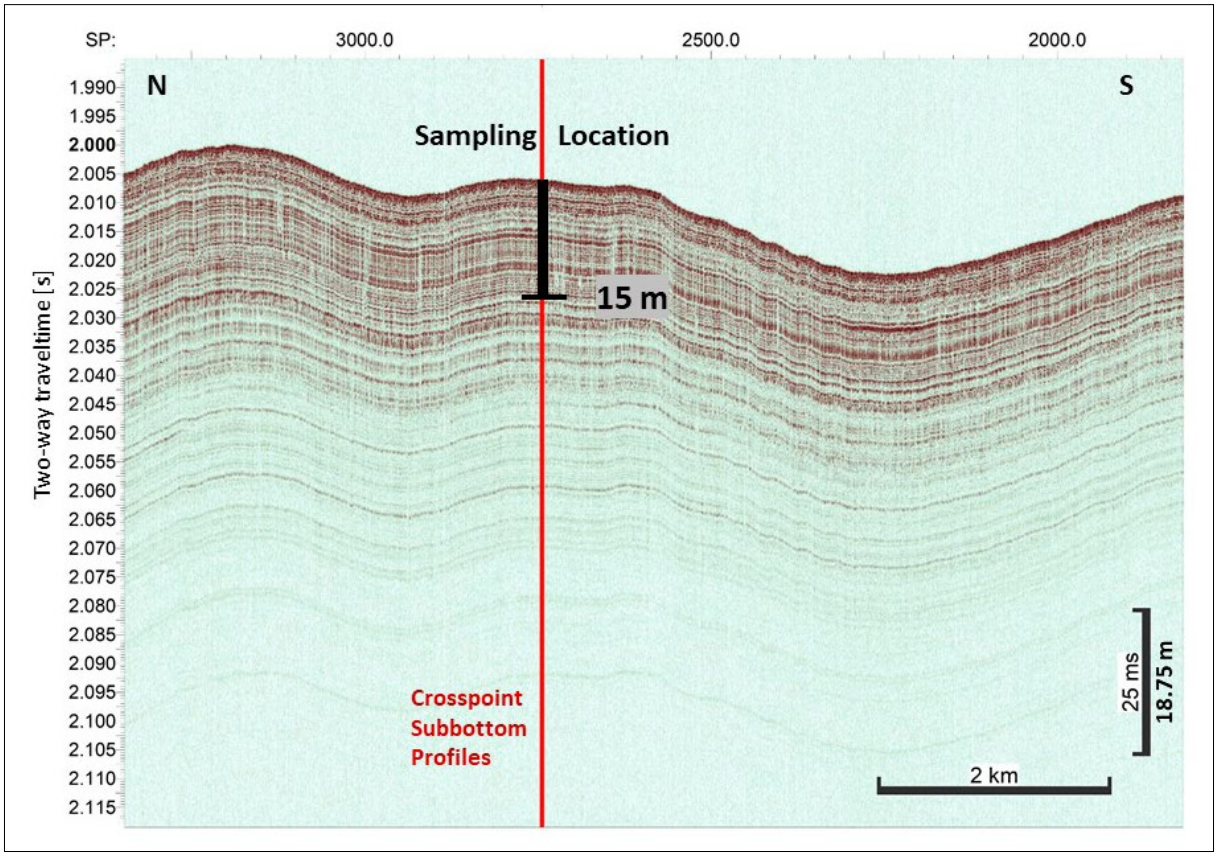

Fig. 2.3.1: Sub-bottom profile imaging sampling location PS141_84-1_GC and cross point location of sub-bottom profiles 2024_0326_093354Freq and 2024_0326_180452.

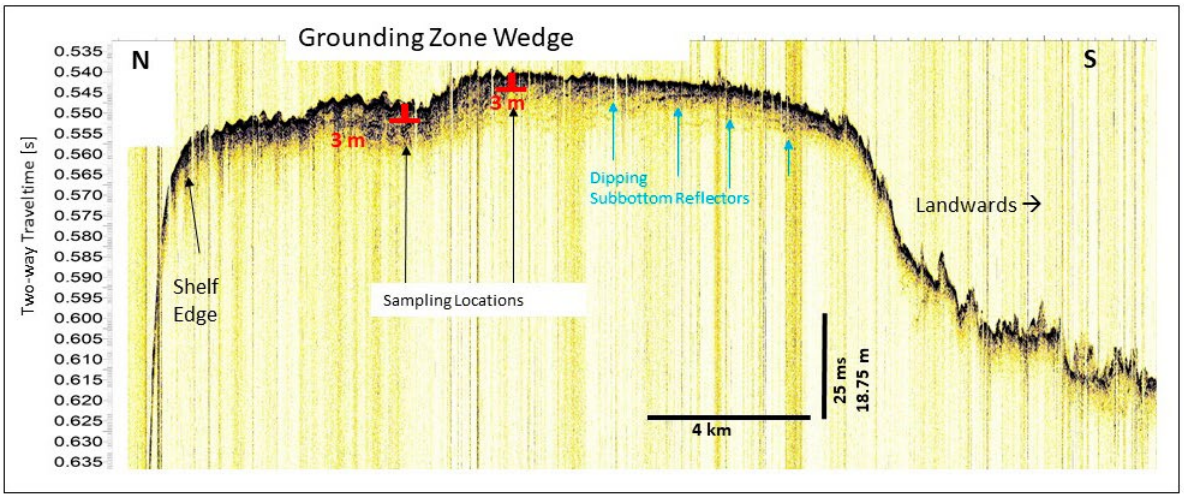

Fig. 2.3.2: Section of a sub-bottom profile imaging a huge grounding zone wedge, sampling locations (red bars), plough marks and scours of icebergs, as well as dipping sub-bottom reflectors (blue arrows)

Data management

Sub-bottom profiling data collected during PS141 were copied to the *Polarstern* data base, from where they will be transferred to the data mass storage at AWI Bremerhaven and linked to the World Data Center PANGAEA Data Publisher for Earth & Environmental Science (https://www.pangaea.de) at AWI.

This expedition was supported by the Helmholtz Research Programme “Changing Earth – Sustaining our Future” Topic 2, Subtopic 2.1.

In all publications based on this expedition, the **Grant No. AWI_PS141_01** will be quoted and the following publication will be cited: Alfred-Wegener-Institut Helmholtz-Zentrum für Polar- und Meeresforschung (2017) Polar Research and Supply Vessel POLARSTERN Operated by the Alfred-Wegener-Institute. Journal of large-scale research facilities, 3, A119. http://dx.doi.org/10.17815/jlsrf-3-163.

References

Evans J, Pudsey CJ, Ó Cofaigh C, Morris P, Domack EW (2005) Late Quaternary glacial history, flow dynamics and sedimentation along the eastern margin of the Antarctic Peninsula Ice Sheet. Quaternary Science Reviews 24:741-774.

Jakobsson M, Anderson JB, Nitsche FO, Dowdeswell JA, Gyllencreutz R, Kirchner N, Mohammad R, O’Regan M, Alley RB, Anandakrishnan S, Eriksson B, Kirshner A, Fernandez R, Stolldorf T, Minzoni R, Majewski W (2011) Geological record of ice shelf break-up and grounding line retreat, Pine Island Bay, West Antarctica. Geology 39:691-694.

Livingstone SJ, Ó Cofaigh C, Stokes CR, Hillenbrand C-D, Vieli A, Jamieson SSR (2012) Antarctic palaeo-ice streams. Earth-Science Reviews 111:90-128.

Ó Cofaigh C, Dowdeswell JA, Evans J, Larter RD (2008) Geological constraints on Antarctic palaeo-ice-stream retreat. Earth Surface Processes and Landforms 33:513-525.

3. MARINE GEOLOGY AND PALEOCEANOGRAPHY

Julia Gottschalk[1], Lester Lembke-Jene[2], Juliane Müller[2], Ole Jasper Ferber[1], Lena Jebasinski[1], Norbert Lensch[2], Anja Müller[2], Gernot Nehrke[2], Tim Beneke Stobbe[1], Anna Völkert[1], Georgios Xydis[1];
Not on board: Ralph R. Schneider[1], Johann P. Klages[2], Oliver Esper[2], Nina Keul[1], Duanne White[3]

[1]DE.UNI-KIEL
[2]DE.AWI
[3]AU.UC

Grant-No. AWI_PS141_02

Objectives

Among Southern Ocean regions, the Indian Ocean sector and its East Antarctic Ice Sheet (EAIS) margin remains one of the least understood areas in terms of its past role in the climate system. However, this region may hold substantial significance for current and future climate and sea-level change. Currently, it is not even known whether the EAIS mass balance is positive or negative, or how it contributes to global and regional sea-level change (The IMBIE Team 2018), severely limiting precise projections of future climate and ice-sheet evolution. The inherently unstable and likely more dynamic marine-based portions of the EAIS (Cook et al. 2013; Wilson et al. 2018) represent a sea-level equivalent of about 19 m (Fretwell et al. 2013). Recent observations indicate considerable thinning and grounding line retreat of some ice streams draining these basins, resulting in a negative mass balance in their catchments (Shen et al. 2018; Picton et al. 2023). Paleoclimate data indicate a close link between extended Antarctic warmth and ice loss from marine-based sectors of the EAIS during past warm, interglacial intervals (Wilson et al. 2018). This raises concerns for future instability of the EAIS, and its potentially higher vulnerability to climatic and oceanographic forcing than previously thought. The current lack of data, both proximal and distal to the EAIS, prevents better understanding of the dynamic past of marine and shelf-based EAIS sectors, despite them being a critical factor for assessing recent changes and providing long-term geological context.

A major goal of this expedition was to advance our process-oriented understanding of Quaternary climatic and oceanographic processes, and their interaction with the cryosphere on orbital to submillennial time-scales. Our particular focus rests on the Holocene, deglacial warming phases and past warmer-than-present time intervals in the East Antarctic ice-ocean-climate system. While sediment cores we obtained along a NE-SW transect across the Austral-Indian sector of the Southern Ocean shall enable the reconstruction of glacial-interglacial shifts in oceanic fronts, sediment cores from the continental margin off the Shackleton Ice Shelf and the Vanderford Glacier provide critically needed material for an assessment of past basal ice shelf melting resulting from warm Circumpolar Deep Water (CDW) intrusions into sub-ice shelf cavities. Such processes and feedback mechanisms, including freshening and sea ice growth or loss, also directly influence the formation rates and characteristic signatures of Antarctic Bottom Water (AABW) sourced from the Ross Sea and Adelie Land coastal regions. Specifically, the newly collected sediment cores will help to address the following three key hypotheses:

A) The marine-based EAIS sectors reacted with rapid and extended phases of retreat to climatic conditions in all relevant warm phases since early glaciations. In this regard, the Davis Sea and Mawson Sea shelf areas are both prime recorders of EAIS dynamics. The Denman Glacier and Vanderford Glaciers form one of the largest ice catchment and drainage areas of East Antarctica. Both glaciers, as well as most of the coastal Davis and Mawson Sea glaciers, are marine-based, making them inherently unstable and thus vulnerable to potential warm CDW incursions. At present, warm-water incursions into the deep submarine basin beneath Denman Glacier are only blocked by a narrow coastal basement ridge (Morlighem et al. 2020). Both glaciers are connected to the vast submarine Wilkes Land and Aurora Subglacial Basins. Though earlier studies suggested a rather constantly stable EAIS, more recent results from the Totten Glacier shelf show that the marine-based sectors of the EAIS behaved dynamically at least throughout the Oligocene to Pliocene, with repeated ice advances and retreats (e.g., Gulick et al. 2017). Moreover, the impact of past (varying) sea-ice conditions on the stability of ice-shelf fronts (Massom et al. 2018) and the formation of dense shelf water contributing to AABW along the East Antarctic continental margin (Ohshima et al. 2016) remain poorly understood. Sea-ice biomarker analyses (e.g., Lamping et al. 2021) paired with diatom assemblage studies of the sediment cores collected on the shelf in front of the Denman and Vanderford Glacier, respectively, will address this crucial knowledge gap along with other multi-proxy reconstructions.

B) The paleo-Denman, Vanderford-, Bond-, Adams- und Underwood Glacier systems extended towards the shelf edge during the last glacial, reacting sensitively to past warm-water incursions and sea-level fluctuations. Current mismatches of model results and proxy-based data of EAIS reconstructions for the Late Quaternary require more detailed, spatially well-resolved evidence for paleo-ice sheet geometries that, in turn, will constrain projections of future ice sheet behavior. Accordingly, Late Quaternary dynamics of vulnerable marine-based EAIS portions on the continental shelf can now be evaluated through a combined approach of swath bathymetry mapping, shallow seismic surveying, and sediment coring to test this hypothesis. This integration shall provide new evidence for ice expansion, paleo-flow pathways, or stillstands in grounding-line retreats to decipher past ice-flow trajectories. Through mapping of sub- and proglacial landforms such as mega-scale glacial lineations, grounding-zone wedges, drumlin and moraine features, as well as subsurface depositional systems and glaciogenic fault tectonics, we aim to define their relative and, if possible, absolute timing throughout the Last Glacial period, including Marine Isotope Stage 3 and the subsequent deglaciation into the Holocene. Until now, such data are still scarce or entirely absent in the working area (Carson et al. 2017; Picton et al. 2023). In combination with time series of environmental proxies from sediment cores, our objective is to establish a four-dimensional reconstruction of ice-sheet advances and retreats for the study area (*cf*. Hillenbrand et al. 2013; Smith et al. 2011, 2014; Klages et al. 2013, 2014, 2015, 2017).

C) EAIS ice-sheet variations were intimately coupled with circum-Antarctic circulation and biogeochemical cycling in the Indian Ocean sector of the Southern Ocean. We hypothesized that profound marginal EAIS fluctuations during the late Quaternary also had a significant impact on circum-Antarctic oceanic circulation and biogeochemical cycling by controlling the amount of dense shelf-slope brine formation, extension of sea-cover supported by catabatic winds, and via contribution to the biogeochemical nutrient inventory through shelf break organic and inorganic matter plumes introduced by ice-margin dynamics (e.g., Smith et al. 2019). Quantifying changes in the supply of these trace elements and nutrient, and their distribution patterns and pathways in sub-Antarctic waters, are key for constraining changes in past environmental conditions as reconstructed from sediment cores in Southern Ocean frontal zones. Notably for nutrients, the processes that govern the quantity and stoichiometry in the source regions, as well as northward advection of water masses, are insufficiently constrained, making it impossible to predict the consequences of Southern Ocean changes in

upwelling or phytoplankton community shifts. While a wealth of knowledge has been gathered on siliceous plankton, surveys for calcifiers, particularly for the ice-sheet margin and shelf water masses, are lacking. While diatoms have high preservation potential in the Southern Ocean Antarctic Margin sediments, and the species distribution patterns provide sufficient information about seawater temperature and trophic conditions (Esper and Gersonde 2014), calcareous tests of planktic foraminifers and shells of pteropods are sparse in circum-Antarctic sediments. Nonetheless, planktic and benthic foraminifera are preserved in sufficient numbers for paleoenviromental reconstructions at high accumulation sites on the shelf.

Work at sea

We performed extensive survey and sediment coring with sites distributed in water depths from the shallow shelf down to depths of 4,000 m in the open ocean. This sampling campaign will enable us to reconstruct physical and chemical water mass characteristics and their influence on EAIS dynamics. The Marine Geology and Paleoceanography work programme comprised two major, distinct sampling efforts:

(1) The paleoceanographic approach focused on sediment cores from the Southern Ocean frontal system between Hobart and Antarctica in the initial pelagic open ocean work area. This transect covers the pelagic sub-Antarctic region in the Austral-Indian sector of the Southern Ocean (SO), and comprises the major frontal zones, the Antarctic Circumpolar Current (ACC), as well as the Antarctic Slope Current (ASC) on the transit towards the Antarctic shelf areas. Due to inclement weather conditions at the start of the expedition that prevented an immediate start of the transect along the desired route, we were only able to collect a lower number of cores than anticipated, i.e., four piston cores and MUCs. These coring sites were chosen to provide information on changes of the oceanic fronts, ocean circulation, productivity and major current characteristics in response to ice sheet variability over the last glacial cycles. Pleistocene to Holocene variations in ACC and ASC dynamics, temperatures, salinity and nutrient concentrations can be determined in shore-based studies, and regional changes will enable us to decipher fluctuations in oceanic heat and salt transfer, while providing information on migrating oceanic fronts and wind fields; while vertical gradients will be used to reconstruct the stratification of the ocean.

(2) The main working area extended along the Antarctic continental margin between 85°E and 110°E, with key areas located along the Wilhelm II, Queen Mary, and Wilkes Land ice rims, where marine geological fieldwork focused on the continental shelf and slope off the West Ice Shelf, Shackleton Ice Shelf and Vanderford Ice Shelf. We used some previously acquired and extensive new high-resolution hydro-acoustic data from swath bathymetry and sub-bottom profiling surveys to identify subglacial sedimentary features (such as grounding-zone wedges and lineations) at the seafloor to target ideal sediment coring sites. Based on these survey results, we collected shorter to medium-length (3–15 m) Gravity Cores (GC) at 36 marine geological coring stations on the shelf and slope. This sampling was again coupled with sediment surface sampling by Multi-Corer (MUC) along the major paleo-ice stream troughs on the continental shelf of the study area, west of the Australian *Casey Station*. We targeted both sites in shallower outer troughs as well as sediment pockets at inner trough margins in order to ensure sampling of undisturbed sediments and carbonate preservation above local carbonate compensation depths (*cf.* Hillenbrand et al. 2017).

Sediment Surface Sampling

Surface and near-surface sediment samples were collected at 30 stations during the cruise by means of a Multicorer (MUC) (Fig. 3.1). The MUC67 (manufactured by Fa. Wuttke, Henstedt-Ulzburg, Germany) is equipped with 12 tubes with an inner tube diameter of 67 mm and a length of 60 cm and was deployed at 31 times. The MUC was lowered with an average speed

of 1 m/s to about a few meters above seafloor and continued with a speed of 0.7 m/s into the sediment. The device was left on the seafloor for a few seconds before being pulled out of the sediment with a speed of 0.2 m/s and subsequently heaved with 1 m/s. Depending on the sediment properties, usually undisturbed surface sediments and overlying bottom water was obtained. All MUCs but one deployment successfully recovered surface sediments.

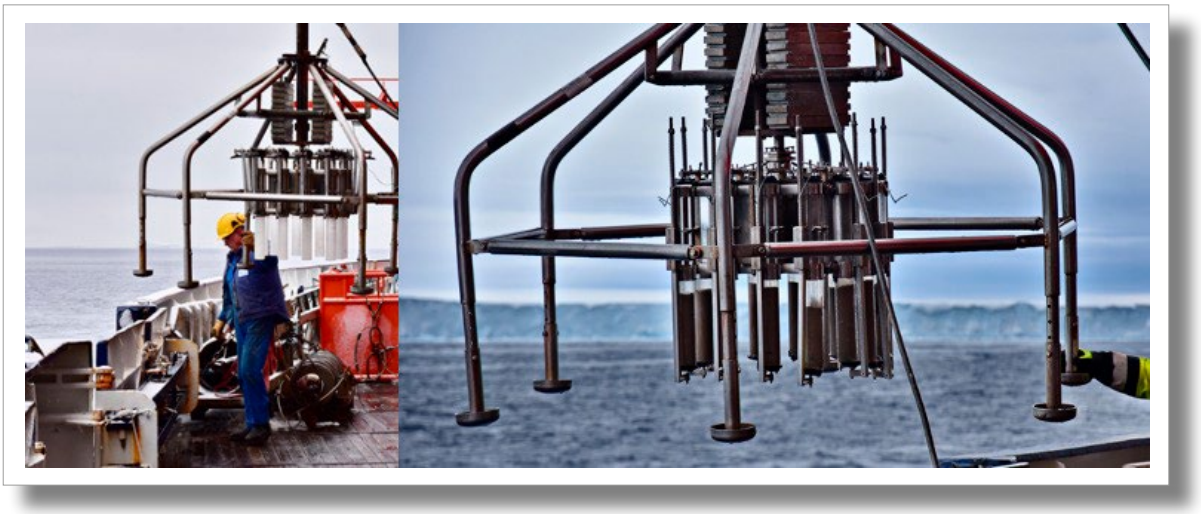

Fig. 3.1: Deployment and retrieval of the multicorer 67 (Fa. Wuttke) during PS141

On average, all 12 tubes contained intact sediments, with average penetration depths around 28 cm (Fig. 3.2; Tab. 3.2). On the outer continental shelf off Bunger Hills, sediment recovery at stations PS141_66-2, PS141_68-2 and PS141_78-2 was relatively low and nil, respectively, due to hard sediment surfaces. At station PS141_74-1, the trigger mechanism for the locking arms was not released but two tubes still recovered sediment.

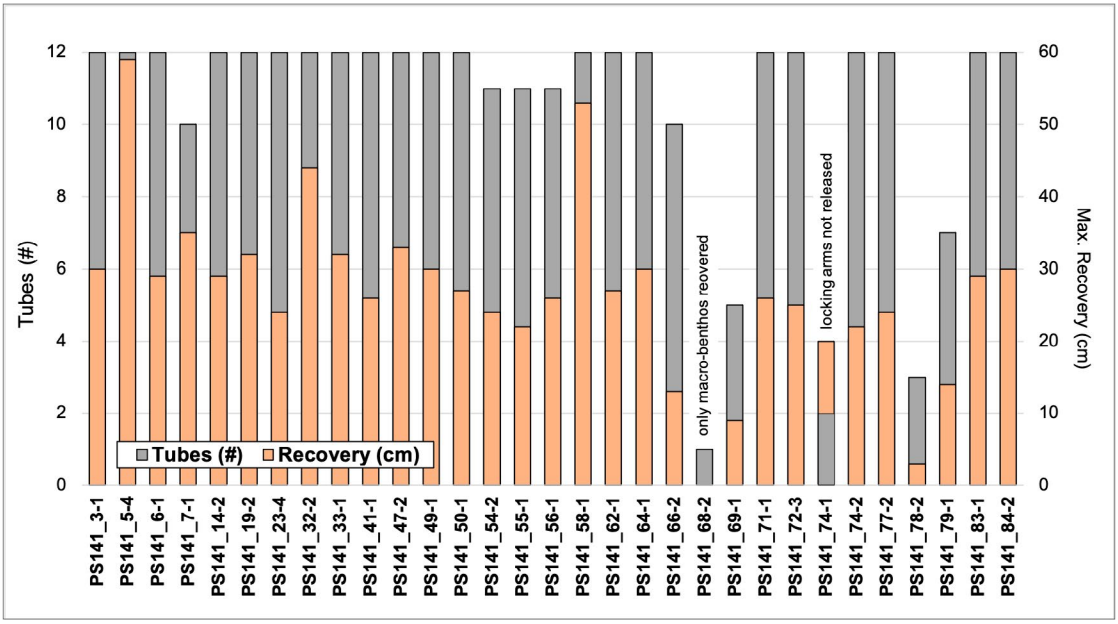

Fig. 3.2: Overview of MUC-deployment core recoveries during PS141.
Grey bars show the number of tubes with recovered sediment (left axis), orange bars indicate the maximum recovery in an individual tube (right axis).

Immediately after recovery of the device, supernatant water was sampled at each station for isotope ($\delta^{18}O$, $\delta^{13}C_{DIC}$, $^{14}C_{DIC}$) and nutrient analyses from three assigned Benthos tubes (BEN I-III). Stable isotope samples were collected in (100 ml for $\delta^{18}O$, 50 ml for $\delta^{13}C_{DIC}$, $^{14}C_{DIC}$) glass bottles with screw tops, the latter series was fixed with 100 µl saturated $HgCl_2$ solution to prevent further biological activity. For nutrient analyses, 50 ml of water were sampled in PE wide-neck bottles and stored frozen at –20°C. For documentation, all MUC tubes were photographed (e.g., Fig. 3.3). The sample and preservation procedure closely follows the established protocols for seater sampling from the CTD Rosette, as described in Chapter 4.

Except for MUC tubes designated as Archive II and DNA, all MUC tubes were sampled immediately after recovery to avoid degradation of organic compounds. For multi-disciplinary investigations of the recovered sediments, the MUC tubes were sampled and stored according to a scheme used with slight alterations for previous EASI expeditions (Tiedemann and Müller 2022, Tab. 3.1).

Tab. 3.1: Sampling series of MUC tubes for different post-cruise investigations

Tubes [#]	Working Group	Sampling	Storage
1	Sedimentology (SED)	1 cm slices in Whirlpack bags	4°C
3	Benthos (BEN I+II+III)	1 cm slices in Kautex bottles (0-10 cm) & Whirlpack bags (11 cm to bottom)	4°C
2	Biomarker (BIO I+II)	1 cm slices in combusted glass vials covered with Al foil	-20°C
1	Physical properties (PP)	1 cm slices in Whirlpack bags	4°C
1	Micropaleontology (PAL)	1 cm slices in Whirlpack bags	4°C
1	Diatoms (DIA)	1 cm slices in Whirlpack bags	4°C
1	Archive I (ARC I)	1 cm slices in Whirlpack bags	4°C
1	Archive II (ARC II)	Entire MUC tube deep frozen, stored wrapped in aluminum foil in evacuated and sealed plastic bag	-20°C
1	Sedimentary DNA (DNA)	Entire MUC tube deep frozen, stored wrapped in aluminum foil in evacuated and sealed plastic bag	-20°C

Fig. 3.3: Example of photo-documented MUC tubes retrieved at station PS141_54-6 in Vincennes Bay (121 m water depth). Note the macro-benthos in the upper part of the sediment.

Tab. 3.2: MUC stations during PS141

Station Number	Gear	Latitude [S°]	Longitude [E°]	Water Depth [m]	Tubes #	Max. Rec. [cm]
PS141_3-1	MUC67	46° 57,106’	134° 45,446’	4,006	12	30
PS141_5-4	MUC67	56° 19,473’	124° 49,039’	4,708	12	59
PS141_6-1	MUC67	59° 44,958’	114° 53,535’	4,527	12	29
PS141_7-1	MUC67	63° 38,548’	107° 05,470’	2,880	10	35
PS141_14-2	MUC67	66° 13,911’	089° 25,277’	540	12	29
PS141_19-2	MUC67	65° 08,536’	095° 28,425’	558	12	32
PS141_23-4	MUC67	65° 38,603’	099° 56,026’	506	12	24
PS141_32-2	MUC67	66° 13,836’	109° 41,167’	1,470	12	44
PS141_33-1	MUC67	66° 02,888’	109° 32,972’	773	12	32
PS141_41-1	MUC67	66° 22,282’	108° 34,237’	1,314	12	26
PS141_47-2	MUC67	65° 39,394’	107° 52,487’	804	12	33
PS141_49-1	MUC67	64° 55,802’	106° 51,598’	2,454	12	30
PS141_50-1	MUC67	66° 15,463’	110° 21,043’	137	12	27
PS141_54-2	MUC67	66° 15,821’	110° 27,411’	121	11	24
PS141_55-1	MUC67	66° 16,222’	110° 29,081’	129	11	22
PS141_56-1	MUC67	66° 16,525’	110° 28,713’	131	11	26
PS141_58-1	MUC67	66° 33,228’	110° 21,251’	2,320	12	53

Station Number	Gear	Latitude [S°]	Longitude [E°]	Water Depth [m]	Tubes #	Max. Rec. [cm]
PS141_62-1	MUC67	66° 18,667’	090° 21,471’	1,088	12	27
PS141_64-1	MUC67	63° 49,782’	098° 02,115’	1,880	12	30
PS141_66-2	MUC67	64° 10,617’	098° 46,148’	406	10	13
PS141_68-2	MUC67	64° 07,429’	099° 05,412’	529	1	0
PS141_69-1	MUC67	64° 18,778’	099° 06,945’	482	5	9
PS141_71-1	MUC67	65° 42,845’	100° 09,181’	540	12	26
PS141_72-3	MUC67	65° 46,700’	100° 13,029’	538	12	25
PS141_74-1	MUC67	65° 06,507’	100° 29,775’	446	2	20
PS141_74-2	MUC67	65° 06,518’	100° 29,803’	446	12	22
PS141_77-2	MUC67	64° 52,941’	100° 15,426’	466	12	24
PS141_78-2	MUC67	64° 23,474’	099° 48,486’	557	3	3
PS141_79-1	MUC67	64° 14,789’	099° 32,760’	504	7	14
PS141_83-1	MUC67	64° 25,124’	101° 46,533’	1,121	12	29
PS141_84-2	MUC67	63° 45,169’	098° 53,939’	1,463	12	30

Sediment coring

Sediment coring during expedition PS141 was performed by means of AWI’s gravity corer (GC) and piston corer (PC), in addition to sub-surface sediment sampling via multi-corer (MUC) (Tab. 3.3). The AWI gravity corer (GC) consists of a steel barrel for Polyvinyl chloride (PVC) plastic core liner that has a diameter of 90 or 125 mm. The steel barrel has an adjustable length (in 5 m-barrel increments with possible connection to a 3m-barrel, or both in isolation) and is attached to a 2.3 t- (125 mm-option) or 2.8 t-weight (90 cm-option) at the top referred to as “bomb” (Fig. 3.4). The maximum barrel length of a gravity corer deployed during expedition PS141 was 15 m (Tab. 3.4).

During deployment, the gravity corer was lowered to the sea floor at a speed of 0.9-1.1 m/s. Upon contact with the sea floor, the gravity corer was left in the sediments for about 30 s until it was retrieved again from the sea floor by heaving at a speed of 0.2 m/s and when released from the seafloor at a speed of 1.0 m/s to deck. Penetration into the sediment and release from the sediments were closely observed through monitoring of the cable tension.

The AWI piston corer consists of a steel barrel for PVC plastic core liner with a 90 mm-diameter that has an adjustable barrel (in 5m-barrel increments) and a 2.8 t-weight on the top (Fig. 3.5). It is connected to a pilot gravity corer that serves as a trigger corer (TC). The piston coring system was purchased from Kawohl-Marinetechnik. The trigger core is attached to the piston corer by a steel rope via a release mechanism and because of its lower position relative to the piston corer is designed to make contact with the sea floor first (Fig. 3.5). Upon contact with the seafloor, the pilot core triggers the release of the piston corer, which then free-falls into the sediment and allows for deeper penetration into the sediments when compared to a gravity corer (that is lowered into the sediment through the winch only). As the piston corer penetrates the seafloor, the piston inside stops at the sediment surface stabilizing the sediment inside the

core liner during core retrieval (Fig. 3.5). Both pilot core and piston core are retrieved from the sediment with the ship's winch.

Fig. 3.4: Deployment of the gravity corer a) with and b) without a core handling rack during Polarstern expedition PS141

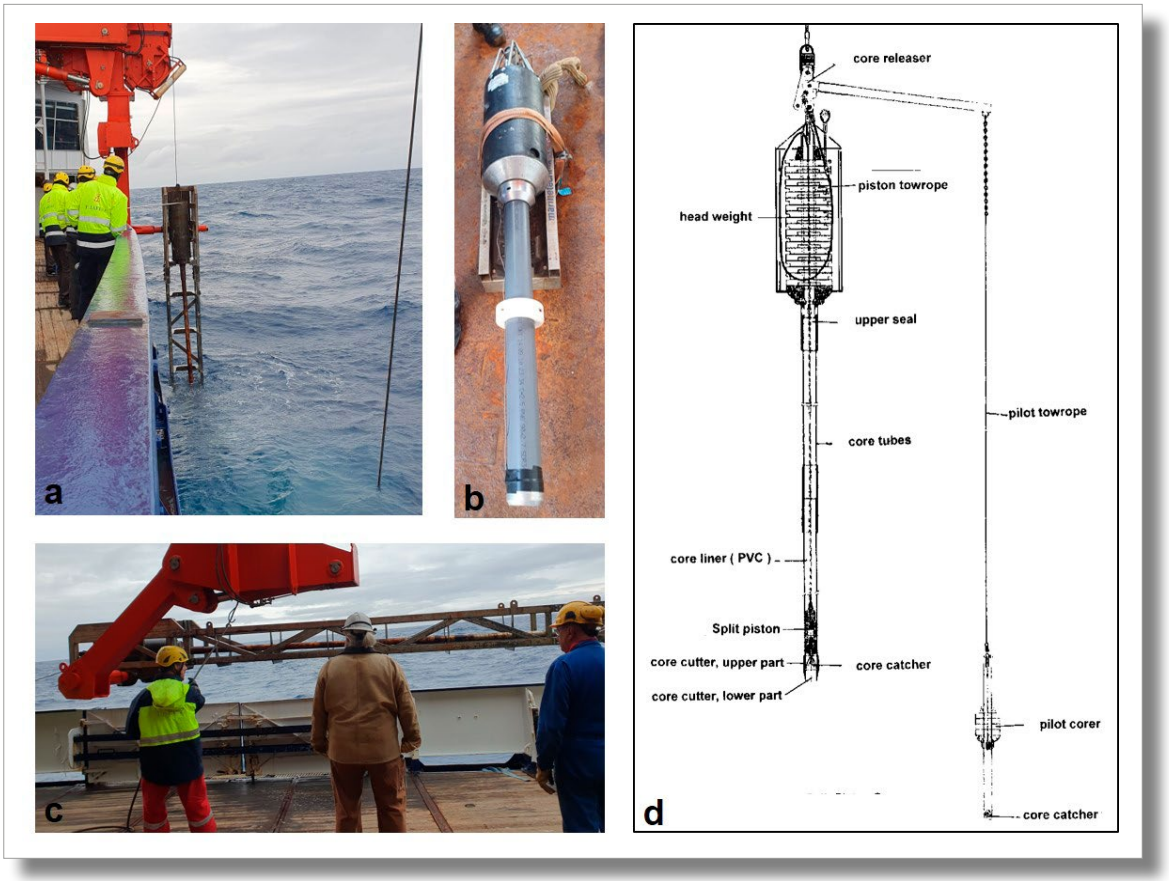

Fig. 3.5: Deployment of the AWI piston corer (PC; Kawohl-Marinetechnik) Polarstern expedition PS141, a) retrieval from the ocean via the ship's core handling rack and b) placement on deck, c) pilot (trigger) corer, and d) schematic drawing of the piston corer with indication of top weight, release mechanism, pilot corer and piston inside the PVC-core liner

During deployment, the piston corer was lowered to the sea floor at a speed of 1.0 m/s, decreasing to 0.3 m/s as the piston corer approached the sea floor and the pilot core eventually made contact with the sediment. The piston corer was left in the sediment for about 30 seconds, and was then released from the sediments through pulling via the winch at a speed of 0.2 m/s. The piston core was raised through the water column at a speed of 1.0 m/s. Penetration into the sediment and release from the sediments were closely observed through monitoring of the cable tension. Gear types and the length of the core barrels of the piston corer and gravity corer were carefully chosen based on hydroacoustic profiles acquired with the ship's shallow sub-bottom profiling system PARASOUND (*cf.* Chapter 2.3). Sediments indicative of mass wasting processes were avoided. The strength, spacing and thickness of shallow sub-surface reflectors and total sub-bottom penetration were considered for device choice.

The gravity corer was deployed 37-times with barrel lengths between 3 and 15 m depending on hydroacoustic characteristics of sea floor conditions (Tab. 3.4, Fig. 3.6). The deployment and retrieval of the gravity corer with barrel lengths of 10 m or longer was aided by the core handling rack of the ship (*German*: "Kernabsatzgestell") (Fig. 3.4). Gravity cores with barrel lengths of 3 or 5 m were retrieved without the ship's core handling rack (Fig. 3.4). 29 deployments of the gravity corer led to the recovery of sediment material, while four deployments resulted in the retrieval of sediments in the core catcher only (sampled in bags; PS141_34-4, PS141_68-1, PS141_77-1, PS141_78-1) and four deployments resulted in an unsuccessful retrieval of sediment material (PS141_48-1, PS141_66-3, PS141_67-1, PS141_76-1) (Tab. 3.4, Fig. 3.6). Gravity cores at station PS141_37 (-1 and -5) are to be combined with the multi-core at station PS141_58, because both are from the same physical station. Gravity core PS141_52-1 was taken at the same station as multi-core PS141_56-1. Gravity core PS141_53-1 was retrieved from the same station as multi-core PS151_5-5-1. An overview of the acquired cores is provided in Table 3.3. Overpenetration was observed for gravity cores PS141_23-2, PS141-32-1, PS141_37-1 and PS141_41-3, as the bomb notably penetrated the sediment. Recent sediments at these stations were likely not recovered via gravity corer, or only in disturbed state (Fig. 3.6). The total recovery of sediments during expedition PS141 via gravity corer (excluding core catcher material sampled in bags) is 143,02 m (Tab. 3.4, Fig. 3.6).

The piston corer was deployed using the ship's core handling rack during stations PS141_5-5, PS141_6-2 and PS141_7-3 (all from the pelagic Indian Southern Ocean) with barrel lengths of 15 and 20 m (Fig. 3.5), depending on hydroacoustic characteristics of ocean floor conditions (Tab. 3.3, Fig. 3.6). The maximum barrel length of a piston corer deployed during expedition PS141 was 20 m (PS141_5-5; Tab. 3.3). While two deployments led to the retrieval of sediments with a total recovery of 32.03 m including trigger core recovery (PS141_7-3, PS141_5-5), one attempt to recover sediments via piston corer failed because of bending of the core barrel upon contact with the sea floor sediment (PS141_6-2, "Banana"; Tab. 3.4, Fig. 3.6).

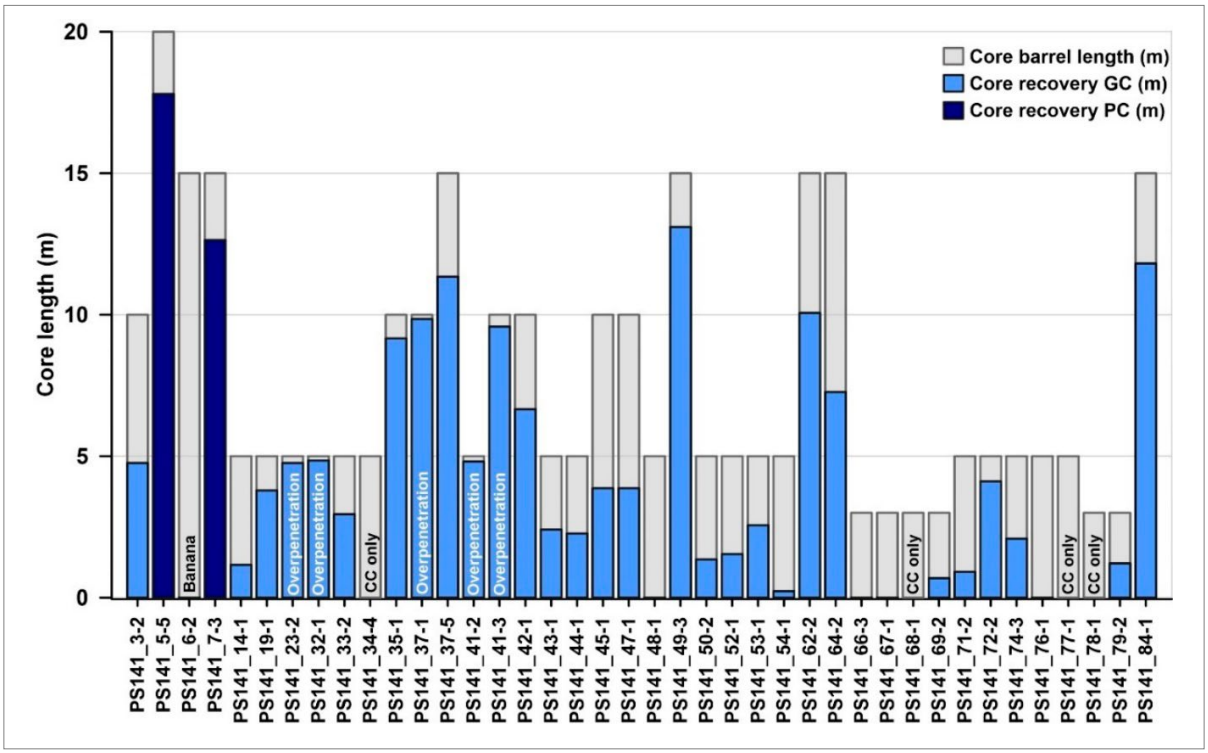

Fig. 3.6: Sediment core recovery (blue) relative to length of gravity core or piston core barrel (gray) during expedition PS141. Instances of overpenetration, bend core barrel ("banana"), sediment recovery in the core catcher only and no recovery at all are highlighted.

Tab. 3.3: Deployments of the multi-corer (MUC), piston corer (PC) and gravity corer (GC) at geological stations during expedition PS141. Number in brackets indicates the barrel lengths of the deployed PC and GC. Three pairs of station names designated one and the same physical station: 1. PS141_37 and PS141_58, 2. PS141_52 and PS141_56, and 3. PS141_53 and PS141_55.

Station	MUC	PC	GC
PS141_3	x		x (10 m)
PS141_5	x	x (20 m)	
PS141_6	x	x (15 m)	
PS141_7	x	x (15 m)	
PS141_14	x		x (5 m)
PS141_19	x		x (5 m)
PS141_23	x		x (5 m)
PS141_32	x		x (5 m)
PS141_33	x		x (5 m)
PS141_34			x (5 m)
PS141_35			x (10 m)
PS141_37	PS141_58		x (10 m, 15 m)
PS141_41	x		x (5 m, 10 m)
PS141_42			x (10 m)
PS141_43			x (5 m)

Station	MUC	PC	GC
PS141_44			x (5 m)
PS141_45			x (10 m)
PS141_47	x		x (10 m)
PS141_48			x (5 m)
PS141_49	x		x (15 m)
PS141_50	x		x (5 m)
PS141_52	PS141_56		x (5 m)
PS141_53	PS141_55		x (5 m)
PS141_54	x		x (5 m)
PS141_55	x		PS141_53
PS141_56	x		PS141_52
PS141_58	x		PS141_37
PS141_62	x		x (15 m)
PS141_64	x		x (15 m)
PS141_66	x		x (3 m)
PS141_67			x (3 m)
PS141_68	x		x (3 m)
PS141_69	x		x (3 m)
PS141_71	x		x (5 m)
PS141_72	x		x (5 m)
PS141_74	x (release failed), x		x (5 m)
PS141_76			x (5 m)
PS141_77	x		x (5 m)
PS141_78	x		x (3 m)
PS141_79	x		x (3 m)
PS141_83	x		
PS141_84	x		x (15 m)

Tab. 3.4: Gravity core (GC) and piston core (PC) stations during PS141

Number following GC or PC marks the loaded core barrel length in meter. CC – core catcher. x marks cores that were opened and described on board. y denotes cores that were multi-sensor core (MSC-)logged.

Station-Gear PS141_	Gear type	PC/GC liner diamet. [mm]	Latitude [S]	Longitude [E]	Water Depth [m]	Core recovery [cm]	Trigger core recov. [cm]	x: opened/ descry. y: MSC-logged
3-2	GC10_PS	90	46° 57.088'	134° 45.418'	4004	476		x
5-5	PC20_PS	90	56° 19.474'	124° 49.045'	4709	1780	76	x
6-2	PC15_PS	90	59° 44.962'	114° 53.564'	4527	0 (Banana)	0	
7-3	PC15_PS	90	63° 38.535'	107° 05.494'	2881	1264	83	x
14-1	GC5_PS	125	66° 13.908'	089° 25.272'	540	116		y
19-1	GC5_PS	125	65° 08.539'	095° 28.394'	558	379		y
23-2	GC5_PS	125	65° 38.631'	099° 56.185'	504	476		x, y
32-1	GC5_PS	125	66° 13.936'	109° 41.214'	1486	485		y
33-2	GC5_PS	125	66° 02.875'	109° 33.051'	758	295		y
34-4	GC5_PS	125	66° 02.784'	109° 33.706'	781	CC only		y
35-1	GC10_PS	125	66° 13.875'	109° 41.178'	1486	916		y
37-1	GC10_PS	125	66° 33.225'	110° 21.212'	2319	985		x, y
37-5	GC15_PS	125	66° 33.226'	110° 21.256'	2296	1134		y
41-2	GC5_PS	125	66° 22.008'	108° 35.049'	1314	481		y
41-3	GC10_PS	125	66° 22.162'	108° 34.812'	1315	958		y
42-1	GC10_PS	125	66° 15.508'	108° 18.362'	1101	666		y
43-1	GC5_PS	125	66° 10.765'	108° 14.536'	924	241		y
44-1	GC5_PS	125	65° 45.541'	107° 55.934'	546	227		y
45-1	GC10_PS	125	65° 39.833'	107° 52.642'	800	387		y
47-1	GC10_PS	125	65° 39.390'	107° 52.497'	804	387		y
48-1	GC5_PS	125	65° 25.682'	107° 25.889'	675	0		y
49-3	GC15_PS	125	64° 55.795'	106° 51.606'	2454	1310		y
50-2	GC5_PS	125	66° 15.465'	110° 21.065'	136	135		y
52-1	GC5_PS	125	66° 16.496'	110° 28.802'	132	154		y
53-1	GC5_PS	125	66° 16.136'	110° 29.090'	130	256		y
54-1	GC5_PS	125	66° 15.749'	110° 27.112'	105	23		y
62-2	GC15_PS	125	66° 18.680'	090° 21.505'	1068	1006		y
64-2	GC15_PS	125	63° 49.766'	098° 02.073'	1880	727		y
66-3	GC3_PS	125	64° 10.611'	098° 46.106'	406	0		y
67-1	GC3_PS	125	64° 11.841'	098° 47.039'	406	0		y
68-1	GC3_PS	125	64° 07.438'	099° 05.387'	529	CC only		y
69-2	GC3_PS	125	64° 18.775'	099° 06.934'	481	69		y
71-2	GC5_PS	125	65° 42.848'	100° 09.248'	540	91		y
72-2	GC5_PS	125	65° 46.696'	100° 13.027'	538	411		y
74-3	GC5_PS	125	65° 06.532'	100° 29.820'	446	209		y
76-1	GC5_PS	125	64° 53.377'	100° 16.669'	452	0		y

Station-Gear PS141_	Gear type	PC/GC liner diamet. [mm]	Latitude [S]	Longitude [E]	Water Depth [m]	Core recovery [cm]	Trigger core recov. [cm]	x: opened/ descry. y: MSC-logged
77-1	GC5_PS	125	64° 52.950'	100° 15.453'	465	CC only		y
78-1	GC3_PS	125	64° 23.468'	099° 48.510'	558	CC only		y
79-2	GC3_PS	125	64° 14.786'	099° 32.775'	504	121		y
84-1	GC15_PS	125	63° 45.179'	098° 53.950'	1265	1181		y

Sediment core handling

After being placed on deck, the core catcher (CC) of the piston-, gravity- or trigger core was removed and the sediment material of the core catcher was sampled in a labelled plastic bag. For gravity cores PS141_49-3, PS141_62-2 and PS141_84-1, the sediments in the core catcher were extracted and sampled in a core liner as an intact sediment section with a length of 25, 21 and 22 cm, comprising the lowermost section of the cores, i.e., 1,285–1,310 cm, 985–1,006 cm and 1,159–1,181 cm, respectively. On deck, the 5 m-long PVC-core liner segments were retrieved from the steel core barrels of the piston corer and gravity corer, thereafter immediately marked with Latin numbers (I, II, III, IV, etc.) and yellow tape on their bottom end. The numbered segments were brought into the Large Wet Laboratory ("Geolab") and cut into 1 m-long whole-round sections that were labelled with roman numbers (1, 2, 3, 4, etc.) starting from the bottom. Before capping the core sections with white caps on both ends, smear slides were taken from each section bottom for biostratigraphic and micropaleontological analyses (Tab. 3.5). Each section was labelled with a yellow tape on the bottom end. Measuring the final lengths of all sections was completed by one operator (LLJ).

Smear slides were prepared with a wooden toothpick, a microscope slide and Norland Optical Adhesive for fixation. Smear slides were examined under transmitted light with a Leitz Orthoplan Petrographic Microscope (100 to 630 x magnification), allowing determination of skeletal remains of siliceous organisms, carbonaceous nanno- and microfossils and minerals under both plane-polarized and cross-polarized light. Smear-slide analysis of bulk sediment was undertaken to check sediment composition and for the preliminary identification of diatoms and radiolarians. Biostratigraphic analyses and determination of assemblage variations of siliceous organisms based on smear slides taken onboard will be completed onshore.

Tab. 3.5: Overview of smear slide samples taken from PS141 sediment cores, either from bottom ends of whole-round sections, opened half-round sections (archive halves) or from core catchers (CC)

Core	Sampling type	Depths [cm]
PS141_5-5	half-round (archive half)	1, 41, 71, 131, 171, 221, 271, 291, 371, 431, 585, 631, 792, 812, 832, 872, 902, 952, 962, 1008, 1020, 1066, 1092, 1152, 1181, 1230, 1255, 1315, 1355, 1390, 1420, 1437, 1456, 1478, 1522, 1552, 1602, 1622, 1644, 1652, 1665, 1672, 1700, 1732, 1760
PS141_7-3	half-round (archive half)	12, 62, 122, 162, 198, 258, 300, 362, 382, 422, 482, 506, 522, 536, 552, 564, 586, 632, 671, 726, 760, 802, 860, 885, 891, 947, 1042, 1064, 1100, 1160, 1260

Core	Sampling type	Depths [cm]
PS141_7-3TC	whole-round	0,80
PS141_19-1	CC	CC
PS141_23-2	half-round (archive half)	0, 50, 99, 112, 146, 216, 326, 416, CC
PS141_32-1	whole-round	86, 185, 285, 385, CC
PS141_33-2	whole-round	0, 95, 195, CC
PS141_35-1	whole-round	30, 130, 230, 330, 515, 615, 716, 816, CC
PS141_37-1	half-round (archive half)	5, 67, 74, 99, 104, 149, 200, 219, 234, 267, 293, 320, 348, 374, 104, 413, 448, 484, 501, 530, 561, 585, 618, 661, 670, 678, 685, 741, 774, 785, 792, 845, 864, 885, 939, CC
PS141_37-5	whole-round	53, 232, 332, 433, 533, 732, 833, 934, CC
PS141_41-2	whole-round	79, 179, 280, 381, CC
PS141_41-3	CC	CC
PS141_42-1	whole-round	81, 265, 366, CC
PS141_43-1	whole-round	60, 141, CC
PS141_44-1	whole-round	60, 127, CC
PS141_45-1	whole-round	0, 87, 187, 287, CC
PS141_47-1	whole-round	86, 187, 287, CC
PS141_49-1	whole-round	47, 97, 197, 397, 498, 599, 699, 984, 1085, 1185, CC
PS141_50-2	whole-round	60
PS141_53-1	CC	CC
PS141_62-2	whole-round	100, 201, 301, 401, 584, 684, 784, 885, CC
PS141_64-2	whole-round	70, 138, 326, 427, 527, 627, CC
PS141_68-1	CC	CC
PS141_69-2	whole-round	69, CC
PS141_71-2	CC	CC
PS141_72-2	whole-round	50, 110, 210, 311, CC
PS141_74-3	whole-round	48, 108, CC
PS141_77-1	CC	CC
PS141_78-1	CC	CC
PS141_79-1	CC	CC
PS141_84-1	whole-round	74, 274, 374, 474, 574, 757, 857, 958, 1058, CC

Labelling of the core sections followed a scheme that is consistent for core liners, storage containers of half-rounds (D-tubes) and the end caps (Fig. 3.7). Label information includes the cruise number, station number, number of device deployment at station, label *A* for archive half, label *W* for working half, an arrow that points to the bottom of the section, the depth interval of the core section (in cm) and an indication of the *Top* and *Bottom* of the section (Fig. 3.7). All whole round-sections were stored for 24 hours at room temperature.

All 125 mm-gravity cores were subsequently analyzed in 1 cm-increments for physical properties (i.e., wet-bulk density, porosity, p-wave velocity and magnetic susceptibility) using a Multi-Sensor-Core-Logger (MSCL, Geotek Ltd.). In contrast, all 90 mm-piston- and trigger cores

(PS141_3-2, PS141_5-5, PS141_6-2, PS141_7-3) will be MSC-logged onshore (Tab. 3.6). All cores not opened and not further processed were finally stored at 4°C in wooden boxes in the reefer container for transport to the home institution and processing onshore.

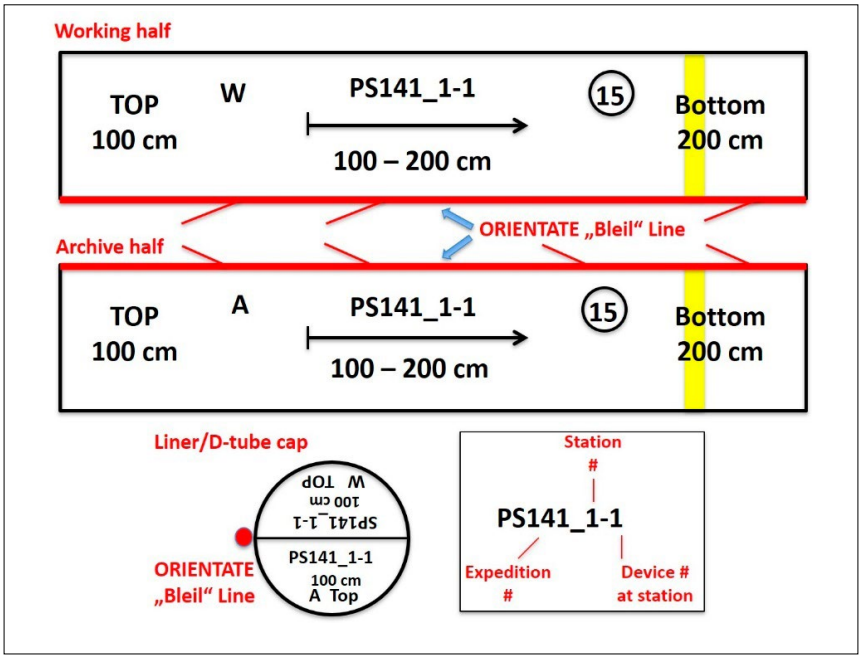

Fig. 3.7: Labelling scheme for core liners (both 90 mm and 125 mm), D-tubes, and liner caps of sediment cores taken during expedition PS141. W indicates working half, while A indicates the archive half. The view shown is of both on the open sediment core as well as on the label of the core liner underside.

Multi-sensor core logging and physical properties measurements

Multi Sensor Core Logging (MSCL) was carried out on all unsplit whole-round 125 mm-thick core segments. Since significant facies and lithological changes are often recognizable in these logging timeseries, one can thus obtain information on variations in biogenic and terrigenous sediment content. These results enable the calculation of key parameters like sediment thickness or continuity of distribution around coring locations and serves for core-to-core correlations as well.

The following parameters were measured on whole-round core sections: magnetic susceptibility, sound velocity of the pressure wave (vP), and the gamma ray attenuation, later calibrated as wet bulk density (WBD). Physical properties of the sediments expressed as wet bulk density, p-wave velocity and magnetic susceptibility were measured on all collected sediment cores using a GEOTEK multi-sensor core logger (MSCL). In addition, core diameter were measured for data processing. The parameters listed in the logger settings of the MSCL software (version 6) and given in Table 3.4 were used for calibration that was conducted following the Geotek MSCL manual and established procedures (Gunn & Best, 1998; Best & Gunn, 1999). An AWI-owned MSCL instrument set-up was used for continuous whole-round core section measurements with a 1 cm resolution. All physical property data were qualitatively controlled on board, and faulty values, *e.g.* at core section boundaries, were flagged in output files. In order to obtain true volume-corrected $\varkappa$ (Kappa) magnetic susceptibility in (10^{-6} SI-units)

values, the magnetic susceptibility sensor data will be further processed onshore, including drift and volume corrections (Tab. 3.6).

MSCL results will be further validated at a later stage with shore-based analyses, hence individual sediment samples were taken from all opened cores with 10 cubic centimetre plastic syringes at 10 cm sample spacing for physical property measurements (water content, sediment density) and further geochemical, sedimentological and mineralogical investigations. To calculate sediment fluxes and mass accumulation rates of specific compounds, the water content and the sediment density will be measured on individual samples taken from the cores that were opened during the cruise. Onshore at AWI, all individual physical properties samples shall be weighed, freeze-dried and milled. Water content, bulk-, grain-, wet-, and dry-bulk-densities, and the porosity shall be determined.

Tab. 3.6: Sensors and parameter settings for measurements with the GEOTEK multi-sensor core logger during PS141 (analog to PS140, cf. Gutjahr et al., 2024).

P-wave velocity and core diameter
Rolling transducers
Transmitter pulse frequency: 250 kHz
P-wave travel time offset: 19.5 µs (PC125, 125 cm outer diam., 2*3.7 mm liner thickness)
P-wave travel time offset: 18.5 µs (PC125, 125 cm outer diam., 2*2.5 mm liner thickness)
Temperature = 20 °C, salinity = 35 psu, not corrected for water depth and *in situ* temperature; calibrated with water core of known temperature and theoretical sound velocity.
Density
Gamma ray source: Cs-137; activity: 370 MBq, Serial No. 0874/13
Aperture diameter: 5.0 mm
Gamma ray detector: 3rd generation; count time 5 s
Gamma ray attenuation measurement and density calculation with equation type $y=Ax^2+Bx+C$, (Coefficients A, B, and C determined with measurements on calibration cores).
Fractional porosity
Mineral grain density = 2.65, water density = 1.026
Magnetic susceptibility (MS)
Coil sensors: BARTINGTON MS-3, Ser. Nr. 0582, and Ser. Nr. 716 (coil sensor)
Nominal inner coil diameter: 14 cm
Coil diameter: 14.8 cm (factors B, Den and LD were deactivated in the GEOTEK processing software).
Alternating field frequency: 565 Hz, count time 5 s, precision 0.1 * 10^{-5} (SI)
Core thickness measurement
Laser detection

Core opening, core documentation and sediment sampling

After MSCL measurements of physical properties of whole-round core sections of the 125 mm-gravity cores, cores PS141_23-2 and PS141_37-1 were selected for opening and sampling. In addition, the gravity core PS141_3-2 (90 mm-liner diameter, run with the piston core without trigger core) and 90 mm-piston cores PS141_5-5 and PS141_7-3 were opened and sampled, although they were not MSC-logged beforehand. This was because the MSC-Logger was not fitted for analysis of 90 mm-whole rounds.

The up to 1 m-long core sections were split lengthwise into a working (W) and an archive (A) half with the Marinetechnik Kawohl vibration saw tool (Fig. 3.8). The sediment surface of both halves was then scrapped with knifes to achieve a clean surface, while also both half-round core liners were cleaned. The cleaned working and archive halves were then immediately photographed to avoid sediment colour changes due to oxidation (Fig. 3.8). The working half proceeded then to initial sampling on board, while the archive half was described and analysed by smear slides (Fig. 3.8, Tab. 3.5). In total, ~51.4 core meters were opened, described and sampled.

Macroscopic descriptions of the archive halves were completed to document the sedimentary composition, colour changes, sediment textures and structures immediately after core opening, and were recorded by hand on digital log sheets. These log sheets were archived as pdf files. The core description was completed by one operator (JG). Sediment colours were qualitatively determined using the Munsell Soil Color Chart (Munsell Color Company, Inc., 2010).

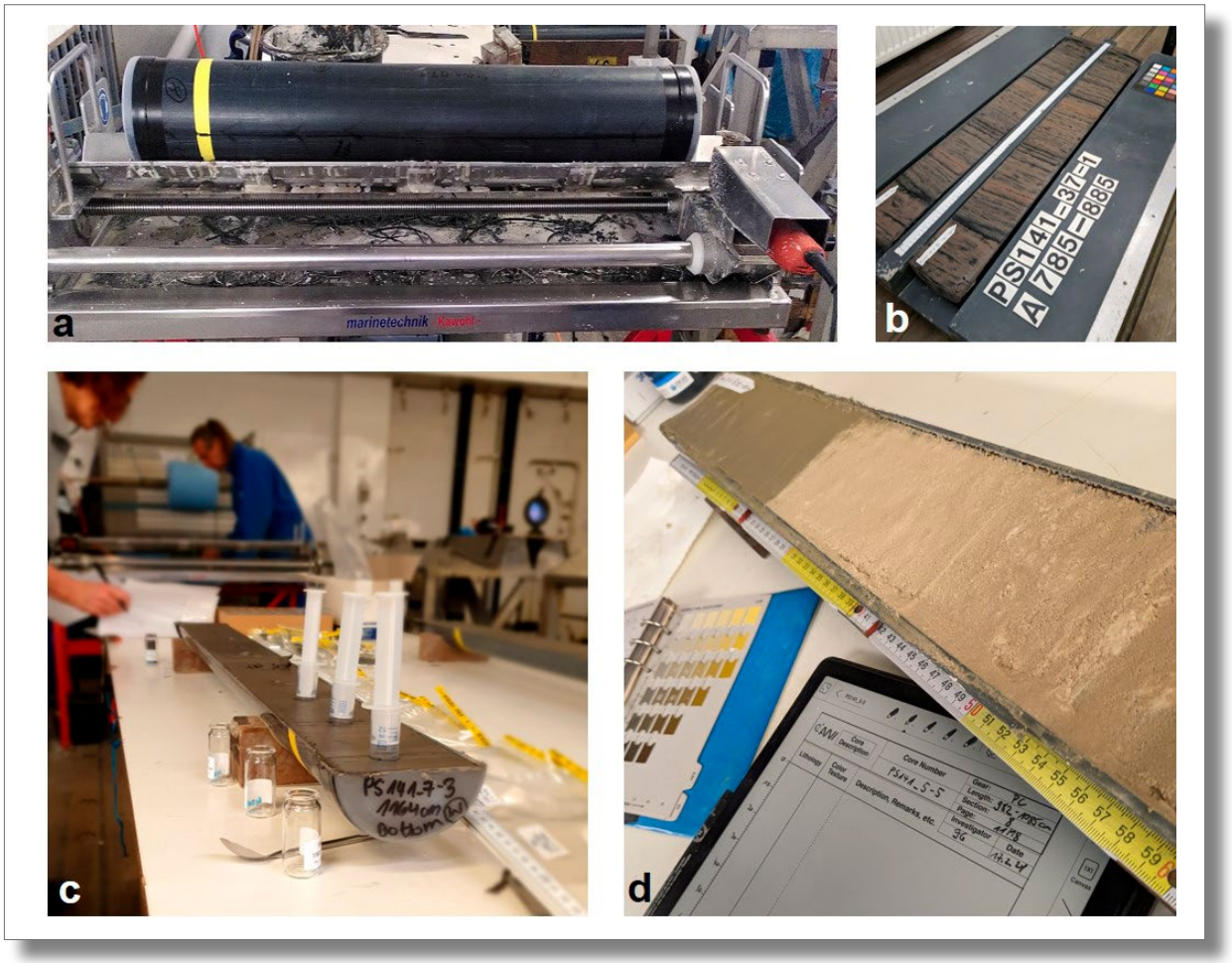

Fig. 3.8: Core handling in the big wet laboratory during Polarstern expedition PS141. a) Splitting of a core section in working and archive halves, using the Marinetechnik Kawohl vibration saw tool, b) photographing of working and archive halves, c) sampling of the working half in 10 cm-increments with 10 ml-syringes and d) core description of PS141_5-5 with Munsell Colour Chart

The principal lithologic name was assigned on the basis of the relative abundances of biogenic and terrigenous clastic grains: The principal name of a sediment with < 50% biogenic grains was based on the grain size characteristics of the terrigenous clastic fraction. If the sediment contains no or minor amounts of gravel, then the principal name was determined by the relative abundances of sand, silt, and clay (Fig. 3.9; after Mazzullo et al. 1988). The principal name of a sediment/rock with ≥ 50% biogenic grains was classified as an ooze and was modified by the most abundant specific biogenic grain type that forms 50 % or more of the sediment (Fig. 3.9). Similar biogenic grain types were grouped together to exceed this 50% abundance threshold (e.g., if diatoms and radiolaria comprised more than 50 % of the sediment, then the sediment was termed "siliceous ooze"). Major and minor modifiers were applied to any of the principal sediment names. The use of major and minor modifiers follows the scheme of Integrated Ocean Drilling Program Expedition 383 (Winckler et al. 2021): Major modifiers (Fig. 3.9) are components with abundances between 25 % and 49 % and are indicated by the suffix "-rich" for the biogenic components (e.g., diatom-rich) and by "clayey," "silty" or "sandy" according to the major terrigenous clastic modifier. Components with abundances < 10% were included with the term "with" after the principal lithological classification. The Wentworth (1922) scale was used to define grain size classes. In addition to the lithological classification, macroscopic description included dropstone observations indicative of the presence of ice-rafted debris, a qualitative estimation of the degree of bioturbation ("slight", "moderate", "strong") and specific types of coring disturbances such as "soupy", "fractured" and "void" (Fig. 3.10). Upon completion of the core description, archives halves were wrapped in transparent cling foil, placed into D-tubes, and stored in reefer containers at ~4°C for transport to the home institution and analyses onshore.

Information from hand-annotated visual core descriptions (VCDs) for each archive core section was recorded and digitized with the APPLECORE software package. These lithologs include relevant descriptive information categories such as lithology, core images, sedimentary structures, bioturbation intensity, drilling disturbances (Appendix A.8).

The working halves were sampled onboard with 10 ml-syringes (with cut-off tops) in 10 cm-increments (1-2 cm, 11-12 cm, *etc*) for the analysis of physical properties and bulk parameters such as dry bulk density as well as carbonate-, total organic carbon- and biogenic silica content (Fig. 3.8). The sediment volume of the samples in the syringes was carefully monitored before extruding and storing the samples in glass vials (resulting in 6-10 cm^3 of sample). In cores PS141_3-2, PS141_5-5 and PS141_7-2, the remainder of the 1 cm-sediment slice, where the syringe sample was taken from, was sampled into a Whirl-Pak bag for micropaleontological analyses. Exact 10 cm-spaced sampling was partly omitted at massive and homogenous sediment layers such as the siliceous oozes encountered in core PS141_5-5. In cores PS141_23-2 and PS141_37-1, 1 cm-sediment slices were only sampled into Whirl-Pak bags at 20 cm-increments (1-2 cm, 21-22 cm, *etc*) to avoid degradation of remaining sediment for further biomarker analyses. Voids in the sediment core resulting from sampling were filled with Styrofoam. After sampling was complete, the working halves were wrapped in transparent cling foil, placed into D-tubes, and stored in reefer containers at ~4°C for transport to the home institution and processing onshore.

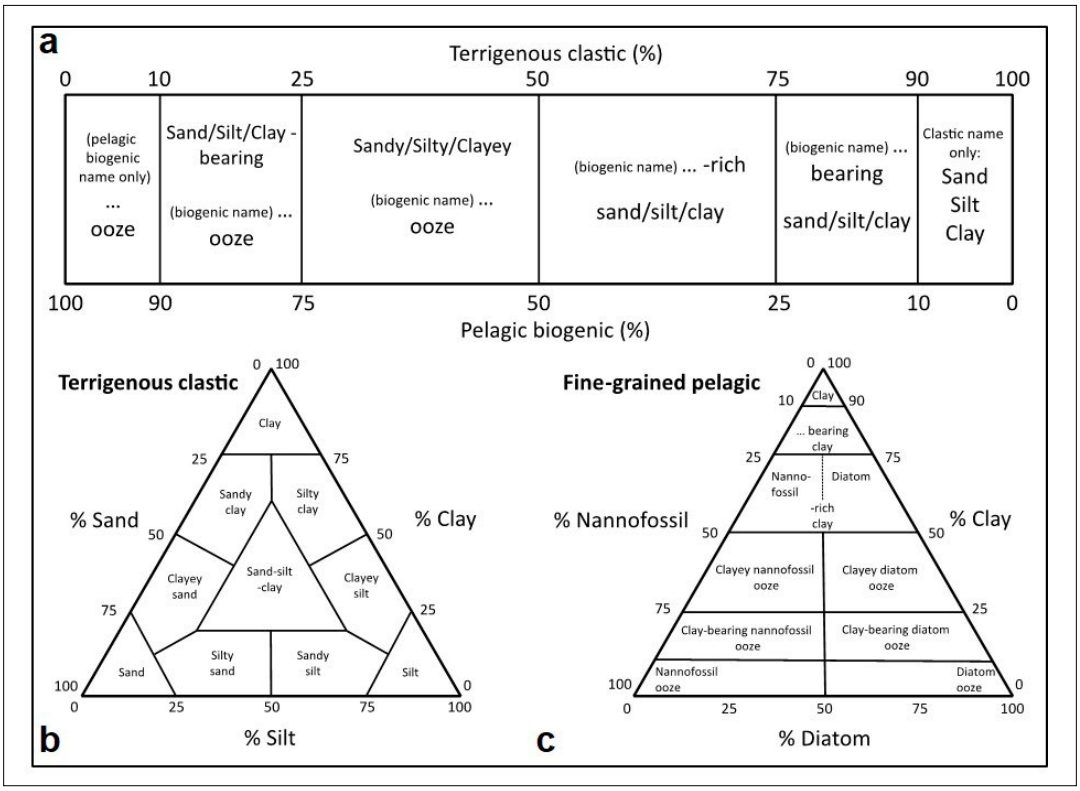

Fig. 3.9: Overview of classification scheme for sediments that are a) mixtures of pelagic biogenic and terrigenous clastic components and ternary diagrams of lithology naming scheme for b) siliciclastic and c) biogenic sediment/rock without gravel after Dean et al. (1985) and Mazzullo et al. (1988) used for shipboard visual core description during Polarstern Expedition PS141. The scheme is based on the classification scheme used by the International Ocean Discovery Programme of Expedition 383 (Winckler et al. 2021).

Preliminary results

Three major anticipated outcomes from the geological sampling conducted during EASI3 will be (i) a longer-term geological context for more recent ice-sheet dynamic changes in the East Antarctic region; (ii) a framework for calibrating and improving numerical ice-sheet models – both urgently needed for this largely understudied region, and (iii) an improved understanding of the connection between nearshore shelf/margin bathymetry, cryosphere processes and more distal oceanographic current dynamics. We further aim to constrain the spatial and temporal variability of potential forcing mechanisms leading to past ice-sheet retreat, e.g., incursions of relatively warm deep water onto continental shelves (*cf*. Hillenbrand et al., 2017) via paleo-ice stream pathways (e.g., Klages et al. 2015) towards the grounding line (e.g., Jacobs et al. 2011; Nakayama et al.,2013; Greenbaum et al. 2015). The previously described ocean access to a cavity beneath Totten Glacier suggests increased vulnerability of such glaciers to warm-water incursions, which requires an understanding of variability from initial post-LGM deglaciation to today. The combined onshore-offshore sampling approach implemented during the EASI2 and 3 expeditions will integrate geological samples collected from the offshore coastal areas of Prydz Bay, Windmill Islands, Bunger Hills and Gaussberg with onshore samples collected during EASI3 (see Chapter 6). This suite of samples will be used to determine proximal ice-sheet dynamics over the last ca. 50,000 years in response to climatic changes, oceanic warm-water intrusions, and relative sea level (RSL) fluctuations at key locations along the present-day ice margin. The results will be an essential reference for ice-sheet models to improve projections of future RSL rise. With the future planned shore-based analytical works we hope to gain more

robust insights into the physical and biogeochemical characteristics of the most distinct water masses of the Southern Indian Ocean. By using elemental and stable isotopic compositions of foraminiferal calcite tests and siliceous diatom frustules as well as various biomarkers we plan to reconstruct past oceanic temperatures, salinities, nutrient conditions and sea-ice cover, as well as past intermediate and deep-water mass properties. Measurements will be carried out on key sites acquired along the three major shelf-based working areas and be complemented by the pelagic sediment cores for comparison to characteristics from the deeper Indian Ocean and its intermediate and deep-water masses, as well as Southern Ocean frontal systems.

Pelagic Southern Ocean transect

Four sediment cores were retrieved from the pelagic Southern Ocean during the transit from Hobart and the working area on the East Antarctic shelf (Fig. 3.10). While sediment retrieval at station PS141_6-2 was not successful (“Banana”), core PS141_3 located in the sub-Antarctic Zone between the sub-Tropical Front (STF) and sub-Antarctic Front (SAF) south of Australia shows massive foraminiferal ooze deposits (details below). Further south, core PS141_5-5 was obtained from the Antarctic Zone south of the Polar Front (PF) and north of the Southern Antarctic Circumpolar Current Front (SACCF) in the northeast Australian-Antarctic Basin (Fig. 3.10). It shows alternations of siliciclastic sediments and siliceous ooze (details below). Core PS141_7-3 was retrieved from a topographic ridge in the vicinity of the Antarctic slope northeast of Law Dome, and consists mostly of silty clay and clay with the minor constituents sand and foraminifera (Fig. 3.10; details below). Due to poor weather conditions sediment coring in the Polar Front Zone between the SAF and the PF was not possible.

Sediment core **PS141_3-2** (-46.9515°S, 134.7570°S) has a total length of 339 cm and was recovered on 10 February 2024 via gravity corer from the northern flank of the Southeast Indian Ridge from a water depth of 4,004 m (Fig. 3.10). The core was retrieved from a weakly stratified sediment sequence with a strong top reflector as hydroacoustically imaged by the ship’s sub-surface bottom profiler Parasound (Fig. 3.11a). The core mostly consists of a massive and homogenous foraminiferal ooze alternating in colour between light gray (10YR 7/2), very pale brown (10YR 7/3, 10YR 8/2) and light yellowish brown (10YR 6/4) (Fig. 3.11b). Transitions between colours and lithologies are gradual (Fig. 3.11b). The planktonic foraminiferal species *Globigerina bulloides* dominates the core catcher sample. Slight to moderate bioturbation is prevalent throughout the entire core and becomes particularly evident at colour transitions (Fig. 3.11b). Weak mottling occurs below 144 cm until core bottom. At 295 and 303 cm, there is a gradual and sharp boundary to very pale brown (10YR 8/2) nannofossil-rich foraminiferal ooze above and below, respectively (Fig. 3.11b). This ~8 cm-long segment shows no signs of bioturbation or mottling.

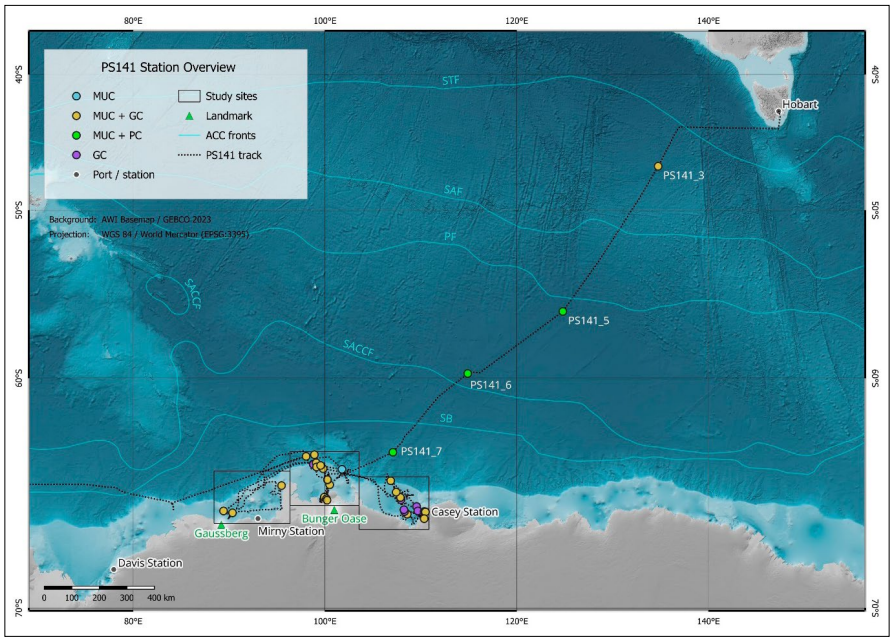

Fig. 3.10: Overview of the geological stations (circles) during PS141 with deployment of multi-corer (MUC), gravity corer (GC) and piston corer (PC) in the Indian Sector of the Southern Ocean south of Australia and in the East Antarctic slope and shelf area between 87°E – 112°E. Background map is based on the General Bathymetric Chart of the Ocean (GEBCO) 2023 (GEBCO Compilation Group, 2023), while high-resolution bathymetry is based on PS141 shipborne bathymetric HYDROSWEEP data (Chapter 2). The boxes indicate detailed maps (from left to right) of the continental shelf-slope area off Vanderford Glacier and Casey Station (Fig. 3.16), off Denman Glacier and Bunger Hills (Fig. 3.20) and off Gaussberg and west of Shackleton Ice Shelf (Fig. 3.24). The dashed line shows the ship's track. Solid lines indicate the fronts of the Antarctic Circumpolar Current (ACC) and the Southern Ocean: Sub-Tropical Front (STF), Sub-Antarctic Front (SAF), Polar Front (PF), Southern Antarctic Circumpolar Current Front (SACCF) and the Southern Boundary (SB).

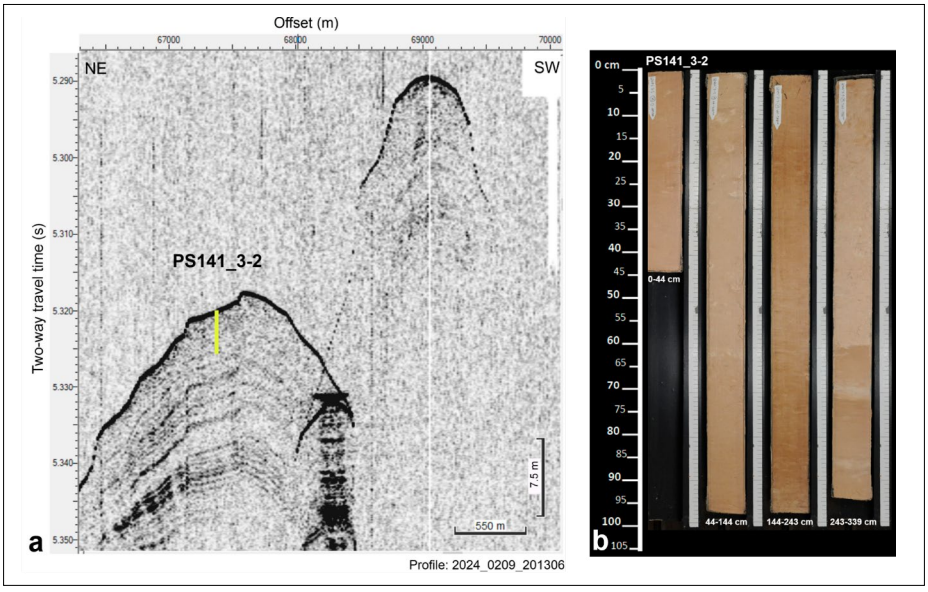

Fig. 3.11: a) Sub-bottom hydroacoustic profile obtained via the ship's PARASOUND system of the ~20 m-thick sedimentary sequence characterized by a hard surface reflector sampled during geological station PS141_3 by gravity corer and multi-corer. The location and penetration depth of core PS141_3-2 is shown by the yellow bar. b) Photograph of working halves of gravity core PS141_3-2.

Sediment core PS141_5-5 (-56.3246°S, 124.8174°E) has a total length of 1,780 cm and was recovered on 14 February 2024 via piston corer from the Northeast Australian-Antarctic Basin south of the Southeast Indian Ridge from a water depth of 4,709 m (Fig. 3.10, Y2). Sub-bottom hydroacoustic profiles obtained via the ship's Parasound system indicated that the core was retrieved from a stratified ~50 m-thick sedimentary sequence that may contain hiatuses (Fig. 3.13). The trigger core of the piston core has a length of 76 cm. Sediment core PS141_5-5 consists of two main sedimentary components: first, clay or silty clay, with different minor constituents comprising of radiolaria, foraminifera or diatoms/opal, and second, siliceous ooze with the major constituents radiolaria and diatoms or diatoms, and the minor constituents clay (Fig. 3.12). While the first varies in colour between dark grayish brown (2.5Y 4/2), grayish brown (2.5Y 5/2), brown (7.5Y 5/3), gray (5Y 5/1) and light brownish gray (2.5Y 6/2), the siliceous ooze varies in color between light olive brown (2.5Y 5/3), olive brown (2.5Y 4/3), pale yellow (2.5Y 8/2) or light yellowish brown (2.5Y 6/3) (Fig. 3.12). Alternations between the two main sedimentary components show a recurring pattern throughout the core: diatom ooze gradually transitions into siliceous ooze comprised of diatoms and radiolaria downcore (and sometimes subsequently into a diatom ooze), which is then followed by clay further down in the core (Fig. 3.12). Although the transitions between the components are often gradual, sharp transitions mostly occur between the base of the clay component and the underlying siliceous ooze (Fig. 3.12). At least 18 of these diatom/siliceous ooze-clay alternations can be identified in the core. From 696 cm to core bottom, the core shows weak to strong bioturbation primarily at lithological transitions. Mottling is present sporadically below 580 cm. The core liner imploded during core recovery, which led to a sediment disturbance (soupy, void) between 308-380 cm due to the liner fragment being sucked up in the core liner.

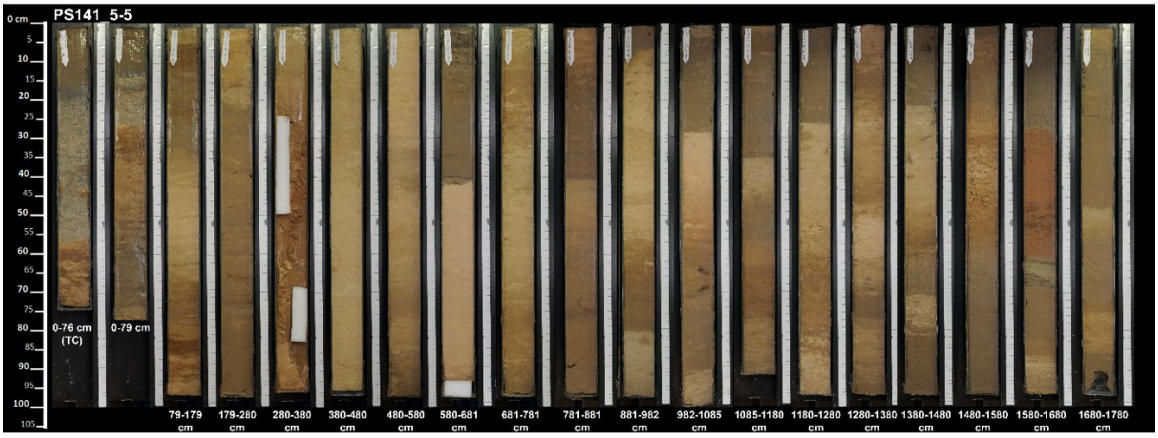

Fig. 3.12: Photo of working halves of piston core PS141_5-5

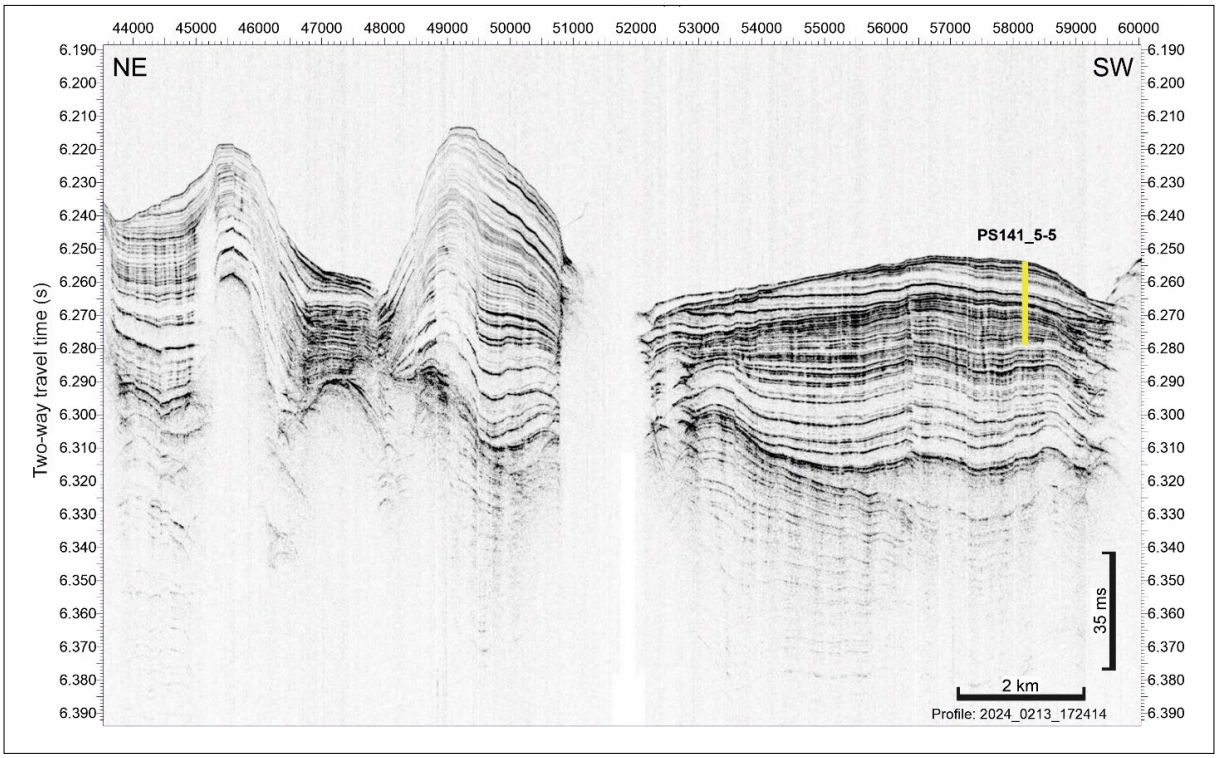

Fig. 3.13: Sub-bottom hydroacoustic profile obtained via the ship's PARASOUND system of a stratified ~50 m-thick sedimentary sequence sampled during geological station PS141_5 by piston corer and multi-corer. The location and penetration depth of core PS141_5-5 is shown by the yellow bar.

Sediment core PS141_7-3 (-63.6422°S, 107.0916°E) has a total length of 1,264 cm and was recovered on 18 February 2024 via piston corer from the Antarctic slope east of Bruce Rise from a water depth of 2,881 m (Fig. 3.10, Y4). The core was retrieved from an undisturbed, well-stratified ~100 m-thick sedimentary sequence as imaged by the sub-bottom profiling Parasound system onboard *Polarstern* (Fig. 3.15). The trigger core of the piston core has a length of 83 cm (Fig. 3.14). In the upper five sections (0-463 cm), sediment core PS141_7-3 consists of grayish brown (2.5Y 5/2), dark grayish brown (2.5Y 4/2) or light olive brown (2.5Y 5/3) silty clay with the minor constituents sand and foraminifera (Fig. 3.14). Gradual lithological transitions occur between clay and silty clay of different colors, or because of changes of the minor constituents (Fig. 3.14). Between 0-463 cm, the core shows moderate to strong bioturbation and sporadic mottling. Dropstones with a size of up to 5 cm appear at 138 cm and 274 cm. The transition to the lowermost core at 463 cm appears disturbed and fractured indicated by a wavy boundary and the presence of soupy silty clay (Fig. 3.14). Sediment core PS141_7-3 from 466-1264 cm is characterized by brown (10YR 4/3), dark brown (7.5YR 3/2), very dark grayish brown (2.5Y 3/2) and very dark gray (2.5Y 3/1) clay with minor constituents sand and foraminifera (Fig. 3.14). The lowermost part of the core distinguishes itself in colour, but it also shows the continuous presence of clayey, stiff layers of up to 1 cm-thickness, dark gray (10YR 4/1) or dark olive gray (5Y 3/2) clay layers of up to 1 cm-thickness, black (2.5Y 2.5/1) laminae (sometimes with coarse-grained material) of up to 0.5 cm-thickness and mm-scale pods/lenses or 1 mm-thick bands of dark gray (10YR 4/1) silty clay and silt (Fig. 3.14). These were mostly absent in the upper part of the core from 0-463 cm. Between 891-900 cm of the core, the core shows a black (GLEY1 2.5/N) and greenish gray (GLEY1 5GY 5/1) claystone/ concretion (likely rich in Mn and Fe) that fills out the entire core liner (Fig. 3.14). Mottles and indications of weak to moderate bioturbation occur only very sporadically throughout the core.

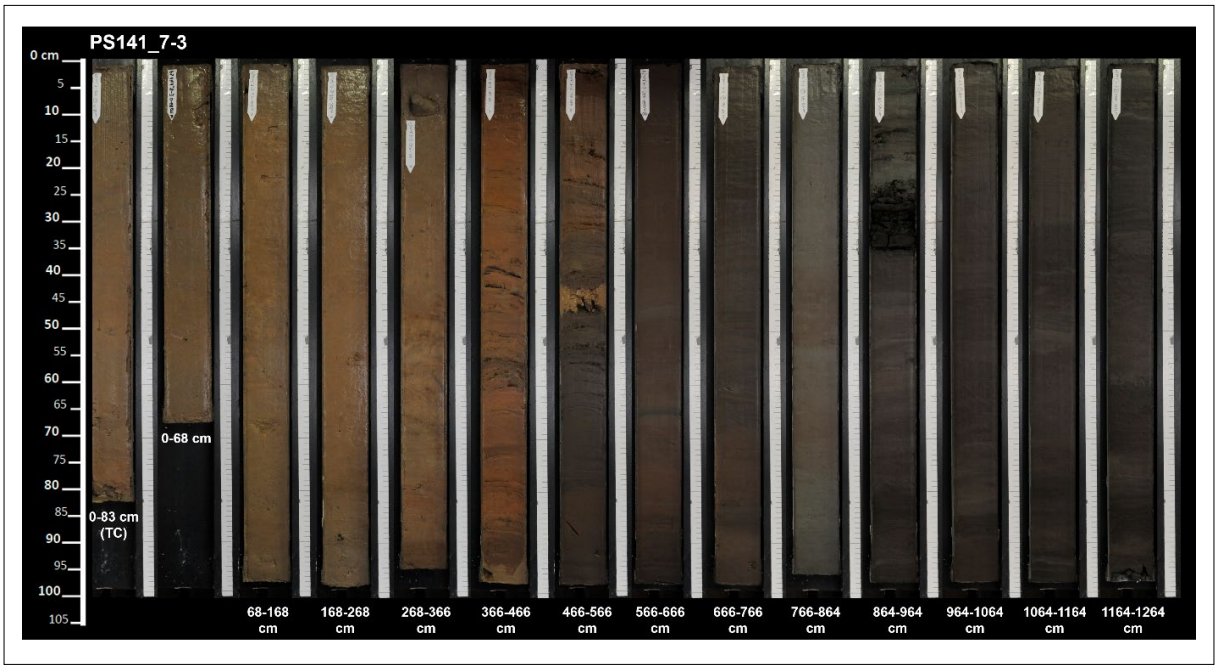

Fig. 3.14: Photo of working half of piston core PS141_7-3

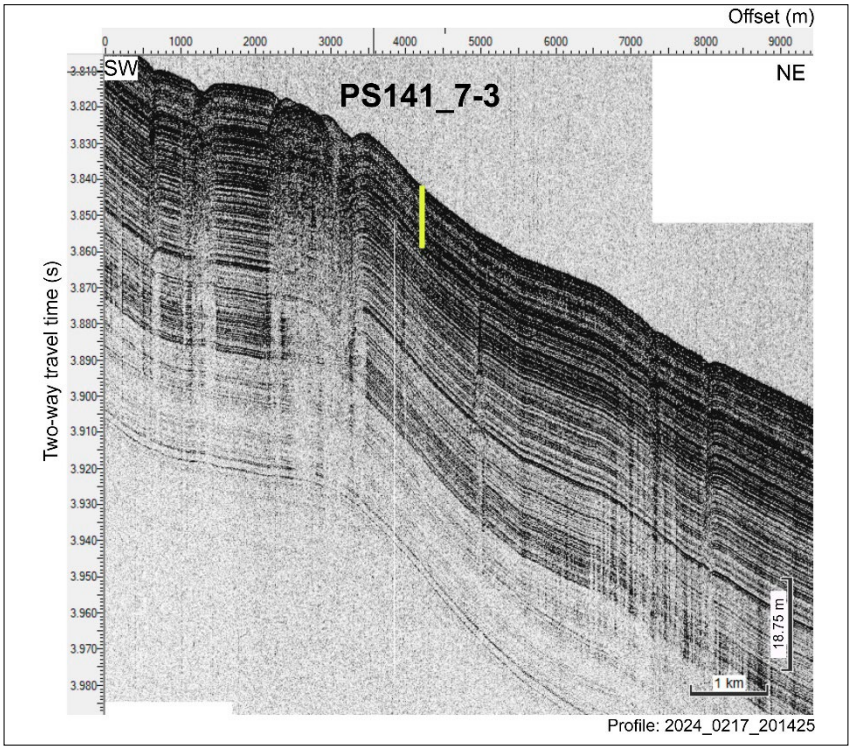

Fig. 3.15: Sub-bottom hydroacoustic profile obtained via the ship's PARASOUND system of an undisturbed, well-stratified ~100m-thick sedimentary sequence sampled during geological station PS141_7 by piston corer and multi-corer. The location and penetration depth of core PS141_7-3 is shown by the yellow bar.

Continental shelf-slope area off Vanderford Glacier and Casey Station

Fifteen coring sites were visited on the continental shelf off Vanderford Glacier and west of *Casey Station*, while one of these geological stations (PS141_49) was retrieved from the slope area in that region (Fig. 3.16). Geological stations PS141_37 (GC), PS141_58 (MUC), PS141_32 and PS141_35 were retrieved from a deep trough off Vanderford Glacier from a water depth of 1.5-2.3 km (Fig. 3.16). Cores PS141_33 and PS141_34 were taken north of Vanderford Glacier trough from a water depth of ~750 m in an area without iceberg ploughmarks (Fig. 3.16). Sediment cores from shallow geological stations (< 200 m water depth) were retrieved off *Casey Station* west of Law Dome, including PS141_50, PS141_54, PS141_55 (MUC) and PS141_53 (GC) as well as PS141_56 (MUC) and PS141_52 (GC) (Fig. 3.16).

Sediment core PS141_41 was retrieved from the vicinity of Bond, Anzac and Adams Glaciers (Fig. 3.16) from an area that is characterized by striations at the surface and a stratified ~12 m-thick sedimentary sequence in the sub-surface (likely indicating the presence of a sub-glacial lake in the past). Sediment cores PS141_42 and PS141_43 were obtained from the northernmost extent of striations and the southernmost extent of iceberg ploughmarks in the area, respectively (Fig. 3.16). While core PS141_44 was taken at the top of a mid-shelf topographic high, likely representing a grounding zone wedge, characterized by ploughmarks, core PS141_45 and PS141_47 were retrieved from the bathymetric depression to the north of it that is not characterized by iceberg ploughmarks (Fig. 3.16, 3.17). Sediment cores PS141_48 and PS141_49 were recovered from the outer shelf that is characterized by iceberg ploughmarks and the continental slope from a water depth of ~2.5 km (Fig. 3.16).

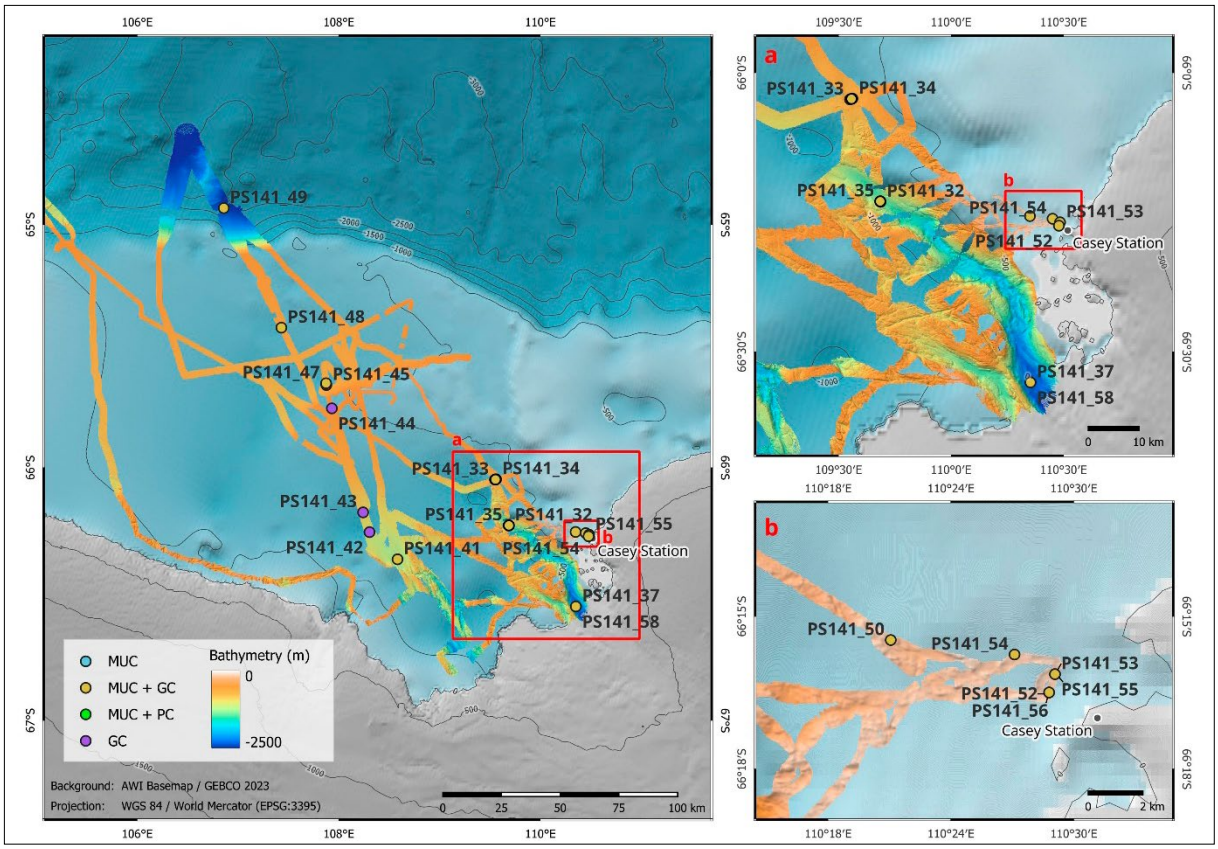

Fig. 3.16: Overview of geological coring stations (circles) in the continental shelf-slope area off Vanderford Glacier and Casey Station completed during Polarstern expedition PS141, including deployment of multi-corer (MUC), gravity corer (GC) and piston corer (PC). Red boxes indicate detailed maps of coring stations a) in the through off Vanderford Glacier and b) in the shallow area (< 200 m water depth) off Casey Station. Background map is based on the GEBCO 2023 (GEBCO Compilation Group, 2023), while high-resolution bathymetry is based on PS141 shipborne bathymetric HYDROSWEEP data. Dashed line shows the ship's track.

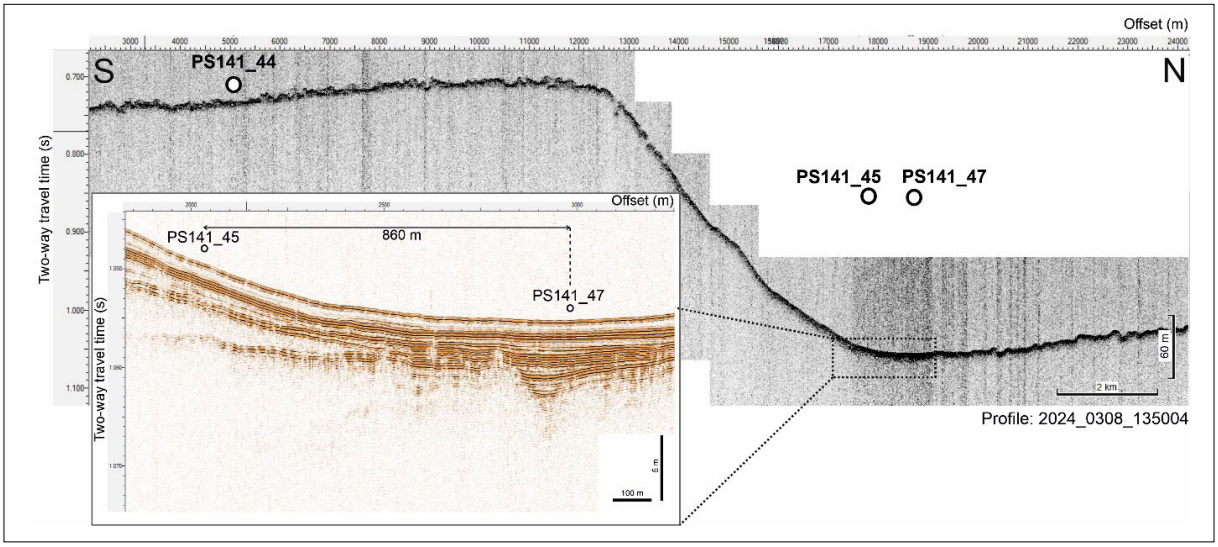

Fig. 3.17: Sub-bottom hydroacoustic profile obtained via the ship's PARASOUND system of the mid-shelf ground zone wedge and the bathymetric depression to the north circles show the location of core PS141_44, PS141_45 and PS141_47. The location of the inset Figure is shown by the stippled box.

Sediment core PS141_37-1 (66.5538°S, 110.3535°E) has a total length of 985 cm and was recovered via gravity corer in a deep trough off Vanderford Glacier from a water depth of 2319 m (Fig. 3.16). Sub-bottom profiles imaged with the ship's Parasound system show that the core was retrieved from a near-transparent, weakly stratified ~25 m-thick sedimentary sequence overlaying harder reflectors (Fig. 3.19). The upper 500 cm of the core are dominated by brown (7.5YR 4/2) silty clay with sand with short intervals (up to 3 cm) of dark brown (7.5YR 3/4) sand-bearing silty clay (Fig. 3.18). Transitions between these lithologies are mostly gradual (Fig. 3.18). The lower half of the core is dominated by brown (7.5YR 4/2) opal-rich clay with silt and clayey silt with sand and opal (Fig. 3.18). While the upper 500 cm show occasional-to-strong mottling, the lower half of the core shows frequent occurrences of black (7.5YR 2.5/1) lenses and (partly discontinuous) bands of mostly (sandy) silt, up to 8 mm in thickness (Fig. 3.18). The occurrence, intensity and thickness of these lenses increase downcore (Fig. 3.18). Between 597-727 cm, very dark gray (10YR 3/1) silty sand occurs in lenses and distinct 1 mm-thick bands. Additionally, dark grayish brown (10YR 4/2) layers of siliceous ooze that are up to 10 mm-thick become frequent in the lower half of the core. These layers are reminiscent of diatom mats and are often associated with black (sandy) silt bands below.

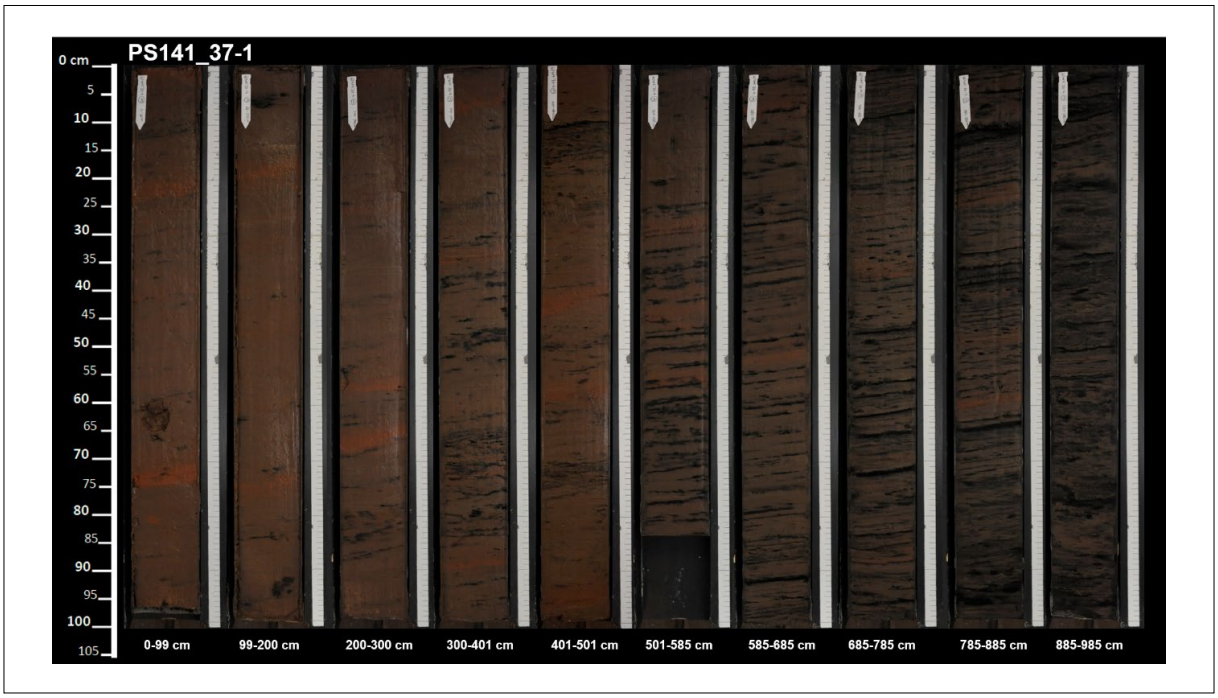

Fig. 3.18: Photo of working half of gravity core PS141_37-1

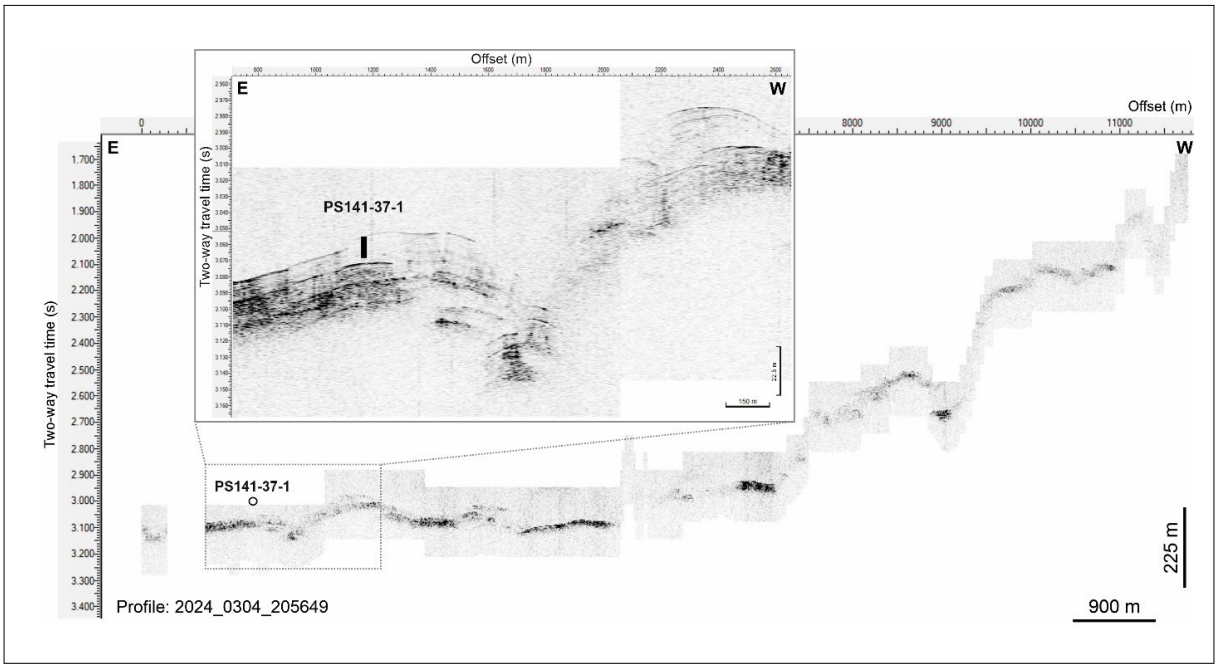

Fig. 3.19: Sub-bottom hydroacoustic profile obtained via the ship's PARASOUND system of a near-transparent, weakly stratified ~25 m-thick sedimentary sequence overlaying harder reflectors sampled during geological station PS141_37 by gravity corer and multi-corer. Circle and black bar show the location and penetration depth of core PS141_7-3. The location of the inset Figure is shown by the stippled box.

Continental shelf-slope area off Denman Glacier and Bunger Hills

Twelve cores were retrieved from the shelf off Denman Glacier and Bunger Hills, with three additional cores (PS141_64, PS141_83 (MUC only), PS141_84) obtained from the slope area in this region (Fig. 3.20). Cores PS141_23 (details below), PS141_71 and PS141_72 were taken off Scott Glacier west of Denman Glacier Tongue from a water depth of ~550 m, while the latter two were retrieved from small-scale trough features (Fig. 3.20). For the retrieval of PS141_71 and PS141_72 advantage was taken from a break in the Shackleton Ice Shelf in Glacier Ice Stream that eventually led to a break-up of an iceberg in the first half of March 2024 and allowed access to this area. Cores PS141_71, PS141_74, PS141_76 and PS141_77 were retrieved from the mid-shelf area (Fig. 3.20) that is characterized by bathymetric features that are likely iceberg ploughmarks (randomly oriented) and mega-berg furrows (SW-NE oriented). Cores PS141_66, PS141_67, PS141_69, PS141_78 and PS141_79 were retrieved from water depths ~400 m from the outer shelf characterized by iceberg ploughmarks, likely representing the top of a grounding zone wedge (Fig. 3.20). Core PS141_68 is located on a narrow plateau at a water depth of 550 m to the north of this grounding zone wedge that transitions into the continental slope northwards (Fig. 3.20, Y9b).

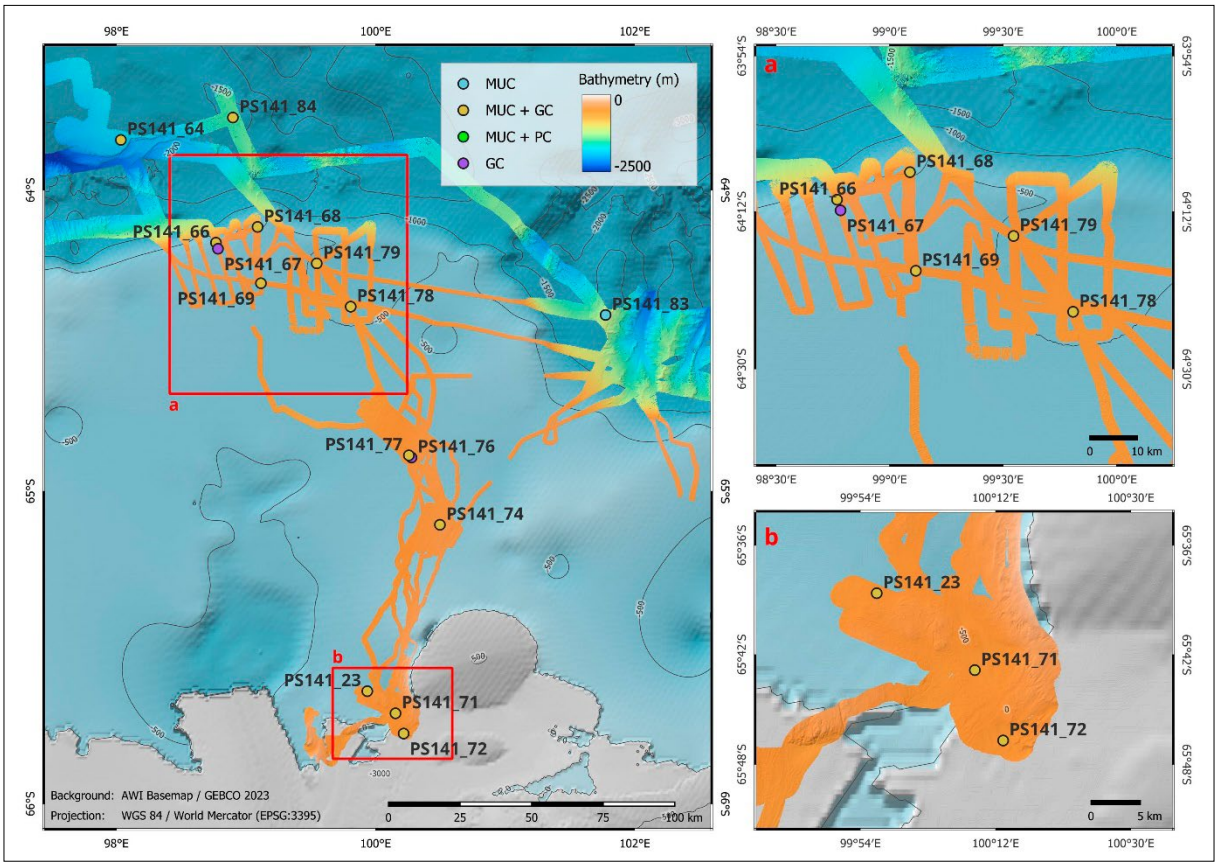

Fig. 3.20: Overview of the geological coring stations (circles) in the continental shelf-slope area off Denman Glacier and Bunger Hills completed during Polarstern expedition PS141, including the deployment of multi-corer (MUC), gravity corer (GC) and piston corer (PC). Red boxes indicate detailed maps of coring stations a) on the outer shelf and b) off Scott Glacier west of Law Dome. The background map is based on the GEBCO 2023 (GEBCO Compilation Group, 2023), while high-resolution bathymetry is based on PS141 shipborne bathymetric HYDROSWEEP data. The dashed line shows the ship's track.

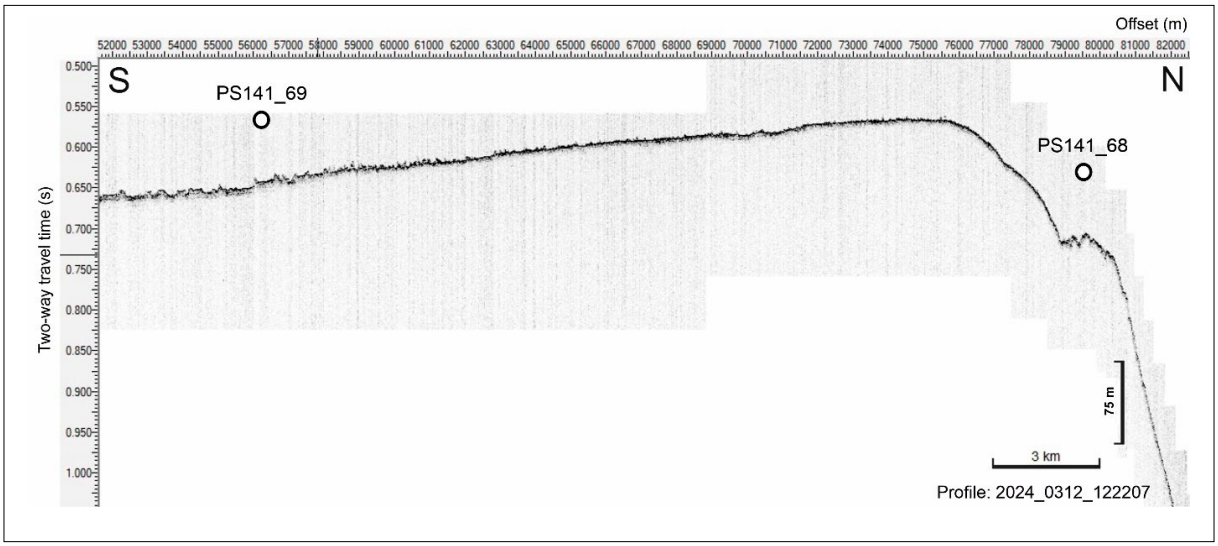

Fig. 3.21: Sub-bottom hydroacoustic profile obtained via the ship's PARASOUND system of the outer shelf off Denman Glacier and Bunger Hills. Circles indicate the position of cores PS141_69 and PS141_68 on and to the north of a grounding zone wedge, respectively.

Sediment core PS141_23-2 (-65.6439°S, 99.9364°E) has a total length of 476 cm and was recovered on 29 February 2024 via gravity corer from the vicinity of the Shackleton Ice Shelf off Scott Glacier, west of Denman Ice Tongue and east of Mill Island, from a water depth of 504 m (Fig. 3.20). The sub-bottom Parasound profiles show that the core was retrieved from a mostly transparent ~5 m-thick sedimentary sequence overlaying another transparent sediment body sample with a hard reflector on the top (Fig. 3.21). In the upper three sections (0-277 cm), sediment core PS141_23-2 mostly consists of dark greyish brown (10YR 4/2) silty clay with sand and diatoms that appears massive and homogeneous, grayish brown (10YR 5/2) silty clay and grayish brown (10YR 5/2) mud with sand (Fig. 3.22). Lithological and color transitions are gradual in the upper three sections from 0-277 cm (Fig. 3.22). Between 69 cm and 111 cm of the core PS141_23-2, we identified a very dark gray (10YR 3/1) highly unsorted, stiff mud clast, with a sharp boundary to surrounding sediment and with rock fragments with a size of up to ~3 cm (Fig. 3.22). In the upper part, this clast is surrounded by dark gray (10YR 3/1) silty clay with sand and diatoms that appears like a contact aureole (Fig. 3.22). In the lower part, it is surrounded by dark greenish gray (GLEY1 10Y 4/1) silty clay with sand and diatoms (Fig. 3.22). From 277 cm to core bottom, grayish brown (10YR 5/2) silty clay transitions into poorly sorted, dark grayish brown (10YR 4/2) mud with gravel and a dark grayish brown (10YR 4/2) sandy mud (Fig. 3.22). Lithological transitions between the latter two are gradual. They are tentatively interpreted as unconsolidated diamicton (Fig. 3.22). At 367 cm, a 0.5 cm-wide carbonate fossil fragment was found (likely bryozoa) in the working half that was sampled in a separate vial.

Fig. 3.22: Photo of working half of gravity core PS141_23-2.

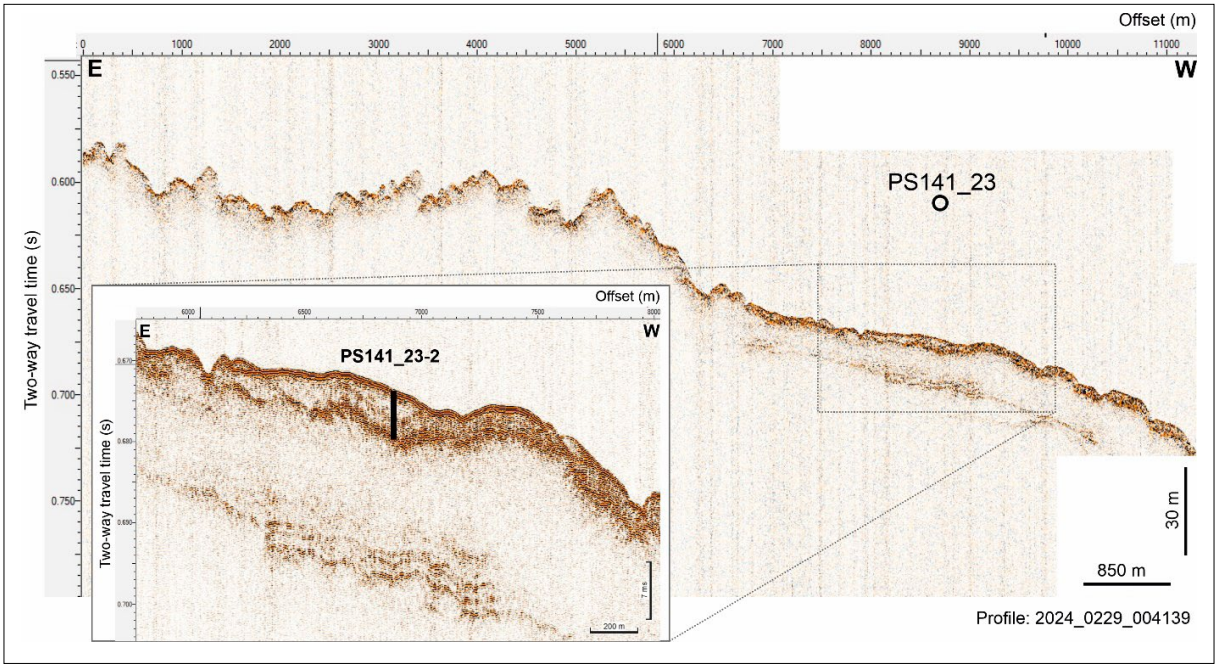

Fig. 3.23: Sub-bottom hydroacoustic profile obtained via the ship's PARASOUND system of a mostly transparent ~5 m-thick sedimentary sequence overlaying another transparent sediment body sample with a hard reflector on the top that was sampled geological station PS141_23 by gravity corer and multi-corer. Circle and black bar show the location and penetration depth of core PS141_23-2. Location of inset figure is shown by stippled box.

Continental shelf-slope area off Gaussberg and west of Shackleton Ice Shelf

Three gravity cores were taken from the East Antarctic shelf off Gaussberg and west of Shackleton Ice Shelf. Core PS141_14 was retrieved from a mid-shelf area characterized by the absence of iceberg ploughmarks (Fig. 3.24). Core PS141_19 was obtained from the outer shelf west of the northern tip of Shackleton Ice Shelf, where iceberg ploughmarks or other remarkable features are not observed either (Fig. 3.24). Core PS141_62 was sampled from an undisturbed, well-stratified ~70 m-thick sedimentary sequence from a mid-shelf trough that is located north of a bedrock outcrop at ~1.1 km water depth (Fig. 3.24; 3.25). This core comprised of a greenish gray diatom ooze that revealed a strong H_2S odor.

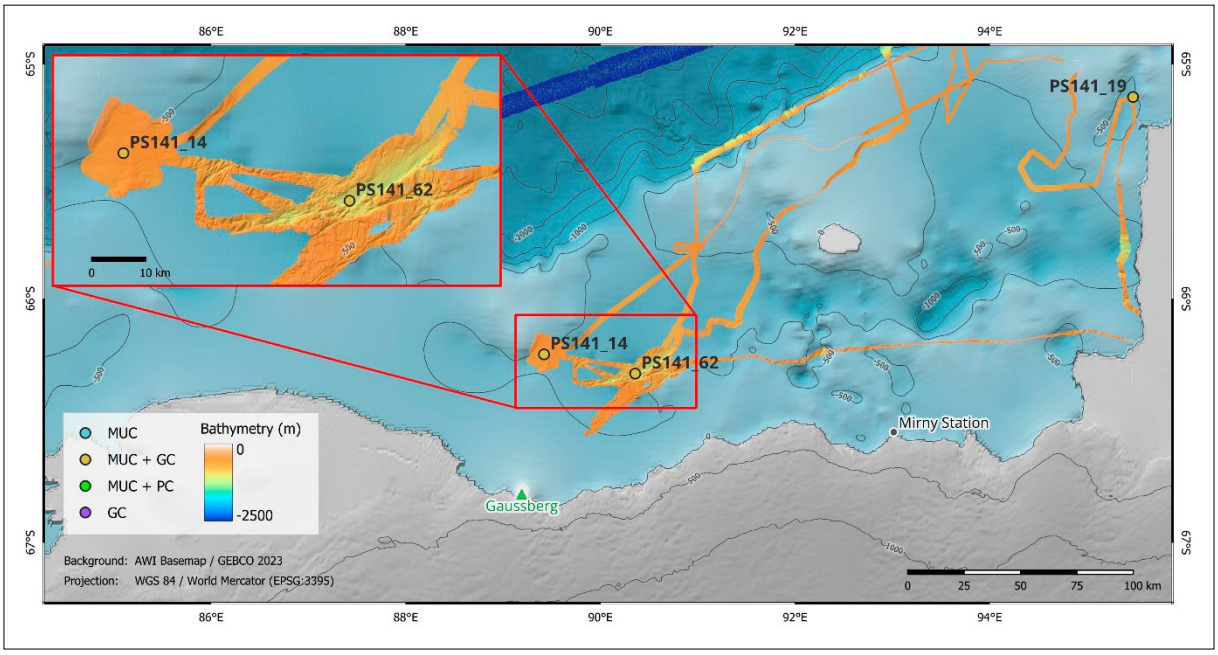

Fig. 3.24: Overview of geological coring stations (circles) in the continental shelf-slope area off Gaussberg and west of the Shackleton Ice Shelf completed during Polarstern expedition PS141, including deployment of multi-corer (MUC), gravity corer (GC) and piston corer (PC). Red box indicates detailed map of coring stations in a) the western shelf area off Gaussberg. A) On the outer shelf and B) off Scott Glacier west of Law Dome. Background map is based on the GEBCO 2023 (GEBCO Compilation Group, 2023), while high-resolution bathymetry is based on PS141 shipborne bathymetric HYDROSWEEP data. Dashed line shows the ship's track.

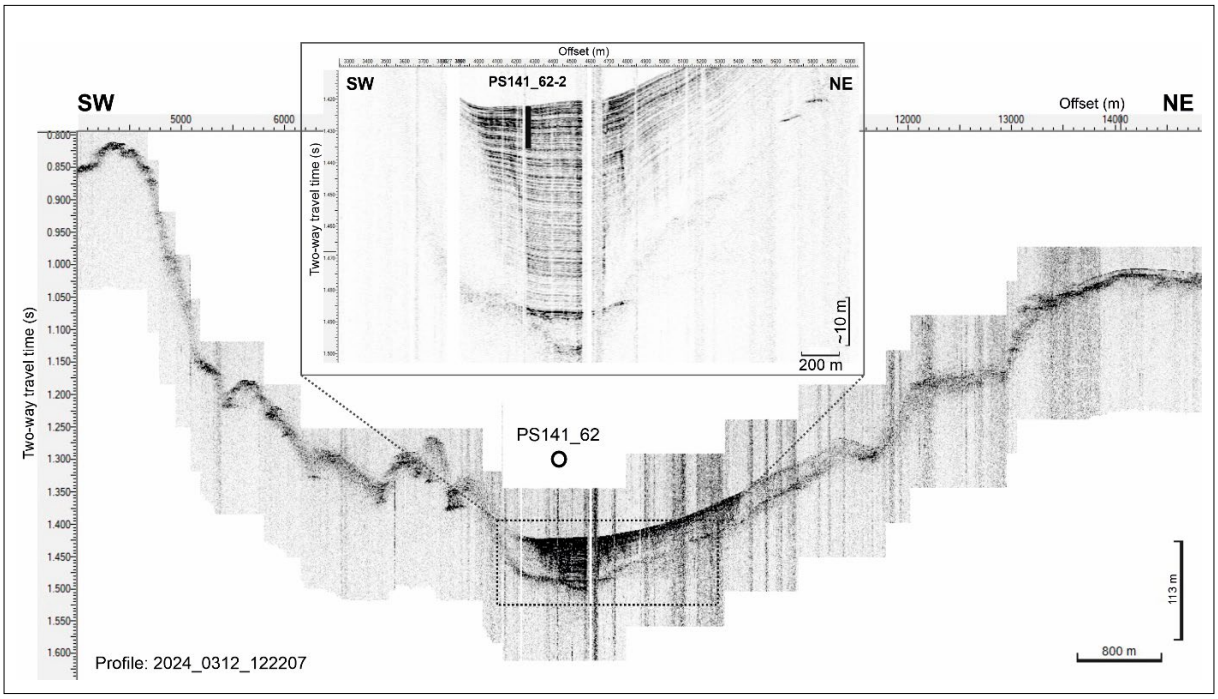

Fig. 3.25: Sub-bottom hydroacoustic profile obtained via the ship's PARASOUND system of an undisturbed, well-stratified ~70 m-thick sedimentary sequence in a trough on the Antarctic shelf off Gaussberg sampled during the geological station PS141_62 via a gravity- and multi-corer. Circle and black bar show the location and penetration depth of the core at PS141_23-2. The location of the inset figure is shown by the stippled box.

Data management

Shipboard data from the expedition are defined as being acquired by the PS141 Shipboard Geoscience Party and is published as part of this cruise report in the AWI open-access series "Reports on Polar and Marine Research". Related meta-data and a short report will be submitted to PANGAEA (https://www.pangaea.de). Sample material retrieved during the cruise has been transferred to shipboard scientists and partners at their respective home institutions according to a jointly agreed sampling plan.

Sample distribution will be recorded, and archive material will be curated and permanently stored at the AWI *Polarstern* Core and Sample Repository, Bremerhaven. Analytical data and scientific results will be published under open access agreements in peer-reviewed journals. All data will be permanently stored in the PANGAEA data repository as a final data product (open access) with a unique digital object identifier for permanent future reference. Access for the science community will be provided via PANGAEA, once the data are published or at the latest 4 years after the end of the expedition (moratorium period).

Availability of sample material from this expedition will be restricted to PS141 participants and collaborators for a maximum post-cruise moratorium period of 4 years, after which material can be made available to the wider scientific community by enquiry to the curator of the AWI Core and Sample Repository and principal investigators.

The research activities are directly related to the objectives of Theme 2 (Ocean and Cryosphere in Climate) with a focus on subtopics 2.1 (Warming Climate), 2.3 (Sea Level Change), and 2.4 (Advanced Research Technologies for Tomorrow).

In publications based on this cruise, **Grant No. AWI_PS141_02** will be quoted and the respective reference article will be cited: Alfred-Wegener-Institut Helmholtz-Zentrum für Polar- und Meeresforschung (2017) Polar Research and Supply Vessel POLARSTERN Operated by the Alfred-Wegener-Institute. Journal of large-scale research facilities, 3, A119. http://dx.doi.org/10.17815/jlsrf-3-163.

References

Alfred-Wegener-Institut Helmholtz-Zentrum für Polar- und Meeresforschung (2017) Polar Research and Supply Vessel POLARSTERN Operated by the Alfred-Wegener-Institute. Journal of large-scale research facilities, 3, A119. http://dx.doi.org/10.17815/jlsrf-3-163

Carson CJ, Post AL, Smith J, Walker G, Waring P, Bartley R, Raymond B (2017) The seafloor geomorphology of the Windmill Islands, Wilkes Land, East Antarctica: Evidence of Law Dome ice margin dynamics. Geomorphology 292:1–15.

Cook CP et al. (2013) Dynamic behaviour of the East Antarctic ice sheet during Pliocene warmth. Nature Geoscience 6:765–770.

Dean WE, Leinen M, and Stow DAV (1985) Classification of deep-sea, fine-grained sediments. Journal of Sedimentary Research, 55(2):250–256. https://doi.org/10.1306/212F868E-2B24-11D7-8648000102C1865DDomack E et al. (1998) Late Quaternary sediment facies in Prydz Bay, East Antarctica and theirrelationship to glacial advance onto the continental shelf. Antarctic Science 10:236–246.

Esper O, Gersonde R (2014) Quaternary surface water temperature estimations: New diatom transfer functions for the Southern Ocean, Palaeogeography Palaeoclimatology Palaeoecology 414:1–19.

Fretwell P et al. (2013) Bedmap2: improved ice bed, surface and thickness datasets for Antarctica. The Cryosphere 7:375–393.

GEBCO Bathymetric Compilation Group 2023 (2023) The GEBCO_2023 Grid - a continuous terrain model of the global oceans and land. https://doi.org/10.5285/F98B053B-0CBC-6C23-E053-6C86ABC0AF7B

Greenbaum J, Blankenship D, Young D, Richter TG, Roberts JL, Atiken ARA, Legresy B Schroeder D, Warner RC, van Ommen TD, Siegert MJ (2015) Ocean access to a cavity beneath Totten Glacier in East Antarctica. Nature Geosci 8:294–298. https://doi.org/10.1038/ngeo2388

Gulick SPS et al. (2017) Initiation and long-term instability of the East Antarctic Ice Sheet. Nature 552:225–229.

Hillenbrand C-D et al. (2013) Grounding-line retreat of the West Antarctic Ice Sheet from inner Pine Island Bay. Geology 41:35–38.

Hillenbrand C-D (2017) West Antarctic Ice Sheet retreat driven by Holocene warm water incursions. Nature 547:43–48.

Jacobs SS, Jenkins A, Giulivi CF, Dutrieux P (2011) Stronger ocean circulation and increased melting under Pine Island Glacier ice shelf. Nature Geoscience 4:519.

Keul N, Peijnenburg KTCA, Andersen N, Kitidis V, Goetze E, Schneider R (2017) Pteropods are excellent recorders of surface temperature and carbonate ion concentration. Sci. Rep. 7:12645. https://doi.org/10.1038/s41598-017-11708-w

Klages JP (2013) First geomorphological record and glacial history of an inter-ice stream ridge on the West Antarctic continental shelf. Quat. Sci, Rev. 61:47–61.

Klages JP et al. (2014) Retreat of the West Antarctic Ice Sheet from the western Amundsen Sea shelf at a pre- or early LGM stage. Quat. Sci. Rev. 91:1–15.

Klages JP et al. (2015) Palaeo-ice stream pathways and retreat style in the easternmost Amundsen Sea Embayment, West Antarctica, revealed by combined multibeam bathymetric and seismic data. Geomorphology 245:207–222.

Klages JP et al. (2017) Limited grounding-line advance onto the West Antarctic continental shelf in the easternmost Amundsen Sea Embayment during the last glacial period. PLOS ONE 12(7), (e0181593). https://doi.org/10.1371/journal.pone.0181593Lamping N, Müller J, Hefter J, Mollenhauer G, Haas C, Shi X, Vorrath ME, Lohmann G and Hillenbrand CD (2021) Evaluation of lipid biomarkers as proxies for sea ice and ocean temperatures along the Antarctic continental margin. Clim. Past 17:2305–2326.

Massom RA, Scambos TA, Bennetts LG, Reid P, Squire VA and Stammerjohn SE (2018) Antarctic ice shelf disintegration triggered by sea ice loss and ocean swell. Nature 558:383–389.

Mazzullo, J.M., Meyer, A., and Kidd, R.B., 1988. New sediment classification scheme for the Ocean Drilling Program. In Mazzullo, J., and Graham, A.G. (Eds.), Technical Note 8: Handbook for Shipboard Sedimentologists. Ocean Drilling Program, 44–67. https://doi.org/10.2973/odp.tn.8.1988

Morlighem M, Rignot E, Binder T et al. (2020) Deep glacial troughs and stabilizing ridges unveiled beneath the margins of the Antarctic ice sheet. Nature Geoscience 13:132–137.

Nakayama Y, Schröder M, Hellmer HH (2013) From circumpolar deep water to the glacial meltwater plume on the eastern Amundsen Shelf. Deep Sea Res. Part I 77:50–62.

Ohshima KI, Nihashi S and Iwamoto K (2016) Global view of sea-ice production in polynyas and its linkage to dense/bottom water formation. Geoscience Letters 3:13.

Picton HJ, Stokes CR, Jamieson SSR, Floricioiu D, Krieger L (2023) Extensive and anomalous grounding line retreat at Vanderford Glacier, Vincennes Bay, Wilkes Land, East Antarcrtica. The Cryosphere 17:3593–3616.

Shen Q et al. (2018) Recent high-resolution Antarctic ice velocity maps reveal increased mass loss in Wilkes Land, East Antarctica. Scientific Reports 8(1):4477.

Smith JA et al. (2011) Deglacial history of the West Antarctic Ice Sheet in the western Amundsen Sea embayment. Quat. Sci. Rev. 30:488–505.

Smith A et al. (2014) New constraints on the timing of West Antarctic Ice Sheet retreat in the eastern Amundsen Sea since the Last Glacial Maximum. Glob. Planet. Change 122:224–237.

Smith JA, Graham AGC, Post AL, Hillenbrand, C-D, Bart, PJ, Powell RD (2019) The marine geological imprint of Antarctic ice shelves. Nat Commun 10:5635. https://doi.org/10.1038/s41467-019-13496-5

The IMBIE team (2018) Mass balance of the Antarctic Ice Sheet from 1992 to 2017. Nature 558:219–222. https://doi.org/10.1038/s41586-018-0179-y

Tiedemann R and Müller J (2022) The Expedition PS128 of the Research Vessel POLARSTERN to the Weddell Sea, Lazarew Sea, Riiser-Larsen Sea, Cosmonaut Sea and Cooperation Sea in 2022 / H. Bornemann and S. Amir Sawadkuhi (editors), Berichte zur Polar- und Meeresforschung = Reports on polar and marine research, Bremerhaven, Alfred Wegener Institute for Polar and Marine Research, 764: 1-235. https://doi.org/10.57738/bzpm_0764_2022

Wentworth CK (1922) A scale of grade and class terms for clastic sediments. Journal of Geology, 30(5):377–392. https://doi.org/10.1086/622910

Wilson DJ et al. (2018) Ice loss from the East Antarctic Ice Sheet during late Pleistocene interglacials. Nature 561:383–386.

Winckler G, Lamy F, Alvarez Zarikian CA, et al. (2021) Expedition 383 Methods, in: Lamy, F., Winckler, G., Alvarez Zarikian, C.A., Expedition 383 Scientists (Eds.), Dynamics of the Pacific Antarctic Circumpolar Current. Proceedings of the International Ocean Discovery Program, 383. College Station, TX (International Ocean Discovery Program). https://doi.org/10.14379/iodp.proc.383.102.2021

4. WATER COLUMN SAMPLING

Jasper Ole Ferber[1], Lester Lembke-Jene[2], [1]DE.CAU
Georgios Xydis[1], [2]DE.AWI
Not on board: Nina Keul[1], Katja Peijnenburg[3], [3]NL.NATURALIS
Sandra Tippenhauer[2]

Grant-No. AWI_PS141_02

Objectives

Currently established, foraminifera-based carbonate system proxies include boron isotopes (pH), B/Ca (CO_3^{2-}), porosity- and weight-based measurements of planktic tests, or the reconstruction of total alkalinity via salinity variations. However, none of these proxies allows the reliable construction of the complete carbonate system and thus paleo pCO_2, due to various limitations and uncertainties associated with the different methods used. In addition, despite extensive methodological calibration works aimed at establishing new foraminifera-based carbonate system proxies, other calcifiers have not yet been as profoundly explored for their potential use as proxy carriers. Yet, without branching out and studying the potential of marine calcifiers, we are left with an inadequate reconstruction of the paleo-carbonate system and thus paleo-atmospheric CO_2. To remedy this gap, we aim for developing new, pteropod-based proxies (e.g., via Boron isotopes), as well as ground-truthing recently developed pteropod-based proxies for temperature and carbonate ion concentration (Keul et al., 2017). We plan to analyse live-sampled pteropod and foraminifera specimen and their geochemical characteristics from plankton net hauls carried out during PS141, and compare assemblage patterns, as well as isotopic and trace elemental compositions of individual samples to acquired instrumental oceanographic data and water column samples from the same stations. The aims of the water column sampling programme were:

A) Ground-truthing of foraminiferal-based and establishing pteropod-based proxies by trace elemental and stable isotopic compositions for reconstructing temperature and CO_2 gradients. A so-far under-used opportunity to establish new C-system proxies is to examine the recorder potential of pteropod shells. Pteropods are ideal candidates as they are abundant in all major ocean bodies, and their physiology is known to be highly sensitive to climate change (Ocean Acidification and Ocean Warming; Lischka et al., 2011). Pteropods are pelagic molluscs, producing shells made out of aragonite, a metastable form of calcium carbonate, which is more soluble than calcite in seawater. Since the presence of pteropods in underlying sediments is governed by the corrosiveness of the water column, pteropods can be used as a “double archive” as they offer the unique chance to quantify both the characteristics of the water column at the time of biomineralization (as imprinted in the trace elemental incorporation in the pteropod shell), and the corrosiveness of the water column (through their presence/absence/ fragmentation in the sediment). Our subsequent, shore-based analyses are planned to lead to novel proxies for both, the carbonate system and temperature. Given the importance of high-latitude areas in the ocean–climate system, there is currently an increasing need for reliable paleo-proxies of low temperature-adapted species.

B) Diversity, abundance and ecology of pteropods and other zooplankton along a latitudinal gradient across the Southern Ocean. Pteropods have been shown to be good indicators of ocean acidification (Manno et al., 2017). However, both abundance and biogeographical distributions are still poorly known in the study area, even though knowledge of their ecology and biogeography is important in order to predict species-specific sensitivity to a changing ocean. We will examine the abundance and diversity patterns of pteropods along two latitudinal and one longitudinal transect in the Indian Sector of the Southern Ocean. These areas have not yet been widely sampled for pteropods, and we will use samples for molecular analyses to establish species boundaries and population structure. Furthermore, many aspects of the basic ecology of pteropods remain poorly known, which limits our ability to assess their response to climate change. During this cruise, we will learn more about their diel vertical migration patterns, trophic level, diet, and depth habitat (where in the water column do they calcify? where and what do they eat?).

Marine zooplankton are the intermediate trophic levels of pelagic marine food webs, and they play an important role in global biogeochemical cycling, facilitating the movement of carbon, nitrogen and phosphorous from the surface ocean into the deep sea. With representatives from 15 animal phyla and > 7,000 species described worldwide, the taxonomic complexity of the assemblage is high. An additional aim of this expdition is to evaluate the diversity of the assemblage in (sub) Antarctic waters, comparing conventual morphological identification of key taxonomic groups with metabarcoding (community amplicon sequencing) approaches.

C) Characterization of regional Southern Ocean physical and biogeochemical characteristics using water column elemental and stable isotope signatures. Geochemical sampling carried out during PS141 included seawater sampling for trace metal and isotopic analyses that shall serve as a reference and calibration dataset for the paleoceanographic proxies and approaches. It will also enhance understanding of Antarctic sub-glacial runoff and nutrient delivery to the Southern Ocean. Large parts of the Southern Ocean Indian sector have not been sampled for trace metals or their isotopic ratios. Conversely, constraining trace metal supply and dispersal in sub-Antarctic waters today is key to developing an accurate reconstruction of past environmental conditions, as well as understanding consequences of ongoing environmental changes. Moreover, the deep and intermediate Antarctic water masses play a crucial role in supplying nutrients to the lower latitude surface ocean. Notably for nutrient metals, the processes that govern the quantity and stoichiometry in the source regions and northward-advected water masses are insufficiently constrained, making it impossible to predict the consequences of Southern Ocean changes in upwelling or phytoplankton community shifts.

Work at sea

During the course of the expedition, we used the following instrumentation and sampling methods: CTD with water sampler rosette, shipboard (ADCP) and Lowered Acoustic Current Doppler Profiler (L-ADCP) systems, a plankton Multi-Net, a handheld plankton net, underway sampling via the shipboard membrane pump system.

A total of 25 water sampling stations were occupied during PS141 (cf. Tab. 4.2, Fig. 4.1), starting on the approach transect to Antarctica and continuing through the three working areas.

CTD rosette

Oceanographic measurements during PS141 were carried out using the *Polarstern* CTD system (CTD-PS, Tab. 4.1). Meta-data of all PS141 CTD stations is listed in Tab. 4.2 and station locations are shown as an overview in Fig. 4.1. The sensors and rosette of CTD-PS are permanently provided on *Polarstern* and maintained by the Section “Physical Oceanography” from DE.AWI. The LADCP system was as well provided by this Section and was already

installed within the metal frame of the CTD following deployment on the preceding PS140 cruise. The fixture of the L-ADCP necessitated the removal of two Niskin bottles (#22&#23) from the original 24-bottle sample rosette set-up.

The standard sensor configuration of the CTD system throughout the cruise consisted of two temperature sensors, two conductivity cells, a pressure sensor, two oxygen sensors, one fluorescence sensor, and a transmissometer (see Tab. 4.1 for more details).

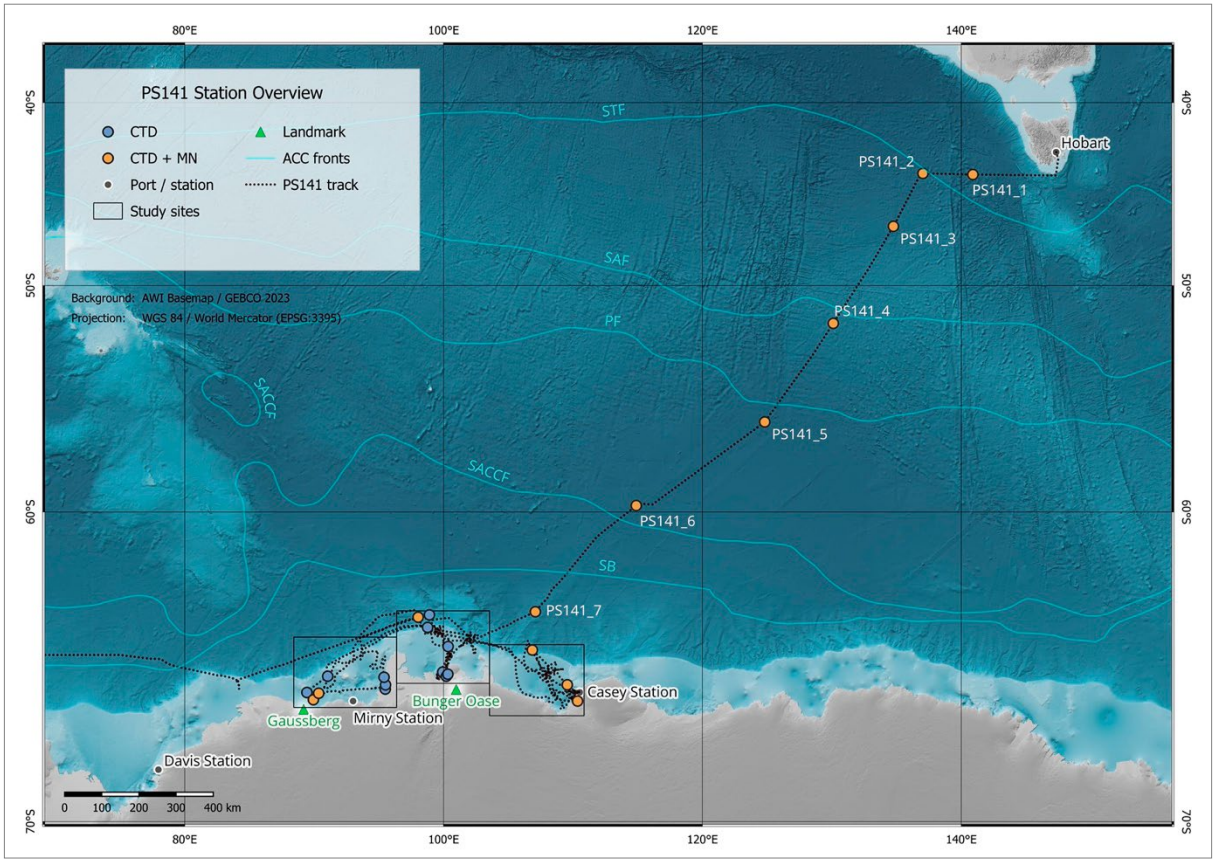

Fig. 4.1: Overview map of study area during PS141 that were addressed with CTD and Rosette water sampler, Multinet (MN), or both, respectively. Major oceanic frontal systems are indicated with light blue lines (after Orsi et al., 1995).

CTD deployments followed standard operating procedures as outlined in the training manuals provided on board with the system. Briefly, the CTD rosette was lowered to 20 m to start pump systems, followed by heaving back to the surface to start the respective downcast with 0.5 m/s for the upper water column, increasing speed up to 1.0 m/s for water depths below 100 – 200 m based on differences in salinity readings between the two sensors. Lowering speed was reduced when approaching the sea floor, downcasts were stopped five to ten meters above the seafloor, depending on sea state and bottom topography. Water sampling was carried out on the upcast. After approaching target water depths with reduced speeds of 0.5 to 0.3 m/s and waiting for 60 s at each target depth, to minimise interference from turbulent water mixing and potentially lagging sensor adjustment, individual Niskin bottles were fired.

Tab. 4.1: Sensor configurations for the CTD-PS system used during PS141, unchanged from the setup of the preceding expedition PS140.

	SN	Calibration Date	Channel	Description
CTD	485			SBE 911plus
Temperature (primary)	1338	22.06.2022	F0	SBE3plus
Conductivity (primary)	3173	23.06.2022	F1	SBE4c
Pressure	0485	14.11.2017	F2	SBE9
Temperature	1374	22.06.2022	F3	SBE3plus
Conductivity	3590	23.06.2022	F4	SBE4c
Oxygen (primary)	4402	20.05.2023	V0	SBE43
Oxygen	4401	20.05.2023	V1	SBE43
Altimeter	46611	--	V2	SBE 171740
Fluorescence	1853	16.11.2021	V3	WETLabs ECO CDOM Fluorometer
Beam Transmission	1220	07.09.2022	V5	WETLabs C-Star
Lowered Acoustic Doppler Current Profiler (LADCP)	23292 and 23293			Teledyne RD Instruments WHM300-I-UG500

Lowered ADCP

Two 300 kHz RDI Workhorse ADCPs were mounted on the rosette to act as lowered ADCPs (L-ADCP), unchanged from the set-up used on the preceding cruise (cf. Gutjahr, 2024). The L-ADCP consists of the two 300 kHz ADCPs and a battery container. Communication was established to a laptop in the winch control room via two cables (for master and slave) and the pre-installed COM1 and COM2 ports. The L-ADCP was operated using the GUI of the LADCP tool V1.7 from GEOMAR. Prior to each deployment, the L-ADCP computer time was synchronized with the shipboard NTP server. During the entire cruise, the settings documented in Table 4.1 were used. Specifically, a bin size of 10 m was used, a maximum range of 200 m, beam coordinates, no blanking after transmission, narrow band processing, and a timing of the Master and Slave such that the acoustic energy of the Master is separated by 0.55 seconds from the acoustic energy of the slave. The Master (downward looking device) and Slave (upward looking device) data file names consist of the station number (three digits), an abbreviation indicating the viewing direction (UP for upward and DN for downward) and a running number with three digits beginning with 000, representing the file number, in case there are multiple files (e.g., 001DN000.000 and 001UP000.000). These files were stored in a folder named according to the station number. Log files documenting all actions conducted as starting (with configurations), stopping and downloading were kept. The match of each CTD cast to the respective L-ADCP profile number is listed in Table 4.2.

Shipboard ADCP

The shipboard hull-mounted Acoustic Doppler Current Profiler (S-ADCP) was in operation from leaving the 12 nm territorial waters off Australia until entering the 12 nm territorial waters of Namibia towards the end of the cruise. The RDI Ocean Surveyor instrument (150 kHz) is mounted at an angle of 45° in the ‘Kastenkiel’ of *Polarstern* and provides a continuous time

series of profiles of ocean current velocity in the upper 300 m of the water column while underway. The instrument was configured in narrowband mode and set up to use a 4 m bin size (configuration file cmd_OS150NB_trigger_off.txt), covering a range from 15 m to around 200 - 300 m water depth below surface, depending on sea state, ship speed and the presence of back-scatterers in the water column.

Overall, the system functioned without any issues and all data was collected entirely in the data files (file format: PS141[three digit deployment number]_000[three digit file number]. ENX, *.ENR, *.ENS, *.N1R, *.N2R, *.NMS, *.STA, *.LTA, *.VMO, *.LOG), as we did not apply any changes to the instrument configuration. The setup of navigational input was used from the vessel's GPS system. The software VmDas (Teledyne RD Instruments) was used to set the ADCP's operating parameters and to record the data. Finally, the data conversion was done using Matlab routines of the Ocean Surveyor Sputum Interpreter (OSSI) version 1.9 (osheader.m, osdatasip.m, osrefine.m, osbottom.m). The processing is to be carried out shore-based.

Discrete Sea*water sampling*

We sampled sea water from all 25 CTD stations with the rosette sampler deployments, for the characterization of modern physical ($\delta^{18}O$) and chemical (PO_4, DIC, NO_3, $\delta^{13}C$, pH, trace elemental composition) oceanographic parameters. The choice of stations and sampled water depth was made in accordance to the water mass status, in the area of scientific interest.

Samples for isotope and nutrient analyses were taken according to standard protocols immediately after the CTD rosette was retrieved from the water column and transferred into the hangar. Clean glass bottles with screw lids were flushed three times with sea water from the Niskin bottles, before fully filling the bottles bubble-free in overflow without air reservoir. From each sampled bottle depth, we took the following standard series of samples: (1) one 100 mL glass bottle for oxygen isotope analysis, (2) two 50 mL glass bottles, one for stable carbon isotope analysis of Dissolved Inorganic Carbon ($\delta^{13}C_{DIC}$), one for DIC content and AMS $^{14}C_{DIC}$, respectively, (3) one 50 mL plastic bottle, for nutrient (NUT) analysis, and (4) one acid-cleaned plastic bottle for Trace Element (TE) analysis. All 50 mL glass bottle samples for DIC measurements were fixed with 100 µL saturated $HgCl_2$ solution under a fume hood to stop biological activity. All glass bottles with screw caps were sealed airtight after sampling with a heated stearin/beeswax mixture to inhibit gas leakage during long-term storage. Samples were thereafter stored refrigerated in cold rooms at +4°C (stable isotopes, TE) or deep-frozen at –20°C (nutrients). Water meant to be analysed for TE was sampled using AcroPak filters and afterwards fixed with ultrapure HNO_3 and stored inside double plastic bags.

Tire-derived compounds and phthalates

Two 1 L water samples were taken from the shallowest CTD bottle at each CTD station and filtered for a solid phase extraction (SPE) of tire-derived compounds and phthalates. For this purpose, precleaned 1 L brown glass bottles were rinsed three times with the water from the respective Niskin bottle of the CTD before the sample was taken. The samples were then extracted using a SPE with a vacuum extraction system, whereby the water is filtered through an SPE cartridge, which allows the enrichment and stabilisation of additives on the SPE cartridge. The filtered water was discarded, and the samples were refrigerated until further analysis at the University of Vienna.

pH measurements

Water samples from every CTD cast were collected in plastic jars (10 samples per CTD cast), in order to conduct pH analyses with a pH electrode connected to a handheld meter (WTW,

Multi 340i). The pH electrode was calibrated on NBS buffers prior to every usage. The choice of water depths for pH measurements was done according to the multinet depth intervals, for further correlation of the pH values and the shell formation of the zooplanktonic organisms that have been collected. pH measurements were also carried out on samples from the underway membrane pump.

Tab. 4.2: Meta-data of all CTD stations from PS141 and the corresponding LADCP profile numbers. The station names refer to the file numbers and headers of the CTD data and correspond to the DSHIP entries.

Station	Event Time [UTC]	Depth [m]	Latitude	Longitude	L-ADCP
PS141_1-2	07.02.2024 23:04	4752	44°08.290‘ S	140°53.562‘ E	2
PS141_2-1	08.02.2024 00:15	4659	44°4.445‘ S	137°1.832‘ E	4
PS141_3-3	10.02.2024 09:44	4004	46°57.076‘ S	134°45.425‘ E	5
PS141_4-1	12.02.2024 05:37	3586	51°50.713‘ S	130°06.720‘ E	6
PS141_5-1	12/13.02.2024 22:15	4708	56°19.477‘ S	124°49.088‘ E	7
PS141_6-3	16.02.2024 10:30	4514	59°44.956‘ S	114°53.317‘ E	8
PS141_7-2	18.02.2024 01:29	2885	63°38.432‘ S	107°5.310‘ E	9
PS141_8-1	19.02.2024 03:45	394	65°42.652‘ S	100°19.818‘ E	no data
PS141_12-1	24.02.2024 06:47	504	65°46.510‘ S	91°02.882‘ E	11
PS141_13-1	25.02.2024 02:23	458	66°17.188‘ S	89°26.344‘ E	13
PS141_16-1	26.02.2024 03:53	180	66°10.891‘ S	95°29.699‘ E	14
PS141_17-1	26.02.2024 05:49	629	66°2.902‘ S	95°31.074‘ E	15
PS141_18-1	26.02.2024 09:08	1027	66°2.922‘ S	95°31.138‘ E	16
PS141_23-1	29.02.2024 03:00	504	65°38.659‘ S	99°56.105‘ E	17
PS141_24-1	29.02.2024 09:55	392	65° 42.709‘ S	100° 19.690‘ E	18
PS141_28-1	01.03.2024 01:29	454	64° 48.740‘ S	100° 21.071‘ E	18
PS141_34-1	04.03.2024 08:37	783	66° 02.818‘ S	109° 33.658‘ E	20
PS141_37-2	05.03.2024 04:37	2296	66° 33.028‘ S	110° 21.168‘ E	21
PS141_49-4	11.03.2024 15:51	2455	64° 55.774‘ S	106° 51.595‘ E	22
PS141_61-1	17.03.2024 02:21	471	66° 30.601‘ S	089° 56.433‘ E	no data
PS141_62-3	17.03.2024 11:00	1054	66° 18.565‘ S	090° 20.565‘ E	23
PS141_64-3	19.03.2024 11:01	1877	63° 49.746‘ S	098° 02.155‘ E	24
PS141_66-1	20.03.2024 03:45	406	64° 10.620‘ S	098°46.102‘ E	25
PS141_72-1	21.03.2024 07:37	538	65° 46.688‘ S	100° 12.969‘ E	26
PS141_84-3	26.03.2024 17:06	1458	63° 45.070‘ S	098° 54.070‘ E	27

Plankton Multi-Net Sampling

During the cruise, plankton was collected using a multiple closing plankton net (Hydrobios Kiel, nominal opening area of 0.25 m^2) with five nets (55 µm mesh size for calcifying plankton), allowing stratified vertical sampling of five depth intervals (Fig. 4.2). A total of 14 stations were sampled. Most stations consisted of two multinet casts (total number of casts: 23). The “shallow” cast comprised five fixed sampling intervals (100–80 m, 80–60 m, 60–40 m 40–20 m, 20–0 m). Following this first cast, a second “deep” cast (surface–600 m) comprised five non-fixed depth intervals. The choice of those sampling intervals was dependant on the individual water mass characteristics and the chlorophyll maxima as indicated from the pre-existing

CTD cast. Usually, depth ranges were chosen based on presumed habitats of deep-dwelling foraminiferal and pteropod species, in connection with the depth distribution of the seasonal mixed layer and mesopelagic water masses. Sampling locations and depth ranges are listed in Table 4.3 for each Multi-Net cast.

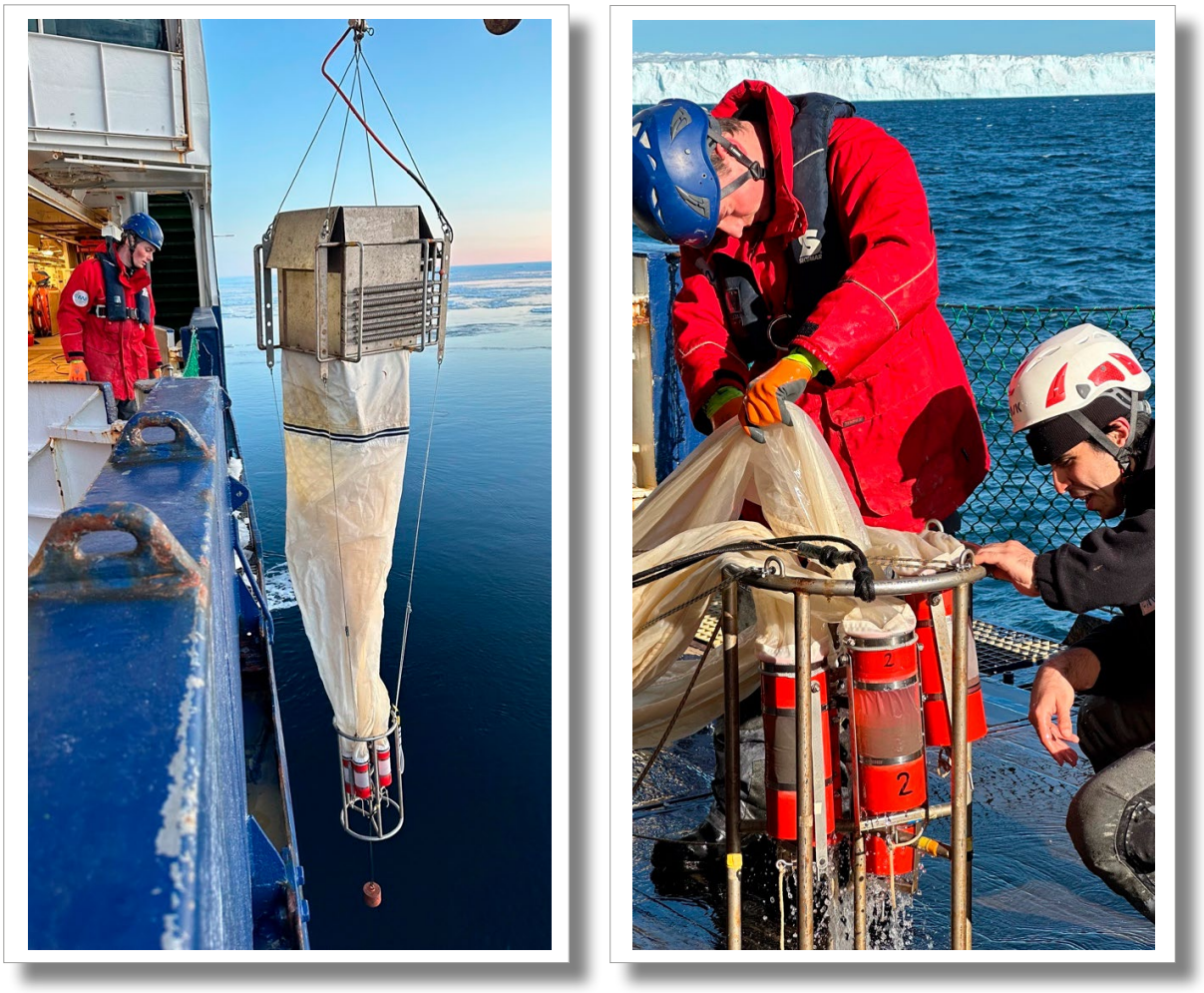

Fig. 4.2: Deployment and retrieval of Hydrobios Multi-Net during PS141.

Slacking was carried out at a speed of 0.5 m/s and hoisting at 0.3 m/s. After each haul the nets were washed with sea water and the net cups were rinsed with filtered sea water. The residue of the net cups, containing the plankton >55 µm was fixed with a filtered seawater – ethanol (1:1) solution and stored at 4°C. Calcifying plankton will be sorted and counted from sampling bottles in shore-based laboratories. The fifth cup of each deep multi-net cast was used to sample the interval between 100 m and the surface and was fixed according to a modified protocol for analysis at the Naturalis in Leiden. Those net cups were rinsed and fixed with 99 % clean ethanol and stored at –20°C.

Tab. 4.3: Locations of Multi-Net stations, hauls and depth ranges during PS141.

Station	Date	Event Time [UTC]	Depth [m]	Latitude	Longitude	Sampling intervals
PS141_01-03	2/8/2024	1:55	4752	44° 08.318‘ S	140° 53.714‘ E	600-400-200-100-60-0
PS141_02-02	2/9/2024	2:08	4650	44° 04.564‘ S	137° 01.964‘ E	100-80-60-40-20-0
PS141_02-03	2/9/2024	2:38	4587	44° 04.640‘ S	137° 02.131‘ E	600-400-300-200-100-0
PS141_03-04	2/10/2024	11:48	4006	46° 57.115‘ S	134° 45.451‘ E	100-80-60-40-20-0
PS141_03-05	2/10/2024	12:18	4005	46° 57.095‘ S	135° 45.407‘ E	600-350-250-172-100-0
PS141_04-02	2/12/2024	7:30	3602	51° 50.685‘ S	130° 06.887‘ E	600-400-300-200-125-0
PS141_05-02	2/14/2024	0:06	4708	56° 19.478‘ S	124° 49.034‘ E	100-80-60-40-20-0
PS141_05-03	2/14/2024	0:33	4708	56° 19.459‘ S	124° 49.103‘ E	600-400-250-200-100-0
PS141_06-04	2/16/2024	14:23	4513	59° 44.968‘ S	114° 53.295‘ E	100-80-60-40-20-0
PS141_06-05	2/16/2024	14:57	4513	59° 45.006‘ S	114° 53.332‘ E	600-400-30-200-100-0
PS141_07-03	2/18/2024	5:12	2880	63° 38.552‘ S	107° 05.466‘ E	Error*
PS141_34-02	3/4/2024	9:35	781	66° 02.788‘ S	109° 33.540‘ E	100-80-60-40-20-0
PS141_34-03	3/4/2024	10:03	782	66° 02.820‘ S	109° 33.586‘ E	500-400-300-225-0
PS141_37-03	3/5/2024	6:09	2304	66° 33.150‘ S	110° 21.197‘ E	100-80-60-40-20-0
PS141_37-04	3/5/2024	6:38	2301	66° 33.140‘ S	110° 21.229‘ E	551-450-300-150-100-0
PS141_49-05	3/11/2024	17:14	2455	64° 55.786‘ S	106° 51.547‘ E	100-80-60-40-20-0
PS141_49-06	3/11/2024	18:03	2458	64° 55.742‘ S	106° 51.516‘ E	500-400-250-150-100-0
PS141_61-02	3/17/2024	3:30	475	66° 30.576‘ S	089° 56.465‘ E	300-200-100-75-50-0
PS141_62-03	3/17/2024	4:28	458	66° 30.505‘ S	089° 56.544‘ E	390-300-200-100-40-0
PS141_62-04	3/17/2024	12:37	1046	66° 18.538‘ S	090° 20.448‘ E	100-80-60-40-20-0
PS141_62-05	3/17/2024	13:11	1046	66° 18.497‘ S	090° 20.163‘ E	600-400-300-220-100-0
PS141_64-03	3/19/2024	12:05	1879	63° 49.749‘ S	098° 02.156‘ E	100-80-60-40-20-0
PS141_64-04	3/19/2024	12:40	1878	63° 49.723‘ S	098° 02.168‘ E	600-400-300-200-100-0

* Net change motor malfunction, cast aborted, no sample retrieval

Multinet sample fixation, for DNA extraction.

At Station PS141_61-2 on 17/03/2024, live pteropod specimen from the deepest multinet (Net No. 3, 75 – 100 m depth) were collected and fixed according to a protocol to allow for later shore-based genetic material extraction. After retrieving the multinet device back to the working deck, net no. 3 was chosen visually as it contained more biological material compared to the other four nets, to extract individual pteropod samples. The biological material was transferred to a petri dish for further microscopic analysis. 26 specimens of the species *Limacina helicina* Antarctica were collected from the petri dish using an Eppendorf pipette and transferred to separate plastic ("Krantz/Fema") storage cells. After the collection of the 26 samples, Milli-Q water was used on each sample cell (five rinses per sample, while trying to remove as much water as possible by using the same pipette in between the cleaning rounds) in order to remove organic and other detrital organic material. After the cleaning step, the samples were dried at room temperature and stored into -80°C freezer afterwards.

Handnet

At five coring stations, additional plankton samples were collected with a Hydrobios Hand net with a mesh size of 200 µm and a diameter of 50 cm (Tab. 4.4). The hand net was lowered manually to an approximate depth range of 5 – 10 m and remained in the water for 10 minutes. The net was dragged along the side of the ship to generate throughflow, which led to a varying depth throughout the deployment. The samples were then fixed according to the same protocol as the Multinet samples in a (1:1) filtered seawater – ethanol mix for further analysis in shore-based laboratories.

Tab. 4.4: List of manual Hand-Net stations during PS141.

Station	Date	Event Time [UTC]	Latitude	Longitude
PS141_23-3	2/29/2024	4:31	65° 38.603‘ S	099° 56.031‘ E
PS141_42-2	3/10/2024	10:26	66° 15.694‘ S	108° 18.720‘ E
PS141_47-3	3/11/2024	2:33	65° 39.426‘ S	107° 52.525‘ E
PS141_48-2	3/11/2024	6:09	65° 25.682‘ S	107° 25.945‘ E
PS141_49-2	3/11/2024	10:11	64° 55.789‘ S	106° 51.595‘ E

Underway membrane pump plankton filtration

Surface water from the ship's membrane pump (11m water depth) were filtered across a 63 µm sieve, in order to be able to collect planktic organisms (e.g. pteropods and foraminifera) in the near-surface seawater during the cruise along routes (Tab. 4.5). Up to three times a day, a varying amount of water was filtered (depending on the plankton density) and fixed according to the same protocol as the multinet samples in a (1:1) filtered seawater, ethanol mix. During each filtering interval, water samples from the same pump system were taken for trace elements, oxygen isotopes and pH measurements. The pH measurements were done immediately on board, while the other samples will be analysed in the home laboratories.

Tab. 4.5: Overview of the filtered seawater samples, locations, time intervals during PS141. *nr=not recorded.*

PF#	Longitude start	Latitude start	Longitude end	Latitude end	filtered volume [m^3]	Comment
1	nr	nr	nr	nr	0.622	missing data
2	135° 14.252’ E	46° 19.256’ S	134° 45.022’ E	46° 58.499’ S	0.631	
3	133° 09.615’ E	48° 47.397’ S	nr	nr	0	sample lost, missing data
4	132° 41.329’ E	49° 17.851’ S	132° 26.473’ E	49° 32.862’ S	0.294	
5	132° 26.480’ E	49° 32.875’ S	131° 51.444’ E	50° 07.945’ S	0.167	
6	131° 19.682’ E	50° 39.397’ S	130° 26.615’ E	51° 31.148’ S	1.337	
7	128° 09.641’ E	53° 37.884’ S	128° 30.324’ E	54° 24.5815’S	1.611	
8	128° 30.324’ E	54° 24.582’ S	126° 21.428’ E	55° 06.409’ S	0.979	
9	126° 21.428’ E	55° 06.409’ S	124° 48.317’ E	50° 20.707’ S	0.540	
10	124° 27.924’ E	56° 28.068’ S	121° 11.451’ E	57° 46.633’ S	0.662	
11	121° 11.451’ E	57° 46.633’ S	119° 53.896’ E	58° 16.879’ S	0.844	
12	114° 20.360’ E	59° 58.119’ S	nr	nr	0.098	missing data
13	110° 30.668’ E	61° 43.546’ S	109° 44.554’ E	62° 10.050’ S	0.099	
14	nr	nr	107° 05.493’ E	63° 38.531’ S	0.038	missing data
15	106° 23.011’ E	63° 47.169’ S	100° 18.503’ E	65° 42.090’ S	0.581	
16	098° 58.274’ E	63° 58.114’ S	097° 52.441’ E	63° 49.391’ S	0.319	
17	096° 16.598’ E	63° 42.576’ S	094° 18.300’ E	64° 06.600’ S	0.677	
18	093° 35.580’ E	64° 25.380’ S	091° 29.520’ E	65° 27.900’ S	0.475	
19	091° 29.520’ E	65° 27.900’ S	nr	nr	0.854	missing data
20	094° 48.620’ E	65° 18.153’ S	093° 43.064’ E	65° 07.993’ S	0.700	
21	100° 15.889’ E	64° 50.560’ S	100° 19.379’ E	65° 42.498’ S	0.467	
22	100° 09.634’ E	65° 30.667’ S	100° 21.058’ E	64° 48.743’ S	0.280	
	105° 02.043’ E	64° 52.923’ S	nr	nr	0.081	sample lost
23	105° 14.161’ E	65° 04.677’ S	109° 42.200’ E	66° 01.808’ S	1.704	
24	107° 44.307’ E	65° 31.410’ S	108° 11.359’ E	65° 40.543’ S	0.133	
25	108° 04.831’ E	65° 33.480’ S	108° 13.476’ E	65° 43.810’ S	0.120	
26	109° 43.260’ E	66° 25.720’ S	108° 44.070’ E	66° 25.740’ S	0.175	
27	039° 22.040’ E	61° 33.564’ S	038° 06.270’ E	61° 05.926’ S	0.207	
28	035° 59.720’ E	60° 18.619’ S	032° 26.420’ E	58° 56.154’ S	1.520	
29	032° 26.420’ E	58° 56.154’ S	030° 40.561’ E	58° 14.048’ S	0.686	
30	030° 36.480’ E	58° 12.334’ S	028° 50.812’ E	57° 29.600’ S	0.704	
31	026° 12.742’ E	56° 23.500’ S	024° 31.541’ E	55° 40.282’ S	0.565	
32	024° 31.542’ E	55° 40.282’ S	023° 02.560’ E	55° 01.587’ S	0.919	
33	022° 28.237’ E	53° 57.518’ S	021° 49.880’ E	52° 39.563’ S	0.624	
34	021° 49.700’ E	52° 39.365’ S	021° 11.118’ E	51° 18.295’ S	0.503	
35	021° 10.460’ E	51° 16.867’ S	020° 36.750’ E	50° 04.163’ S	0.663	
36	020° 36.750’ E	50° 04.163’ S	019° 53.161’ E	48° 27.305’ S	0.798	
37	019° 52.342’ E	48° 25.519’ S	019° 22.883’ E	47° 18.190’ S	0.823	
38	019° 19.767’ E	47° 10.978’ S	018° 53.425’ E	46° 09.496’ S	0.778	
39	018° 50.491’ E	46° 02.482’ S	018° 26.188’ E	45° 04.583’ S	0.843	

PF#	Longitude start	Latitude start	Longitude end	Latitude end	filtered volume [m^3]	Comment
40	018° 23.273' E	44° 57.492' S	017° 43.141' E	43° 19.521' S	0.701	
41	017° 40.969' E	43° 14.067' S	017° 14.900' E	42° 06.301' S	0.356	
42	017° 14.900' E	42° 06.301' S	016° 44.319' E	40° 50.622' S	1.307	
43	016° 44.319' E	40° 50.622' S	016° 08.525' E	39° 17.160' S	0.175	
44	016° 07.454' E	39° 14.522' S	015° 29.694' E	37° 33.617' S	0.507	
45	015° 28.700' E	37° 30.900' S	015° 06.622' E	36° 30.855' S	0.568	

Preliminary results

Due to the extensive work programme during the expedition, we kept analyses as well as sample and data processing to generate shipboard results to a minimum. Almost all subsequent works are planned to be carried out shore-based after receiving all samples and data during the shipyard port of call of *Polarstern* in Bremerhaven in May 2024. Expected results for the individual aims are to establish novel pteropod-based proxies for both carbonate system and temperature. Furthermore, we expect to be able to ground-truth selected foraminifera-based proxies. We hypothesize that the biogeographical distribution of pteropod assemblages will largely mirror the distribution of Longhurst's biogeochemical provinces (Longhurst et al., 1995). Furthermore, we hope to discover new pteropod species diversity within the *Limacina* genus with distinct ecologies. We expect to add to reference DNA barcoding libraries (Biodiversity of Life Database: https://www.boldsystems.org/ and MetaZooGene: https://metazoogene.org/mzgdb/), with voucher specimens and DNA stored at Naturalis Biodiversity center. Lastly, we hope to enhance the understanding of trace metal supply and dispersal in sub-Antarctic waters, a key to developing a reference frame for more accurate reconstructions of past oceanic conditions.

Out of the total 25 CTD stations with water sampling, seven stations track the transit across the frontal zone region in the Austral-Indian Southern Ocean (Figs. 4.1 and 4.3). All major water masses along this transect: Antarctic Bottom Water (AABW), Lower and Upper Circumpolar Deep Water (LCDW and UCDW), as well as Antarctic Intermediate Water (AAIW) and Antarctic Surface Waters (AASW) were covered by the hydrocasts and sampled with a total of 525 samples taken for each primary tracer ($\delta^{18}O$, $\delta^{13}C_{DIC}$, nutrients) and lower respective numbers for AMS ^{14}C, DIC, trace metals, etc. In total about 2,000 discrete water samples were taken. In addition, on 12 stations we sampled about 120 samples with mostly double net tows, despite the challenging weather conditions and sea states and a flooded Multi-net control unit.

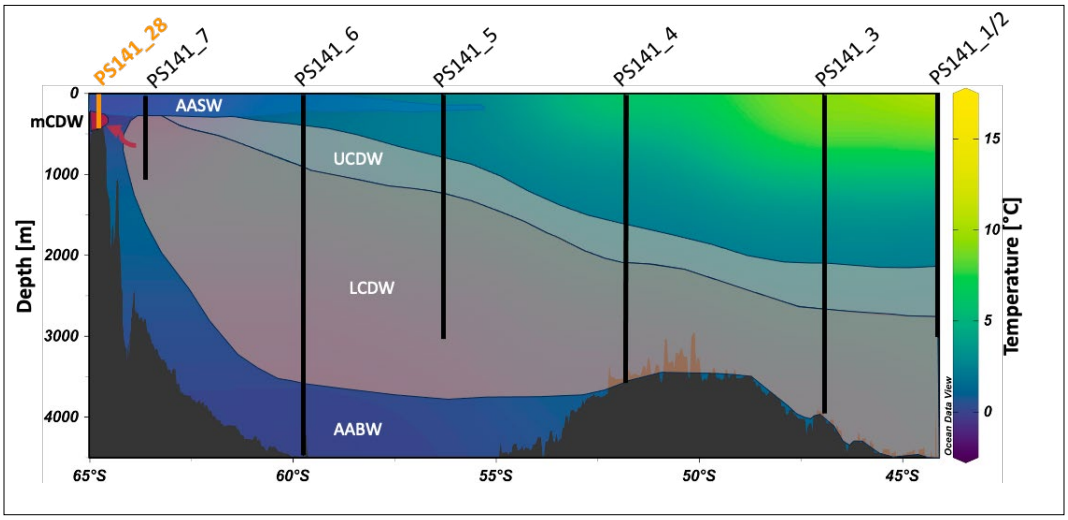

Fig. 4.3: Cross-section of transect across oceanic frontal zones on PS141, showing temperatures in colour shading. Black lines denote stations on which CTD and Rosette water sampler, Multinet (MN), or both were deployed. Ocean Data View software was used for visualisation of data (Schlitzer, 2004)

Along the shelf areas, the three major work areas were from West to East (i) The E' Davis Sea off Gaussberg and W' Shackleton Ice Shelf (Fig. 4.4); (ii) the W' Mawson Sea off Denman Glacier and Bunger Hills (Fig. 4.6); and (iii) Vincennes Bay off Casey Station and Vanderford Glacier (Fig. 4.8).

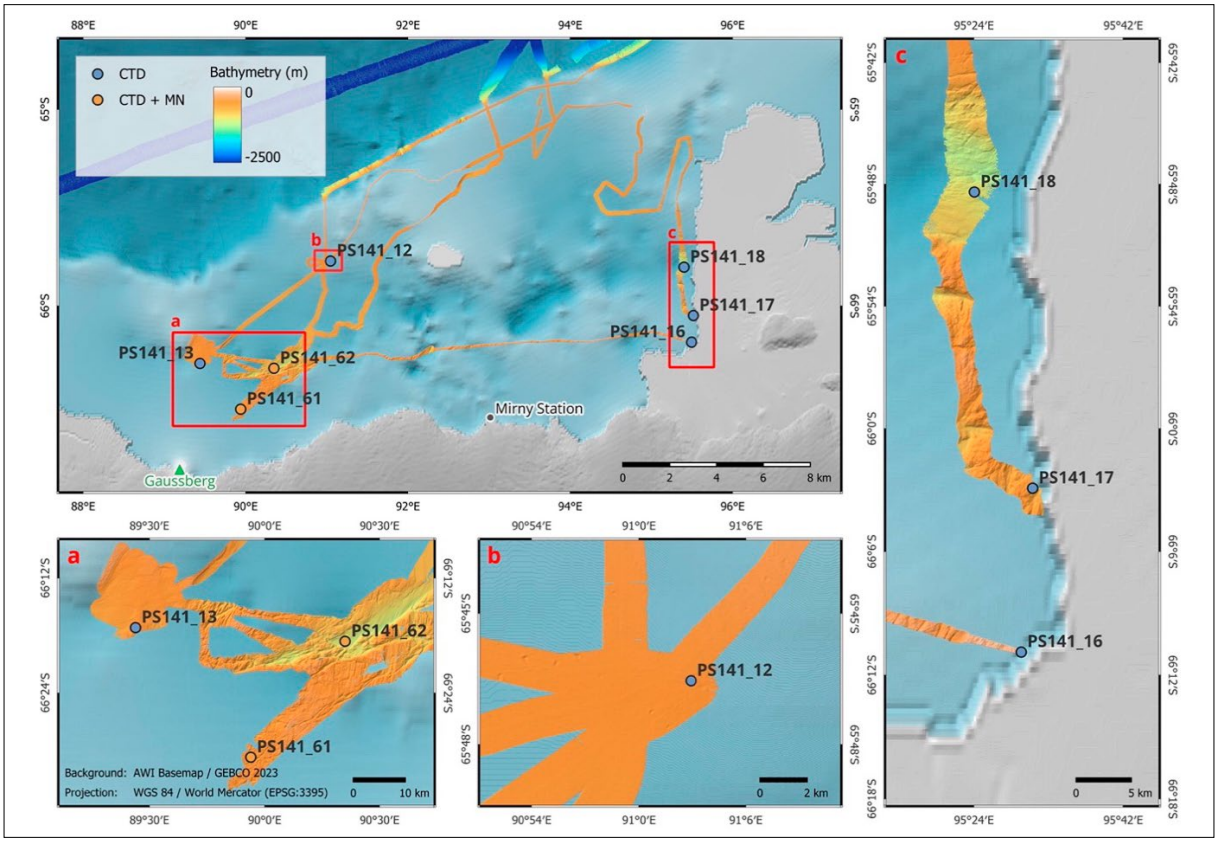

Fig. 4.4: Map of Hydrocast and plankton-net station in working area E' Davis Sea off Gaussberg and W' Shackleton Ice Shelf (Fig. 4.1). Bathymetric shading is a composite of IBSCO data (Dorschel et al., 2022) and swath bathymetry data acquired during PS141.

PS141/EASI-3 CTD

PS141_16-1

Longitude: 95.495874
Latitude: -66.181042
UTC (Time): 26.02.2024 03:41
Water depth: 169 m

Bottle	Depth [m]	Pressure [db]	Salinity [PSU]	Temperature [°C]	Oxygen [ml/l]	Density [kg/m^2]	Fluorecence [mg/m^2]
1	180.234	182.113	34.3176	-1.8518	6.8984	1028.5046	-0.0532
2	175.252	177.078	34.3159	-1.8556	6.89309	1028.4792	-0.0015
3	170.646	172.421	34.3133	-1.8616	6.89742	1028.4549	-0.0044
4	165.034	166.749	34.308	-1.8721	6.89413	1028.4236	-0.0348
5	155.229	156.838	34.3063	-1.8757	6.90016	1028.3747	0.0546
6	145.556	147.061	34.294	-1.888	6.92194	1028.318	0.0277
7	124.841	126.126	34.2823	-1.9057	6.92067	1028.2083	0.124
8	100.102	101.126	34.2774	-1.9168	6.91208	1028.0843	0.0764
9	74.821	75.582	34.2732	-1.9197	6.91946	1027.9578	0.7773
10	50.519	51.03	34.2561	-1.9127	6.9702	1027.8253	0.6043
11	25.12	25.372	34.1903	-1.8482	7.25275	1027.6464	1.876
12	20.85	21.059	34.2218	-1.878	7.11969	1027.652	1.1877
13	10.83	10.939	34.0747	-1.8573	7.65255	1027.483	2.3907
14	5.154	5.205	34.0602	-1.8317	7.73825	1027.4429	2.1121
15	0.837	0.845	34.0463	-1.8666	7.75201	1027.4114	1.4215
16	0.906	0.915	34.0532	-1.8673	7.7502	1027.4173	1.3379
17	1.021	1.031	34.0495	-1.8668	7.75637	1027.4148	1.2215
18	0.918	0.927	34.0499	-1.867	7.7555	1027.4146	1.0708
19	0.867	0.875	34.0487	-1.8668	7.74834	1027.4135	1.2932
20	0.866	0.875	34.0517	-1.8669	7.76007	1027.4159	1.2507
21	0.767	0.775	34.054	-1.8682	7.76074	1027.4173	1.1522
24	0.88	0.889	34.0546	-1.8666	7.7448	1027.4183	1.0954

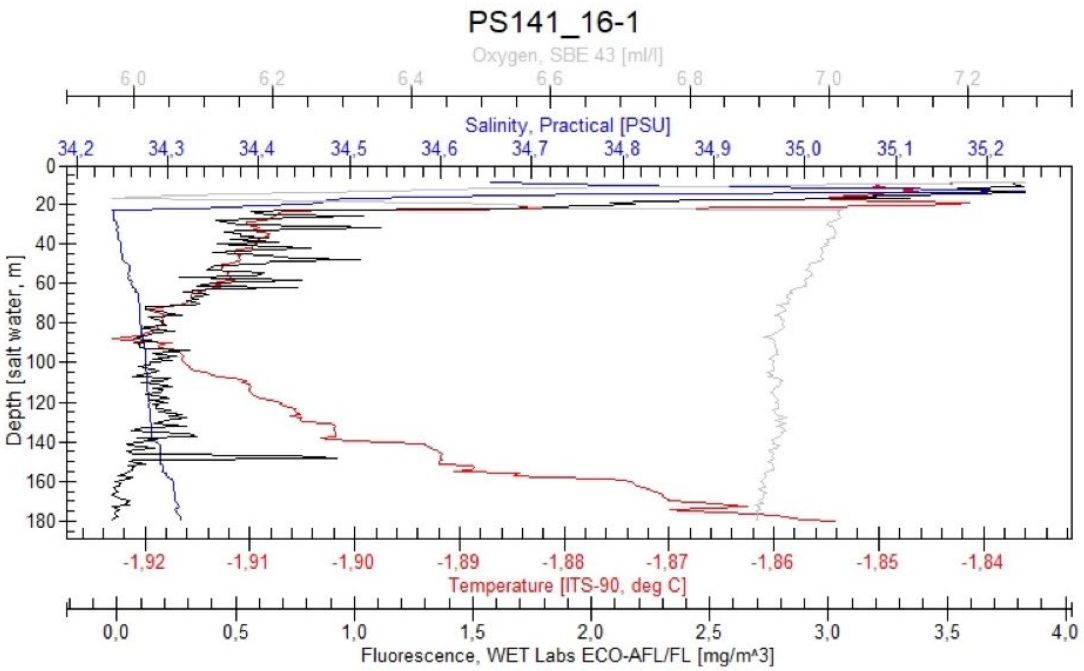

Fig. 4.5: CTD cast at Station PS141_16 (66°10.891' S, 95°29.699' E), an exemplary cast in the in working area E' Davis Sea off Gaussberg and W' Shackleton Ice Shelf (see Fig. 4.4).

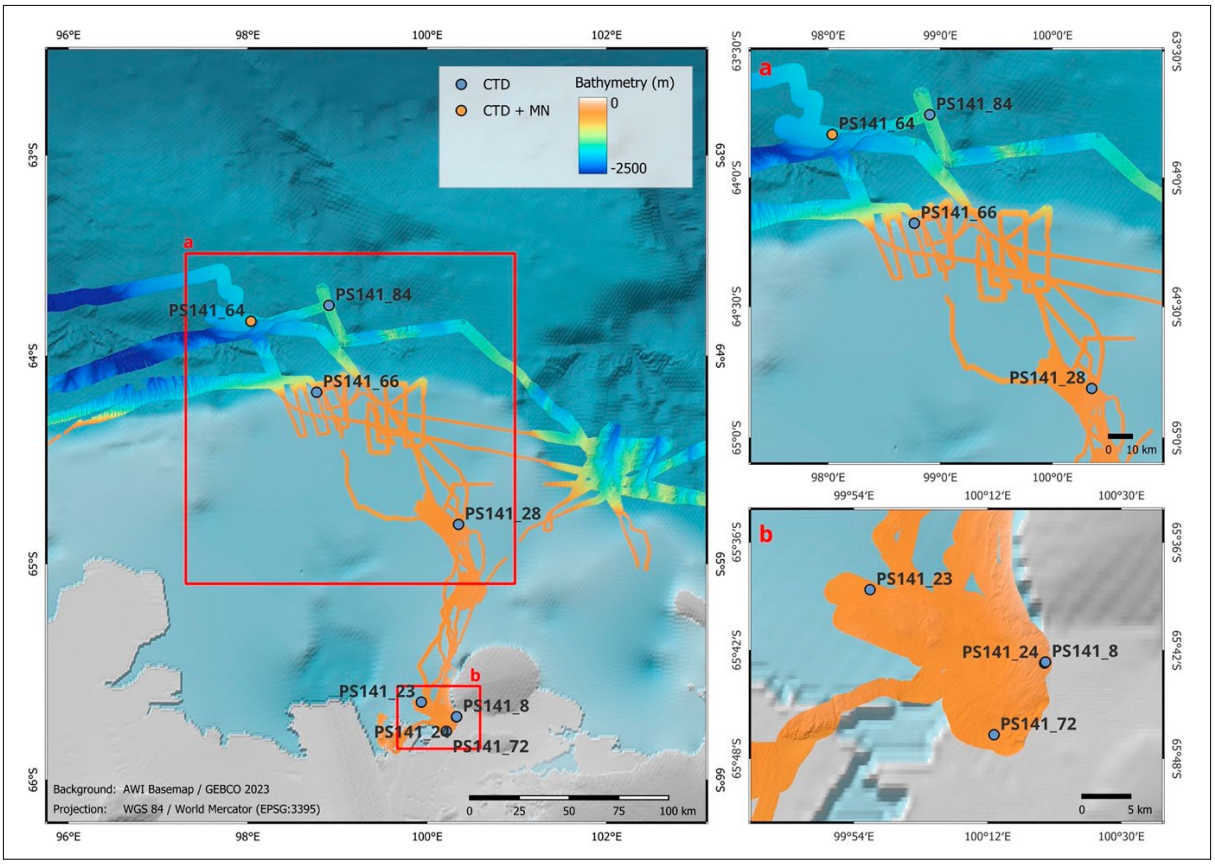

Fig. 4.6: Map with station locations of Hydrocast and plankton-net station in working area W' Mawson Sea off Denman Glacier and Bunger Hills (see Fig. 4.1). Bathymetric shading is a composite of IBSCO data (Dorschel et al., 2022) and swath bathymetry data acquired during PS141.

PS141/EASI-3 CTD

PS141_66-1

Longitude: 98.769154
Latitude: -64.176898
UTC (Time): 20.03.2024 03:27
Water depth: 406 m

Bottle	Depth [m]	Pressure [db]	Salinity [PSU]	Temperature [°C]	Oxygen [ml/l]	Density [kg/m^2]	Fluorecence [mg/m^2]
1	392.943	397.191	34.4684	-1.2741	6.38132	1029.6333	-0.0549
2	381.533	385.647	34.4586	-1.3449	6.45818	1029.5736	0.0174
3	360.873	364.746	34.4336	-1.5211	6.64671	1029.4614	-0.0509
4	351.695	355.461	34.4293	-1.5483	6.68918	1029.4148	-0.0509
5	340.568	344.206	34.42	-1.6136	6.74717	1029.3561	-0.052
6	324.85	328.307	34.4205	-1.6142	6.75111	1029.2805	-0.0554
7	301.816	305.011	34.416	-1.6317	6.77077	1029.1661	-0.0549
8	275.759	278.661	34.4028	-1.6961	6.83062	1029.0317	-0.0514
9	250.647	253.269	34.3917	-1.7278	6.86211	1028.9021	-0.0526
10	225.288	227.63	34.388	-1.7363	6.87692	1028.7765	-0.048
11	201.017	203.095	34.3744	-1.763	6.9012	1028.6486	-0.0302
12	149.702	151.23	34.3504	-1.788	6.94688	1028.3808	0.0048
13	124.083	125.342	34.3419	-1.7955	6.9759	1028.2497	-0.0251
14	106.66	107.738	34.3358	-1.798	6.99907	1028.1601	-0.0273
15	100.338	101.35	34.3267	-1.8006	7.02586	1028.122	0.0059
16	76.835	77.605	34.2814	-1.7783	7.09437	1027.9702	0.0294
17	55.071	55.62	34.2081	-1.7176	7.17888	1027.803	0.061
18	46.379	46.841	34.1409	-1.6868	7.30963	1027.7053	0.1194
19	30.025	30.323	33.885	-1.6053	7.69435	1027.4154	0.2713
20	20.585	20.788	33.8217	-1.532	7.7788	1027.3159	0.2827
21	10.689	10.794	33.8024	-1.476	7.78154	1027.2504	0.2558
24	1.946	1.965	33.8023	-1.4713	7.77873	1027.2077	0.1715

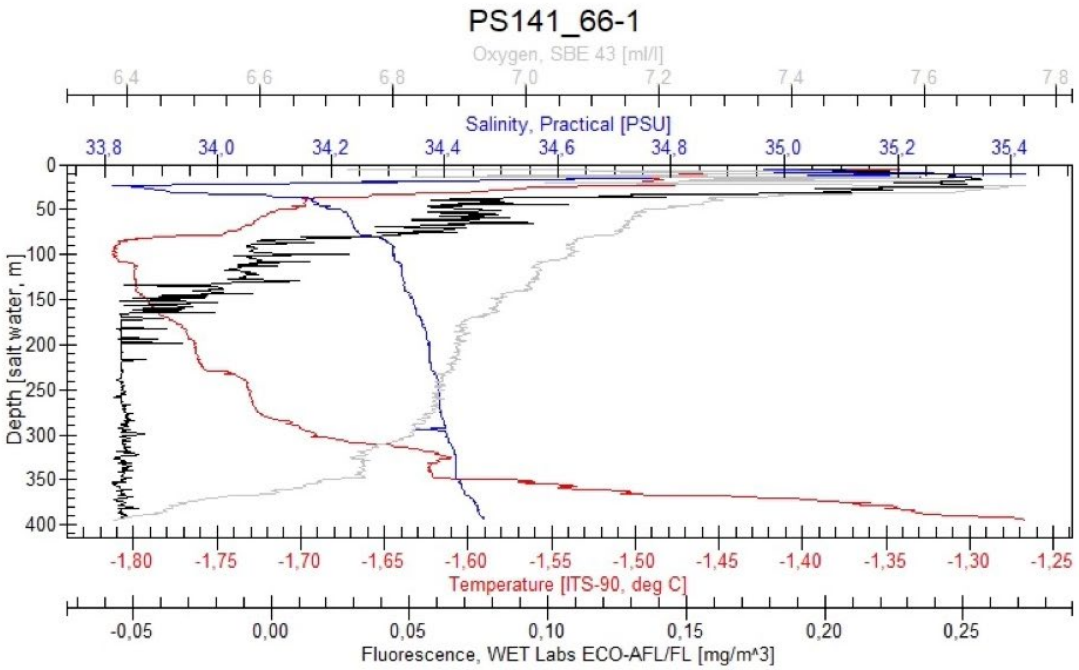

Fig. 4.7: CTD cast at Station PS141_66 (64° 10.620' S, 098°46.102' E), an exemplary cast in the in working area W' Mawson Sea off Denman Glacier and Bunger Hills (see Fig. 4.6).

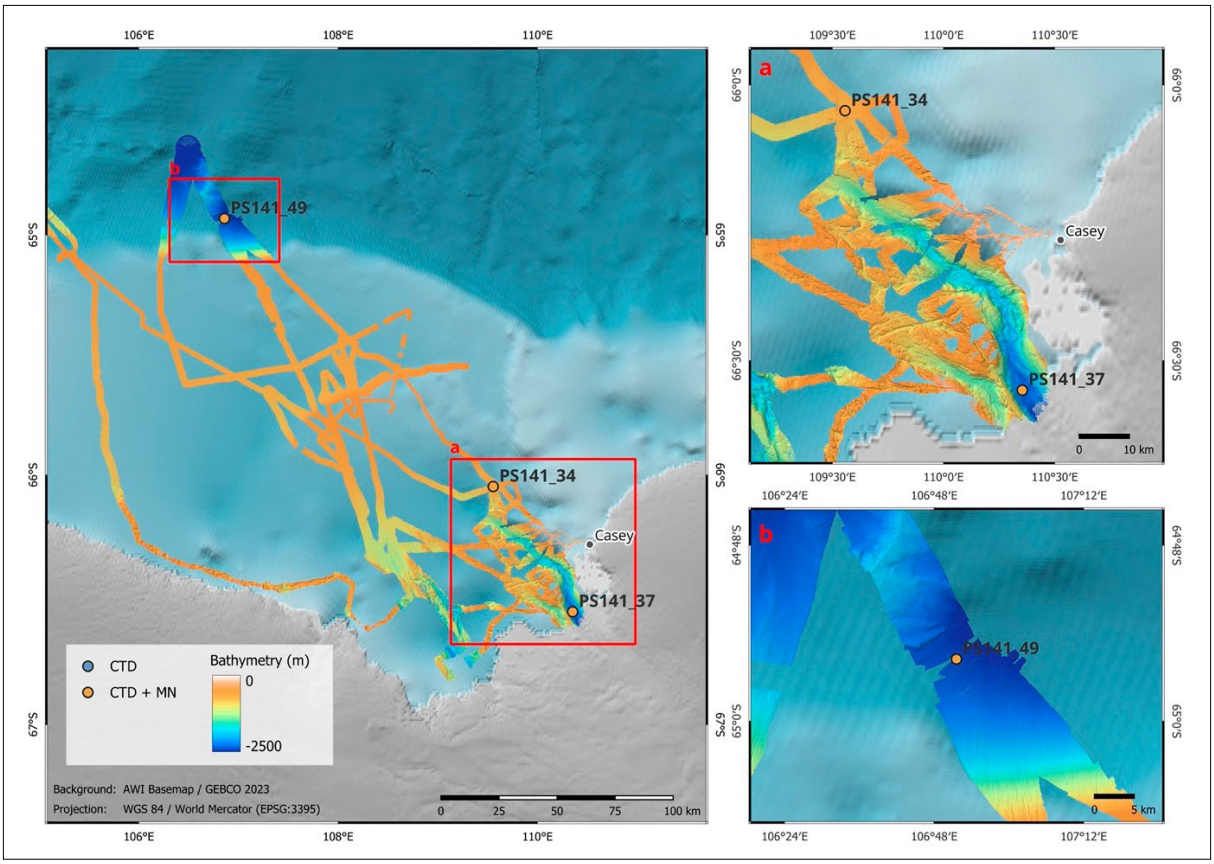

Fig. 4.8: Map with station locations of Hydrocast and plankton-net station in working area in Vincennes Bay off Casey Station and Vanderford Glacier (see Fig. 4.1). Bathymetric shading is a composite of IBSCO data (Dorschel et al., 2022) and swath bathymetry data acquired during PS141

PS141/EASI-3 CTD

PS141_49-4

Longitude: 106.860158
Latitude: -64.929946
UTC (Time): 11.03.2024 14:59
Water depth: 2455 m

Bottle	Depth [m]	Pressure [db]	Salinity [PSU]	Temperature [°C]	Oxygen [ml/l]	Density [kg/m^2]	Fluorecence [mg/m^2]
1	2407.941	2445.938	34.6443	-0.2216	5.05229	1039.1993	-0.0737
2	2200.463	2234.083	34.6458	-0.2005	5.02159	1038.2371	-0.0829
3	1999.049	2028.616	34.6512	-0.1254	4.9456	1037.2973	-0.0697
4	1799.432	1825.175	34.6542	-0.0687	4.89978	1036.3632	-0.0898
5	1599.076	1621.174	34.6573	0.0078	4.79794	1035.4212	-0.0846
6	1399.999	1418.667	34.6601	0.0831	4.74911	1034.4826	-0.0875
7	1199.306	1214.71	34.6646	0.1797	4.66104	1033.5334	-0.0926
8	1000.217	1012.576	34.6681	0.2898	4.59546	1032.5875	-0.0737
9	899.545	910.438	34.667	0.3113	4.59571	1032.109	-0.0703
10	800.57	810.07	34.6749	0.4344	4.54248	1031.6367	-0.0697
11	725.292	733.765	34.6731	0.4647	4.53072	1031.2761	-0.0726
12	599.434	606.251	34.6818	0.6278	4.44716	1030.6732	-0.0577
13	499.9	505.463	34.685	0.729	4.41337	1030.1952	-0.0898
14	450.477	455.435	34.6803	0.7283	4.4368	1029.9565	-0.068
15	400.027	404.38	34.6647	0.6497	4.51166	1029.7098	-0.0566
16	249.549	252.172	34.4953	-0.7097	5.70327	1028.9369	-0.056
17	150.35	151.894	34.3714	-1.6215	6.43115	1028.3956	-0.0503
18	90.028	90.939	34.3039	-1.6685	6.45025	1028.0494	0.0724
19	70.264	70.972	34.2854	-1.6973	6.47666	1027.9392	0.0736
20	50.409	50.914	34.2561	-1.6952	6.50077	1027.8187	0.3974
21	30.029	30.329	34.0981	-0.9994	6.76251	1027.5679	0.9837
24	9.696	9.793	33.9309	-0.198	7.19737	1027.2997	0.6977

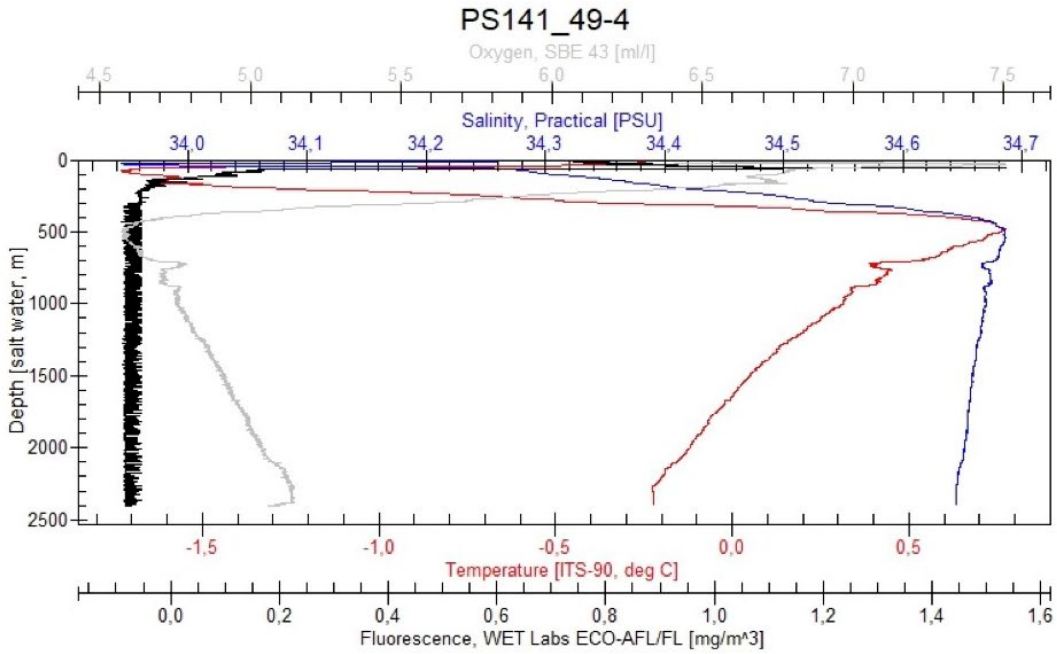

Fig. 4.9: CTD cast at Station PS141_49 (64° 55.774' S, 106° 51.595' E), an exemplary cast in the in working area W' Mawson Sea off Denman Glacier and Bunger Hills (see Fig. 4.8)

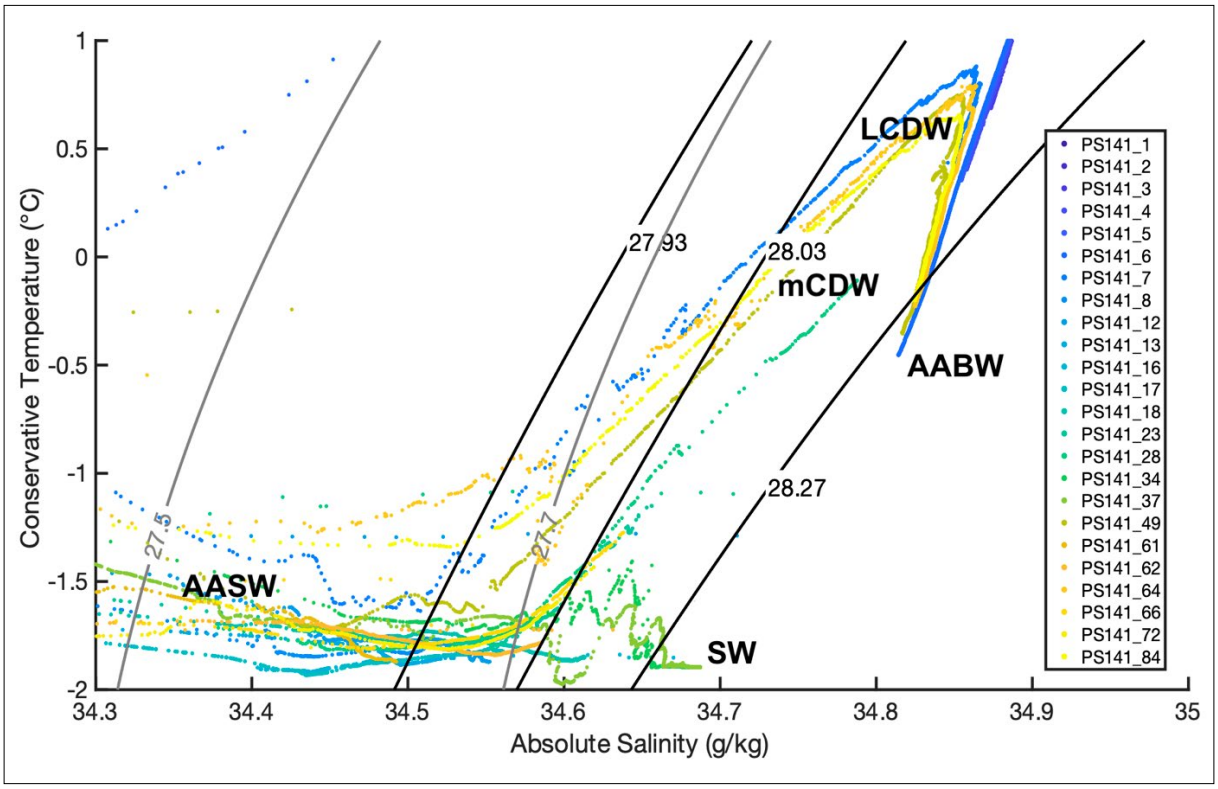

Fig. 4.10: Temperature-Salinity relationship for CTD stations of PS141 with bounding neutral density anomaly contours (black) and potential density anomaly contours (grey). AASW (Antarctic Surface Water); SW (Shelf Water); mCDW (modified Circumpolar Deep Water); LCDW (Lower circumpolar Deep Water); AABW (Antarctic Bottom Water)

We performed a total of seven CTD casts along the transect from Hobart to Antarctica, seven in the working area E' Davis Sea off Gaussberg and W' Shackleton Ice Shelf (Fig. 4.4), eight in the working area W' Mawson Sea off Denman Glacier and Bunger Hills (Fig. 4.6) and three in the working area in Vincennes Bay off Casey Station and Vanderford Glacier (Fig. 4.8). Water depths were largest on transit stations (4,752 m, station PS141_1), while shelf stations had lower water depths (e.g. 180 m on Station PS141_16, Fig. 4.5). The temperature vs. salinity (T-S) diagram is shown in Fig. 4.10, with T and S as conservative tracers, modified only by the interaction with the atmosphere and by mixing with other waters, not by biological or chemical activities. These properties allowed us to identify water masses along the PS141 transect, corroborating water mass characteristics already indicated in the temperature profile along the transect (Fig. 4.3). The major water masses identified are Shelf Water (SW), Antarctic Surface Water (AASW), Upper and Lower Circumpolar Deep Water (UCDW, LCDW), Antarctic Bottom Water (AABW) and modified Circumpolar Deep Water (mCDW). This water mass could likely be traced to selected shelf sites in one working area, being especially pronounced at stations along 100 °E with temperatures of up to -0.1 °C. On other stations proximal to the ice shelf, water temperatures were slightly higher at near-bottom depth, but remained close to overlying waters.

Data management

Plankton and water samples retrieved during the cruise will be transferred to CAU and AWI-Bremerhaven. Analytical data obtained on all samples will be published in peer-reviewed journals. Access for the science community will also be provided via the geoscientific database PANGAEA (https://www.pangaea.de), once the data are published or at the latest 4 years

after the end of the expedition (moratorium period). Directly after publication, data will be freely accessible. To avoid research overlap, the availability of the sample material from this expedition will be restricted to PS141 EASI-3 participants and collaborators for a period of a maximum of 4 years after the cruise. Afterwards, the material will be available for the wider scientific community.

The research activities are directly related to the objectives of Topic 2 (Ocean and Cryosphere in Climate) with a focus on Subtopics 2.1 (Warming Climate), 2.3 (Sea Level Change), and 2.4 (Advanced Research Technologies for Tomorrow).

In all publications, based on this cruise, the Grant No. AWI_PS141_02 will be quoted and the following article will be cited: Alfred-Wegener-Institut Helmholtz-Zentrum für Polar- und Meeresforschung (2017) Polar Research and Supply Vessel POLARSTERN Operated by the Alfred-Wegener-Institute. Journal of large-scale research facilities, 3, A119. http://dx.doi.org/10.17815/jlsrf-3-163.

References

Dorschel B, Hehemann L, Viquerat S, Warnke F, Dreutter S, Tenberge Y.S, Accettella D, An L, Barrios F, Bazhenova E, Black J, Bohoyo F, Davey C, De Santis L, Dotti CE, Fremand AC, Fretwell PT, Gales JA, Gao J, Gasperini L, Greenbaum JS, Jencks JH, Hogan K, Hong JK, Jakobsson M, Jensen L, Kool J, Larin S, Larter RD, Leitchenkov G, Loubrieu B, Mackay K, Mayer L, Millan R, Morlighem M, Navidad F, Nitsche FO, Nogi Y, Pertuisot C, Post AL, Pritchard HD, Purser A, Rebesco M, Rignot E, Roberts JL, Rovere M, Ryzhov I, Sauli C, Schmitt T, Silvano A, Smith J, Snaith H, Tate AJ, Tinto K, Vandenbossche P, Weatherall P, Wintersteller P, Yang C, Zhang T, Arndt JE. The International Bathymetric Chart of the Southern Ocean Version 2 (2022) Scientific Data, 9(1):275. https://doi.org/10.1038/s41597-022-01366-7

Gutjahr M, Esper, O (2024) The Expedition PS140 of the Research Vessel POLARSTERN to the Cooperation Sea and Davis Sea in 2023/2024. Bornemann H and Amir Sawadkuhi S (eds), Berichte zur Polar- und Meeresforschung = Reports on polar and marine research, Bremerhaven, Alfred-Wegener-Institut Helmholtz-Zentrum für Polar- und Meeresforschung, 790, 185 p. https://doi.org/10.57738/BzPM_0790_2024

Keul N, Peijnenburg KTCA, Andersen N, Kitidis V, Goetze E, Schneider R (2017) Pteropods are excellent recorders of surface temperature and carbonate ion concentration, Sci. Rep., 7:12645. https://doi.org/10.1038/s41598-017-11708-w

Lischka S, Büdenbender J, Boxhammer T, Riebesell U (2011) Impact of ocean acidification and elevated temperatures on early juveniles of the polar shelled pteropod Limacina helicina: mortality, shell degradation, and shell growth. Biogeosciences 8:919–932.

Longhurst A, Sathyendranath S, Platt T, Caverhill C (1995) An estimate of global primary production in the ocean from satellite radiometer data. J. Plankt. Res. 17 (6):1245–1271.

Manno C, Bednaršek N, Tarling GA, Peck VL et al. (2017) Shelled pteropods in peril: assessing vulnerability in a high CO2 ocean. Earth Sci. Rev. 169:132–145.

Orsi AH, Whitworth T, Nowlin WD (1995) On the meridional extent and fronts of the Antarctic Circumpolar Current. Deep Sea Res. Part I 42 (5):641–673.

5. ANTARCTIC KRILL STUDIED BY CRABEATER SEALS BENEATH THE SEA ICE: SEAL TAGGING

Sara Labrousse[1], Laurene Trudelle[1]; [1]FR.CNRS
not on board: Marc Eleaume[2], Michelle LaRue[3], [2]FR.MNHN
Jean-Benoit Charrassin[1] [3]NZ.UC

Grant-No. AWI_PS141_09

Objectives

Over the past half century, many climate-induced physical processes have changed the structure and functioning of Antarctic marine ecosystems and the Southern Ocean. The latter is absorbing more and more CO_2 due to the increase in greenhouse gas emissions caused by human activities. The resulting acidification affects calcifying organisms, and also leads to implications for the physiology of crustaceans such as krill (Kawaguchi et al. 2013). Furthermore, increasing ocean temperature, regional and local changes in sea ice thickness and seasonal coverage, and increasing ocean stratification have the potential to profoundly alter marine primary production, its duration and intensity; these changes are already visible in some regions (Meredith et al. 2019). These ongoing changes thus impact the entire local food web, whether it be phytoplankton, zooplankton (krill, primarily), fish, cephalopods, marine mammals and birds, or benthos.

In response to these changes, the distribution of krill in regions of the South Atlantic where the sea ice extent has significantly decreased, has, for example, shifted southward over the past 90 years (Atkinson et al. 2019). This can be easily explained by krill's life traits: their larvae use the sea ice area in winter both as a food source (by grazing on algae growing on the submerged side of the pack ice) and as a refuge from predators and surface currents (Meyer 2012). In doing so, by following the retreat of the sea ice, krill larvae could continue to benefit from refuge areas from their predators. However, it still remains unclear whether or not krill, at the Southern Ocean's scale, will follow their thermal niche southward - under the constraint of climate change - due to the importance of other factors such as depth and amount of primary production. For marine birds and mammals, the degree to which they will be influenced by changes in the Southern Ocean, meanwhile, depends on many factors such as their flexibility to alter their diets, move to alternative foraging areas or resting/breeding habitats for sea-ice-dependent predators, the energy expenditure of longer or more complex foraging trips, or interspecies competition for concentrated or reduced resources (Constable et al. 2014).

Beyond this patchy knowledge, threats to this food web resulting from changes in the Antarctic sea ice remain largely unknown. Mechanistic understanding of the linkages between sea ice, biogeochemical processes, and lower and upper trophic levels remains poor (Ducklow et al. 2007). For example, studies on krill are generally restricted to ice-free waters, as sea ice – when present – hinders both navigation of research icebreakers and satellite visibility of waters beneath the ice. Furthermore, setting up observatories using moorings (fixed buoys equipped with sensors) remains logistically difficult and only allows the collection of information at specific points. The richness, range of opportunities and spatial coverage that polar predator bio-telemetry has provided and will continue to provide in this region are thus essential to

study the Antarctic ecosystem. Indeed, krill is very abundant under the sea ice (Brierley 2002), and many predators feed there. Far from being a homogeneous area, sea ice is a habitat of great heterogeneity that supports very specific biotic and abiotic conditions (Worby et al. 2008; Williams et al. 2014; Meiners et al. 2017). Thus, it is crucial to focus on a mechanistic understanding of the linkages between sea ice and the underlying ecosystem. This is what we propose in this project, focusing on krill, a key link in the Antarctic ecosystem and component of one of the two dominant polar pelagic food webs, as well as its predators.

The objective of our project is to elucidate the mechanisms by which the Antarctic sea ice controls the distribution of krill by studying the functional relationships of krill with their predators. We will study how the functional traits of krill - based on the organization of the swarms they form (e.g. surface area, length, perimeter, average depth, etc.) – influence the functional hunting/foraging/feeding responses of a polar predator – based on its diving behaviour (e.g. dive depths and durations, horizontal and vertical travel speeds, 3D acceleration peaks, etc.).

Work at sea

We deployed tags on 15 individuals opportunistically during the cruise in pack ice zones along the ship-track around Shackleton ice shelf, Bowman Island and Vincennes Bay (Fig. 5.1). Tags were deployed between 27 February and 23 March 2024 just after the crabeater seal moulting period. The helicopter stayed with us on the ice floe for the whole experiments. The total helicopter time used during the cruise including the time they stayed on the ice floe (rotor shut down) was 38 hours 58 minutes corresponding with 13 flights. Tag deployments happened over 10 flights. Flights corresponding with deployments on three individuals lasted ~5 hours (2 flights), on two individuals ~3,5 hours (one flight) and on one individual between 2.2 and 3.5 hours (seven flights). We noticed that crabeater seals were less alarmed by the helicopter when in groups of 1–4 on larger floes or sheltered by ridges from blowing snow (refer to examples of surveyed floes with seals in Fig. 5.2). During specific deployments, certain factors hindered our ability to remain on the ice floe for longer periods to tag multiple seals simultaneously. These included the unpredictable weather conditions typical of this time of year and the distance of the ship (no ship time allocated preventing the boat to wait for us to be back). By late March, heavy snow on top of ice floes made some helicopter landings impossible. Sightings along the ship track or helicopter flights are reported in Fig. 5.3.

Details:

- Seals were located by helicopter in the pack ice areas as previously done by Nordøy and Blix (2009), Nachtsheim et al. (2016) and Wege et al. (2021). Once the seals were observed and inspected at close range, and the state of sea ice for landing was evaluated, the helicopter dropped the staff on ice and stayed. If the animals did not escape to the water, they were immobilized.
- The helicopter dropped four persons on an ice floe in the wider vicinity of sighted crabeater seals. Some equipment was positioned near the helicopter, while the remainder was carried in backpacks. As a precaution, we always had a red survival box containing essentials for an overnight stay on the ice in case of emergency. An ice pick was utilized to identify any hazards like holes and cracks while navigating the floe. AWI and *Polarstern* respectively have long standing experience with seal work on ice (*cf*. Bornemann 2019, 2017, 2014), and protocols have been applied accordingly. Communication devices, including one radio, two GPS units, and one iridium phone, were brought along onto the ice for safety and coordination.
- Fieldworkers wore the helicopter dry suit and life jacket. The helicopter life jacket was changed with the ship life jacket once landed on the ice floe.

- We carefully circled the seals at a safe distance to avoid startling them, moved on the ice floe slowly, ensuring minimal disturbance, and positioned ourselves strategically to block their access to the water. Three fieldworkers used wooden sticks for this purpose.
- Prior to immobilization, all four staff members remained low, seated on the ice floe to minimize stress to the animals.
- Seals were immobilized using a jabstick with a combination of 300 mg Xylazine, 500 mg Ketamine, known as "Hellabrunner Mischung" (HM). Additional doses of 125 mg Xylazine and 100-200 mg Ketamine were supplemented if necessary after 15 minutes. Maintenance of narcosis will be ensured by manual follow-up doses of Ketamine, and/or Xylazine on demand. The immobilization procedure is described in detail by Bornemann et al. (1998) and Bornemann and Plötz (1993) and dose rates available on PANGAEA (https://doi.pangaea.de/10.1594/PANGAEA.438929). While the seals are immobilized, their standard body length have been measured with the animal lying on its venter. Standardized (blood, whiskers) and opportunistic sampling protocols (scat) complemented the procedure.
- Tags were attached to the fur on the animal's head and back with quick setting loctite 420 glue. This new glue has been tested on southern elephant seals and Weddell seals. We hypothesized that the durability of this new glue might vary depending on the animals' behaviour, as we observed certain individuals rubbing their tags against the ice, potentially leading to tag detachment. Consequently, we transitioned to a two-part epoxy (Araldite AW 2101 and Hardener HW 2951) for seals 6-12. Later, due to running out of epoxy, we reverted to Loctite 420. Our observation led us to conclude that Loctite 420 is highly effective for seals that do not engage in rubbing behaviours on the ice.
- After completing the anesthesia and tag deployment process, the field team communicated with the helicopter pilot to determine whether there was sufficient time to attend to another seal or if it was necessary to return to the ship.

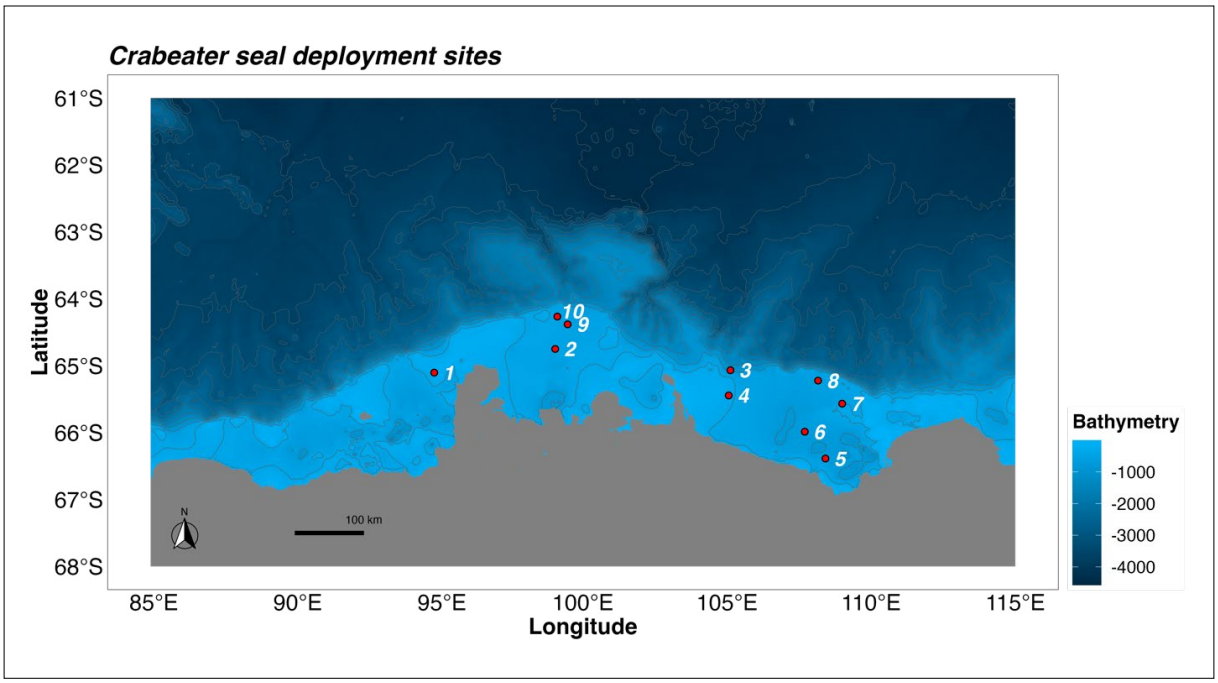

Fig. 5.1: Map showing deployment sites numbered over time, with bathymetry based on GEBCO data (2023).

Fig. 5.2: Examples of surveyed ice floes with seals; from left to right first row corresponds with 27 February, 5 March then second row 7 March and 23 March 2024.

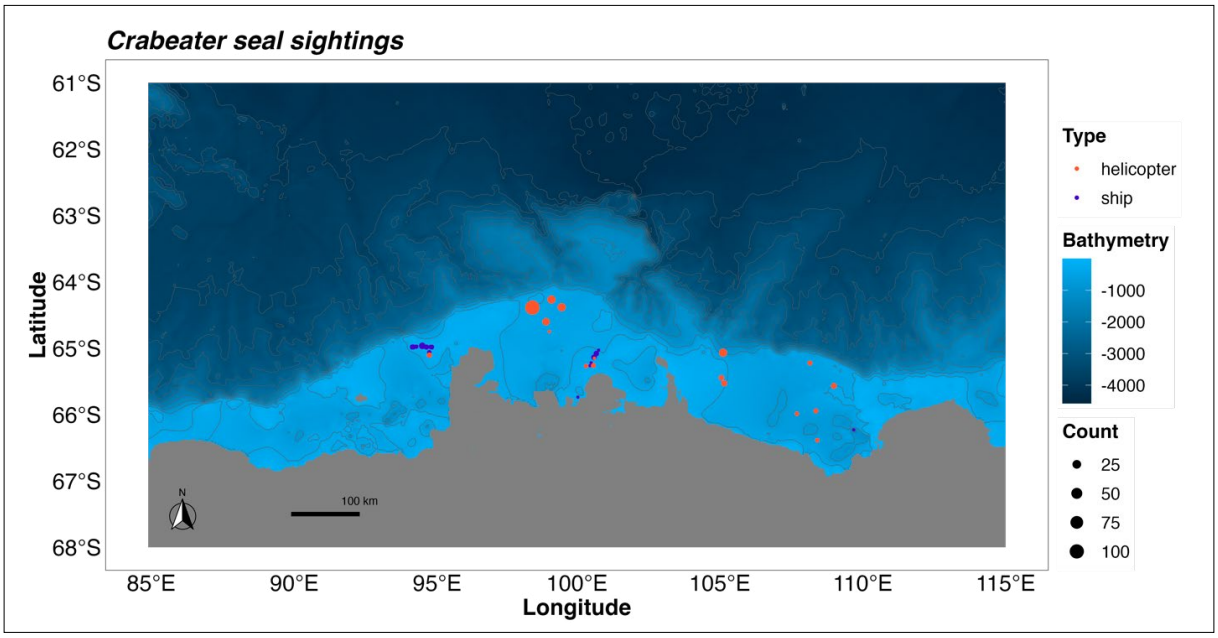

Fig. 5.3: Map showing crabeater seal sightings along the ship track or helicopter flights, with bathymetry based on GEBCO data (2023).

Tab. 5.1: Tracking information for the 15 crabeater seals tagged during PS141 cruise.

No	Sex	Start	End (of the last tag)	Head tag	Back Tag
1	NA	27.02.2024	17.03.2024	SCOUT-DSA-296G	SPLASH10-BF-297A
2	M	27.02.2024	04.03.2024	SCOUT-DSA-296G	SPLASH10-BF-297A
3	NA	27.02.2024	*	SCOUT-DSA-296G	NA
4	F	28.02.2024	*	SCOUT-DSA-296G	NA
5	F	02.03.2024	03.03.2024	SCOUT-DSA-296G	SPLASH-F-391A
6	F	07.03.2024	*	SPLASH-F-391A	SCOUT-DSA-296G
7	M	07.03.2024	*	SCOUT-DSA-296G	NA
8	NA	07.03.2024	*	SCOUT-DSA-296G	NA
9	M	10.03.2024	*	SCOUT-DSA-296G	NA
10	F	10.03.2024	*	SCOUT-DSA-296G	NA
11	F	11.03.2024	*	SCOUT-DSA-296G	NA
12	F	11.03.2024	*	SCOUT-DSA-296G	NA
13	M	11.03.2024	11.03.2024	SPLASH-F-391A	NA
14	F	23.03.2024	*	SCOUT-DSA-296G	NA
15	M	23.03.2024	*	SCOUT-DSA-296G	NA

M=male F=female **still transmitting (5/04/2024)*

Preliminary results

The continuous monitoring of crabeater seals in East Antarctica using high-resolution accelerometers (SCOUT-DSA, Wildlife Computers) positioned on their heads provide the opportunity to record acceleration: Prey capture attempts; dive depths; and Argos positions.

By tracking changes in crabeater seal distribution and behaviour, we can uncover seasonal shifts in krill distribution under sea ice – a crucial knowledge gap. Although there is currently no substantial krill fishery in East Antarctica, indications of growing interest necessitate timely monitoring and surveys in the absence of fishing pressure, aligning with CCAMLR CEMP's (Commission for the Conservation of Antarctic Marine Living Resources Ecosystem Monitoring Program) objective of distinguishing environmental changes from resource harvesting impacts on krill-centered ecosystems.

The urgency of our pursuit is heightened by the ongoing decline of Antarctic sea ice. Identifying feeding zones for krill-eating predators across both vertical and horizontal dimensions is vital to unraveling krill distribution patterns and understanding the regional impact of sea ice changes (SC-CAMLR-41 Annex 4, Tab. 2, Section 2a,e). Our research will offer valuable insights into the distribution of krill beneath the sea ice, their significance for predators, and the dynamic trophic relationships that necessitate monitoring.

This research will serve as a basis for (i) including the crabeater seal as a sentinel species in the CCAMLR CEMP monitoring program; and (ii) setting up a long-term monitoring program with annual deployments in East Antarctica. These deployments will utilise international collaboration between Australia, Germany, and the French Polar program at Dumont d'Urville, and will enable ongoing monitoring of changes in krill distribution and important habitats for krill-dependent predators in relation with changes in sea ice in East Antarctica. There is no significant krill fishery in this region, but an MPA proposal is currently in discussion and includes, particularly for the Dumont d'Urville-Mertz area, a no take zone for krill.

We deployed the first tags on three individuals on 27 February 2024 west of Queen Mary Coast; subsequent tracking revealed one of them migrating to the western part of the region, while another remained local, and the last individual ventured eastward (see Fig. 5.4).

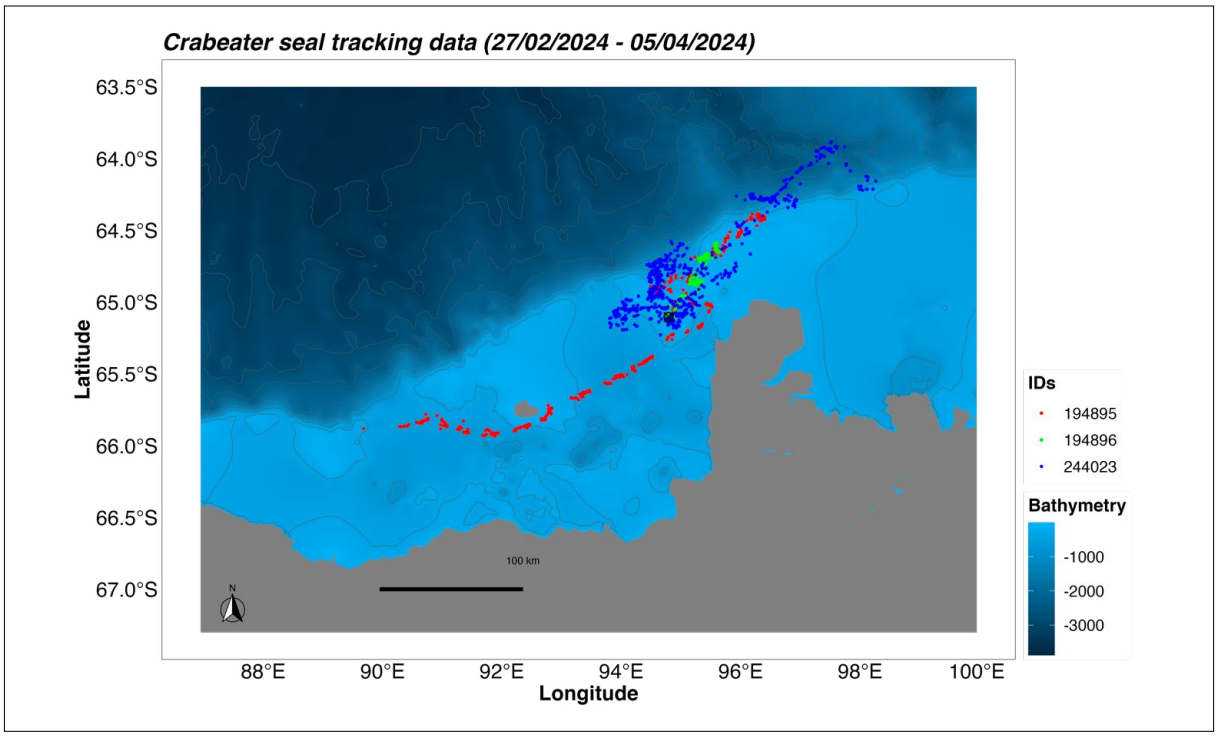

Fig. 5.4: Tracking data from three individuals equipped on 27February 2024. The deployment site is noted in black. The bathymetry is based on GEBCO data (2023).

On 28 February, one individual was equipped east of Queen Mary Coast and on 7 March, three individuals were equipped southeast of Bowman Island (Fig. 5.5). Intriguingly, all four of these individuals exhibited an eastward movement pattern, either close to the shelf break or on the continental shelf. Notably, the trio tagged on the 7th followed similar routes as they progressed eastward.

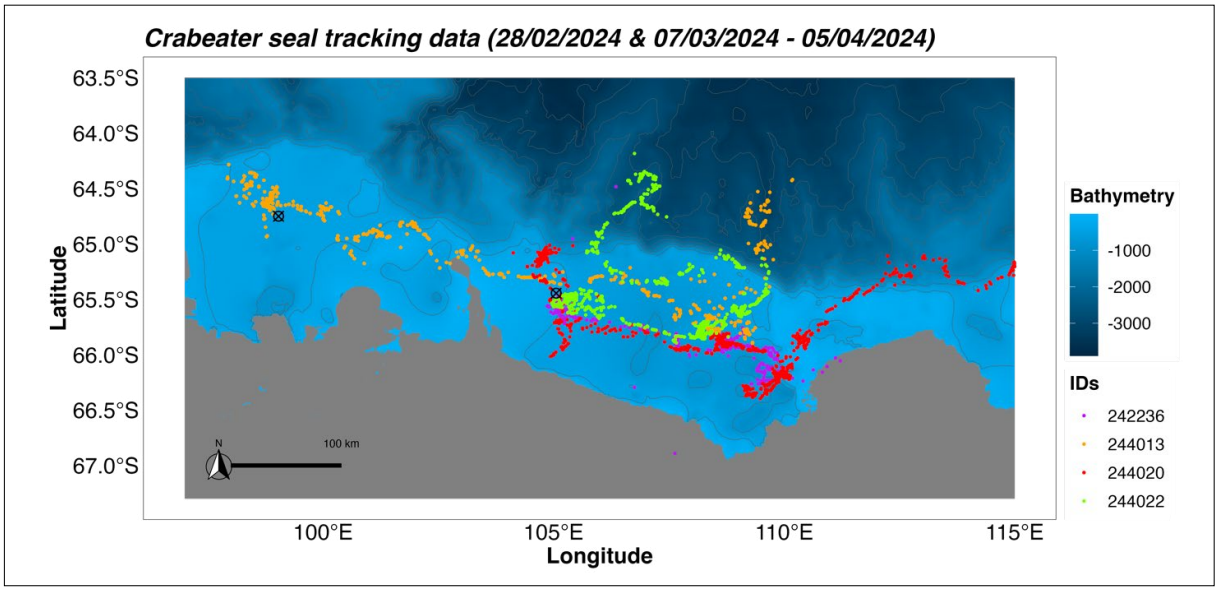

Fig. 5.5: Tracking data from four individuals equipped in 28 February and 7 March 2024. The deployment sites are noted in black. The bathymetry is based on GEBCO data (2023).

On 10 and 11 March, we equipped four more individuals in Vincennes Bay (Fig. 5.6); the two individuals equipped on 10 March on two different ice floes had similar paths and moved northwards. The two individuals equipped on 11 March moved within Vincennes Bay and one of them towards the outer shelf break.

Finally, two seals were equipped on 23 March east of Queen Mary Coast, one opted to remain proximate to the shelf break, while the other embarked on a southward journey before veering along the shelf break (see Fig. 5.7). Notably, the 5th and 13th individuals are not reported, as tag failures or detachments may happened following several hours of deployment and despite a full recovery after the anaesthesia. Diving behaviour analysis on the 15 crabeater seals will be performed on the full deployments.

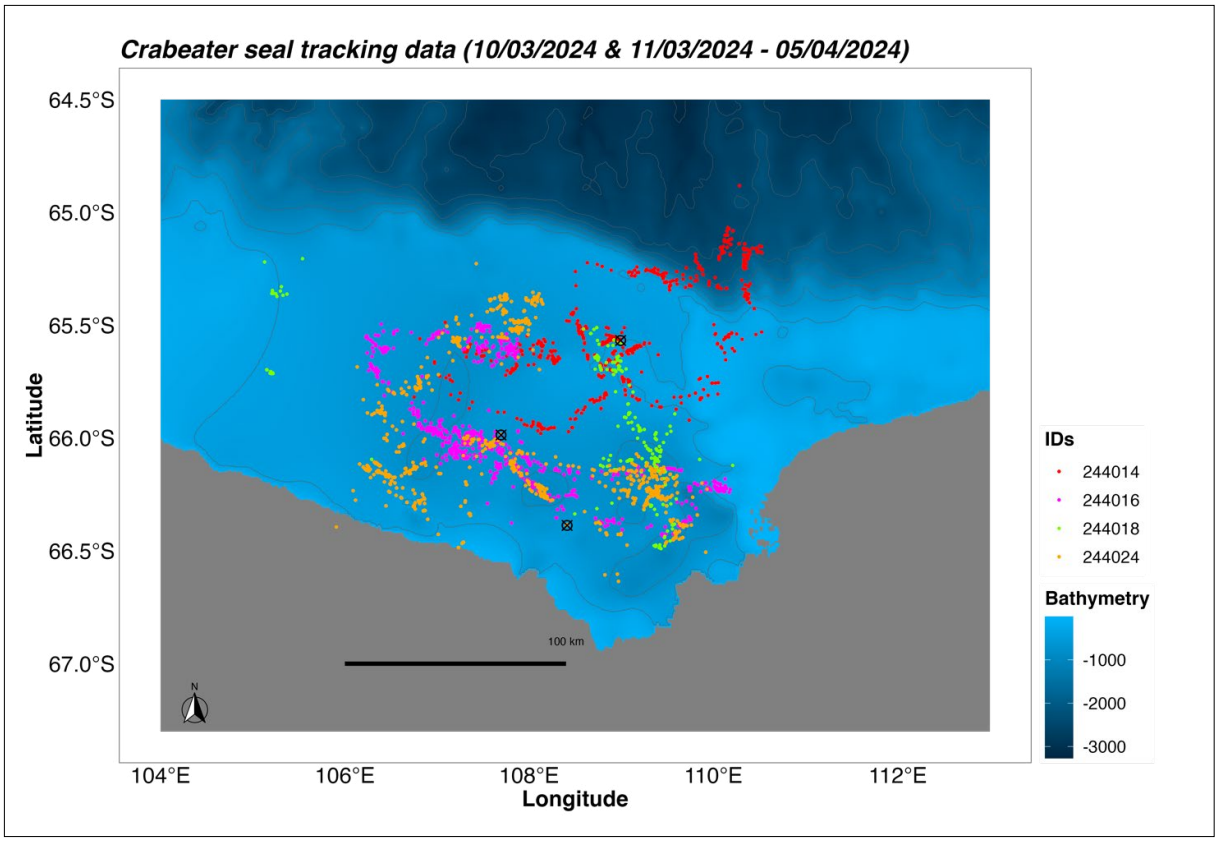

Fig. 5.6: Tracking data from four individuals equipped in 10 Marchand 11 March 2024. The deployment sites are noted in black. The bathymetry is based on GEBCO data (2023).

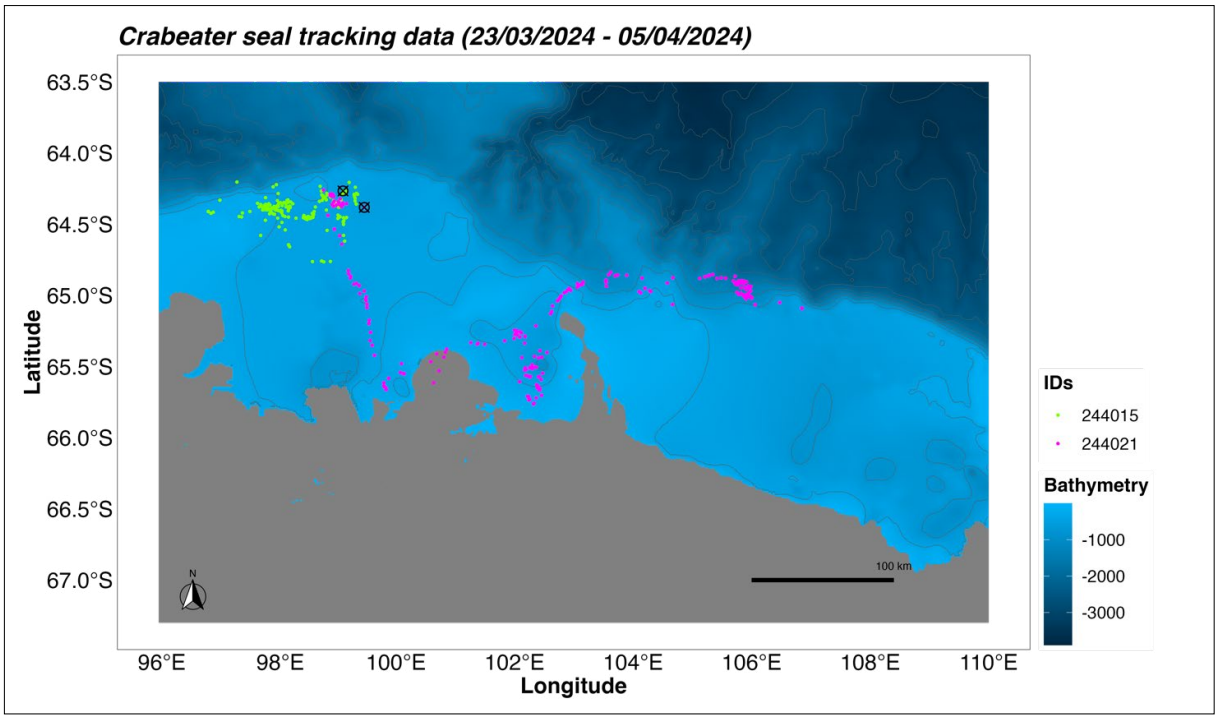

Fig. 5.7: Tracking data from 2 individuals equipped on 23 March 2024. The deployment sites are noted in black. The bathymetry is based on GEBCO data (2023).

Data management

Environmental data will be archived, published and disseminated according to international standards by the World Data Center PANGAEA Data Publisher for Earth & Environmental Science (https://www.pangaea.de) within two years after the end of the expedition at the latest. By default, the CC-BY license will be applied.

Any other data will be submitted to an appropriate long-term archive that provides unique and stable identifiers for the datasets and allows open online access to the data. This expedition was supported by the Helmholtz Research Programme “Changing Earth – Sustaining our Future”.

In all publications based on this expedition, the **Grant No. AWI_PS141_09** will be quoted and the following publication will be cited: Alfred-Wegener-Institut Helmholtz-Zentrum für Polar- und Meeresforschung (2017) Polar Research and Supply Vessel POLARSTERN Operated by the Alfred-Wegener-Institute. Journal of large-scale research facilities, 3, A119. http://dx.doi.org/10.17815/jlsrf-3-163.

References

Atkinson A, Hill SL, Pakhomov EA, et al. (2019) Krill (*Euphausia superba*) distribution contracts southward during rapid regional warming. Nature Clim Change 9:142–147. https://doi.org/10.1038/s41558-018-0370-z

Bornemann H, Plötz J (1993) A field method for immobilizing Weddell seals. Wildlife Society Bulletin 21:437–441.

Bornemann H, Mohr E, Plötz J & Krause G (1998) The tide as zeitgeber for Weddell seals. Polar Biology 20:396–403.

Bornemann H (2014) Documentation of 9 Weddell seals during the FIL2014 campaign. https://hdl.handle.net/10013/epic.44433

Bornemann H (2017) Documentation of 2 Weddell seals during the DRE2015 campaign. http://hdl.handle.net/10013/epic.50679

Bornemann H (2019) Marine Mammals Tracking-MMT-Processing report, FIL2018 campaign. https://hdl.handle.net/10013/epic.47618f1f-8e24-4e8d-a069-f6790739ed6c

Brierley AS (2002) Antarctic Krill Under Sea Ice: Elevated Abundance in a Narrow Band Just South of Ice Edge. Science 295:1890–1892. https://doi.org/10.1126/science.1068574

Constable AJ, Melbourne-Thomas J, Corney SP et al. (2014) Climate change and Southern Ocean ecosystems I: how changes in physical habitats directly affect marine biota. Global Change Biology 20:3004–3025. https://doi.org/10.1111/gcb.12623

Ducklow HW, Baker K, Martinson DG et al. (2007) Marine pelagic ecosystems: the West Antarctic Peninsula. Philosophical Transactions of the Royal Society B: Biological Sciences 362:67–94. https://doi.org/10.1098/rstb.2006.1955

GEBCO Bathymetric Compilation Group 2023 (2023) The GEBCO_2023 Grid - a continuous terrain model of the global oceans and land. https://doi.org/10.5285/F98B053B-0CBC-6C23-E053-6C86ABC0AF7B

Kawaguchi S, Ishida A, King R et al. (2013) Risk maps for Antarctic krill under projected Southern Ocean acidification. Nature Clim Change 3:843–847. https://doi.org/10.1038/nclimate1937

Meiners KM, Arndt S, Bestley S et al. (2017) Antarctic pack ice algal distribution: Floe-scale spatial variability and predictability from physical parameters: Mapping Antarctic Sea Ice Algae. Geophys Res Lett 44:7382–7390. https://doi.org/10.1002/2017GL074346

Meredith M, Sommerkorn M, Cassotta S et al. (2019) Polar regions: IPCC Special Report on the Ocean and Cryosphere in a Changing Climate. IPCC https://www ipcc ch/srocc/chapter 2

Meyer B (2012) The overwintering of Antarctic krill, Euphausia superba, from an ecophysiological perspective. Polar Biol 35:15–37. https://doi.org/10.1007/s00300-011-1120-0

Nachtsheim DA, Jerosch K, Hagen W et al. (2016) Habitat modelling of crabeater seals (*Lobodon carcinophaga*) in the Weddell Sea using the multivariate approach Maxent. Polar Biology. https://doi.org/10.1007/s00300-016-2020-0

Nordøy ES, Blix AS (2009) Movements and dive behaviour of two leopard seals (*Hydrurga leptonyx*) off Queen Maud Land, Antarctica. Polar Biol 32:263–270. https://doi.org/10.1007/s00300-008-0527-8

Wege M, Salas L, LaRue M (2021) Ice matters: Life-history strategies of two Antarctic seals dictate climate change eventualities in the Weddell Sea. Global Change Biology gcb.15828. https://doi.org/10.1111/gcb.15828

Williams G, Maksym T, Wilkinson J et al. (2014) Thick and deformed Antarctic sea ice mapped with autonomous underwater vehicles. Nature Geoscience 8:61–67. https://doi.org/10.1038/ngeo2299

Worby AP, Geiger CA, Paget MJ et al. (2008) Thickness distribution of Antarctic sea ice. J Geophys Res 113:C05S92. https://doi.org/10.1029/2007JC004254

6. CONTINENTAL GEOLOGY AND GEODESY

Mirko Scheinert[1], Sonja Berg[2]

[1]DE.TU-DRESDEN
[2]DE.UNI-KÖLN

Grant-No. AWI_PS141_04, AWI_PS141_05

Outline

Geoscientific research during expedition PS141 covered three study areas in East Antarctica (Fig. 6.1). Bunger Hills and Windmill Islands in Wilkes Land were target areas for terrestrial geological and limnological work. Gaussberg was the main working area for the onshore geophysical-geodetic work. Camps were set up in Bunger Hills and at Gaussberg in order to conduct onshore work. Several sites were also visited for short-term stays in order to maintain existing GNSS sites and install new GNSS sites. Details are summarized in Chapters 6.1 and 6.2.

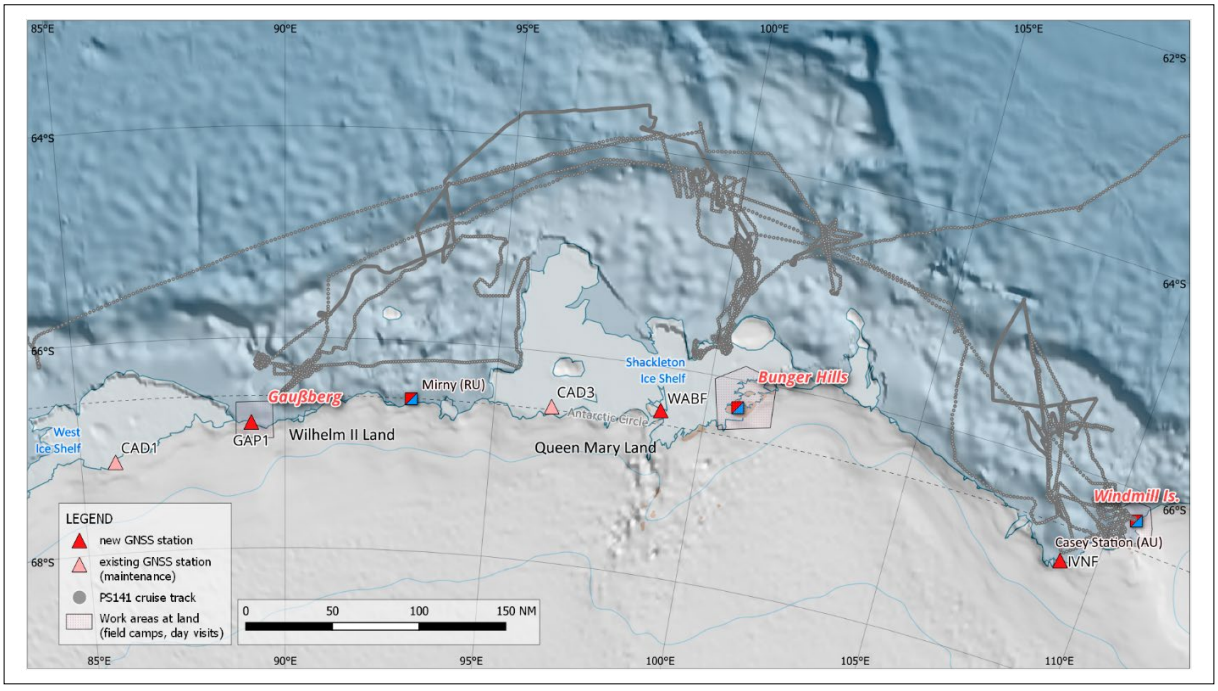

Fig. 6.1: Overview map of the coastal region of East Antarctica with the cruise track of PS141 and the onshore locations that were visited. A field camp for terrestrial geological and limnological work was set up at Bunger Hills (Chapter 6.1). At Gaussberg a field camp was maintained for three weeks (Chapter 6.2). All other sites were visited during day visits for short-term stays. Three new Global Navigation Satellite Systems (GNSS) stations could be set up during PS141 (Chapter 6.2). The station CAD1 was visited for maintenance, while the station CAD3 was already visited during the previous cruise PS140.

6.1 Terrestrial Geology and Limnology

Sonja Berg[1], Bernd Wagner[1], Damian B. Gore[2], Daniela Dägele[1], Amber Howard[3], Timo Lange[1], Stephanie Scheidt[1], Marie Weber[4]; not on board: Duanne White[3], Krystyna Saunders[5], Martin Melles[1]

[1]DE.UNI-KÖLN
[2]AU.MACQUARIE
[3]AU.UC
[4]DE.TU-DRESDEN
[5]AU.ANSTO

Grant-No. AWI_PS141_04

Objectives

It has long been assumed that the EAIS is stabilised by resting on bedrock above sea level (in contrast to the largely marine-based West Antarctic Ice Sheet). In recent years, however, modelling approaches and field experiments have shown that processes associated with basal melting of ice shelves through the intrusion of relatively warm deep water could also destabilise marine-based portions of the EAIS (e.g. Rintoul et al. 2016), especially in Wilkes Land, where the highest ice mass losses in East Antarctica are observed (Rignot et al. 2019). Possible causes lie not only in interactions of the ice sheet with the ocean, but also local topography beneath the ice sheet. To better understand the drivers of ice sheet stability/ instability in relation to regional features, detailed studies from the presently ice-free regions of Wilkes Land are required. Bunger Hills and Windmill Islands, two ice-free coastal sites, provide a unique opportunity to obtain information on temporal/spatial ice sheet changes at the margins of the major glaciers (Denman/Scott Glacier and Vanderford/Totten Glacier), which are particularly dynamic under present-day conditions (Rignot et al. 2019). To gain insights into regional ice sheet history, and interactions between ocean and ice during the Holocene, we collected geological samples and data at Bunger Hills and Windmill Islands. The new material will provide the basis for a significantly improved spatial and temporal resolution of palaeoenvironmental and paleoclimate information in this region.

Work at sea and on land

During PS141 we visited Thomas Island in the north of Bunger Hills (Fig. 6.1.1) from 19 to 29 February 2024. After a reconnaissance flight, a site on the western shore of Ear Lake (informal name) was defined for setting up the camp (Fig. 6.1.1). Equipment and the team of eight persons were brought to this location by helicopter during 19 February and the camp was set up so that work could be carried out without direct support from *Polarstern*. The work programme comprised lake sediment coring, surveying/sampling of ancient shorelines and glacial-geomorphological mapping and sampling and was carried out in parallel by specific groups within the team. However, the passage of a low-pressure system with winds of up to 11 Bft delayed the start of work until 23 February. Unfortunately, the programme had to be terminated well before completion due to a second low pressure system that was forecasted to reach winds of up to 12 Bft. The team and parts of the equipment were brought back on board *Polarstern* on 29 February, but weather conditions prevented evacuation of the entire equipment. This was achieved later, on 21 March, after completing marine-based work around Windmill Islands. In Windmill Islands several sites were visited for several hours for sampling mumiyo (fossil snow petrel stomach oil deposits) and glacial erratics between 5 and 13 March.

The glacial geology of Thomas Island (Bunger Hills) is little described, both in terms of sedimentology or chronology of deposition. In order to resolve the glaciation history of the area a sampling programme was undertaken to characterise glacial sediments, describe glacial drift weathering patterns (e.g. Augustinus 2002) and to provide quantitative ages for deglaciation using terrestrial cosmogenic nuclides (TCN) on bedrock and glacially transported erratics (e.g. White et al. 2022). Additional sampling of glacial erratics was carried out on offshore islands at Windmill Islands to better understand the dynamics of the Vanderford/Totten Glaciers.

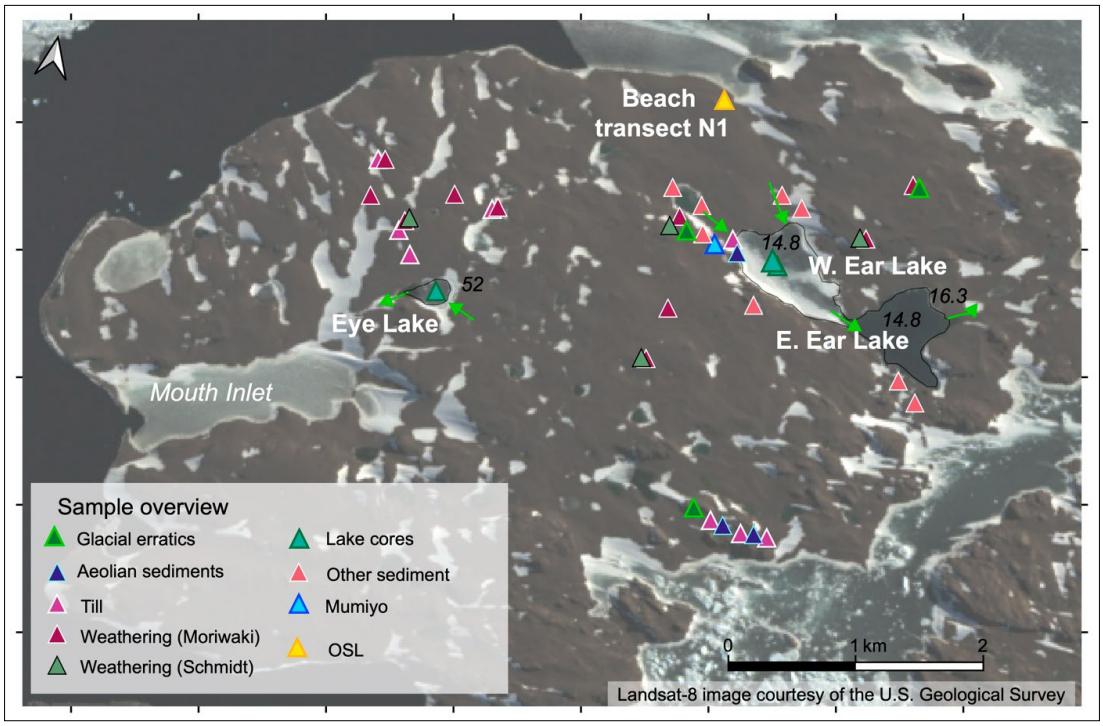

Fig. 6.1.1: Sampling sites on Thomas Island colour coded by type of sampling. Numbers give altitudes above sea level of lake level and sill heights of potential outflow of Ear Lake. Green arrows indicate in- and outflow pathways of both investigated lakes.

Field work at Bunger Hills included sediment coring on lakes to reconstruct the timing of ice retreat and Holocene paleoclimate. In order to obtain records that are not affected by relative sea level (RSL) changes during their history, we selected lakes at higher elevations that likely have not experienced marine incursions during the Holocene (i.e. higher than c. 10 m above sea level; Verkulich et al. 2002). Measurements of lakes and sills (highest elevation between lake and sea) was done by geodetic measurements (Chapter 6.2). Collection of sediment cores was complemented by sampling of sediments from the lake shore and catchment for characterising inputs into the lakes, which is important for palaeoenvironmental reconstructions. On some samples mineral magnetic/biomagnetic investigations will be carried out, focussing on patterns of the concentration and diversity of magnetofossils, which are the fossil remains of magnetotactic bacteria. Recent studies show that different bacterial species or strains synthesise different crystal morphologies (e.g. Li et al. 2020), suggesting that the shape of magnetofossils could become a new environmental indicator. However, the study of magnetofossils in Antarctica is currently limited to just a few studies in marine environments. Therefore, this was the first detailed study of the abundance and variability of freshwater magnetofossils in Antarctica.

Geophysical measurements on land were carried out to complement the findings from sedimentary archives. Ground penetrating radar (GPR) profiles were measured to provide information on the stratigraphy of ancient beach deposits, reflecting past changes in RSL and aiding in selecting suitable sites for sampling beach deposits for age determination by optically stimulated luminescence (OSL) dating.

A further focus was the sampling of fossil stomach oil deposits of snow petrels (*Pagodroma nivea*), so-called mumiyo deposits. These deposits provide geological evidence for the distribution of snow petrels in the past (e.g. Berg et al. 2019a). They can be well dated by radiocarbon dating

(e.g. Mackintosh et al. 2011) and have been used as an archive for environmental conditions in the coastal ocean, which is the feeding ground of the birds (e.g. Hiller et al. 1988; Ainley et al. 2006; Berg et al. 2019b, 2023). The lipid and isotopic composition of stomach oil deposits can provide evidence for changes in the food composition of snow petrels (Berg et al. 2023), which is linked to oceanic environmental parameters, such as the sea ice distribution during summer, polynyas and shifts of the southern boundary of the ACC. Stomach oil deposits form in the vicinity of nesting cavities of snow petrels, which are distributed on nunataks and rocky coastal sites. The occurrence of snow petrel stomach oil deposits in Bunger Hills and Windmill Islands has been reported in previous studies (Ainley et al. 2006; Berg et al. 2023) and the record from southern Bunger Hills dates to the early Holocene (Ainley et al. 2006).

Isotopic and hydrochemical data from lakes provide direct information on the response of the catchment to changing precipitation, evapotranspiration, nutrient cycling, and ecosystem conditions (Meredith et al. 2022). These techniques have rarely been applied to lakes in the high latitudes of the Southern Hemisphere. We sampled water from one lake in order to carry out hydrochemical and isotopic studies. These data will be used in a larger study that addresses environmental processes and ecological effects of seasonal, annual and long-term fluctuations.

Biological soil crusts are an important component of Antarctic terrestrial ecosystems. Their microbial biodiversity, however, is not well known. The material collected at one site in Windmill Islands, therefore represents an essential contribution to biodiversity research and also provides functional evidence of microbial networks.

Results

Air temperature and pressure was recorded at three locations during the fieldwork (Fig. 6.1.2). The first was a rock surface in a crevice sheltered from direct insolation; the second was just underneath the sediment surface, and the third logger was placed at the base of the ~30 cm deep snowpack. The first logger remained exposed to the sky at all times, while the sediment logger was buried by snow intermittently. The loggers were Van Essen “Cera-Diver” model D1701, firmware version 1.06, read with software for Windows version 11.2.0.1. The logging interval was set at five minutes. Temperature resolution was 0.001°C and pressure resolution was 0.001 cm H_2O. The logger exposed subaerially exhibited the greatest diurnal range in temperature, and the highest and lowest maxima. This short record indicates that snow-covered rock surfaces might undergo many fewer freeze-thaw cycles per year than exposed rock surfaces. Snow then provides thermal protection, and thus relief from weathering influences. This has geomorphological implications for the rates of surface lowering in the landscape, and requires further quantification under saline Antarctic conditions.

Lakes and lake sediment coring

On Thomas Island, two lakes were sampled (Ear Lake and Eye Lake, informal names). The topography of the island suggests that the lakes are part of stream systems that connect several lakes on the northern side of Thomas Island (Fig. 6.1.1).

The water flow in streams, and the resultant water balance of lake basins, affects their salinity, tendency to desiccation and the sediment accumulation within them. Understanding inflows and outflows into lake basins is therefore crucial for a deeper understanding of lacustrine palaeoenvironmental records. Accordingly, the water sources flowing into and from Ear Lake and Eye Lake were assessed.

Eye Lake is an oval basin, with no clearly defined stream system flowing into it. At the time of visiting, unchannelised sheet flow was partly obscured by snowlie, but it appears that minor

flow from an unnamed lake to the east seeps gently along an unchannelised flowpath into Eye Lake. The lake likely receives input of melt water from ephemeral snow lie around the lake during spring and summer. Eye Lake drains to the west, into Mouth Inlet (informal name, Fig. 6.1.1).

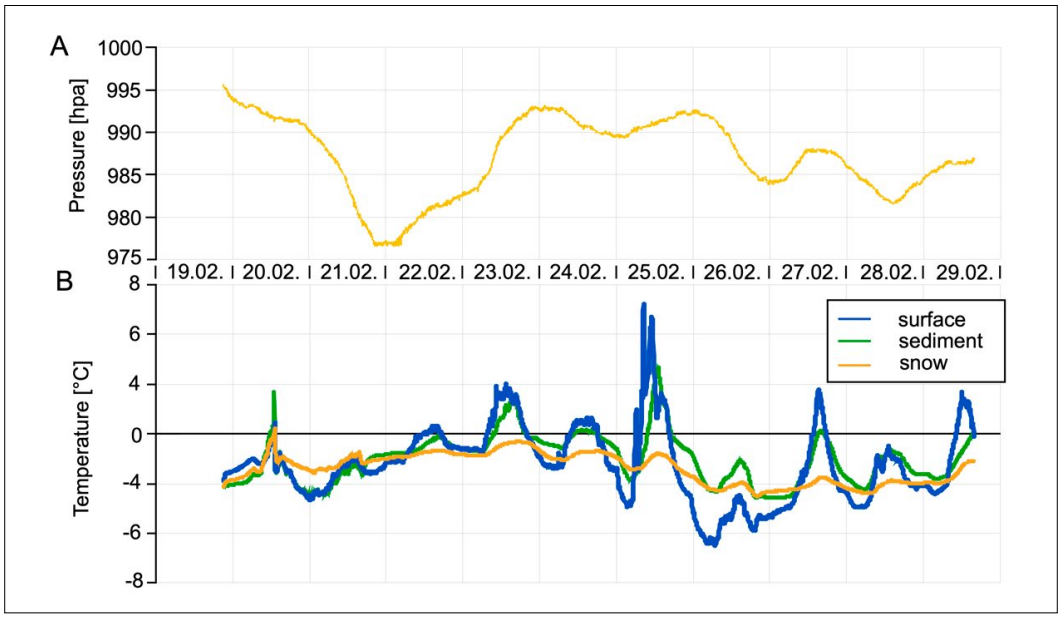

Fig. 6.1.2: Air pressure and temperature recorded at Thomas Island from 19.2. to 29.2.2024 A) The pressure curve depicts changes in air pressure, notably the decrease of air pressure during the storm on 21. and 22.2.2024 and B) Temperature recordings from three different settings (at the surface, inside sediments and below snow) show how the snow cover moderates daily temperature fluctuations.

Ear Lake has at least three inflows at the western lobe (Western Ear Lake) and two possible outflows towards the sea on the eastern end of the eastern lobe (East Ear Lake). It is possible that both flowpaths are active from time to time, depending on the snow accumulation in southeastern Ear Lake. These scenarios are important because they control the amount of freshwater flushing through the location of the coring site in Ear Lake, and the accumulation of solutes in the basin there. By the time of our observations the stream system was not active and the water level of Ear Lake was at 14.8 m asl, which is 1.5 m below the lowest sill of potential outflows (Fig. 6.1.1).

While the eastern lobe of Ear Lake was only partly covered by lake ice and therefore not accessible for sediment coring, Western Ear Lake was ice covered. The ice surface was smooth but showed a pronounced topography of undulations of c. 0.5 m height and wavelengths of several meters. Ice thickness and water depth were investigated at two sites by drilling through the lake ice cover. At coring sites W Ear1 and W Ear2 (Tab. 6.1.1) the lake ice thickness varied between 1.4 and 1.5 m (n=8). The lake ice was not homogenous, but showed a layering with a more solid, 0.3 – 0.4 m thick top layer of ice and alternating layers of more and less slushy ice below. Water depth ranged from 13.1 to 15.1 m. For site W Ear1, water properties (temperature, conductivity and oxygen saturation) were measured (Fig. 6.1.3), showing that the lake water is saline (19.9 mS cm^{-1} at 0.5 m below the ice) with an increase in salinity to 47.5±2.3 mS cm^{-1} below 5 m and an inverse temperature profile, with warmer water in the

lower water column than directly below the ice (Fig. 6.1.3). One water sample from Western Ear Lake was taken for analysis of isotopic and hydrochemical properties.

Sediment coring was performed using a gravity corer and a 2 m-long core barrel with hammering option (UWITEC Co.) (Tab. 6.1.1). The gravity corer is routinely equipped with a 60 cm or 120 cm PVC liner of 62 mm outer diameter and a ball core catcher. For the recovery of longer sediment cores with the gravity corer, the corer was modified for hammering and a stainless-steel core catcher was used. For even deeper penetration, a 2 m-long steel core barrel with an interior PVC liner of 62 mm outer diameter was hammered into the sediments. Penetration progress in all holes decreased distinctly at a sediment depth of ~1.2 m. Two attempts to recover deeper sediments failed because the stainless-steel core catcher could not keep the sediment material. However, very stiff, greyish to olive sediments sticking to the outer core barrel in its lowermost end indicated that it prevented further penetration and caused the loss of the sediments.

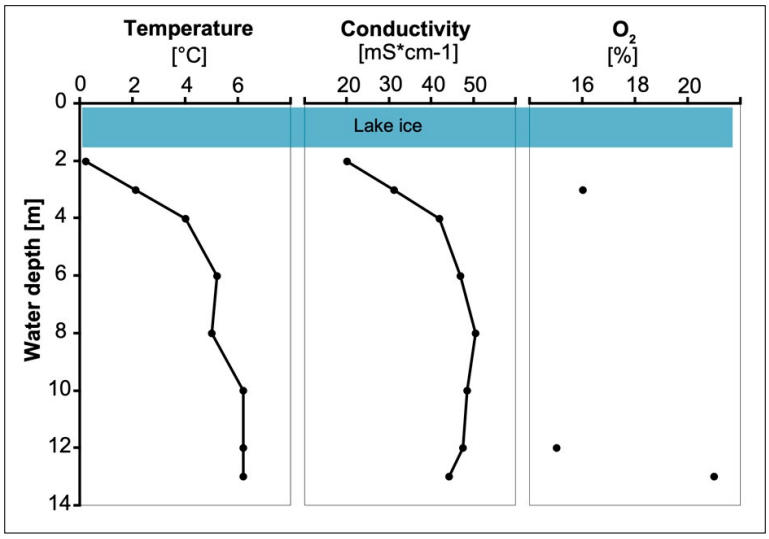

Fig. 6.1.3: Water properties at site W-EAR 1. Values were determined from water samples collected with a UWITEC water sampler and temperature, conductivity and oxygen saturation were measured.

Sediments recovered from the W Ear1 site showed 5-10 cm of microbial mats at the top and increasing clastic matter with dark greyish color and interspersed light grey flakes below. Sand layers were observed in the core catchers of W Ear1-3 and W Ear1-4 (Fig. 6.1.4).

After recovery of two sediment cores with the gravity corer at the W Ear 2 site, two attempts with the 2m-long core failed, apparently also because till hampered penetration at > 1.2 m sediment depth and the core catcher was not able to keep the sediment material. However, 40 cm-long remnants of these cores, most likely originating from the sediment surface, flushed onto the lake ice, when the PVC liners were removed from the core barrel. They were cut lengthwise and showed a slightly different lithology compared to the cores recovered at W Ear1, with alternating layers of greyish and blackish sediments of 1-2 cm and a few thin sand layers at > 20 cm depth. At both sites, W Ear1 and W Ear2, a strong smell of H_2S was detected during core processing. Zooplankton was not observed in the water above the sediment surface, consistent with low oxygen concentrations in the bottom water of Western Ear Lake.

Eye Lake was visited on 28 February (Fig. 6.1.5). Three holes were drilled through the lake ice cover at a distance of ~30 m to each other. The ice thickness was ~0.9 m, with a solid top layer of ice 40-50 cm thick and alternating layers of more or less slushy ice below. The ice was mostly transparent, and contained patches of microbial mats (that likely detached from the

lake bed and floated up) and gas bubbles, mostly close to the shore. Water depths at the three holes varied between 4.1 and 4.5 m. The location with 4.5 m water depth was selected for the recovery of two gravity cores (Tab. 6.1.1). Core Eye1-1 was 72 cm long, while core Eye1-2 was only 28 cm long (Fig. 6.1.5). The surface of Eye1-1 consisted of a fluffy layer of reddish to brownish microbial mats. Downcore, sediments became more greyish and appeared enriched in clastic material. Several horizons down to the core base showed brownish filamentsthat were likely remnants of subaquatic mosses. The sediment cores did not smell of H_2S. A sample from the water surface revealed a specific conductivity of 559 µS cm^{-1} and a pH around 5.5. Deeper waters were not recovered.

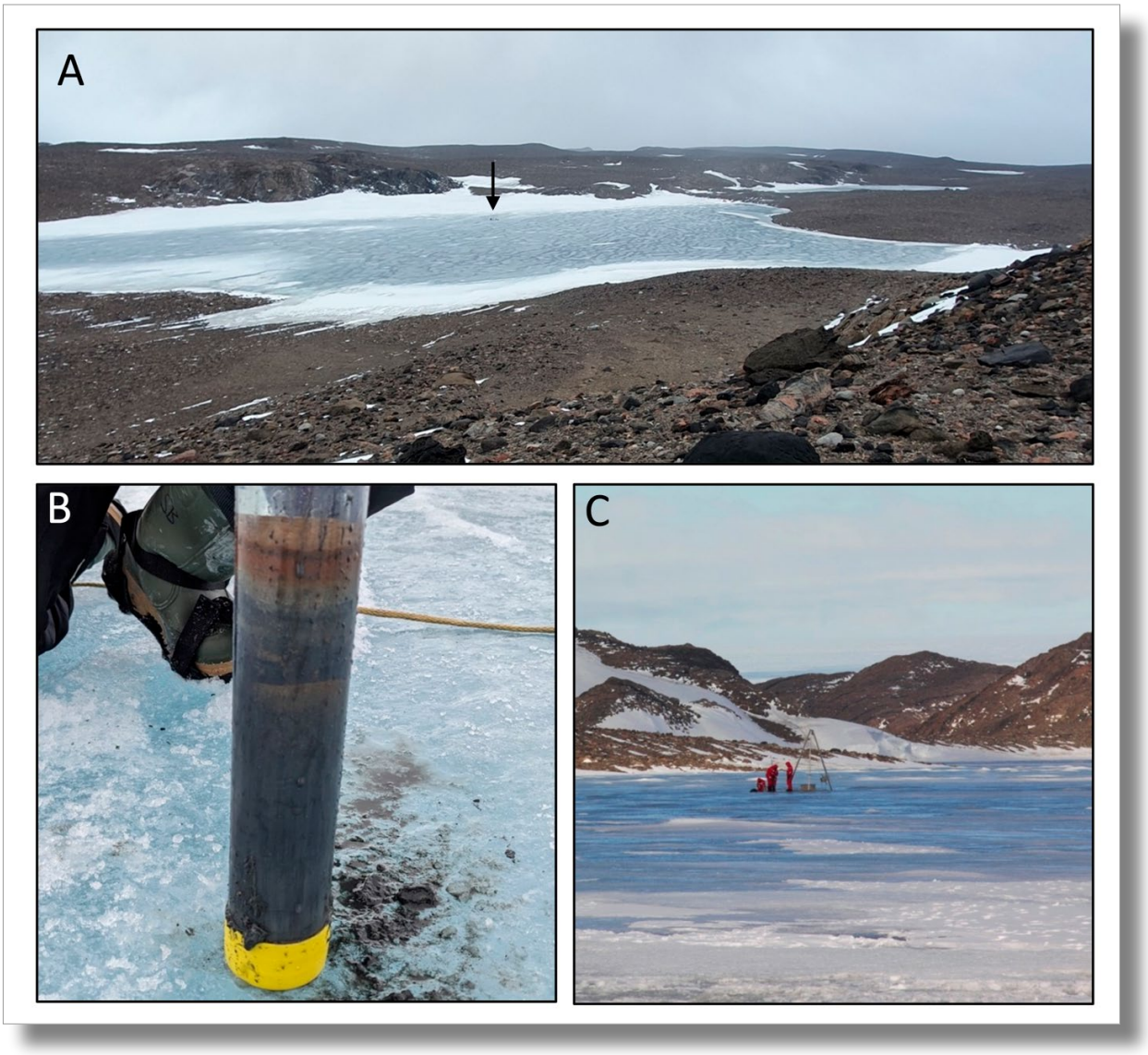

Fig. 6.1.4: A) Coring location on Western Ear Lake (indicated by arrow), view towards the west, B) gravity core from coring site W Ear1. Sediments show clear layering and microbial mats in the top-most centimeters C) Coring location W Ear1 and bedrock ridges on the western shore of the lake.

Tab. 6.1.1: Lake sediment cores collected at Thomas Island. Gear refers to coring device (GC120-gravity corer with 120 cm length, GC60-gravity corer with 60 cm length, GC/H-gravity corer with hammering, HC200-hammer core with 200 cm steel core barrel and internal PVC liner).

Lake	Core ID	Latitude South [°]	Longitude East [°]	Water depth [m]	Core depth [cm]	Gear
W Ear	W Ear1-1	66.10621	100.95924	14.4	0-48	GC120
W Ear	W Ear1-2	66.10621	100.95924	14.4	0-46	GC120
W Ear	W Ear1-3	66.10621	100.95924	14.4	2-112*	HC200
W Ear	W Ear1-4	66.10621	100.95924	14.4	0-108*	HC200
W Ear	W Ear1-5	66.10621	100.95924	14.4	0-27	GC60
W Ear	W Ear1-6	66.10621	100.95924	14.4	0-27	GC60
W Ear	W Ear1-7	66.10621	100.95924	14.4	0-101*	HC200
W Ear	W Ear2-1	66.10580	100.95823	13.6	0-29	GC60
W Ear	W Ear2-2	66.10580	100.95823	13.6	0-32	GC60
W Ear	W Ear2-3	66.10580	100.95823	13.6	0-72.5**	GC/H
Eye	Eye1-1	66.10621	100.95924	4.5	0-72	GC120
Eye	Eye1-2	66.10621	100.95924	4.5	0-28	GC

* Core depth does not include material in core catcher (7 cm) and core tip (5 cm), i.e. total penetration is plus 12 cm; till prevented deeper penetration

*** Core depth does not include material in core catcher (7 cm), i.e. total penetration is plus 7 cm*

Fig. 6.1.5: A) Eye Lake, arrow indicates towards outlet of the lake, B) gravity core from Eye Lake with laminated, biogenic sediments.

Glacial-geomorphological mapping and sampling

The glacial geology of Thomas Island is little described, both in terms of sedimentology or chronology of deposition. Regional overriding by the ice sheet flowing toward the northwest created striations which are, in rare places, preserved on bedrock surfaces (Adamson and Colhoun 1992; Augustinus et al. 1997; Augustinus 2002). The rarity of striations is due to extensive subaerial weathering of bedrock surfaces due to frost and salt crystallization pressures, and abrasion by wind-borne particles (sensu Gore and Leishman 2020a, b). Except for a few radiocarbon dates of marine shells in a raised beach, ranging from 7.7 – 0.2 ka BP (corrected for a 1,300 a marine reservoir effect; see Adamson and Colhoun 1992), no direct constraints on the chronology of the glacial history of Thomas Island are available.

The pattern of glaciation and deglaciation is slightly better constrained. The regional overriding of Thomas Island by the ice sheet flowing to the northwest is well established (Adamson and Colhoun 1992; Augustinus et al. 1997). Impingement of the northeasterly flowing Edisto Ice Tongue onto the western coast is also clear, with two (Older Edisto, Younger Edisto; Colhoun and Adamson 1992) to three (Edisto 1, 2, 3; Augustinus 2002) sets of moraines having formed just before the mid-Holocene to late Holocene times. Preliminary interpretation of satellite imagery and aerial photography of Thomas Island shows the existence of the well-defined Edisto moraines in the western part of the island and a thermokarsted, dimpled drift sheet in the northwestern part of the island. In order to help resolve some of these details, a sampling programme was undertaken to characterise glacial sediments, describe glacial drift weathering patterns (e.g. Augustinus 2002) and to provide quantitative ages for deglaciation using terrestrial cosmogenic nuclides on bedrock and glacially transported erratics. These are described in subsequent chapters.

Weathering – Rock hardness

As rocks weather chemically their structure is weakened, and so their hardness can reflect their age since deglaciation. This is represented by a large geomorphological literature from formerly glaciated environments around the world, including Antarctica (e.g. White et al. 2009) and in particular, Thomas Island at Bunger Hills (Augustinus 2002). Less commonly discussed is that microstructural features (such as angular grain boundaries) can form asperities which crush during measurement of rock hardness. In this way, physically weathered rock can also decline in apparent strength as the surface weathers progressively with increasing age. This is particularly useful at Bunger Hills, where rocks are physically weathered more than chemically weathered (Fig. 6.1.6).

Researchers have used for several decades an instrument, the Schmidt Hammer, to measure the unconfined compressive strength of rocks for geomorphological studies (e.g. Matthews and Winkler 2022). The instrument we used to measure unconfined compressive rock strength was a Proceq (Screening Eagle) “Rock Schmidt” RS8000 (Proceq 2024). In an attempt to constrain mineralogical effects, clasts were classified into mafic (M), intermediate (I) and felsic (F) categories, and a single measurement was made from each of 25-34 clasts from each category at a site. This measurement strategy follows current best-practise outlined in Matthews and Winkler (2022) and Winkler (personal communication with DG 2023). Site locations that were recorded using the methods outlined previously, are listed in Table 6.1.2.

Tab. 6.1.2: Schmidt hammer study sites on Thomas Island, Bunger Hills

Sample code	Latitude South [°]	Longitude East [°]	Altitude [m]	# of clasts measured
TISc1	66.10487	100.94130	62	102
TISc2	66.10320	100.97321	89	102
TISc3	66.11421	100.94023	96	75
TISc4	66.10801	100.89533	107	75

Weathering - Moriwaki rock weathering index

Since surficial weathering of erratic boulders and bedrock takes time to occur, it follows that the extent of weathering may reflect age since emplacement by ice or exposure from an eroding, overriding ice mass. This relationship between age and weathering stage of boulders was quantified for sediments from the Sør Rondane Mountains of Antarctica (Moriwaki et al. 1991, 1994), where the presence of “staining” from chemical weathering, cavernous weathering (tafoni) (Fig. 6.1.6), ventifact development and crumbling (Fig. 6.1.6) of individual clasts > 30 cm diameter was noted in five categories (Tab. 6.1.3). The degree of weathering of 100 clasts at a site were combined to create a weathering class;

W = (0 x N0) + (1 x N1) + (2 x N2) + (3 x N3) + (4 x N4)

The subscripts refer to the degree of weathering classes and the numbers N0-4 indicate the number of clasts in each weathering class.

Tab. 6.1.3: Weathering descriptions for an individual clast (after Moriwaki et al., 1991).

Code	Description
DW0	Fresh
DW1	Stained without cavernous weathering, ventifaction or crumbling
DW2	Stained, cavernously weathered or ventifacted; but not crumbled
DW3	Distinctly stained and moderately crumbled
DW4	Strongly stained and crumbled

Similar classifications for 100 nearest neighbour clasts (following Augustinus 2002 and White et al. 2009), rather than 100 clasts in a quadrat (sensu Moriwaki et al. 1991) were then combined to form a degree of weathering index. This assessment of weathering class was conducted at 11 sites on Thomas Island (Tab. 6.1.4).

Tab. 6.1.4: Clast weathering class assessments (Moriwaki scheme) on Thomas Island. Site locations were recorded using methods outlined previously.

Site code	Latitude South [°]	Longitude East [°]	Altitude [m]
TIM1	66.10487	100.94130	
TIM2	66.10320	100.97321	67
TIM3	66.09903	100.98052	
TIM4	66.11050	100.94227	
TIM5	66.11421	100.94023	96
TIM6	66.10801	100.89533	107
TIM7	66.10419	100.88889	

Site code	Latitude South [°]	Longitude East [°]	Altitude [m]
TIM8	66.10673	100.88876	97
TIM9	66.10556	100.90282	105
TIM10	66.10608	100.90961	84
TIM11	66.12492	100.96020	37

Terrestrial Cosmogenic Nuclide dating of deglaciation

Felsic, particularly quartz-rich erratics or bedrock were identified from areas with abundant exposure of the clast to radiation from space. The size of the erratic needed to yield at least 30 g of processed quartz, so the more quartz in a rock type, the smaller the selected clast could be. Clasts thus identified from high, exposed positions in the landscape, were marked with a sample code and an arrow indicating true north, and photographs were taken *in situ* showing the location and the view toward the cardinal points north, east, south and west (e.g. Fig. 6.1.6).

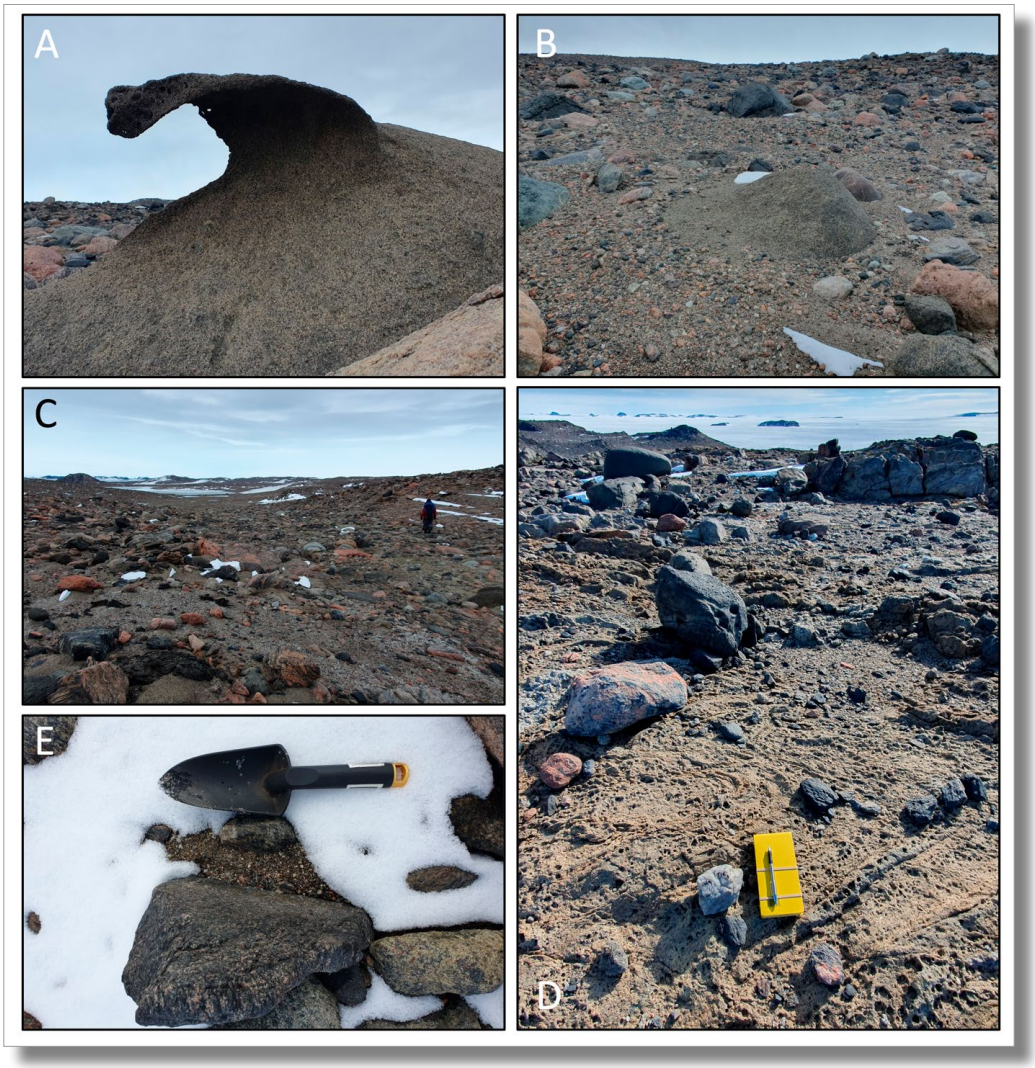

Fig. 6.1.6 A) Extensive tafoni development, B) Granular disintegration of a boulder (dominant wind right to left), C) Glacial sediments exposed between boulders at lower right. D) Quartz cobble TIE4 for cosmogenic isotope measurement, on strongly weathered gneiss bedrock in northeastern Thomas Island E) Aeolian sediments collected in the lee-side of a cobble. Dominant wind direction bottom to top of the image.

Angles of the azimuth from the clast to the horizon were recorded every 30˚ from 0, 030, 060 … 330˚, using a Nikon Forestry Pro II laser rangefinder, with 0.1˚ vertical increments. The location of each clast was then recorded using a hand-held Global Positioning System Garmin Etrex 22x, with data recorded in the World Geodetic System WGS84, in decimal degrees to five decimal places. Greater than 15 satellites were typically visible, and positional uncertainties were typically ±3 m. Nominal heights above datum were also recorded, with their greater uncertainties understood. Some locations were not recorded with Garmin GPS due to field time constraints, and these locations were estimated using Google Earth.

Because Google Earth images of different dates appear to have different georeferencing which influences their location, we first plotted the sites for which Garmin locations existed and then plotted the remainder of the locations. In Table 6.1.5, the source of the latitude and longitude measurement is recorded as “Garmin” or “Google Earth” with the date of the relevant image (e.g. “Google Earth February 2012”). Samples will be prepared for analysis at the University of Cologne or collaborating laboratories, following standard methods (e.g. White et al. 2011).

Tab. 6.1.5: Summary collection locations for samples for cosmogenic isotope dating.

Location name	Sample code	Latitude South [°]	Longitude East [°]	Positioning	Altitude [m]
Bunger Hills	TIB1a, 1b	66.10465	100.94160	Garmin Etrex 22x	66
Bunger Hills	TIE1	66.10487	100.94217	Garmin Etrex 22x	67
Bunger Hills	TIE2	66.10501	100.94276	Google Earth Feb 2012	67
Bunger Hills	TIE3	66.10471	100.94169	Garmin Etrex 22x	65
Bunger Hills	TIE4	66.09903	100.98050	Google Earth Feb 2012	89
Bunger Hills	TIE5	66.09903	100.98054	Google Earth Feb 2012	89
Bunger Hills	TIE6	66.09903	100.98056	Google Earth Feb 2012	89
Bunger Hills	TIB2	66.12371	100.95310	Garmin Etrex 22x	66
Bunger Hills	TIB3	66.12374	100.95305	Garmin Etrex 22x	67
Bunger Hills	TIB4	66.12363	100.95308	Google Earth Feb 2012	67
Bunger Hills	TIE7a, 7b	66.12372	100.95305	Google Earth Feb 2012	67
Bunger Hills	TIE8	66.12367	100.95333	Google Earth Feb 2012	66
Windmill Islands	NIE1	66.22953	110.19025	Garmin Etrex 22x	55
Windmill Islands	NIE2	66.22961	110.19052	Google Earth Jan 2011	55
Windmill Islands	NIE3	66.22962	110.19055	Google Earth Jan 2011	55

Glacial and Aeolian sediments

Surficial exposures of glacial (Fig. 6.1.6) and aeolian (Fig. 6.1.6) sediments were sampled where encountered (Tab. 6.1.6). For this, 50 to 100 g of sediment was collected and stored in plastic bags until further analysis. Glacial sediments were identified as silty diamictons outcropping beneath, in places, a thin grus formed from coarse sand and fine gravel liberated by frost and salt weathering of bedrock and glacially transported clasts. The finer-grained component of the glacial sediment imparts a shear strength which allows it to resist surficial erosion, transport and redeposition, whereas the coarse sand and fine gravel liberated by subaerial weathering blows readily across the land surface, forming sandy gravel deposits in the lee of larger cobbles and boulders. Ten representative samples of both of these types of sedimentary materials were sampled for textural analysis (Tab. 6.1.6).

Glacial sediments will be dispersed in sodium hexametaphosphate (Calgon®) for 24 h before wet sieving at 2,000 µm. The coarse fraction will be sieved at half phi intervals. The fine fraction will be measured using laser diffractometry, with a Malvern Mastersizer 3,000 optical bench and Hydro G accessory. Cumulative particle size distribution curves and derived statistics will be compared for each of the depositional environments.

Tab. 6.1.6: Summary of glacial and aeolian sediment samples from Thomas Island.

Sample material	Sample code	Latitude South [°]	Longitude East [°]	Altitude [m]
Glacial sediment	TIG1	66.11024	100.89726	95
Glacial sediment	TIG2	66.10749	100.89295	96
Glacial sediment	TIG3	66.10419	100.88889	74
Glacial sediment	TIG4	66.10608	100.90961	84
Glacial sediment	TIG5	66.10608	100.90961	
Glacial sediment	TIG6	66.10520	100.95037	25
Glacial sediment	TIG7	66.12435	100.95629	
Glacial sediment	TIG8	66.12446	100.95760	
Glacial sediment	TIG9	66.12485	100.96175	
Glacial sediment	TIG10	66.12474	100.96514	
Aeolian sediment	TIA1	66.10510	100.95088	25
Aeolian sediment	TIA2	66.10508	100.95076	25
Aeolian sediment	TIA3	66.10508	100.95064	26
Aeolian sediment	TIA4	66.10506	100.95047	26
Aeolian sediment	TIA5	66.10504	100.95030	27
Aeolian sediment	TIA6	66.12454	100.95849	
Aeolian sediment	TIA7	66.12463	100.95956	
Aeolian sediment	TIA8	66.12476	100.96398	
Aeolian sediment	TIA9	66.12435	100.95683	
Aeolian sediment	TIA10	66.12445	100.95672	

Survey and sampling of raised beaches

Raised beach ridges are sequences of paleoshorelines that represent a lowering of sea level which may be due to eustatic or isostatic sea level changes through time. These sequences are considered proxies to evaluate and characterise shore displacement (Muru et al. 2018). Antarctic beaches offer unique records of coastal environmental change. Ancient beaches are preserved above present-day sea level due to relative sea-level fall caused by glacial-isostatic adjustment (GIA) following ice sheet retreat after the Last Glacial Maximum (LGM). Thus, Antarctic beaches have been extensively used for Holocene relative sea-level (RSL) reconstructions, providing constraints on GIA and ice-sheet models (Simkins et al. 2015).

We investigated a sequence of raised shorelines in the north of Thomas Island (Profile N1; Fig. 6.1.1). The elevation of different beaches will provide evidence for the magnitude of RSL changes at northern Bunger Hills. Subsurface imaging and sampling for OSL dating has been performed to characterise the stratigraphy and produce age estimates of their formation (Fig. 6.1.7 and 6.1.8; Tab. 6.1.7). The investigated beaches face an open ocean embayment with the highest depositional sea level evidence (ridge) c. 8 metres above the modern shoreline, likely containing one of the most complete paleoshoreline sequences in the region (Fig. 6.1.7).

We surveyed the beach ridges using a Nikon Forestry Pro 2 laser range finder with a measured vertical closing error of 0.1-0.2 m per 100 m, creating a topographic beach profile of identified ridge sequences. Elevation data were also collected from GNSS receivers (Chapter 6.2). To produce a detailed elevation model of the geomorphic features, photogrammetry data were obtained. Data will be processed by the TU Dresden group (Chapter 6.2).

We used ground penetrating radar (GPR) to image the subsurface and nearshore stratigraphy of site N1 (Fig. 6.1.8). This is important when sediment structure variations are expected from different geomorphic features. We employed a sled-mounted Mala GX 160 MHz GPR antennae, taking four transect scans. Three of the four GPR transects ran perpendicular to the sea starting at the top of the slope, downwards towards the modern-day shoreline. One transect followed parallel to the modern shoreline, between the beach ridge sequences to capture information on lateral changes in deposition (Fig. 6.1.8).

To assess subsurface structure and to sample sandy beach material for OSL dating of these paleoshorelines, we dug a pit at the top of every second targeted beach ridge (three of six observed beaches) (Tab. 6.1.7). Pits ranged from 16 to 40 cm deep (Fig. 6.1.7), and had a relatively consistent structure and sedimentology. The surface consisted of clast-supported sandy gravels overlying sand. No fossilised shells or materials were found in the OSL pits. OSL samples were obtained from three beach ridges from sand intervals that resulted from coastal processes and avoided sands formed from aeolian processes. Sampling was difficult due to the sandy materials being frozen, which limited the depth of the excavation to a maximum of 40 cm.

OSL sampling was conducted by hammering a 24 cm long, 5 cm diameter metal tube into the side of a pit until the tube had completely penetrated the sandy material (Fig. 6.1.7). Prior to removing the metal tube, a sediment sample was taken for dosimetry and water content.

Tab. 6.1.7: OSL samples obtained from the beach ridges of N1.

Sample ID	Sample Type	Latitude South [°]	Longitude East [°]
TI_N1_T4_R2	OSL	66.09561	100.94498
TI_N1_T4_R4	OSL	66.09545	100.94528
TI_N1_T4_R6	OSL	66.09528	100.94567

The tube was then removed, ensuring sediment was tightly packed along its length so that sediment in the tube remained undisturbed/mixed. Each end of the tube was then sealed with tape. The PVC endcaps should ensure that no light has access to the grains at the centre of the sample. OSL samples were then placed into a light proof bag.

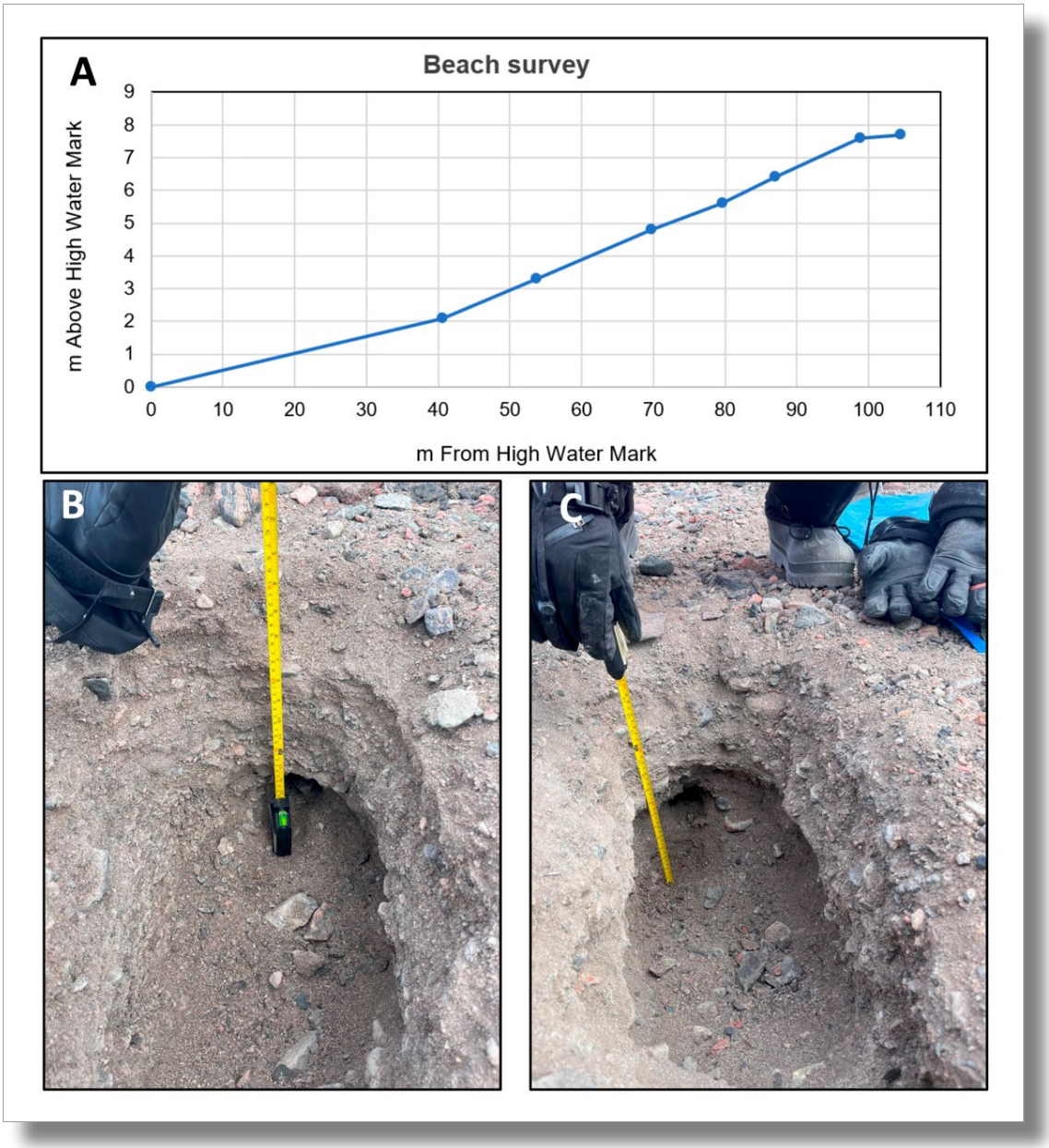

Fig. 6.1.7: A) Topographic survey of the beach, where each point represents an identified paleoshoreline with its elevation and distance between each ridge. B) and C) pits for OSL sampling

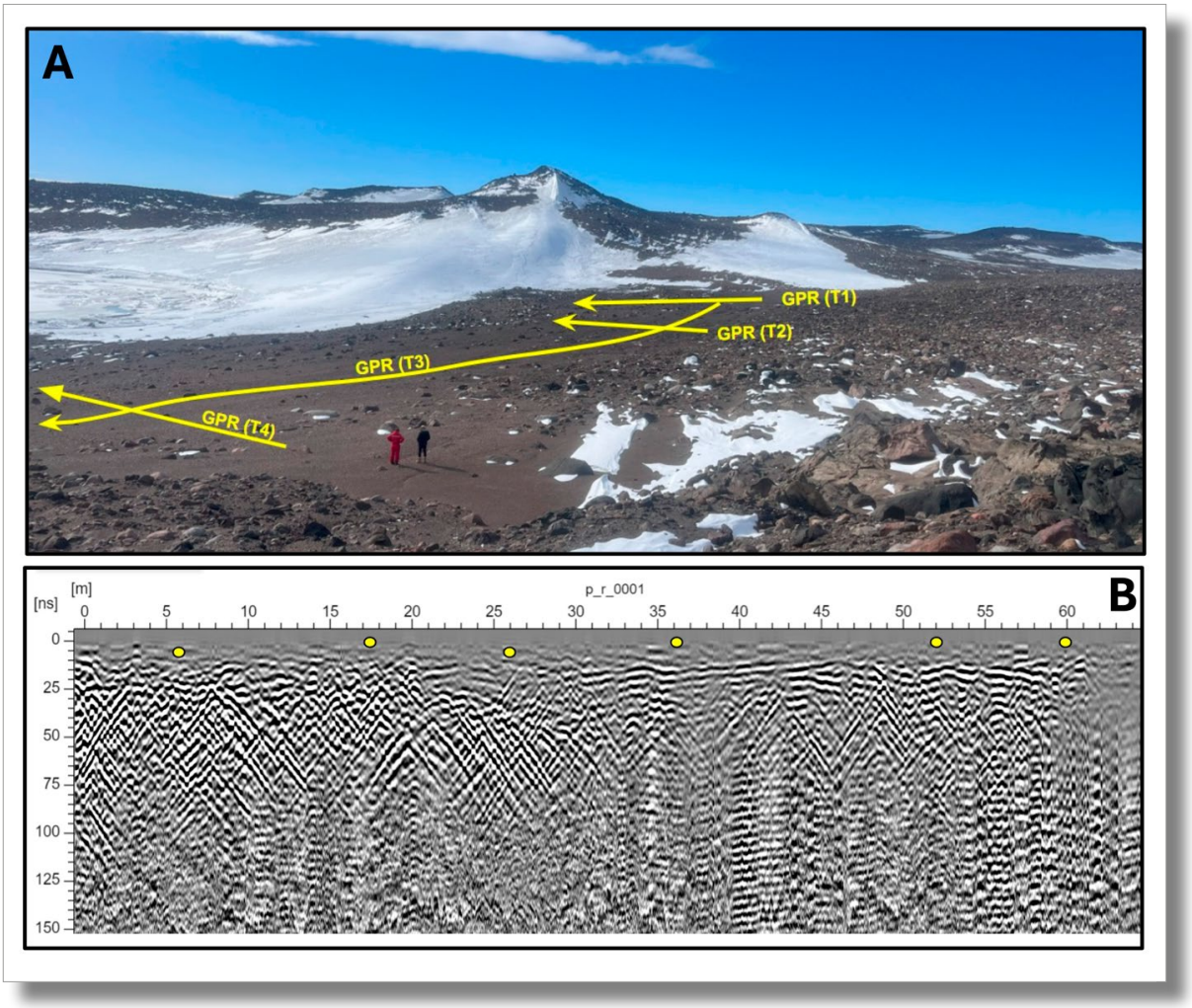

Fig. 6.1.8: Raw GPR data from one transect taken at raised beaches site N1 (location in Fig. 6.1.1). Annotated with yellow dots are the locations of the beach ridges where some variation in direction of depositional layers can be seen.

Snow petrel stomach oil deposits (mumiyo)

On Thomas Island, rock cavities on bedrock ridges and moraines in the surroundings of the field camp were searched for mumiyo deposits. During our stay, no flying snow petrels were observed, but three birds were found sitting in rock cavities, one of which was only identified acoustically. Samples were collected at two locations of un-occupied cavities (Tab. 6.1.8). At site BH-MUM-01, highly-weathered mumiyo deposits were found on the lee side of a rock cavity. The sample is palm-sized, flat, slightly stratified and about 1.5 cm thick. At the second location (BH-MUM-02) a very thin layer of mumiyo covered loose pebbles at the entrance of a narrow crevice. The sample was collected from the ground with a spoon and spatula and wrapped in pre-cleaned aluminium foil.

On Browning Peninsula (Windmill Islands), two snow petrels were observed in rock cavities. The cavities were not sampled so as not to disturb snow petrels. Thin mumiyo deposits were found in, and in front of, several empty rock cavities and were sampled at six sites (Tab. 6.1.8). While most samples are 0.1-0.5 cm thick, at one site a 2-5 cm thick, stratified deposit on the floor and wall inside a rock cavity of an abandoned cavity (BP-MUM-1-5) was sampled.

On Herring Island (Windmill Islands) one flying snow petrel was observed and foot prints of birds were visible in the snow around some rock cavities. Mumiyo deposits on Herring Island were mostly thin yellow-grayish crusts (< 0.5 cm). Nine sites were suitable for sampling, three of which contained deposits > 5 cm thick (Fig. 6.1.9). At the site HI-MUM-03 an unoccupied cavity in bedrock contained mumiyo as thin crusts on the cavity floor, but also stalactite-like mumiyo deposits on the ceiling, as well as a 5-6 cm thick deposit with a waxy and smooth surface on the cavity wall. The other sites with thicker mumiyo deposits were HI-MUM-1-6, where a 5 cm-long stalactite-like mumiyo deposit was found and site HI-MUM-09, where a patch-like 10 cm-thick mumiyo deposit was collected.

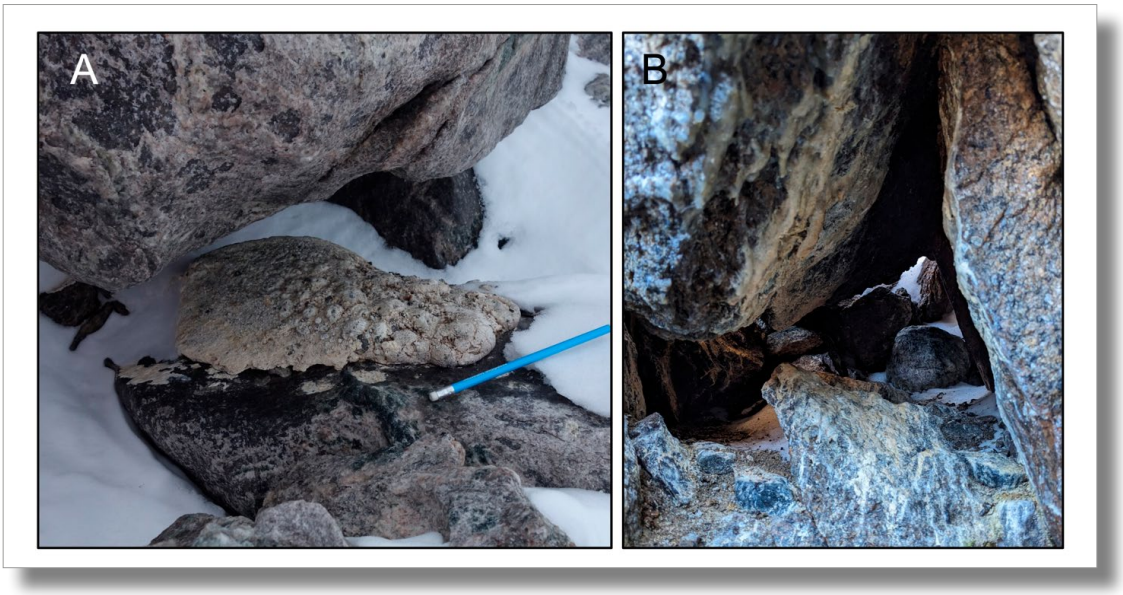

Fig. 6.1.9: A) Mumiyo deposit HI-MUM-09 showing a typical white crust. B) Thin mumiyo crusts on the floor and walls of an empty cavity

Tab. 6.1.8: Summary of mumiyo samples collected at Bunger Hills and Windmill Islands

Location	Site ID	Latitude South [°]	Longitude East [°]
Thomas Island	BH-MUM-01	66.10542	100.94732
Thomas Island	BH-MUM-02	66.10554	100.94801
Browning Peninsula	BP-MUM-1-1	66.46467	110.54615
Browning Peninsula	BP-MUM-1-2	66.46463	110.54390
Browning Peninsula	BP-MUM-1-3	66.46962	110.55582
Browning Peninsula	BP-MUM-1-5	66.46933	110.55595
Browning Peninsula	BP-MUM-2-1	66.46601	110.55449
Browning Peninsula	BP-MUM-2-2	66.46085	110.54332
Herring Island	HI-MUM-01	66.40832	110.61429
Herring Island	HI-MUM-02	66.40917	110.61451
Herring Island	HI-MUM-03	66.41058	110.61472
Herring Island	HI-MUM-04	66.41108	110.61437
Herring Island	HI-MUM-05	66.41164	110.61548

Location	Site ID	Latitude South [°]	Longitude East [°]
Herring Island	HI-MUM-06	66.40427	110.60863
Herring Island	HI-MUM-07	66.40429	110.60843
Herring Island	HI-MUM-08	66.40440	110.60716
Herring Island	HI-MUM-09	66.41309	110.41572

Other samples

Sediment samples were collected from the catchment and shore area of Western Ear Lake to characterize potential inputs of organic and minerogenic components into this and other lakes (Fig. 6.1.10, Tab. 6.1.9). Geochemical and biogeochemical analyses on these samples will help to develop new environmental proxies for paleoclimate reconstructions based on lake sediment sequences. Mineral magnetic/ biomagnetic investigations will be carried out on the material to study the abundance and variability of the fossil remains of magnetotactic bacteria in the lake sediments. These magnetofossils are thought to be ubiquitous in aquatic environments and are likely to be an important contributor to magnetic enrichment in aquatic sediments and thus to the record of palaeomagnetic signals. However, the study of magnetofossils in Antarctica has been limited to a few studies in marine environments (e.g. Vali et al. 1987). Therefore, this study will provide the first detailed evidence on the abundance and variability of magnetofossils in limnic environments in Antarctica. In order to characterize the mineral-magnetic background signal that results from physical weathering, a variety of frequently occurring rock types were collected from the catchment area of Western Ear Lake as reference material (Fig. 6.1.10, Tab. 6.1.9).

The microbial biodiversity of biological soil crusts in Antarctica is little known, although they are an important component of Antarctic terrestrial ecosystems (e.g. Colesie et al. 2014). For contributing to research on biodiversity and functional evidence of microbial networks, one site on Browning Peninsula was sampled for biological soil crusts (Tab. 6.1.9). On Thomas Island, however, we did not observe soil crusts, lichens or mosses although fine-grained material was widely abundant (Fig. 6.1.10).

Tab. 6.1.9: Summary of samples taken for geochemical and biogeochemical analyses

ID	Latitude South [°]	Longitude East [°]	Comment
BH_SoSa01	66.10448	100.95096	Sediment from inlet drainage channel
BH_SoSa02PM	66.10197	100.96146	Till from slope above the lake
BH_SoSa02	66.10141	100.95789	Quartz pebble with green algae and underlying sediment
BH_SoSa03	66.10309	100.94461	Sediment from waterline (incl. algae)
BH_SoSa04PM	66.10233	100.94441	Grey till near lake shore
BH_SoSa04	66.10309	100.94461	Algae and soil from shore line
BH_SoSa05PM	66.10500	100.94570	Sediment from dry meltwater pond
BH_SoSa05	66.10224	100.93916	Sediment with filamentous algae at lake shore
BH_SoSa06PM	66.10474	100.94794	Sediment from dry overflow channel
BH_SoSa06	66.11369	100.98674	Grey till near lake shore
BH_SoSa07PM	66.11242	100.98325	Sediment from the shore

ID	Latitude South [°]	Longitude East [°]	Comment
BH_SoSa07	66.10224	100.93916	Sediment with filamentous algae at lake shore
BH_SoSa08	66.10918	100.95652	Sandy sediment from lake shore, including brown algae mats
BP_SC032024	66.45883	110.54169	Soil crust and sediment

Fig. 6.1.10: Sampling site of surface sediments in the catchment and along the shore of Ear Lake on Thomas Island (A-E). A) Thin salt crusts, B) decaying algae mats along shore line of lake, C) fine-grained sediments from inactive drainage channel E) green filamentous algae at the waterline, D) fine-grained gray till. E) green filamentous algae at the waterline, F) Soil crust sampled at Windmill Islands: three petri dishes indicate the position of soil crust samples. For scale: The pencil has got a length of 18.5 cm.

Data management

Environmental data will be archived, published and disseminated according to international standards by the World Data Center PANGAEA Data Publisher for Earth & Environmental Science (https://www.pangaea.de) within two years from the end of the expedition. By default, the CC-BY license will be applied. Any other data will be submitted to appropriate long-term archives that provide unique and stable identifiers for the datasets and allow open online access to the data. This expedition was supported by the Helmholtz Research Programme “Changing Earth – Sustaining our Future”.

In all publications based on this expedition, the **Grant No. AWI_PS141_04** will be quoted and the following publication will be cited: Alfred-Wegener-Institut Helmholtz-Zentrum für Polar- und Meeresforschung (2017) Polar Research and Supply Vessel POLARSTERN Operated by the Alfred-Wegener-Institute. Journal of large-scale research facilities, 3, A119. http://dx.doi.org/10.17815/jlsrf-3-163.

References

Adamson DA, Colhoun EA (1992) Late Quaternary glaciation and deglaciation of the Bunger Hills, Antarctica. Antarctic Science 4:435-446.

Ainley DG, Hobson KA, Crosta X, Rau GH, Wassenaar LI, Augustinus PC (2006) Holocene variation in the Antarctic coastal food web: linking δD and δ13C in snow petrel diet and marine sediments. Marine Ecology Progress Series 306:31-40.

Augustinus PC, Gore DB, Leishman MR, Zwartz D, & Colhoun EA (1997) Reconstruction of ice flow across the Bunger Hills, East Antarctica. Antarctic Science 9:347-354.

Augustinus PC (2002) Weathering Characteristics of the Glacial Drifts, Bunger Hills, East Antarctica. Arctic, Antarctic, and Alpine Research 34:65-75.

Berg S, White DA, Hermichen WD, Emmerson L (2019a) Late Holocene colonisation of snow petrels (Pagodroma nivea) of the Prince Charles Mountains, Antarctica. Polar Biology 42:1167-1173.

Berg S, Melles M, Hermichen WD, McClymont EL, Bentley MJ, Hodgson DA, Kuhn G (2019b) Evaluation of mumiyo deposits from East Antarctica as archives for the Late Quaternary environmental and climatic history. Geochemistry, Geophysics, Geosystems 20:260-276.

Berg S, Emmerson L, Heim C, Buchta E, Fromm T, Glaser B, Hermichen W-D, Rethemeyer J, Southwell C, Wand U, Zech M, Melles M (2023) Reconstructing the paleo-ecological diet of snow petrels (*Pagodroma nivea*) from modern samples and fossil deposits - implications for Southern Ocean paleoenvironmental reconstructions. Journal of Geophysical Research: Biogeosciences 128: e2023JG007454.

Colesie C, Gommeaux M, Green TA, Büdel B (2014) Biological soil crusts in continental Antarctica: Garwood Valley, southern Victoria Land, and Diamond Hill, Darwin Mountains region. Antarctic Science 26:115-123.

Goodwin ID (1993) Holocene deglaciation, sea-level change, and the emergence of the Windmill Islands, Budd Coast, Antarctica. Quaternary Research 40:55-69.

Gore DB, Rhodes EJ, Augustnus PC, Leishman MR, Colhoun EA, Rees-Jones J (2001) Bunger Hills, East Antarctica: ice free at the Last Glacial Maximum. Geology 29:1103-1106.

Gore DB, Leishman MR (2020a) Tafoni show postglacial and modern wind azimuths that are similar at Bunger Hills. Antarctic Science, 32(2):132-137. https://doi.org/10.1017/S095410201900035XGore DB, Leishman MR (2020b) Salts, sediments and weathering environments in Bunger Hills. Antarctic Science 32(2):138-152. https://doi.org/10.1017/S0954102020000073Hiller A, Wand U, Kämpf H,

Stackebrandt W (1988) Occupation of the Antarctic continent by petrels during the past 35 000 years: inferences from a ^{14}C study of stomach oil deposits. Polar Biology 9:69-77.

Li J, Menguy N, Roberts AP, Gu L, Leroy E, Bourgon J, Yang X, Zhao X, Liu P, Changela HG, Pan Y (2020) Bullet-Shaped Magnetite Biomineralization Within a Magnetotactic Deltaproteobacterium: Implications for Magnetofossil Identification. Journal of Geophysical Research: Biogeosciences 125: e2020JG005680.

Mackintosh A, Golledge N, Domack E, Dunbar R, Leventer A, White D, Lavoie C (2011) Retreat of the East Antarctic ice sheet during the last glacial termination. Nature Geoscience 4:195-202.

Matthews JA, Winkler S (2022) Schmidt-hammer exposure-age dating: a review of principles and practice, Earth-Science Reviews 230:104038. https://doi.org/10.1016/j.earscirev.2022.104038

Meredith KT, Saunders KM, McDonough LK, McGeoch M (2022) Hydrochemical and isotopic baselines for understanding hydrological processes across Macquarie Island. Scientific Reports 12:21266.

Moriwaki K, Hirakawa K, Matsuoka N (1991) Weathering stage of till and glacial history of the central Sør Rondane Mountains, East Antarctica. Proceedings of NIPR Symposium on Antarctic Geosciences 5:99-111.

Moriwaki K, Iwata S, Matsuoka N, Hasegawa H, Hirakawa K (1994) Weathering Stage as a Relative Age of Till in the Central Sør Rondane. Proceedings of NIPR Symposium on Antarctic Geosciences 7:156-161.

Muru M, Rosentau A, Preusser F, Plado J, Sibul I, Jõeleht A, Kriiska A (2018) Reconstructing Holocene shore displacement and Stone Age palaeogeography from a foredune sequence on Ruhnu Island, Gulf of Riga, Baltic Sea. Geomorphology 303:434-445.

Rignot E, Mouginot J, Scheuchl B, Van Den Broeke M, Van Wessem MJ, Morlighem M (2019) Four decades of Antarctic Ice Sheet mass balance from 1979–2017. Proceedings of the National Academy of Sciences 116:1095-1103.

Rintoul SR, Silvano A, Pena-Molino B, van Wijk E, Rosenberg M, Greenbaum JS, Blankenship DD (2016) Ocean heat drives rapid basal melt of the Totten Ice Shelf. Science Advances, 2:e1601610.

Screening Eagle (Proceq) (2024) Rock Schmidt RS8000. https://www.screeningeagle.com/en/products/rock-schmidt-rs8000

Simkins LM, Simms AR, DeWitt R (2015) Assessing the link between coastal morphology, wave energy and sea ice throughout the Holocene from Antarctic raised beaches. Journal of Quaternary Science 30(4):335-348.

Vali H, Förster O, Amarantidis G, Petersen N (1987) Magnetotactic bacteria and their magnetofossils in sediments. Earth and Planetary Science Letters 86:389-400.

Verkulich SR, Melles M, Hubberten HW, Pushina ZV (2002) Holocene environmental changes and development of Figurnoye Lake in the southern Bunger Hills, East Antarctica. Journal of Paleolimnology 28:253-267.

White D, Bennike O, Berg S, Harley SL, Fink D, Kiernan K, McConnell A, Wagner B (2009) Geomorphology and glacial history of Rauer Group, East Antarctica. Quaternary Research 72:80-90. https://doi.org/10.1016/j.yqres.2009.04.001

White D, Fink D, Gore DB (2011) Cosmogenic nuclide evidence for enhanced sensitivity of an East Antarctic ice stream to change during the last deglaciation. Geology 39(1):23-26. https://doi.org/10.1130/G31591.1

White DA, Fink D, Lilly K, O'Brien P, Dorschel B, Berg S, Wagner B (2022) Rapid ice sheet response to deglacial and Holocene paleoenvironmental changes in eastern Prydz Bay, East Antarctica. Quaternary Science Reviews 280:107401.

6.2 Geodetic-Geophysical Investigations

Mirko Scheinert[1], Lutz Eberlein[1], Erik Loebel[1], [1]DE.TU-DRESDEN
Xabier Blanch Gorriz[1], Jodi Fox[2], Jack Beardsley[2], [2]AU.UTAS
Marie Weber[1], [3]AU.UC
not on board: Matt King[2], Kate Selway[2],
Tobias Stål[2], Anya Reading[2], Duanne White[3]

Grant-No. AWI_PS141_05

Objectives

The glacial history of the Antarctic Ice Sheet – from the last glacial maximum up to present day – directly affects the deformation of the Earth. The response of the Earth is governed by the properties of its interior, the rheology of the Earth (especially effective elastic thickness of the lithosphere, and viscosity of the upper and lower mantle). Both quantities – ice-load history and Earth's rheology – lead to the process of glacial-isostatic adjustment (GIA, e.g. Whitehouse et al. 2019; Scheinert et al. 2021). Thus, a main goal of the geodetic-geophysical programme was to realise geodetic GNSS observations and to link them, where possible, to measurements of further geophysical sensors.

Hence, it was the aim to visit already existing permanently recording GNSS sites for maintenance which was successfully accomplished for one location. At three locations new permanent GNSS stations were set up. Additionally, geophysical observations of magnetotellurics (MT) were planned but could not be realised. The map in Figure 6.2.1 gives an overview of all locations at the East Antarctic coastal margin relevant to this project.

Furthermore, a geodetic-geological field campaign at Gaussberg was carried out. Gaussberg, with a height of about 370 m, is of volcanic origin, erupted subglacially about 56 ka B.P. and, as the most isolated Quaternary volcanic centre in Antarctica, is of great importance for the paleoenvironment (Smellie and Collerson 2021). In April/May 1902 and in September/ October 1902, during the 1st German South Polar Expedition under the leadership of Erich von Drygalski, an extensive geodetic survey of Gaussberg was performed determining horizontal coordinates of points at the mountain and on the ice surface as well as their heights relative to sea level (Drygalski et al. 1906; Drygalski 1921). Therefore, our re-survey of the Gaussberg will allow us to infer height changes as well as changes of the ice-flow velocity in its direct vicinity over a time span of 120 years. This survey was accompanied by photogrammetric measurements to generate a high-resolution digital elevation model (DEM) of the Gaussberg area which can be used for further geomorphological-glaciological investigation as well as to aid the inference of contemporary ice-flow velocity. Geological sampling was done in order to improve our knowledge on the geologic-vulcanological characteristics of Gaussberg and to aid the reconstruction of climate history.

GNSS stations at bedrock for GIA and further geodynamic studies

Except Gaussberg, all land locations were reached during day visits (Fig. 6.2.1). For shorter visits the helicopter stayed on site especially for the maintenance of an existing GNSS site. For the installation of new GNSS sites, which took about three to four hours, the helicopter returned to the ship or was used for further actions in the meantime. This programme was accomplished in collaboration with the group of Matt King (University of Tasmania) who is already running a number of permanent GNSS sites along the East Antarctic coast (King et al. 2022). The details of each GNSS site are given in Table 6.2.1 and 6.2.2.

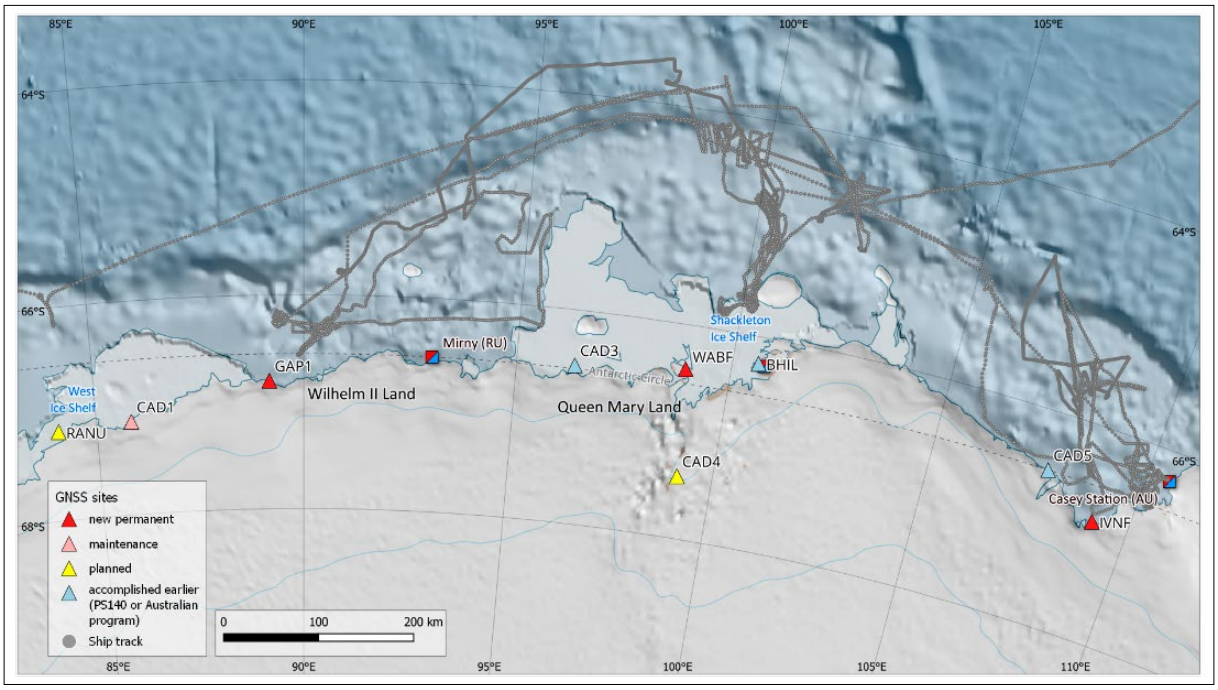

Fig. 6.2.1: Overview map showing the locations of the GNSS sites. The GNSS site CAD3 was serviced during cruise PS140, maintenance at the sites BHIL and CAD5 was not planned for this cruise, but all three locations are also shown for completeness. Site CAD6 (not shown) is located in a distance of about 470 km southeast of Casey.

Tab. 6.2.1: GNSS sites on bedrock. Column “Date 2024” gives the day of visit or the day of first observation (in case of a new site).

ID	Location	Latitude South [°]	Longitude East [°]	Remark	Date
RANU	Ravich Nunatak (West Ice Shelf)	67.1670	84.0689	new installation planned, could not be performed	
CAD1	Carey Nunatak (West Ice Shelf)	67.1306	85.8365	maintenance successfully performed	28.03.2024
GAP1	Gaussberg	66.80248	89.17860	new permanent installation	12.03.2024
WABF	Watson Bluff (Shackleton Ice Shelf)	66.4167	98.9500	new permanent installation	21.03.2024
CAD4	Mt. Strathcona	67.41955	99.14367	maintenance planned, could not be performed	
IVNF	Ivanhoff Head	66.88037	109.12976	new permanent installation	05.03.2024
CAD6	Chick I.	66.7894	120.9886	maintenance planned, could not be performed	

Of the already existing GNSS sites only the site CAD1 (Carey Nunatak) could be reached during this cruise and was visited on 28 March 2024. At this site the installation was accomplished in the season 2016/2017, but the site had not been visited since then. During the visit, the

station was successfully upgraded (replacement of receiver and further electronic parts; see Tab. 6.2.2 and Fig. 6.2.2 and 6.2.3). The original receiver was returned to the ship, so that the data could be downloaded. Data was successfully recorded from January 2017 to March 2024 (with some data breaks in the austral winter).

Furthermore, three new permanent GNSS installations were deployed, namely at Gaussberg (GAP1), at Watson Bluff (WABF) in the region of the Shackleton Ice Shelf, and at Ivanhoff Head (IVNF) southwest of *Casey Station* (see Fig. 6.2.1 and Tab. 6.2.1 for location details).

The setup at GAP1 was done by TUD during the Gaussberg field campaign. Two Zarges boxes (each 80 cm x 60 cm x 60 cm) containing the receiver, Iridium Certus, batteries and further electronics were placed in a distance of about 30 m from the antenna pillar. These boxes are secured by a steel frame which also carries the Iridium antenna. Adjacent to these, six solar panels were mounted close to the ground, with a slight slope towards northern direction. See Table 6.2.2 for the details of the equipment, and Figures 6.2.4 and 6.2.5 for an overview of the setup.

The setup at WABF (Fig. 6.2.6 and 6.2.7) and IVNF (Fig. 6.2.8) follows the UTAS layout and consists of one aluminium frame that secures the solar panel, Iridium antenna and GNSS enclosure, and a GNSS monument plus antenna up to 25 m from the frame. The GNSS monument is anchored directly into bedrock using expanding rock anchors, while the GNSS frame is secured using chain and climbing bolts. Both sites use two batteries (250 Ah total) and 160 W of solar input to keep them charged (cf. also Tab. 6.2.2).

Tab. 6.2.2: Overview of permanent GNSS installations. At IVNF, WABF and GAP1 new installations were set up. At CAD1 maintenance was done, and equipment changed / upgraded (old and new equipment given in subsequent rows).

Location	Receiver	Antenna	Satellite communication	Batteries	Solar panel
Ivanhoff Head (IVNF)	REFTEK Resolute Polar S/N 0530	Septentrio PolaNt-x MF S/N 14708	Internal Iridium modem with AeroAntenna AT1621-142	250 Ah (2x 125 Ah VRLA- AGM GPL-31XT)	160 W (1x 160 W Symmetry PV SY3-M160W/ LH4)
Watson Bluff (WABF)	REFTEK Resolute Polar S/N 0529	Septentrio PolaNt-x MF S/N 14713	Internal Iridium modem with AeroAntenna AT1621-142	250 Ah (2x 125 Ah VRLA- AGM GPL-31XT)	160 W (1x 160 W Symmetry PV SY3-M160W/ LH4)
Gaussberg (GAP1)	Septentrio Mosaic-X5 S/N 3684492	navXperience NAX3g+C S/N RE0521	Iridium Certus SkyLink 5100	600 Ah (6x 100 Ah VRLA-AGM Kung Long MP-10012C)	210 W (6x 35 W Phasun PN-SPR S35)
Carey Nunatak (CAD1)	Trimble Net R9, S/N 5502R50058	Trimble 59800.00 with SCIGN radome, S/N 5508356075	N/A	98 Ah (1x GelTech 8G-31DTM)	80 W (1x SHARP NE-80EJEA)
	REFTEK Resolute Polar S/N 0341		Internal Iridium modem with AeroAntenna AT1621-142	196 Ah (2x GelTech 8G-31DTM)	

Fig. 6.2.2: GNSS receiver setup at CAD1/Carey Nunatak after upgrade was complete (Iridium antenna installed on frame and enclosure swapped for new GNSS receiver)

Fig. 6.2.3: GNSS monument and antenna at CAD1/Carey Nunatak, looking true east

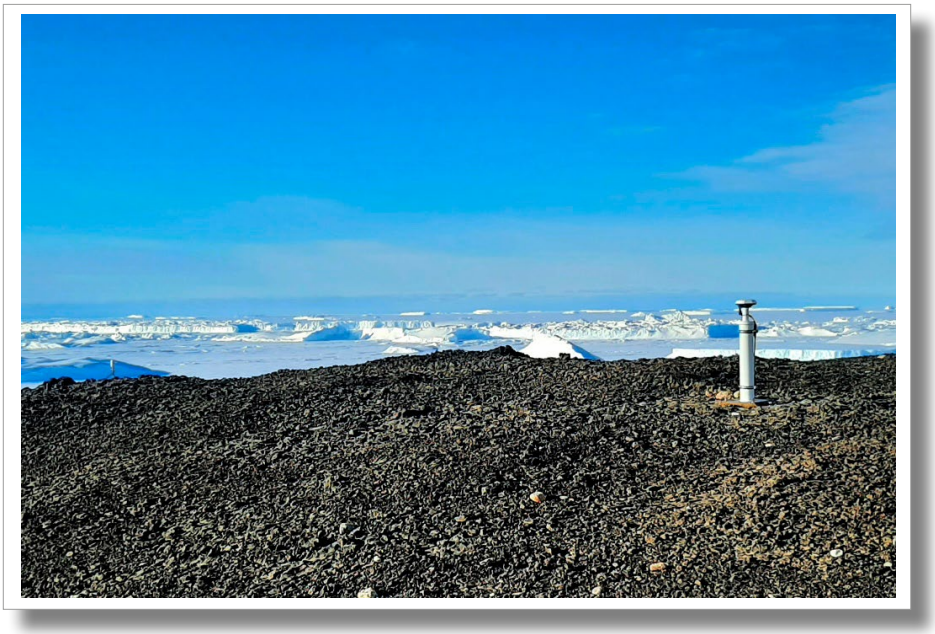

Fig. 6.2.4: GNSS pillar and antenna at GAP1/Gaussberg, looking north. To the left, just at the edge of the rim, the Iridium antenna can be seen (mounted at top of the frame, cf. Fig. 6.2.5).

Fig. 6.2.5: GNSS setup at GAP1/Gaussberg, with receiver, Iridium Certus, batteries and further parts contained in the two Zarges aluminium boxes, Iridium antenna on top of the frame, and solar panels installed close to the ground

Fig. 6.2.6: GNSS monument and antenna at WABF/Watson Bluff, looking true west

Fig. 6.2.7: New GNSS frame at WABF/Watson Bluff after installation (frame features 160 W solar panel, enclosure with batteries, receiver and Iridium antenna). GNSS antenna located about 15 m true east

Fig. 6.2.8: (Left) GNSS monument and antenna at IVNF/Ivanhoff Head, looking true west. (Right) New GNSS frame at IVNF/Ivanhoff Head after installation (frame features 160 W solar panel, enclosure with batteries, receiver and Iridium antenna)

Field campaign at Gaussberg

At Gaussberg a field campaign was carried out for a duration of three weeks, from 25 February to 16 March 2024. Two helicopter flights were already performed on 24 February 2024 to transport the first equipment to Gaussberg. The remaining scientific and camp equipment as well as all five participants were flown on 25 February 2024. The weight of the entire equipment (without persons) was 3.8 tons. The pick-up and return transport took place mainly on 16 March 2024 with two additional helicopter flights accomplished on 17 March 2024. A general view of Gaussberg is given in Figure 6.2.9, including some annotations on principal geographical features and the location of the field camp.

For the field camp the following equipment was used, provided by AWI logistics: a light-weight stable igloo fibreglass cabin (‘tomato’), two Scott tents, five Bergans tents used as sleeping tents, field parties, 2 kW Honda generators, and further equipment. To travel on ice surface, two snowmobiles (Lynx) and two Nansen sledges were available. Figures 6.2.10 to 6.2.12 illustrate the setup of the field camp.

Due to weather conditions, of the 21 days the group spent at Gaussberg, in total only 11 days could be used for work. Considering the work hours needed to establish, secure and dismantle the field camp, there were only about 9 days left to accomplish the tasks of the scientific programme. We faced especially disadvantageous conditions on 3 March 2024, with a low pressure system affecting the Gaussberg area which resulted in a minimum air pressure of 947 hPa and wind velocities of about 30 m/s with gusts of up to 40 m/s, which forced us to take down all five sleeping tents and one Scott tent. All five participants spent the subsequent four nights in the igloo as well as most of the days. The field camp could not be re-established until

the 7 March 2024 (Fig. 6.2.11). Three Bergans tents (out of five) were usable for sleeping (two persons continued to spent the nights in the igloo), and only one Scott tent was used for the remaining time.

Fig. 6.2.9: Aerial view of Gaussberg, direction south-east, with annotations. See also maps in Fig. 6.2.13 and 6.2.14.

Fig. 6.2.10: Initial setup of field camp at Gaussberg (left), with storm and snow drift (right)

Fig. 6.2.11: Setup of field camp after 8 March 2024, looking north-west from the GNSS site GAU1

According to the scientific programme the following works were planned:

1. Rediscovery and identification of those locations at Gaussberg that were marked (by cairns) by the Drygalski expedition in 1902, and RTK measurement by GNSS;
2. Static and kinematic GNSS measurements at the ice surface close to Gaussberg covering the area of the measurements accomplished by the Drygalski expedition in 1902;
3. Set-up of one temporary GNSS installation to measure the sea surface at the northern shore of Gaussberg utilizing the method of GNSS reflectometry;
4. Static photogrammetric recordings to infer ice-surface geometry and ice-flow velocity, and (supplementing GNSS reflectometry) of the sea surface;
5. UAV-based photogrammetric survey to infer a high-resolution digital elevation model of Gaussberg and the ice surface in its vicinity, and to infer ice-flow velocity;
6. Sampling for geological investigation and climate reconstruction.

All but one of the above-mentioned topics could be fulfilled to a certain extent. It was not possible to do any work on the ice surface (topic b) – we simply lacked the time due to the above described weather conditions. In the following, the different topics will be discussed in detail. Maps of the Gaussberg area with all measurement points are given in Figures 6.2.12. (general map) and 6.2.13 (detailed map of camp area at western side of Gaussberg). The locations of geologic samplings are shown in Figure 6.2.22.

Geodetic survey at Gaussberg

To facilitate the geodetic survey at Gaussberg, a GNSS campaign site was established previously during cruise PS140 on 7 January 2024 (see cruise report of PS140, Chapter 6). Unfortunately, due to a receiver failure, data was recorded only on 7 and 8 January 2024. The receiver was replaced, and the recording was re-started on 28 February 2024. Later (after the heavy storm on 3 March 2024), the two solar panels had to be replaced, the 30 m antenna cable was replaced by a 10 m cable, and a radio modem with antenna was installed on 8 March 2024 to enable the transmission of correction data for the real-time kinematic (RTK) measurements (Fig. 6.2.14). Details on the location and equipment of the reference site and the RTK rover can be found in the Tables 6.2.3 and 6.2.4.

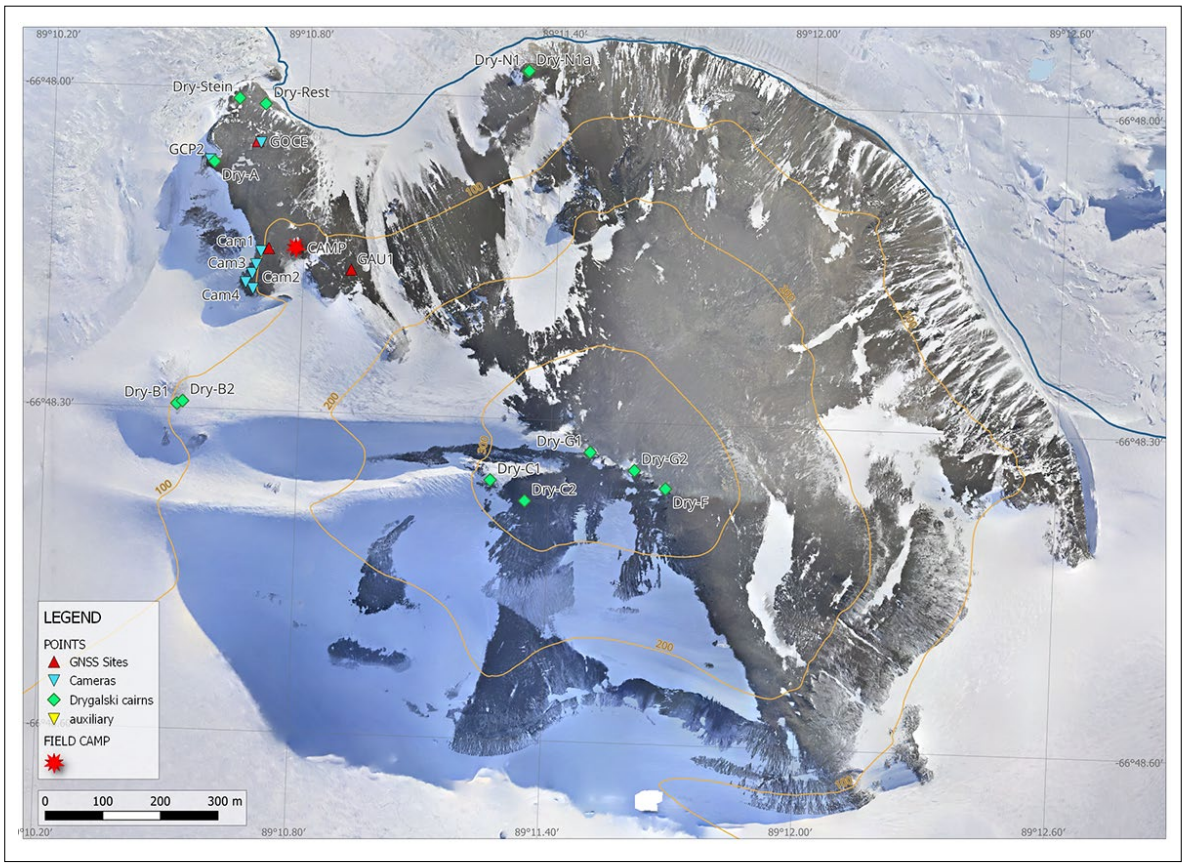

Fig. 6.2.12: Map of Gaussberg with measurement points
Background: preliminary orthophoto inferred from photogrammetric survey

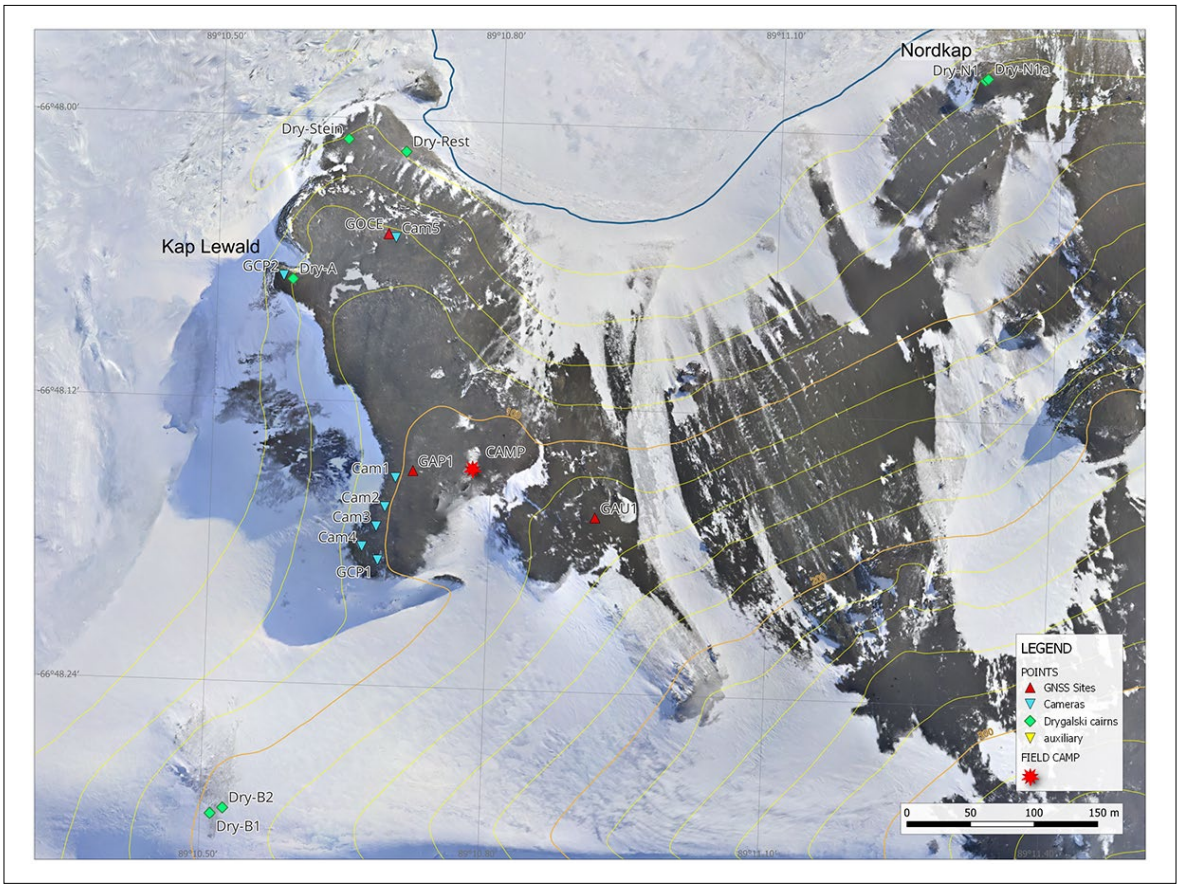

Fig. 6.2.13: Detailed map of the plateau at the western side of Gaussberg, where the camp and majority of measurement points were located.

Tab. 6.2.3: GNSS sites temporarily established during the field campaign at Gaussberg

ID	Longitude East [°]	Latitude South [°]	Remark	Date
GAU1	89.18189	66.80276	campaign site, RTK reference	7/8 Jan, 28.02.-15.03.2024
RTK Rover			rover equipment, different points	
GOCE	89.17803	66.80081	ocean observation at northwestern bay	27.02.-03.03.2024, 11.-15.03.2024

Tab. 6.2.4: Overview of additional GNSS sites and equipment temporarily established during the Gaussberg field campaign. At the site GOCE the receiver had to be replaced after the heavy storm on 3 March 2024.

Location	Receiver	Antenna	Batteries	Solar panel
Gaussberg RTK reference (GAU1)	Leica GR25 S/N 1831215 (only DOY 7 to 8) S/N 1831210 (DOY 59 to 75)	Leica AR10 S/N 17280009 (with separator 9) direction: 0° to mag north	1x 34 Ah, from DOY 68: 100 Ah VRLA-AGM Kung Long, MP-3412C and MP-10012C, resp.	2x 35 W Phasun PN-SPR S35
Gaussberg RTK Rover	Leica GS25 S/N 1823511 with controller CS15 S/N 2906612	Leica AX1203+GNSS S/N 092400097	internal battery	none
Gaussberg ocean (GOCE) 27.02.-03.03.2024 // 11.-15.03.2024	Leica GRX1200+ GNSS S/N 495286	Leica AX1203+GNSS S/N 09240086	1x 34 Ah VRLA-AGM Kung Long, MP-3412C	2x 35 W Phasun PN-SPR S35
	Septentrio Mosaic-X5 S/N 3613414			1x 35 W Phasun PN-SPR S35

Fig. 6.2.14: GNSS campaign station GAU1, looking north. Foreground left: Zarges box with receiver, battery, radio modem and solar panels mounted on top, and radio antenna fixed at a tripod. Center to the right: GNSS antenna, mounted at a special bolt which is fixed into the ground.

Some of the accessible locations where the Drygalski expedition established cairns to mark the mountain points (“Bergpunkte”) for the Gaussberg survey were visited when weather permitted. It was possible to identify these points by help of the estimated location given in the

maps published by Drygalski (1906, 1921). For mountain points at the summit of Gaussberg, additionally approximate coordinates were used which were predicted by application of a Helmert transformation (see below). The positions of the former cairns were identified by the still existing piles of rocks, although no real cairns exist anymore (examples see Figs. 6.2.15 and 6.2.16). Since the volcanic material is not well suited to erect cairns they had to use erratic rocks as far as possible. Drygalski (1904) reported, that they had to repeatedly deploy the bamboo canes and to re-erect the cairns since volcanic rocks simply rolled away, and it was hard to find erratics at the different locations. These erratic rocks were found to form a reasonable cluster still today. However, the exact position of the bamboo cane marking the respective mountain point can be identified with an accuracy of only 1 to 2 m (which is still in the range of the measurement precision of Drygalski's survey). All found and identified mountain points were re-measured by RTK, where the antenna was mounted on top of a special antenna rod. The length of this rod (exactly 2 m) was automatically taken into consideration during the RTK measurement. The receiver (powered by an internal battery) was carried in a special backpack.

The mountain points A (Fig. 6.2.15), B and N1 (Nordkap) where measured on 8 and 10 March 2024, respectively. At the location of the mountain points B and N1 (Nordkap) two remaining piles of rocks were found, which were both measured and named B1 and B2, and N1 and N1a, respectively. The (more likely) correct location can be identified by the subsequent analysis.

For this, a preliminary analysis was done already in the field. The so-called Helmert transformation links the horizontal coordinates of the first system – here the local coordinates of the Drygalski survey – with the horizontal coordinates of the second system, here coordinates in the UTM zone 45 south (UTM45S). The vector denotes the shift of the origin, and the rotation matrix

- which, for small rotation angle, can be approximated by the second term. To determine the transformation parameters and, the local coordinates and the UTM coordinates of identical points are needed. In a preliminary analysis, this was accomplished using the mountain points A, B and N1, where the UTM45S coordinates were inferred from the RTK measurements (with a subsequent map projection of ellipsoidal coordinates to UTM45S). It turned out that using the locations B2 and N1a (together with A) gives the best result. Applying the (preliminary determined) parameters in the Helmert transformation, UTM45S and, thus, ellipsoidal coordinates of the other mountain points could be predicted.
- On 15 March 2024, during the ascent to and work at the summit of Gaussberg, the mountain points G1, G2 (Fig. 6.2.16), F, C1 and C2 could be measured by RTK. A thorough analysis to determine the 'best' parameters of the Helmert transformation will be done at the home institution. Subsequently, the Helmert transformation can be applied for the ice points of the Drygalski expedition, too, where the ice surface heights will be inferred. This will also be subject for later processing.
- The details of all points measured by RTK are given in Appendix A.9.

Fig. 6.2.15: Mountain point A: RTK measurement (left), remnants of the cairn (right)

Fig. 6.2.16: Mountain point G2: RTK measurement (left), remnants of the cairn looking west towards G1 (right)

- A further GNSS equipment was installed about 250 m north-west of the field camp, at the edge of the plateau such that the antenna is allowed to receive the indirect signal reflected from the ice-covered ocean surface at the northern bay (Fig. 6.2.17 left). This temporary installation should enable to apply the technique of GNSS reflectometry in order to infer height changes of the local sea level. Installed on 27 February 2024, the set-up was destroyed during the storm on 3 March 2024. The Zarges aluminium box, the antenna cable as well as one solar panel were blown away by heavy gusts. Fortunately, the receiver and the battery could be found later down at the bay, although damaged. The recording was re-started on 11 March 2024 (using another receiver), and lasted until 15 March 2024, see Figure 6.2.17 as well as Table 6.2.3 for coordinates and 6.2.4 for technical details.

Fig. 6.2.17: Set-up of the GNSS site GOCE, looking at the northern bay of Gaussberg to infer measurements of the local sea level by GNSS reflectometry. Left: Initial set-up (28.02.- 03.03.2024). Right to the GNSS antenna the tripod with the time-laps camera was installed (see also Fig. 6.2.20). At the right margin in the middleground: Nordkap. Right: Second set-up (11.-15.03.2024)

- Close to the GNSS installation a time-laps camera was installed as well, which also was blown away on 3 March 2024 (and, too, found later), see the subsequent paragraph. The data will be analysed at the home institution, and will be combined with the results of the time-laps camera and of UAV flights which were repeated over this area.

Photogrammetric static measurements at Gaussberg

- Two temporary photogrammetric installations have been done at Gaussberg. The first installation comprised a single fixed RGB camera facing the northern bay with the aim of detecting tidal displacement of the ice-covered sea surface from 2D images. This camera was installed on 27 February 2024 and was operational until 3 March 2024 (see Figs. 6.2.17, left, and 6.2.18). It captured images every 30 minutes (cf. Tab. 6.2.5). The georeferencing of these images will be done with the support of a photogrammetric UAV-flight of the area and the corresponding 3D model.

Fig. 6.2.18: Camera installed at the right tripod, pointing towards the northern bay of Gaussberg for 2D monitoring of ocean tides. At the left tripod the antenna of the temporary GNSS station GOCE is mounted (see also Fig. 6.2.19).

Tab. 6.2.5: Images acquired by the installed time-laps cameras

Camera No.	Orientation towards	Date and Time of		Number of images
		first image	last image	
1	glacier	28.02.2024 09:18	15.03.2024 01:42	350
2	glacier	28.02.2024 09:19	15.03.2024 01:43	337
3	glacier	28.02.2024 09:19	15.03.2024 01:43	323
4	glacier	28.02.2024 09:19	15.03.2024 01:43	444
5	northern bay	27.02.2024 10:52	03.03.2024 04:51	228

- The second installation comprised a set of four cameras installed at the edge of the plateau (Fig. 6.2.19), about 100 to 150 m from the field camp. The goal of this system was to monitor the displacement of the glacier located to the west of Gaussberg. The four cameras successfully captured images from 28 February to 15 March 2024. The images were taken simultaneously by all four cameras at 30-minute intervals during the daylight (Tab. 6.2.5). Using the data of these acquisitions will make it possible to detect the movements of the glacier both in 2D (from a single image) and in 3D, as it will be possible to use the simultaneous images to infer photogrammetric models. In order to georeference the images, the coordinates of the cameras as well as the coordinates of five control points that appear in each of the images were obtained by the geodetic RTK measurements (see Appendix A.9).

Fig. 6.2.19: System of four cameras installed at the edge of the camp plateau for 2D and 3D monitoring of the glacier west of Gaussberg

UAV-based measurements

- The UAV flights on the Gaussberg expedition took place in four different areas, each with its own objectives. In general, the flights were conducted with a DJI Phantom 4 RTK drone. Further flights were performed with a DJI Mavic 2 Pro drone. Additionally, photogrammetric acquisitions could be performed based on the helicopter flights to Gaussberg. Appendix A.10 lists all flights with their designated area, times and number of images acquired.

- Together with the image acquisition the drone recorded GNSS data along its flight trajectory. With the additional support by the ground-based GNSS measurements, this will allow us to realise the georeferencing with an accuracy in the centimetre level in the post processing. The flights were performed following specific flight plans each configured according to the areas of interest. Starts and landings were supported by using a special landing pad (Fig. 6.2.20). The landings were performed manually in order to have full control of the UAV. In all flights the pilot was assisted by an observer. Due to the absence of any colonies of animals there was no risk in that respect. Likewise, there was no conflict with birds during the flight. The surveyed areas and specific goals were:

- the camp plateau: to support the two fixed terrestrial photogrammetric installations (see previous paragraph), and to yield a mapping in support of the geological sampling and its geomorphological interpretation;

- *the northern bay*: to support the 2D measurements made by the fixed camera as well as to obtain a comparison between 3D models, and to infer the displacement of the ice-covered sea surface due to ocean tides;

- *the glacier*: to facilitate the inference of 3D models of the glacier and to be able to detect its displacement from the comparison of subsequent models;
- *the summit*: to provide support and georeference to the models made from the images acquired during the helicopter flights, since this flight covers an important area of the Gaussberg.
- As previously mentioned, images were also captured during helicopter flights. These images lack georeferencing, but thanks to the defined flight paths, it has been possible to obtain images that cover the entire Gaussberg, allowing the creation of 3D models and mapping. To support the georeferencing of these images, points measured by GNSS RTK (ground control points GCP1 and GCP2, coordinates see Appendix A.9, photo Fig. 6.2.21) as well as drone flights will be used.

Fig. 6.2.20: UAV DJI Phantom 4 RTK used as the main platform for the acquisition of aerial images of the different study areas. This photo shows the take-off and landing area, supported by the special landing pad, used as a basis for the flight over the glacier.

Fig. 6.2.21: Temporarily established ground control point GCP1 (close to Kap Lewald)

Geological survey at Gaussberg

- Geological sampling was conducted at Gaussberg via simple hand specimen collection from a mixture of *in situ* outcrops and from erratic samples located on the surface of the lavas. Sampling was restricted to the northwest slope and summit of Gaussberg (Fig. 6.2.22) due to weather and subsequent time restraints. Gaussberg volcanic rocks are typically fragile, poorly exposed and heavily eroded by wind and/or ice-jacking. Pillow lavas are best exposed in cliff outcrops but careful observation on flat platforms also provided useful information and appropriate locations for sampling (Fig. 6.2.23). A total of 83 rock samples were collected during the campaign (see Appendix A.11).

- Cosmogenic sampling was conducted at six sites and comprised a total of 27 samples (cf. Fig. 6.2.23a). At each site three to four erratic rock samples and one bedrock (if present) sample were collected. Cosmogenic analysis will be conducted by D. White at the University of Canberra, Australia. These data will be used to reconstruct the history of glacier advance and retreat at Gaussberg.

- A total of 56 samples were collected for geological studies including volcanology (36 samples, cf. Fig. 6.2.23b–d) and metamorphic petrology (20 samples). The volcanology samples comprised mostly *in situ* lamproite lavas and xenoliths from within the lava. Together with the detailed field observations of lava morphology and contact relationships, these samples will be used to understand both the volcanic history of Gaussberg and the paleo-icesheet thickness at the time of eruption. Xenoliths from within the lava will be examined to determine the nature of the significantly older basement rocks beneath Gaussberg. The volcanology samples will be examined at the University of Tasmania, Australia and the National Museum for Science and Nature, Japan.

- Twenty metamorphic erratic samples will be examined at University of Tasmania, Australia and will provide important data for understanding the regional geology of East Antarctica.

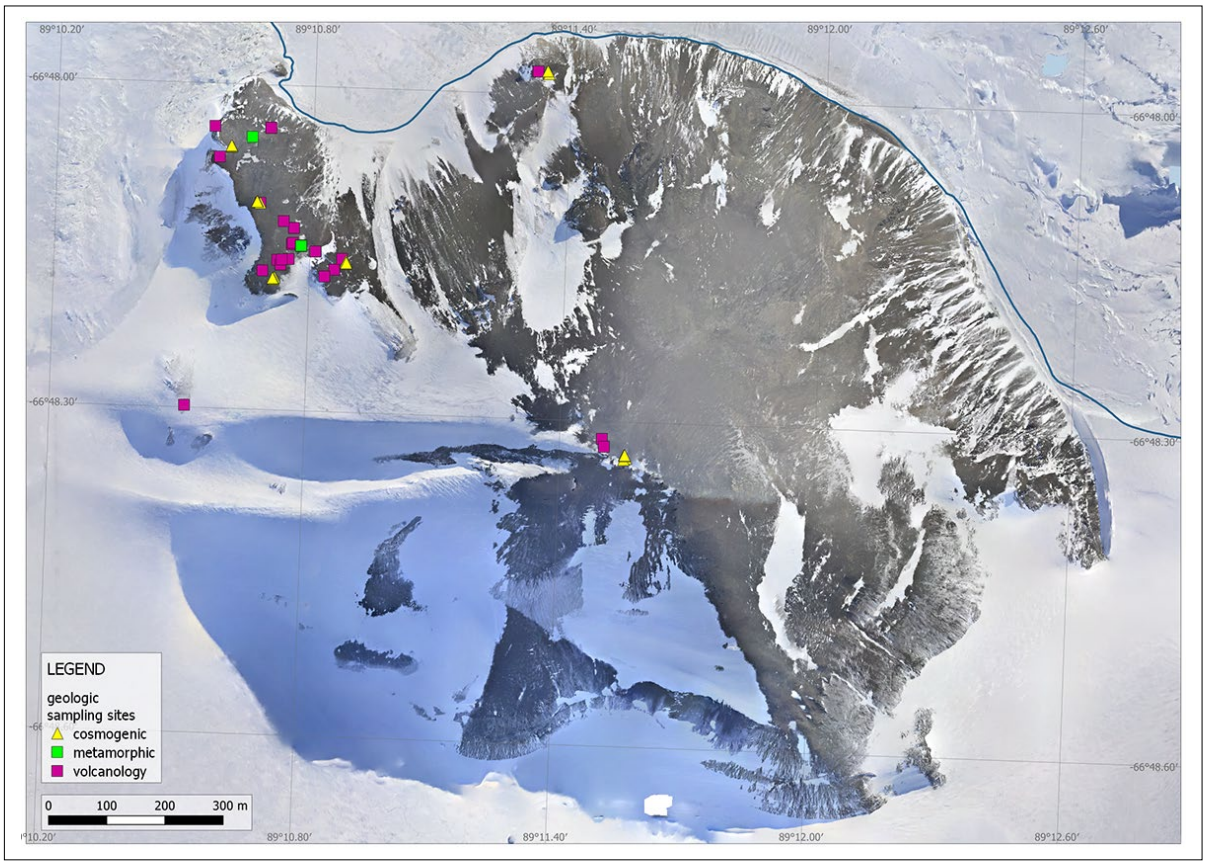

Fig. 6.2.22: Overview on the locations of geological sampling.
Background: preliminary orthophoto inferred from photogrammetric survey

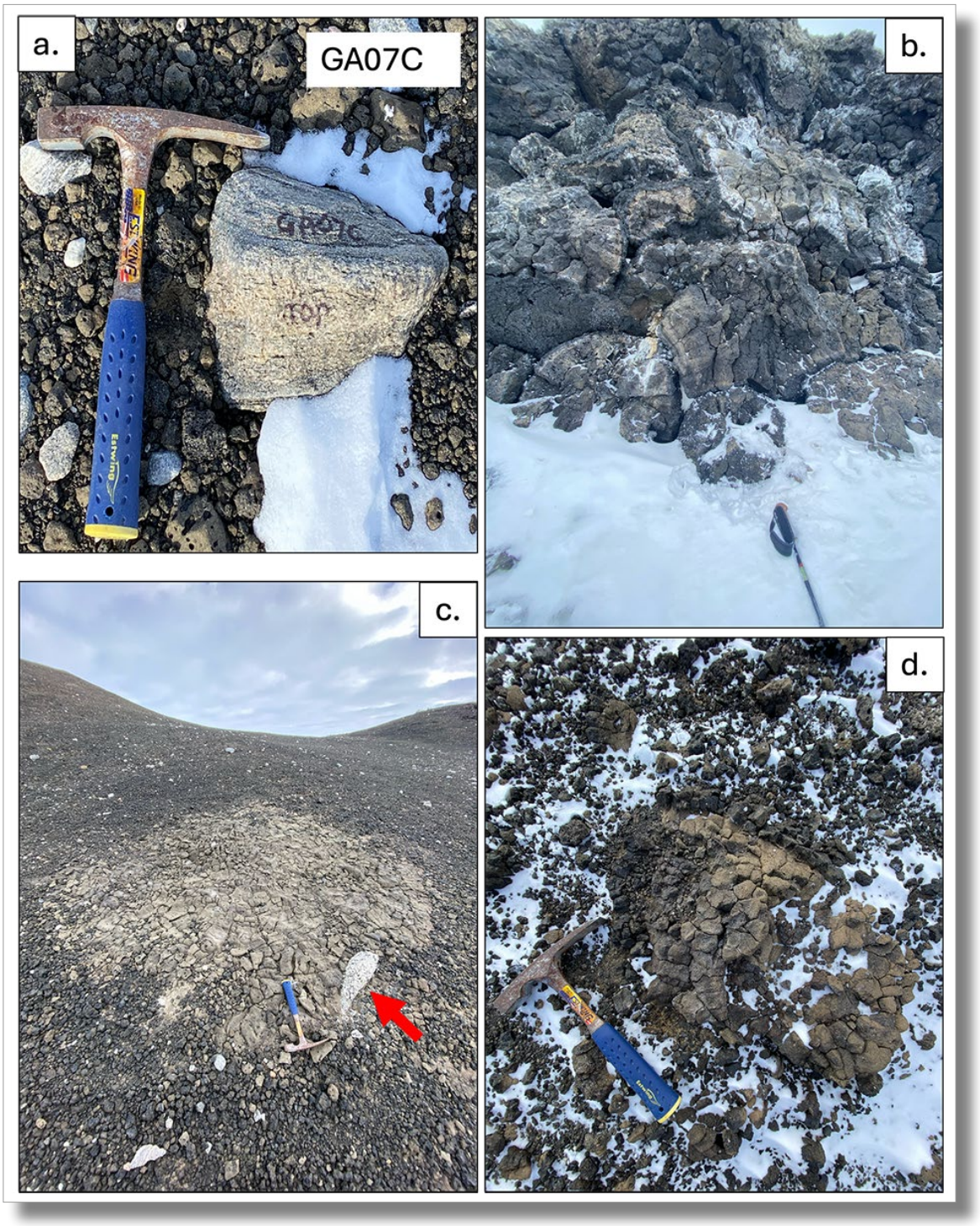

Fig. 6.2.23: Representative outcrops, samples or sampling sites at Gaussberg:
a. Quartz-feldspar-magnetite gneiss erratic sampled at cosmogenic sample site GA07.
b. Lamproite pillow lava pile exposed at the base of Kap Lewald.
c. Lamproite lava lobe exposed plan view, hosting a quartz-magnetite xenolith.
d. Lamproite pillow lava at Nordkap

Geodetic measurements in support of the land geology group

The geological field work of the land geology group (see Section 6.1) was supported by geodetic measurements to georeferencing sampling sites as well as to measure the height of lake and sea levels. This refers especially to the outlet structure of the Ear Lake system and various sampling sites at raised beaches (see Fig. 6.2.24 and 6.2.25). For an overview map of the work area at Thomas Island (Bunger Hills) see Section 6.1. Due to the rough weather conditions in the first stage of the field campaign, it was not possible to set up a GNSS reference station. Thus, point measurements were realized using a GNSS rover system, consisting of a Leica ATX1203+GNSS antenna and a Leica GR25 receiver (see Tab. 6.2.6 for details). The antenna was mounted at a height of 2m on a measuring pole. The measurement duration at each point was typically in the range of 5 to 10 minutes (see also Tab. 6.2.7). The data will be analysed at TU Dresden applying the technique of precise point positioning (PPP) in the post-processing.

Tab. 6.2.6: GNSS equipment used for the surveys at Thomas Island, Bunger Hills

Location	Receiver	Antenna	Batteries	Solar panel
Bunger Hills (Thomas I.)	Leica GR25 S/N 1831212	Leica AX1203+GNSS S/N 09110050	internal battery	none

Tab. 6.2.7: List of GNSS point measurements of geomorphological sites at Thomas Island, Bunger Hills

ID	Location	Date/Time UTC	Remarks
TI_BN1_T1 to TI_BN1_T4	raised beach	25 Feb 2024 04:08 – 09:33	Terrace slope points for GPR georeferencing
MP1 to MP9	eastern Ear Lake outlets	27 Feb 2024 02:23 – 07:40	Elevation measurements for outflow reconstruction

Fig. 6.2.24: GNSS positioning to document heights of emergent marine shorelines, Thomas I.

Fig. 6.2.25: GNSS positioning of outlet sills draining lakes, Thomas I., Bunger Hills

Preliminary results

All measurements and geologic samples will be analysed at the home and partner institutions, respectively. This refers to the GNSS recordings at bedrock sites as well as those taken during the Gaussberg survey. Here, the so-called post-processing will be employed using the Bernese GNSS Software v5.4 applying the methods of differential GNSS and PPP. In the analyses, latest standards have to be incorporated used in geodesy (e.g. precise realization of the reference frame, consistent treatment of corrections and reductions). For the Gaussberg survey we will infer transformation parameters to facilitate the transformation of the local geodetic system realized by Drygalski's work in 1902 to the modern system supported by GNSS. Likewise, the photogrammetric data (from static cameras as well as from the UAV-based survey) will be processed at home to infer 3D models at different resolutions. As a result of the Gaussberg survey, first insights will be gained in terms of quality and plausibility of the data. The geological samplings will also be analysed at the home and partner institutions, mainly in Australia.

Data management

Environmental data will be archived, published and disseminated according to international standards by the World Data Center PANGAEA Data Publisher for Earth & Environmental Science (https://www.pangaea.de) within two years after the end of the expedition at the latest. By default, the CC-BY license will be applied.

Any other data will be submitted to an appropriate long-term archive that provides unique and stable identifiers for the datasets and allows open online access to the data. This refers especially to GNSS data where archiving will be done in the framework of the SCAR Expert Group "Geodetic Infrastructure in Antarctica" (GIANT).

Geological samples will be stored and analysed at the cooperation partners in Australia (University of Tasmania, Hobart, and University of Canberra).

In all publications based on this expedition, the **Grant No. AWI_PS141_05** will be quoted and the following publication will be cited:

Alfred-Wegener-Institut Helmholtz-Zentrum für Polar- und Meeresforschung (2017) Polar Research and Supply Vessel POLARSTERN Operated by the Alfred-Wegener-Institute. Journal of large-scale research facilities, 3, A119. http://dx.doi.org/10.17815/jlsrf-3-163.

References

Drygalski E von (1904) Zum Kontinent des eisigen Südens. Deutsche Südpolarexpedition. Fahrten und Forschungen des „Gauß“ 1901–1903. XIV, 668 S., Georg Reimer, Berlin.

Drygalski E von (1921) Deutsche Südpolar-Expedition 1901-1903. Band I: Geographie, Heft 4: Das Eis der Antarktis und der subantarktischen Meere. Walter de Gruyter, Berlin und Leipzig.

Drygalski E von, Philippi E, Reinisch R(1906) Deutsche Südpolar-Expedition 1901-1903. Band II: Geographie und Geologie, Heft 1. Georg Reimer, Berlin.

King MA, Watson CS, White D (2022) GPS rates of vertical bedrock motion suggest late Holocene ice-sheet readvance in a critical sector of East Antarctica. Geophys. Res. Lett. 49: e2021GL097232.

Scheinert M, Engels O, Schrama EJO, van der Wal W and Horwath M (2021): Geodetic observations for constraining mantle processes in Antarctica. In: A. P. Martin and W. van der Wal (eds.), The Geochemistry and Geophysics of the Antarctic Mantle. Geological Society, London, Memoirs, 56. https://doi.org/10.1144/M56-2021-22Smellie JL and Collerson KD (2021) Gaussberg: volcanology and petrology, Chapter 5.5, 615-628. In: Smellie, J.L., K.S. Panter, A. Geyer (eds.), Volcanism in Antarctica: 200 Million Years of Subduction, Rifting and Conti-nental Breakup. Geological Society, London, Memoirs, 55(1). https://doi.org/10.1144/M55-2018-85.

Whitehouse PL, Bentley MJ, Milne GA et al. (2012) A new glacial isostatic adjustment model for Antarctica: calibrating the deglacial model using observations of relative sea-level and present-day uplift rates. Geophys. J. Int. 190:1464-1482.

7. ISOMETHANE: ONBOARD *IN SITU* ANALYSES OF METHANE CONCENTRATION AND ITS STABLE CARBON ISOTOPIC SIGNATURE ($\delta^{13}C\text{-}CH_4$) IN THE LOWER TROPOSPHERE ABOVE THE SOUTHERN OCEAN

Lisa Rüther[1] [1]DE.AWI
not on board: Ellen Damm[1], Markus Rex[1]

Grant-No. AWI_PS141_11

Objectives

Methane is the second most important human-influenced greenhouse gas in terms of climate forcing. For methane, both bottom-up and top-down modelling approaches are subject to large uncertainties, leading to a significant mismatch. We aimed to record a time series of methane concentration and its stable carbon isotopic signature in the lower troposphere during the cruise. This time series will contribute to the quantification of methane sources and sinks in the Southern Ocean needed for the improvement of model parameterizations.

Work at sea

The continuous ship-borne measurements of CH_4 concentration and $\delta^{13}C\text{-}CH_4$ were carried out by Cavity Ring-Down Spectroscopy (CRDS) using a Picarro G2132-i isotope analyser (Picarro, Inc., Santa Clara, USA). CRDS is a highly sensitive gas analysis technique that measures the near-infrared absorption spectra of small gas-phase molecules within a high-reflectivity cavity using a laser diode. Air was sucked from the starboard side of the Peildeck at about 21 m above sea-ice/water surface using a Teflon tube. A constant flow was generated with a 3KQ Diaphragma pump (Boxer, Ottobeuren, Germany). The recorded raw data was processed with a spike detection code to distinguish the background signal from contamination by local pollution (like pollution from the ship stack). The Picarro G2132 was maintained during the cruise to ensure high data quality.

Preliminary (expected) results

Variations in CH_4 mixing ratio and $\delta^{13}C\text{-}CH_4$ ratios over time will help to understand and validate source and sink capacities. The data evaluation focuses on using backwards airmass trajectories to monitor air masses and to distinguish locally induced signals from signals transported from remote areas. Combined with the time series recorded during MOSAiC (Multidisciplinary drifting Observatory for the Study of Arctic Climate 2019 – 2020), the project aims to study differences in the source-sink balance along a global North-South transect.

As an example for the recorded data, Figures 7.1 and 7.2 show data on CH_4 mixing ratio and $\delta^{13}C\text{-}CH_4$ ratio gathered in the Vincennes Bay in front of *Casey Station*. The area was visited twice during the cruise. Once between 2 February and 5 March 2024 and a second time between 10 March and 13 March 2024. In Figure 7.1 the mixing ratio of CH_4 (left) and the ratio of $\delta^{13}C\text{-}CH_4$ (right) on the ships track can be seen. Figure 7.2 shows a time series for mixing

ratio of CH_4 (left) and the ratio of $\delta^{13}C$-CH_4 (right) for the 2 February 2024 to 5 March 2024 (top) and the 10 March to 13 March 2024 time period (bottom). CH_4 mixing ratio values are mostly between 1.82 and 1.83 ppm, while values are somewhat higher, the second time Vincennes Bay was visited with a peak of more than 1.83 ppm on 13 March 2024. This peak corresponds to a minimum of less than -48‰ in the $\delta^{13}C$-CH_4 ratio. Apart from this minimum the air in the area is mostly slightly enriched in ^{13}C compared to the background of -47‰.

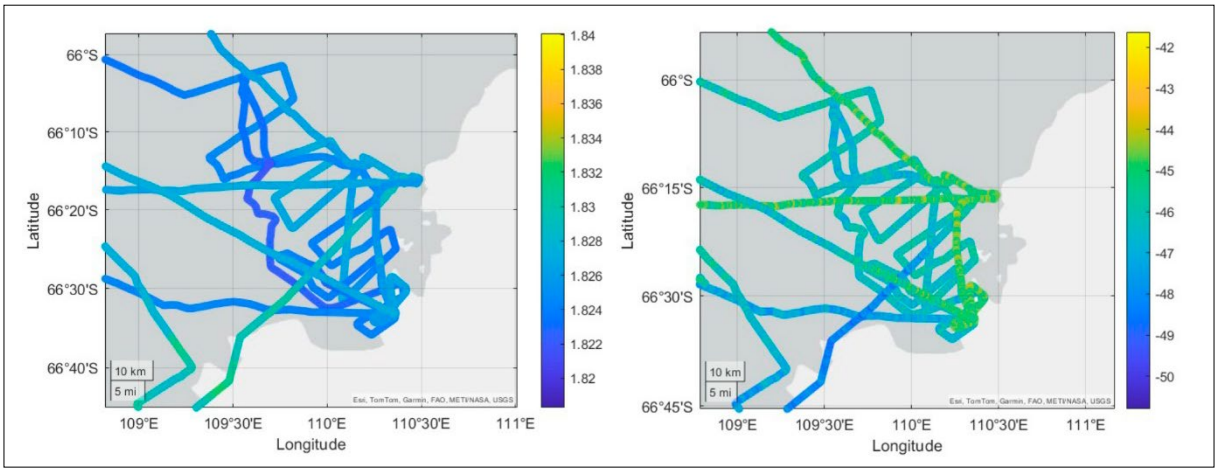

Fig. 7.1: CH_4 mixing ratio (left) and $\delta^{13}C$-CH_4 ratio (right) recorded on the ships track in Vincennes Bay, close to Casey-Station

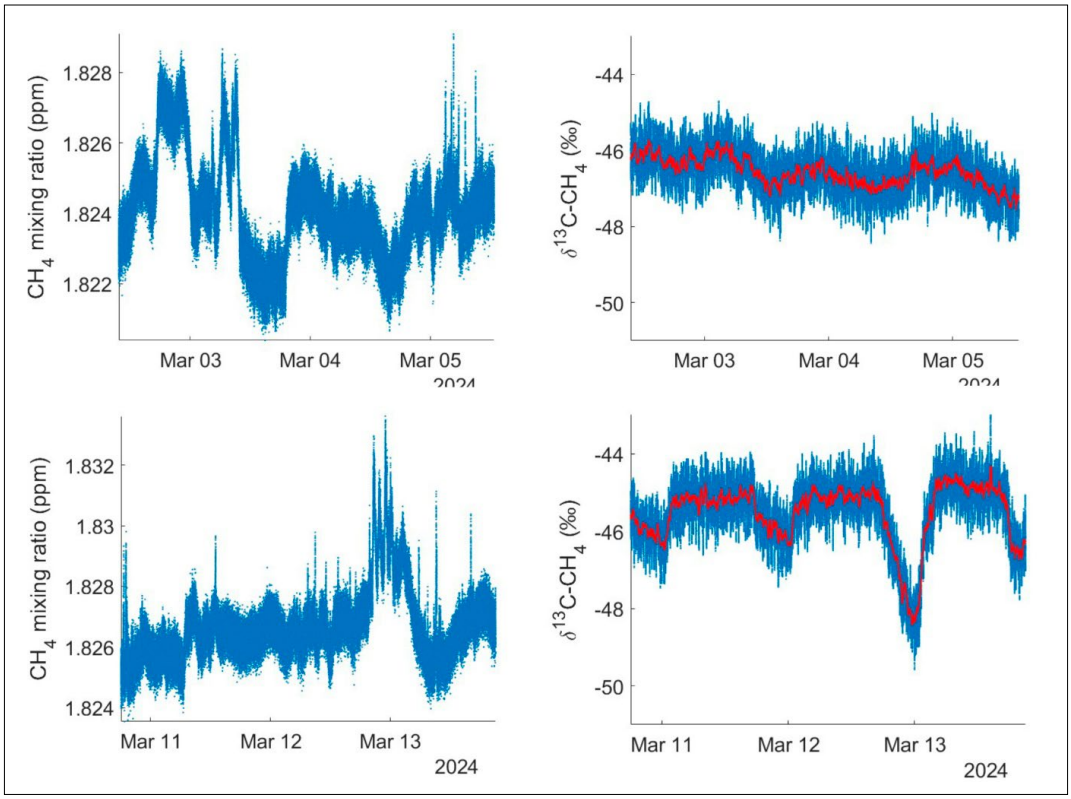

Fig. 7.2: Processed time series of atmospheric CH_4 mixing ratio (left) and $\delta^{13}C$-CH_4 ratio (right) recorded in Vincennes Bay, close to Casey Station for both time periods spent in that region

Data management

The atmospheric data will be archived, published and disseminated according to international standards by the World Data Center PANGAEA Data Publisher for Earth & Environmental Science (https://www.pangaea.de) within two years after the end of the expedition at the latest. By default, the CC-BY license will be applied.

This expedition was supported by the Helmholtz Research Programme “Changing Earth – Sustaining our Future” Topic 1.

In all publications based on this expedition, the **Grant No. AWI_PS140_11** will be quoted and the following publication will be cited: Alfred-Wegener-Institut Helmholtz-Zentrum für Polar- und Meeresforschung (2017) Polar Research and Supply Vessel POLARSTERN Operated by the Alfred-Wegener-Institute. Journal of large-scale research facilities, 3, A119. http://dx.doi.org/10.17815/jlsrf-3-163.

8. DEPLOYMENT OF ARGO FLOATS

Katharina Hochmuth[1]
Not on board: Esmee van Wijk[2,3*],

[1]AU.UTAS
[2]AU.CSIRO
[3]AU.AAPP
[*]not on board

Grant-No. AWI_PS141_00

Objectives

The international Argo programme provides real-time and delayed-mode data for climate and oceanographic research from profiling floats which observe temperature, salinity and currents in the global ocean (Roemmich et al. 2019). Throughout their lifetime, these robotic floats perform scheduled measurement cycles all year round by decending to a predetermined parking depth and drifting with the currents, before descending to profile depth and collecting water column data on the ascent (Wong et al. 2020). After surfacing, the profile data are transmitted via satellite to national data centres and subsequently disseminated by two global data access centres (GDACs). Argo float data are freely available from the Coriolis or USGODAE GDACs (please see the Data Management section below). Argo floats can also be monitored via https://fleetmonitoring.euro-argo.eu/.

The behaviour of the East Antarctic Ice Sheet is closely coupled with the Southern Ocean and its unique current systems. In the Southern Ocean, the stability of the East Antarctic Ice Sheet is potentially threatened by warm water masses intruding onto the Antarctic continental shelf and into deep troughs that extend beneath glaciers (Herraiz-Borreguero et al. 2022; van Wijk et al. 2022). Warmer modified Circumpolar Deep Water (mCDW) has been detected on the continental shelf in some sectors of East Antarctica; however, understanding the spatial and temporal extent and the variability of mCDW on the shelf has been hampered by a lack of observations. The pathways of mCDW from the outer shelf break to the deep troughs of the inner shelf are not well known. The distribution and seasonal to interannual variability of water masses on the shelf such as mCDW, Dense Shelf Water (DSW), Antarctic Bottom Water (AABW), Ice Shelf Water (ISW) and the meltwater fraction that leaves glacier cavities is also poorly understood. Argo floats are a valuable tool for collecting year-round measurements that can help fill observational gaps on the Antarctic continental shelf.

During PS141, we deployed seven Argo floats on the continental shelf in East Antarctica from approximately 92°E to 101°E, on behalf of the Australian Antarctic Programme Partnership (AAPP), CSIRO and UTAS researchers (Fig. 8.1). Profiling floats were deployed into deep troughs or in regions with water depths > 450 dbar. Floats have been programmed to either park on the sea floor between profiles or to drift at the expected depth of mCDW intrusions. Researchers from AAPP will use profile data collected by the floats to study mCDW intrusions onto the continental shelf, ocean-ice interactions near glaciers, water mass formation regions and polynya processes.

Work at sea

Seven ARGO floats were deployed during PS141; comprising two ARVOR- and five APEX APF11 floats (Fig. 8.1 and Tab. 8.1). Both float types are about 1m long with a cylindrical hull. The sensors and the satellite antenna are mounted on the head (end cap) of the float. The main body of the float is dedicated to the CPU, batteries and the buoyancy engine, which allows the depth control of the float. A disk and/or foam flotation around the upper part of the float increases the stability of the float in the water.

ARVOR-I floats are produced by nke Instrumentation (France) (Fig. 8.2B) and carry a CTD sensor, measuring conductivity (salinity), temperature, and pressure (depth) and an optional optode sensor measuring dissolved oxygen. The specified mission, detailing cycle patterns as well as the collected data are exchanged via the IRIDIUM satellite system. The mission includes the cycle time, drift and profile depths and other parameters that can be changed from cycle to cycle. The data collected by these floats are transmitted to the operating institution, CSIRO Environment in Hobart. Prior to deployment, these floats need to be activated by removing a magnet from the floats hull. The float then undergoes a start-up procedure and connects to the satellite system to receive updates on the programmed mission. During PS141, we fixed the float in its upright position to the ship's side with a clear view of the sky during activation.

The APEX Profiling Floats are produced by TELEDYNE WEBB RESEARCH (USA) (Fig. 8.2A) and are equipped with a CTD (salinity, temperature, depth) sensor. Two APEX floats are additionally carrying an Aanderaa 4330 optode to measure dissolved oxygen and an iceguard. The iceguard is designed to prevent damage to the antenna/sensors in case the float is surfacing below sea-ice by providing an additional buffer. One APEX float was equipped with an ice guard but did not carry any additional sensors. There are no additional steps for the activation of the APEX floats as they are pressure-activated and can be deployed straight into the water without connecting to IRIDIUM satellites first.

During PS141, we deployed the ARGO floats from the aft of the vessel on the portside using a rope to lower the instrument to the water line at reduced speed (Fig. 8.2CD). Open water conditions were preferred for the deployment; however, we also deployed some floats in sea-ice cover.

All seven floats have made contact with the satellite IRIDIUM system, however so far only six floats have collected profiles. It is possible the remaining float was trapped below sea ice and unable to surface after the first profile. As the floats were deployed late in the season, all seven floats are now under sea ice and we do not expect to hear from them again before the ice melts in spring.

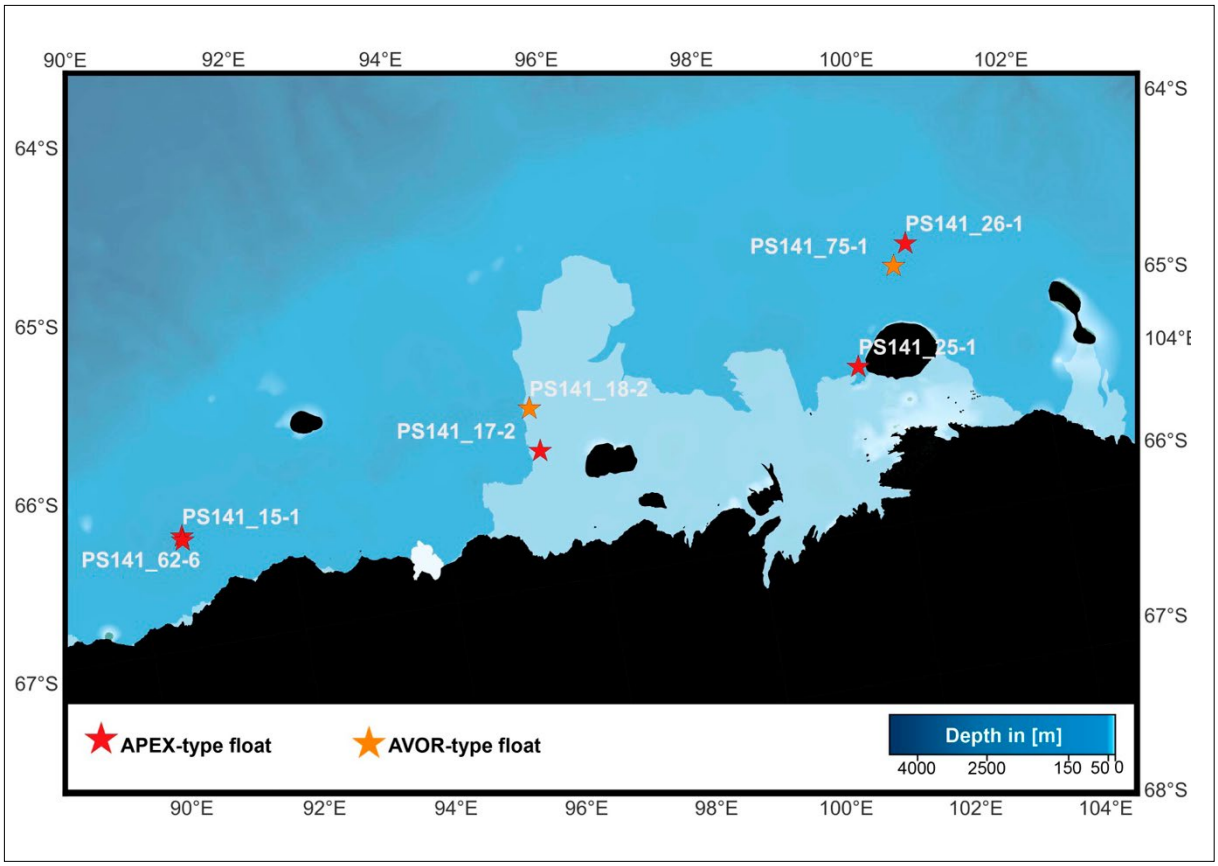

Fig. 8.1: Bathymetric map of the working area for Argo float deployments on the continental shelf of East Antarctica. The map depicts the deployments as stars (red for the deployment of an APEX-type float, orange for the deployment of an ARVOR-type float) indicating the station number. The bathymetry is taken from the International Bathymetric Chart of the Southern Ocean, Version 2 (IBCSO v2; Dorschel et al. 2022).The gray-shaded areas show the position of the Shackleton Ice Shelf.

Tab. 8.1: Overview on Argo float deployments during PS141

Station PS141_	Float Type	Serial number	Date and Time	Depth (m)	Latitude South [°]	Longitude East [°]	Additional Sensors & Features
15-1	APEX	10359	25.02.24 12:56	838	66.28394	90.32112	Iceguard
17-2	APEX	10343	26.02.24 06:38	549	66.05134	95.50964	Optode & Iceguard
18-2	ARVOR	AU002	26.02.24 10:08	1054	65.80441	95.40496	Optode
25-1	APEX	9756	29.02.24 13:54	500	65.64192	99.9974	
26-1	APEX	10358	29.02.24 20:27	431	64.93699	100.62890	Optode & Iceguard
62-6	APEX	9755	17.03.24 14:36	1028	66.3079	90.32329	
75-1	ARVOR	AU201	22.03.24 03:47	477	65.06603	100.47393	Optode

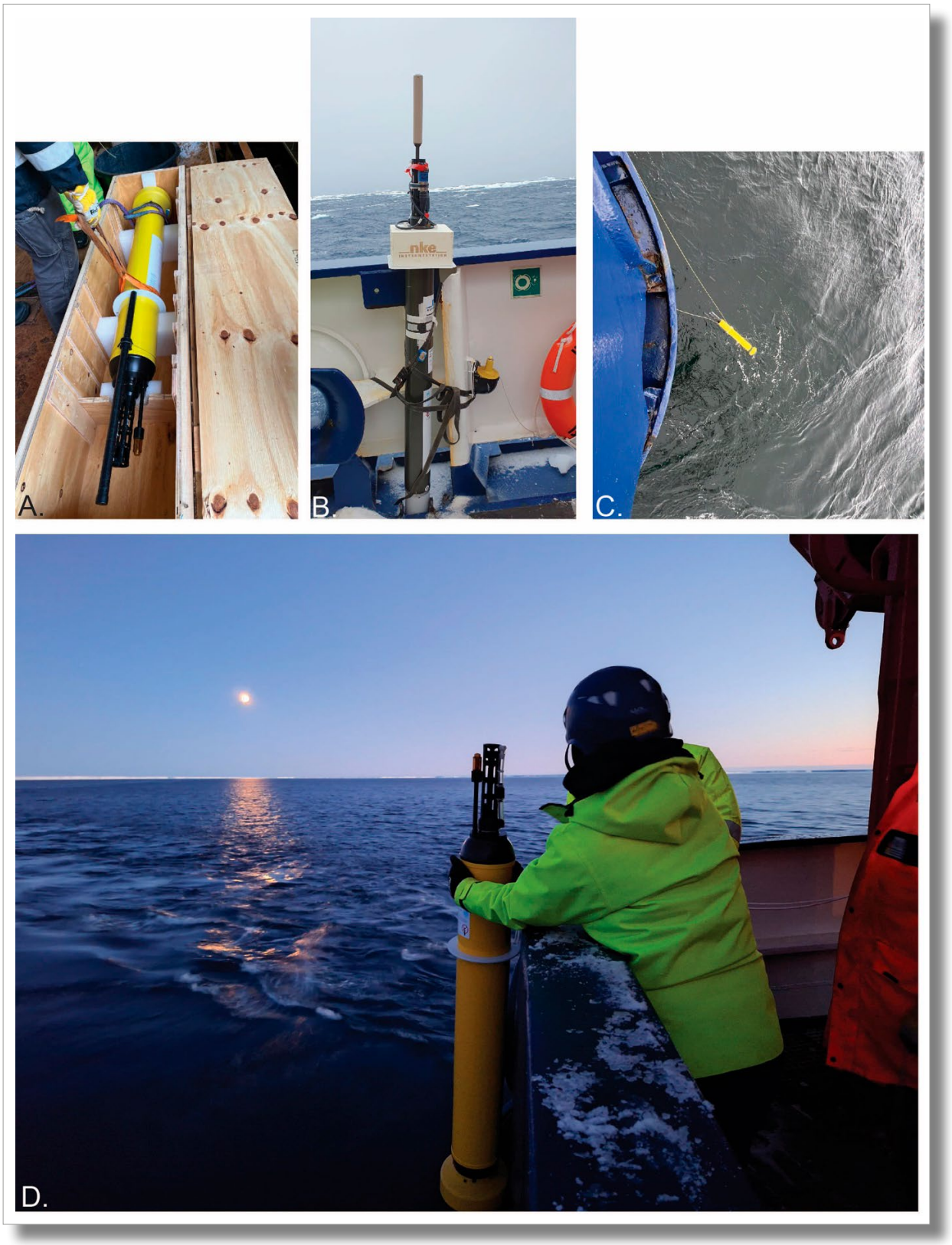

Fig. 8.2: ARGO Float deployments during PS141: A. APEX-type float in transport box prior to deployment (Photo: K. Gohl) B. ARVOR-type float fixed to the ship's wall prior to deployment (Photo: A. Völkert) C. APEX-type float is lowered to the water line (Photo: K. Gohl) D. Night deployment of APEX-type float (Photo: T. Krause)

Preliminary results

Seven ARGO floats were successfully deployed during PS141 (Fig. 8.1). Six of these floats have so far returned profile data with the seventh float making initial satellite contact and now presumed to be under sea ice.

APEX-type float *7900960* is shown here as an example of the Argo float profiling close to the West Ice Shelf and the Gaussberg operational area during PS141. So far, the float has surfaced 4 times returning water column profiles (Fig. 8.3). The float has travelled approx. 100 km between 25.02.2024 and 8.03.2024. We can assume that it is now continuing to profile under the quickly evolving sea ice in the region.

Float 7900960 collected two profiles in a relatively deep depression on the shelf (~760 dbar) before moving towards the shelf break for profiles 3 and 4 (Fig. 8.3 – 8.6). For the first two profiles collected in the depression colder (< 1.8°C) and fresher (~34.4) waters were present at the bottom of the profile (Fig. 8.4 and 8.6). At the third profile collected by the float we can see warm and salty modified Circumpolar Deep Water (> 0.25°C, > 34.65 psu) at depths of 800 to 931 dbar, close to the shelf break (Fig. 8.4 – 8.6).

Data returned by the floats in the following summer (late 2024/early 2025) will be used by CSIRO and UTAS researchers to study ice-ocean interactions, warm water intrusions on the shelf, water mass formation and distribution and polynya dynamics.

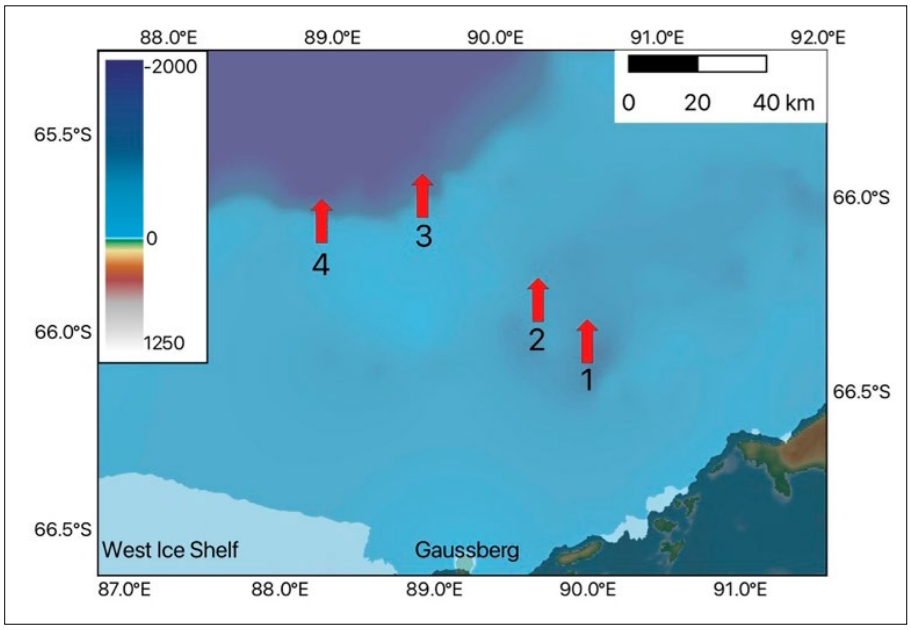

Fig. 8.3: APEX-type float 7900960 drift pathway between deployment on 25.02.2024 and 8.03.2024 showing 4 surfacing locations (red arrow) from which data was transmitted from east of the West Ice Shelf in the area of the flight operations to the Gaussberg field camp during PS141.

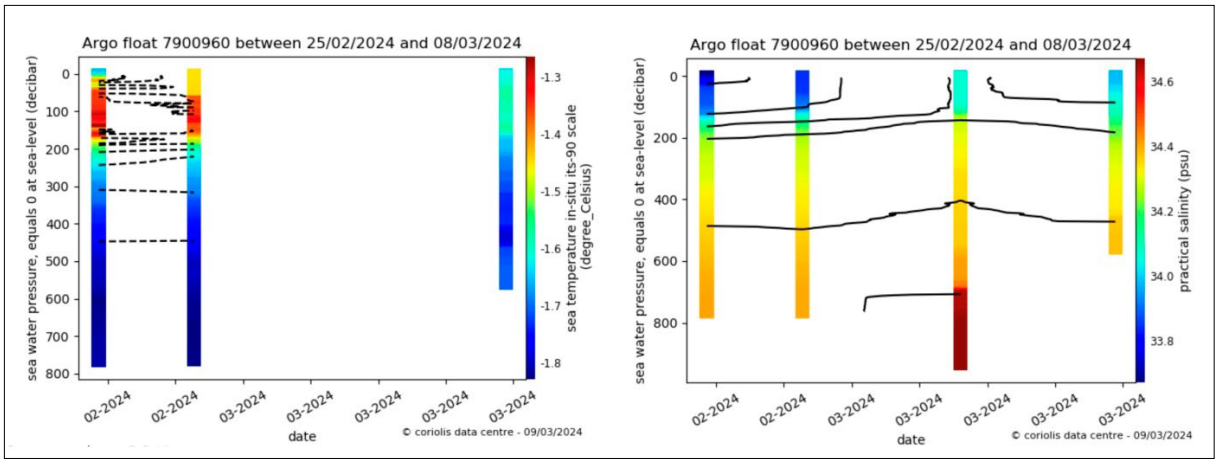

Fig. 8.4: Profiling data of APEX-type ARGO float 7900960 between 25.02.2024 and 8.03.2024 displaying A. the temperature and B. the salinity of the water column

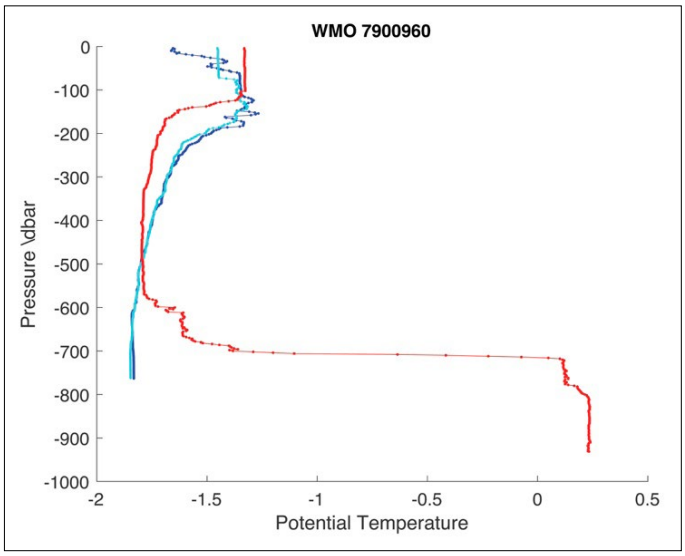

Fig. 8.5: Temperature profiles of Float 7900960: Profile 1 in dark blue, profile 2 in light blue and profile 3 in red

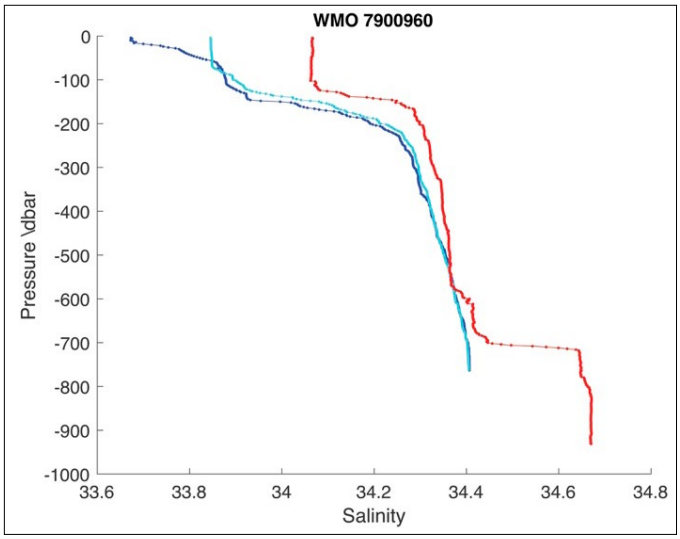

Fig. 8.6: Salinity data of Float 7900960: Profile 1 in dark blue, profile 2 in light blue and profile 3 in red

Data management

Incoming oceanographic profile data from the floats is transmitted to CSIRO in Hobart, Australia where it undergoes checks and RTQC (real-time quality control checks). All oceanographic data collected by the floats is available in near real-time from the two Argo global access data centres:

- Coriolis (https://www.coriolis.eu.org/Data-Products)
- USGODAE (https://usgodae.org/pub/outgoing/argo/)

Climate quality data is made available within one year and can be found in the Delayed Mode netcdf files (D*wmoid*.nc) at the above data centres. This data has undergone additional rigourous Delayed Mode quality control checks where sensors are checked for drift and/or offsets and QC flags and error estimates for the various parameters are adjusted. For more information see https://argo.ucsd.edu/data/ and the data manuals available at: http://www.argodatamgt.org/Documentation

Note that wherever possible, Delayed Mode Argo data should be used in preference to real-time data. Individual floats and profile data can also be monitored at: https://fleetmonitoring.euro-argo.eu

References

Herraiz-Borreguero L & Garabato ACN (2022) Poleward shift of Circumpolar Deep Water threatens the East Antarctic Ice Sheet. Nature Climate Change 1–7. https://doi.org/10.1038/s41558-022-01424-3

Roemmich D, Alford MH, Claustre H, Johnson K, King B, Moum J et al. (2019) On the Future of Argo: A Global, Full-Depth, Multi- Disciplinary Array. Front. Mar. Sci. 6:439. https://doi.org/10.3389/fmars.2019.00439

van Wijk E M, Rintoul SR, Wallace LO, Ribeiro N, Herraiz-Borreguero L (2022) Vulnerability of Denman Glacier to Ocean Heat Flux Revealed by Profiling Float Observations. Geophysical Research Letters 49(18). https://doi.org/10.1029/2022gl100460

Wong APS, Wijffels SE, Riser SC, Pouliquen S, Hosoda S, Roemmich D et al. (2020). Argo Data 1999–2019: Two Million Temperature-Salinity Profiles and Subsurface Velocity Observations from a Global Array of Profiling Floats. Front. Mar. Sci. 7:700. https://doi.org/10.3389/fmars.2020.00700

9. ACKNOWLEDGEMENTS

Sebastian Krastel[1] [1]DE.CAU

On behalf of the entire scientific crew of PS141, I would like to thank Captain Thomas Wunderlich and the crew of *Polarstern* for their outstanding support and assistance in coordinating, preparing and carrying out our scientific work on board. Their great flexibility and perfect technical support contributed significantly to the scientific success of this cruise. We also appreciate the great atmosphere on board, which makes the work very pleasant.

We would also like to thank the many colleagues from the AWI Logistics and Research Platforms Department, who supported us perfectly and competently in the planning, preparation, realisation and public relations work for and in connection with the expedition.

The expedition was part of the Helmholtz Association's programme-oriented funding (PoF) in the research programme "Changing Earth – Sustaining our Future". Funding for the university participants was provided by the priority programme "Antarctic Research" of the German Research Foundation (DFG), among others.

APPENDIX

A.1 TEILNEHMENDE INSTITUTE / PARTICIPATING INSTITUTES

Affiliation	Address
AR.MARYBIO	Marybio Foundation Alvarez Thomas 3550 1431 Buenos Aires Argentina
AU.GA	Geoscience Australia Cnr Jerrabomberra Ave and Hindmarsh Drive Symonston 2609 Canberra ACT Australia
AU.MACQUARIE	Macquarie University Eastern Road 2109 North Ryde Australia
AU.UC	University of Canberra 11 Kirinari Street Bruce 2617 Canberra Australia
AU.UTAS	University of Tasmania Clark Road Level 3, Geography Building 7005 Sandy Bay Australia
DE.AWI	Alfred-Wegener-Institut Helmholtz-Zentrum für Polar- und Meeresforschung Postfach 120161 27515 Bremerhaven Germany
DE.CAU	Christian-Albrechts-Universität zu Kiel Christian-Albrechts-Platz 4 24118 Kiel Germany

Affiliation	Address
DE.DRF	DRF Luftrettung AG Laval Avenue E312 77836 Rheinmünster Germany
DE.DWD	Deutscher Wetterdienst Seewetteramt Bernhard Nocht Str. 76 20359 Hamburg Germany
DE.GEOMAR	GEOMAR Helmholtz-Zentrum für Ozeanforschung Wischhofstr. 1-3 24148 Kiel Germany
DE.NHC	Northern HeliCopter GmbH Gorch-Fock-Str. 103 26721 Emden Germany
DE.TU-DRESDEN	Technische Universität Dresden Helmholtzstr.10 01069 Dresden Germany
DE.TUM	Technische Universität München Arcisstraße 21 80333 München Germany
DE.UNI-KÖLN	Universität zu Köln Albertus-Magnus-Platz 50923 Köln Germany
DE.UNI-POTSDAM	Universität Potsdam Am Neuen Palais 10 14469 Potsdam Germany
FR.CNRS	CNRS/Laboratoire d'Océanographie et du Climat 4 Place Jussieu 75005 Paris France

Affiliation	**Address**
Not on board / Not in the field	
AU.AAPP	Australian Antarcic Program Partnership 20 Castray Esplanade 7004 Battery Point, TAS Australia
AU.ANSTO	Australian Nuclear Science and Technology Organisation New Illawarra Road Lucas Heights NSW 2234 Australia
AU.CSIRO	Commonwealth Scientific and Industrial Research Organisation (CSIRO) Hobart Castray Esplanade 7004 Battery Point, TAS Australia
FR.MNHN	Muséum national d'Histoire naturelle 57 Rue Cuvier 75005 Paris France
NL.NATURALIS	Naturalis Darwinweg 2 2333 CR Leiden The Netherlands
NZ.UC	University of Canterbury Private Bag 4800 Christchurch 8140 New Zealand

A.2 FAHRTTEILNEHMER:INNEN / CRUISE PARTICIPANTS

Name/ Last name	Vorname/ First name	Institut/ Institute	Beruf/ Profession	Fachrichtung/ Discipline
Barrett	Rachel Sian	DE.CAU	Scientist	Geophysics
Baumann	Lenya Mara	DE.CAU	Student (Bachelor)	Geophysics
Beardsley	Jack	AU.UTAS	Scientist	Geophysics
Berg	Sonja	DE.UNI-KÖLN	Scientist	Geology
Blanch Gorriz	Xabier	DE.TU-DRESDEN	Scientist	Earth Science
Brauer	Jens	DE.NHC	Pilot	Helicopter Service
Cammareri	Alejandro	AR.MARYBIO	Scientist	MMO
Cornish	Natalie Roslyn	DE.AWI	Scientist	Earth Science
Dägele	Daniela	DE.UNI-KÖLN	Student (Master)	Earth Science
Eberlein	Lutz	DE.TU-DRESDEN	Engineer	Earth Science
Ferber	Ole Jasper	DE.CAU	Student (Master)	Earth Science
Fox	Jodi	AU.UTAS	Scientist	Geology
Gohl	Karsten	DE.AWI	Scientist	Geophysics
Gore	Damian	AU.MACQUARIE	Scientist	Earth Science
Gottschalk	Julia	DE.CAU	Scientist	Geology
Hochmuth	Katharina	AU.UTAS	Scientist	Geophysics
Höppner	Laura Katharina	DE.TUM	Student (Master)	Geophysics
Howard	Amber	AU.UC	Student (Bachelor)	Geology
Jebasinski	Lena	DE.CAU	PhD Student	Oceanography
Krastel	Sebastian	DE.CAU	Scientist	Geophysics
Krause	Timo	DE.AWI	PhD Student	Geophysics
Labrousse	Sara	FR.CNRS	Scientist	Biology
Lange	Timo	DE.UNI-KÖLN	Student (Bachelor)	Earth Science
Lembke-Jene	Lester	DE.AWI	Scientist	Geology
Lensch	Norbert	DE.AWI	Technician	Geology
Loebel	Erik	DE.TU-DRESDEN	Scientist	Glaciology
McNeil	Mardie	AU.GA	Scientist	Geology
Miehe	Kai	DE.DRF	Technician	Helicopter Service
Müller	Anja	DE.AWI	Technician	Geology
Müller	Juliane	DE.AWI	Scientist	Geology
Nehrke	Gernot	DE.AWI	Scientist	Earth Science
Panter	Gabriel	DE.DRF	Technician	Helicopter Service
Pena	Ursula	AR.MARYBIO	Scientist	MMO
Pfeiffer	Adalbert	DE.AWI	Technician	Geophysics

Name/ Last name	**Vorname/ First name**	**Institut/ Institute**	**Beruf/ Profession**	**Fachrichtung/ Discipline**
Rohleder	Christian	DE.DWD	Technician	Logistics
Rüther	Lisa	DE.UNI-POTSDAM	Student (Master)	Physics
Scheidt	Stephanie	DE.UNI-KÖLN	Scientist	Geology
Scheinert	Mirko	DE.TU-DRESDEN	Scientist	Earth Science
Schwarzbach	Patrick	DE.AWI	Engineer	Geophysics
Scrigna	Andres Alejandro	AR.MARYBIO	Scientist	MMO
Stobbe	Tim Beneke	DE.CAU	PhD Student	Geology
Tobisch	Chiara Alina	DE.CAU	PhD Student	Geophysics
Trudelle	Laurène Servane	FR.CNRS	Scientist	Biology
Vaupel	Lars	DE.NHC	Pilot	Helicopter Service
Völkert	Anna	DE.CAU	Student (Master)	Earth Science
Wagner	Bernd	DE.UNI-KÖLN	Scientist	Earth Science
Weber	Marie	DE.TU-DRESDEN	Student (Bachelor)	Earth Science
Weigelt	Estella	DE.AWI	Scientist	Geophysics
Wenzel	Anna Julia	DE.DWD	Scientist	Meteorology
Xydis	Georgios	DE.GEOMAR	Student (Master)	Biology

A.3 SCHIFFSBESATZUNG / SHIP‘S CREW

No	Name / Last Name	Vorname / First name	Position / Rank
1	Wunderlich	Thomas	Master
2	Langhinrichs	Jacob	C/M
3	Grafe	Jens	C/E
4	Strauß	Erik	2/M Cargo
5	Hering	Igor	2/M
6	Rathke	Jannik	2/M
7	Dr. Gößmann-Lange	Petra	Doc
8	Dr. Hofmann	Jörg	E/E Com.
9	Brose	Thomas	2/E
10	Bähler	Stephanie	2/E
11	Farysch	Tim	2/E
12	Redmer	Jens	E/E SET
13	Kliemann	Olaf	E/E Brücke
14	Hüttebräucker	Olaf	E/E Labor
15	Pliet	Johannes	E/E Sys
15	Jäger	Vladimir	E/E Winde
17	Sedlak	Andreas	Bosun
18	Neisner	Winfried	Carpenter
19	Burzan	Gerd-Ekkehard	MPR
20	Klee	Philipp	MPR
21	Klähn	Anton	MPR
22	Meier	Jan	MPR
23	Rhau	Lars-Peter	MPR
24	Schmidt	Patrick	MPR
25	Thöndel	Christoph	MPR
26	Schwarz	Uwe	MPR
27	Klinger	Dana	MPR

No	Name / Last Name	Vorname / First name	Position / Rank
28	Wendt	Meyk	MPR
29	Münzenberger	Börge	MPR
30	Schwarz	Uwe	MPR
31	Preußner	Jörg	Fitter/E
32	Hofmann	Werner	Cook
33	Hammelmann	Louisa	2./Cook
34	Dietrich	Emilia	2./Cook
35	Pieper	Daniel	C/Stew.
36	Hinz	Nina	Stew./Nurse
37	Dibenau	Torsten	2./Stew.
38	Stocker	Eileen	2./Stew.
39	Brändli	Monika	2./Stew.
40	Arendt	René	2./Stew.
41	Cheng	Qi	2./Stew.
42	Chen	Dansheng	2./Stew.
43	Klett	Onno	Trainee

A.4 STATIONSLISTE / STATION LIST PS141

Station list of expedition PS141 from Hobart – Walvis Bay;
the list details the action log for all stations along the cruise track.

See https://www.pangaea.de/expeditions/events/PS141 to display the station (event) list for expedition PS141.
This version contains Uniform Resource Identifiers for all sensors listed under https://sensor.awi.de. See https://www.awi.de/en/about-us/service/computing-centre/data-flow-framework.html for further information about AWI's data flow framework from sensor observations to

Event label	Optional label	Date/Time	Latitude	Longitude	Depth [m]	Gear	Action	Comment [*]
PS141-track		2024-02-06T00:00:00	-42.89320	147.34110		CT	Station start	Hobart – Walvis Bay
PS141-track		2024-04-14T00:00:00	-22.94100	14.50300		CT	Station end	Hobart – Walvis Bay
PS141_0_Underway-51		2024-02-06T21:38:36	-44.18259	145.99419		SWEAS	Station start	
PS141_0_Underway-51		2024-04-14T04:09:14	-22.84982	14.40396	44	SWEAS	Station end	
PS141_0_Underway-28		2024-02-07T19:34:32	-44.14300	141.16900	4557	DS3	Station start	Event shows start/ end point (date/time & coordinates) of first/ last data record using Hydrosweep DS 3 multibeam during PS141
PS141_0_Underway-28		2024-04-10T05:00:30	-36.20200	14.99710	4809	DS3	Station end	Event shows start/ end point (date/time & coordinates) of first last data record using Hydrosweep DS 3 multibeam during PS141
PS141_0_Underway-24		2024-02-07T20:16:00	-44.14116	141.01916		GRAV	Station start	
PS141_0_Underway-24		2024-04-14T04:05:53	-22.85031	14.39910	46	GRAV	Station end	

** Comments are limited to 130 characters. See https://www.pangaea.de/expeditions/events/PS141 to show full comments in conjunction with the station (event) list for expedition PS141*

Event label	Optional label	Date/Time	Latitude	Longitude	Depth [m]	Gear	Action	Comment [*]
PS141_0_Underway-23		2024-02-07T20:16:00	-44.14116	141.01916		MAG	Station start	
PS141_0_Underway-23		2024-04-14T04:06:22	-22.85023	14.39984	46	MAG	Station end	
PS141_0_Underway-39		2024-02-07T20:34:09	-44.13990	140.95037	4569	PS	Station start	
PS141_0_Underway-39		2024-04-10T05:00:00	-36.20335	14.99760	4809	PS	Station end	
PS141_0_Underway-31		2024-02-07T20:34:45	-44.13987	140.94821	4579	NEUMON	Station start	
PS141_0_Underway-31		2024-04-14T04:09:30	-22.84978	14.40435	44	NEUMON	Station end	
PS141_0_Underway-11		2024-02-07T20:35:40	-44.13983	140.94469	4598	MYON	Station start	
PS141_0_Underway-11		2024-04-14T04:09:14	-22.84982	14.40396	44	MYON	Station end	
PS141_1-1		2024-02-07T20:39:45	-44.13941	140.93052	4661	MAG	Station start	
PS141_1-1		2024-02-07T22:36:37	-44.13912	140.91729	4772	MAG	Station end	
PS141_0_Underway-3		2024-02-07T21:25:02	-44.12572	140.94818	4672	ADCP	Station start	
PS141_0_Underway-3		2024-04-14T04:03:09	-22.85079	14.39490	48	ADCP	Station end	
PS141_0_Underway-34		2024-02-07T22:37:37	-44.13908	140.91492	4776	pCO2	Station start	
PS141_0_Underway-34		2024-04-14T04:04:40	-22.85054	14.39721	47	pCO2	Station end	
PS141_0_Underway-13		2024-02-07T22:37:55	-44.13906	140.91425	4778	FBOX	Station start	
PS141_0_Underway-13		2024-04-14T04:04:16	-22.85061	14.39663	47	FBOX	Station end	
PS141_0_Underway-43		2024-02-07T23:55:53	-44.13860	140.89510	4752	TSG	Station start	
PS141_0_Underway-43		2024-04-14T04:07:54	-22.84999	14.40211	45	TSG	Station end	
PS141_0_Underway-44		2024-02-07T23:56:14	-44.13859	140.89507	4751	TSG	Station start	
PS141_0_Underway-44		2024-04-14T04:08:19	-22.84994	14.40270	44	TSG	Station end	
PS141_0_Underway-42		2024-02-07T23:57:01	-44.13856	140.89502	4750	SNDVELPR	Station start	
PS141_0_Underway-42		2024-04-14T04:07:23	-22.85007	14.40136	45	SNDVELPR	Station end	
PS141_1-2		2024-02-08T00:04:48	-44.13826	140.89468	4752	CTD-RO	max depth	
PS141_1-3		2024-02-08T01:45:22	-44.13846	140.89540	4752	MSN	Station start	
PS141_1-3		2024-02-08T03:10:36	-44.14700	140.90705	4772	MSN	Station end	
PS141_2-1		2024-02-09T00:15:56	-44.07409	137.03053	4650	CTD-RO	max depth	
PS141_2-2		2024-02-09T01:59:21	-44.07609	137.03207	4636	MSN	Station start	

Event label	Optional label	Date/Time	Latitude	Longitude	Depth [m]	Gear	Action	Comment [*]
PS141_2-2		2024-02-09T02:30:45	-44.07693	137.03442	4604	MSN	Station end	
PS141_2-3		2024-02-09T02:31:30	-44.07696	137.03454	4603	MSN	Station start	
PS141_2-3		2024-02-09T03:59:36	-44.08390	137.04059	4573	MSN	Station end	
PS141_3-1		2024-02-10T02:45:00	-46.95177	134.75743	4006	MUC	max depth	
PS141_3-2		2024-02-10T06:09:00	-46.95147	134.75697	4004	GC	max depth	
PS141_3-3		2024-02-10T09:44:04	-46.95130	134.75690	4004	CTD-RO	max depth	
PS141_3-4		2024-02-10T11:38:21	-46.95143	134.75779	4005	MSN	Station start	
PS141_3-4		2024-02-10T12:05:41	-46.95138	134.75951	4009	MSN	Station end	
PS141_3-5		2024-02-10T12:05:57	-46.95138	134.75958	4009	MSN	Station start	
PS141_3-5		2024-02-10T13:20:21	-46.95037	134.75798	4006	MSN	Station end	
PS141_4-1		2024-02-12T05:36:18	-51.84525	130.11185	3604	CTD-RO	max depth	
PS141_4-2		2024-02-12T07:21:32	-51.84478	130.11266	3604	MSN	Station start	
PS141_4-2		2024-02-12T09:19:42	-51.84079	130.15016	3538	MSN	Station end	
PS141_5-1		2024-02-13T22:15:15	-56.32450	124.81727	4710	CTD-RO	max depth	
PS141_5-2		2024-02-13T23:53:11	-56.32460	124.81733	4708	MSN	Station start	
PS141_5-2		2024-02-14T00:26:13	-56.32469	124.81720	4709	MSN	Station end	
PS141_5-3		2024-02-14T00:27:08	-56.32461	124.81717	4709	MSN	Station start	
PS141_5-3		2024-02-14T01:44:59	-56.32441	124.81766	4708	MSN	Station end	
PS141_5-4		2024-02-14T03:29:58	-56.32455	124.81731	4708	MUC	max depth	
PS141_5-5		2024-02-14T08:08:29	-56.32457	124.81741	4709	PC	max depth	
PS141_6-1		2024-02-16T03:53:56	-59.74930	114.89225	4527	MUC	max depth	
PS141_6-2		2024-02-16T07:36:16	-59.74937	114.89274	4527	PC	max depth	
PS141_6-3		2024-02-16T12:01:48	-59.74926	114.88903	4514	CTD-RO	max depth	
PS141_6-4		2024-02-16T14:12:47	-59.74954	114.88894	4514	MSN	Station start	
PS141_6-4		2024-02-16T14:46:38	-59.74947	114.88911	4513	MSN	Station end	
PS141_6-5		2024-02-16T14:47:28	-59.74948	114.88923	4513	MSN	Station start	
PS141_6-5		2024-02-16T16:07:51	-59.75068	114.89156	4513	MSN	Station end	

Event label	Optional label	Date/Time	Latitude	Longitude	Depth [m]	Gear	Action	Comment [*]
PS141_7-1		2024-02-17T23:46:20	-63.64246	107.09116	2880	MUC	max depth	
PS141_7-2		2024-02-18T01:29:13	-63.64021	107.08823	2885	CTD-RO	max depth	
PS141_7-3		2024-02-18T03:41:59	-63.64225	107.09158	2881	PC	max depth	
PS141_7-4		2024-02-18T05:07:09	-63.64233	107.09101	2881	MSN	Station start	
PS141_7-4		2024-02-18T06:40:36	-63.64562	107.09376	2871	MSN	Station end	
PS141_8-1		2024-02-19T03:45:27	-65.71088	100.33025	394	CTD-RO	max depth	
PS141_9-2		2024-02-19T08:48:09	-65.71222	100.31840	392	PS	Station start	
PS141_9-2		2024-02-20T01:59:33	-65.60589	100.17645	427	PS	Station end	
PS141_9-1		2024-02-19T08:49:45	-65.71212	100.31049	386	DS3	Station start	
PS141_9-1		2024-02-20T01:58:32	-65.60584	100.17636	427	DS3	Station end	
PS141_10-1		2024-02-20T02:00:41	-65.60598	100.17650	427	SEIS	Station start	
PS141_10-1		2024-02-20T05:39:18	-65.62796	100.23671	242	SEIS	Station end	
PS141_11-1		2024-02-20T09:28:08	-65.06329	100.36730	469	SEIS	Station start	
PS141_11-1		2024-02-24T05:31:09	-65.77056	90.99707	472	SEIS	Station end	
PS141_12-1		2024-02-24T06:45:45	-65.77563	91.04886	503	CTD-RO	max depth	
PS141_13-1		2024-02-25T02:24:09	-66.28642	89.43977	458	CTD-RO	max depth	
PS141_14-1		2024-02-25T08:54:37	-66.23180	89.42120	540	GC	max depth	
PS141_14-2		2024-02-25T09:43:41	-66.23185	89.42128	540	MUC	max depth	
PS141_15-1		2024-02-25T12:50:35	-66.28368	90.31034	832	ARVORFL	Station start	
PS141_15-1		2024-02-25T12:59:10	-66.28469	90.32728	818	ARVORFL	Station end	
PS141_16-1		2024-02-26T03:53:21	-66.18141	95.49494	169	CTD-RO	max depth	
PS141_17-1		2024-02-26T05:49:27	-66.04842	95.51772	629	CTD-RO	max depth	
PS141_17-2		2024-02-26T06:35:36	-66.05185	95.51643	613	ARVORFL	Station start	
PS141_17-2		2024-02-26T06:38:54	-66.05113	95.50858	542	ARVORFL	Station end	
PS141_18-1		2024-02-26T09:08:52	-65.80634	95.40105	1030	CTD-RO	max depth	
PS141_18-2		2024-02-26T10:04:30	-65.80506	95.40349	1028	FLOAT	Station start	
PS141_18-2		2024-02-26T10:08:45	-65.80436	95.40501	1054	FLOAT	Station end	
PS141_19-1		2024-02-26T15:06:53	-65.14231	95.47324	558	GC	max depth	

Event label	Optional label	Date/Time	Latitude	Longitude	Depth [m]	Gear	Action	Comment [*]
PS141_19-2		2024-02-26T15:58:40	-65.14227	95.47375	558	MUC	max depth	
PS141_20-1		2024-02-27T08:16:36	-65.24723	93.56167	558	SEIS	Station start	
PS141_20-1		2024-02-27T12:17:34	-64.97485	93.62506	435	SEIS	Station end	
PS141_21-2		2024-02-28T09:00:27	-64.90859	100.32996	446	PS	Station start	
PS141_21-2		2024-02-28T15:30:46	-64.88407	100.41175	433	PS	Station end	
PS141_21-1		2024-02-28T09:00:49	-64.90793	100.32810	446	DS3	Station start	
PS141_21-1		2024-02-28T15:30:47	-64.88411	100.41179	433	DS3	Station end	
PS141_22-1		2024-02-29T00:44:20	-65.71052	100.32527	391	PS	Station start	
PS141_22-1		2024-02-29T02:30:16	-65.64489	99.93361	504	PS	Station end	
PS141_22-2		2024-02-29T00:44:23	-65.71049	100.32509	389	DS3	Station start	
PS141_22-2		2024-02-29T02:30:38	-65.64479	99.93365	504	DS3	Station end	
PS141_23-1		2024-02-29T03:00:53	-65.64390	99.93633	504	CTD-RO	max depth	
PS141_23-2		2024-02-29T04:06:58	-65.64386	99.93642	504	GC	max depth	
PS141_23-3		2024-02-29T04:30:29	-65.64339	99.93388	506	HN	Station start	
PS141_23-3		2024-02-29T04:41:56	-65.64333	99.93345	506	HN	Station end	
PS141_23-4		2024-02-29T05:02:36	-65.64338	99.93376	506	MUC	max depth	
PS141_24-1		2024-02-29T09:50:27	-65.71182	100.32816	392	CTD-RO	max depth	
PS141_25-1		2024-02-29T13:52:09	-65.64249	99.99869	496	ARVORFL	Station start	
PS141_25-1		2024-02-29T13:54:33	-65.64166	99.99732	500	ARVORFL	Station end	
PS141_26-1		2024-02-29T20:26:27	-64.93872	100.62931	432	ARVORFL	Station start	
PS141_26-1		2024-02-29T20:28:36	-64.93584	100.62909	428	ARVORFL	Station end	
PS141_27-1		2024-02-29T21:32:00	-64.86762	100.40387	433	PS	Station start	
PS141_27-1		2024-03-01T01:00:01	-64.81231	100.35098	452	PS	Station end	
PS141_27-2		2024-02-29T21:32:01	-64.86760	100.40378	433	DS3	Station start	
PS141_27-2		2024-03-01T01:00:00	-64.81231	100.35098	452	DS3	Station end	
PS141_28-1		2024-03-01T01:29:17	-64.81239	100.35111	452	CTD-RO	max depth	
PS141_29-1		2024-03-01T02:11:01	-64.81210	100.35026	452	SEIS	Station start	
PS141_29-1		2024-03-01T17:31:09	-64.62399	100.28822	519	SEIS	Station end	

Event label	Optional label	Date/Time	Latitude	Longitude	Depth [m]	Gear	Action	Comment [*]
PS141_30-2		2024-03-02T12:15:00	-66.08596	109.22924	961	PS	Station start	
PS141_30-2		2024-03-02T21:30:00	-66.23696	110.15248	193	PS	Station end	
PS141_30-1		2024-03-02T12:15:01	-66.08598	109.22933	961	DS3	Station start	
PS141_30-1		2024-03-02T21:29:00	-66.23691	110.15275	192	DS3	Station end	
PS141_31-2		2024-03-03T02:36:00	-66.30350	110.28134	202	PS	Station start	
PS141_31-2		2024-03-03T07:58:22	-66.23419	110.15385	59	PS	Station end	
PS141_31-1		2024-03-03T02:36:01	-66.30354	110.28130	202	DS3	Station start	
PS141_31-1		2024-03-03T07:58:21	-66.23419	110.15385	59	DS3	Station end	
PS141_32-1		2024-03-04T02:27:46	-66.23226	109.68690	1486	GC	max depth	
PS141_32-2		2024-03-04T03:55:35	-66.23061	109.68611	1470	MUC	max depth	
PS141_33-1		2024-03-04T06:28:18	-66.04814	109.54953	773	MUC	max depth	
PS141_33-2		2024-03-04T07:32:27	-66.04792	109.55085	758	GC	max depth	
PS141_34-1		2024-03-04T08:38:30	-66.04674	109.56037	782	CTD-RO	max depth	
PS141_34-2		2024-03-04T09:14:42	-66.04649	109.56091	782	MSN	Station start	
PS141_34-2		2024-03-04T09:59:44	-66.04683	109.56084	782	MSN	Station end	
PS141_34-3		2024-03-04T10:00:06	-66.04684	109.56079	769	MSN	Station start	
PS141_34-3		2024-03-04T11:12:37	-66.04705	109.56384	782	MSN	Station end	
PS141_34-4		2024-03-04T11:42:57	-66.04640	109.56177	781	GC	max depth	
PS141_35-1		2024-03-04T14:36:42	-66.23125	109.68631	1486	GC	max depth	
PS141_36-2		2024-03-04T15:15:00	-66.23186	109.68679	1485	PS	Station start	
PS141_36-2		2024-03-05T01:40:28	-66.55438	110.34637	2298	PS	Station end	
PS141_36-1		2024-03-04T15:15:01	-66.23186	109.68679	1485	DS3	Station start	
PS141_36-1		2024-03-05T01:39:27	-66.55430	110.34641	2215	DS3	Station end	
PS141_37-1		2024-03-05T02:25:34	-66.55375	110.35354	2319	GC	max depth	
PS141_37-2		2024-03-05T04:37:45	-66.55051	110.35282	2296	CTD-RO	max depth	
PS141_37-3		2024-03-05T06:00:18	-66.55243	110.35435	2299	MSN	Station start	
PS141_37-3		2024-03-05T06:32:36	-66.55241	110.35339	2304	MSN	Station end	

Event label	Optional label	Date/Time	Latitude	Longitude	Depth [m]	Gear	Action	Comment [*]
PS141_37-4		2024-03-05T06:35:18	-66.55243	110.35345	2298	MSN	Station start	
PS141_37-4		2024-03-05T07:45:45	-66.55283	110.35390	2300	MSN	Station end	
PS141_37-5		2024-03-05T08:37:09	-66.55376	110.35427	2296	GC	max depth	
PS141_38-1		2024-03-05T12:46:29	-66.48852	108.88024	1064	SEIS	Station start	
PS141_38-1		2024-03-08T02:11:35	-65.74127	108.50133	458	SEIS	Station end	
PS141_39-1		2024-03-08T02:12:19	-65.74205	108.50124	456	SEIS	Station start	
PS141_39-1		2024-03-08T07:50:09	-65.67910	108.19213	462	SEIS	Station end	
PS141_40-1		2024-03-08T09:47:08	-65.50722	107.98045	700	SEIS	Station start	
PS141_40-1		2024-03-09T16:56:50	-65.45360	108.17567	648	SEIS	Station end	
PS141_41-1		2024-03-10T02:07:35	-66.37136	108.57062	1314	MUC	max depth	
PS141_41-2		2024-03-10T03:32:27	-66.36680	108.58415	1314	GC	max depth	
PS141_41-3		2024-03-10T04:37:01	-66.37605	108.58600	1329	GC	max depth	
PS141_42-2		2024-03-10T07:25:00	-66.26190	108.31283	1107	HN	Station start	
PS141_42-2		2024-03-10T07:37:00	-66.25918	108.30797	1104	HN	Station end	
PS141_42-1		2024-03-10T07:46:09	-66.25847	108.30603	1101	GC	max depth	
PS141_43-1		2024-03-10T09:34:25	-66.17941	108.24226	924	GC	max depth	
PS141_44-1		2024-03-10T13:27:30	-65.75902	107.93223	546	GC	max depth	
PS141_45-1		2024-03-10T15:07:29	-65.66388	107.87736	800	GC	max depth	
PS141_46-2		2024-03-10T15:50:00	-65.66722	107.88459	788	PS	Station start	
PS141_46-2		2024-03-11T01:07:00	-65.65505	107.87390	761	PS	Station end	
PS141_46-1		2024-03-10T15:51:00	-65.66772	107.88580	785	DS3	Station start	
PS141_46-1		2024-03-11T01:06:00	-65.65484	107.87367	761	DS3	Station end	
PS141_47-1		2024-03-11T01:38:08	-65.65651	107.87495	804	GC	max depth	
PS141_47-3		2024-03-11T02:33:41	-65.65710	107.87542	804	HN	Station start	
PS141_47-3		2024-03-11T02:44:40	-65.65655	107.87484	804	HN	Station end	
PS141_47-2		2024-03-11T02:53:41	-65.65656	107.87479	804	MUC	max depth	
PS141_48-1		2024-03-11T06:02:27	-65.42803	107.43148	675	GC	max depth	

Event label	Optional label	Date/Time	Latitude	Longitude	Depth [m]	Gear	Action	Comment [*]
PS141_48-2		2024-03-11T06:06:27	-65.42800	107.43194	675	HN	Station start	
PS141_48-2		2024-03-11T06:30:00	-65.42941	107.43241	673	HN	Station end	
PS141_49-2		2024-03-11T10:11:22	-64.92994	106.85984	2470	HN	Station start	
PS141_49-2		2024-03-11T10:19:37	-64.92998	106.85997	2454	HN	Station end	
PS141_49-1		2024-03-11T10:58:49	-64.93003	106.85997	2454	MUC	max depth	
PS141_49-3		2024-03-11T13:43:04	-64.92991	106.86011	2454	GC	max depth	
PS141_49-4		2024-03-11T15:51:07	-64.92955	106.85989	2455	CTD-RO	max depth	
PS141_49-5		2024-03-11T17:05:45	-64.93000	106.86007	2455	MSN	Station start	
PS141_49-5		2024-03-11T17:38:45	-64.92961	106.85882	2456	MSN	Station end	
PS141_49-6		2024-03-11T17:39:45	-64.92963	106.85881	2456	MSN	Station start	
PS141_49-6		2024-03-11T19:07:36	-64.92706	106.85789	2469	MSN	Station end	
PS141_50-1		2024-03-12T11:12:55	-66.25772	110.35071	137	MUC	max depth	
PS141_50-2		2024-03-12T11:54:14	-66.25775	110.35108	136	GC	max depth	
PS141_51-2		2024-03-12T12:45:00	-66.26276	110.38784	204	PS	Station start	
PS141_51-2		2024-03-13T03:40:45	-66.27490	110.47998	131	PS	Station end	
PS141_51-1		2024-03-12T12:46:00	-66.26292	110.39442	176	DS3	Station start	
PS141_51-1		2024-03-13T03:40:57	-66.27490	110.48003	131	DS3	Station end	
PS141_52-1		2024-03-13T03:51:21	-66.27494	110.48003	132	GC	max depth	
PS141_53-1		2024-03-13T04:20:21	-66.26893	110.48483	130	GC	max depth	
PS141_54-1		2024-03-13T04:50:08	-66.26249	110.45186	105	GC	max depth	
PS141_54-2		2024-03-13T05:27:36	-66.26368	110.45685	121	MUC	max depth	
PS141_55-1		2024-03-13T06:08:36	-66.26981	110.48523	132	MUC	Station start	
PS141_55-1		2024-03-13T06:18:09	-66.27036	110.48468	129	MUC	Station end	
PS141_56-1		2024-03-13T06:53:44	-66.27542	110.47856	131	MUC	max depth	
PS141_57-1		2024-03-13T08:27:54	-66.39457	110.25911	1845	SEIS	Station start	
PS141_57-1		2024-03-13T13:52:42	-66.47735	110.35465	1555	SEIS	Station end	
PS141_58-1		2024-03-13T15:11:41	-66.55380	110.35419	2320	MUC	max depth	

Event label	Optional label	Date/Time	Latitude	Longitude	Depth [m]	Gear	Action	Comment [*]
PS141_59-2		2024-03-13T16:18:00	-66.55021	110.35484	2295	PS	Station start	
PS141_59-2		2024-03-14T00:16:00	-66.46277	108.79323	739	PS	Station end	
PS141_59-1		2024-03-13T16:19:00	-66.54846	110.35233	2298	DS3	Station start	
PS141_59-1		2024-03-14T00:15:00	-66.46215	108.79259	743	DS3	Station end	
PS141_60-2		2024-03-16T12:20:00	-66.52142	89.94290	513	PS	Station start	
PS141_60-2		2024-03-17T02:09:32	-66.51169	89.93937	473	PS	Station end	
PS141_60-1		2024-03-16T12:21:00	-66.52173	89.94431	523	DS3	Station start	
PS141_60-1		2024-03-17T02:09:00	-66.51168	89.93934	473	DS3	Station end	
PS141_61-1		2024-03-17T02:40:23	-66.51098	89.93941	471	CTD-RO	max depth	
PS141_61-2		2024-03-17T03:27:04	-66.50973	89.94110	473	MSN	Station start	
PS141_61-2		2024-03-17T04:12:44	-66.50870	89.94193	460	MSN	Station end	
PS141_61-3		2024-03-17T04:25:18	-66.50848	89.94239	458	MSN	Station start	
PS141_61-3		2024-03-17T05:23:09	-66.50704	89.93908	483	MSN	Station end	
PS141_62-1		2024-03-17T08:14:27	-66.31112	90.35785	1088	MUC	max depth	
PS141_62-2		2024-03-17T10:13:52	-66.31134	90.35841	1068	GC	max depth	
PS141_62-3		2024-03-17T11:26:24	-66.31025	90.34977	1053	CTD-RO	max depth	
PS141_62-4		2024-03-17T12:33:21	-66.30905	90.34134	1046	MSN	Station start	
PS141_62-4		2024-03-17T13:00:21	-66.30850	90.33772	1045	MSN	Station end	
PS141_62-5		2024-03-17T13:00:46	-66.30849	90.33764	1045	MSN	Station start	
PS141_62-5		2024-03-17T14:22:10	-66.30708	90.32585	1042	MSN	Station end	
PS141_62-6		2024-03-17T14:22:54	-66.30707	90.32574	1042	FLOAT	Station start	
PS141_62-6		2024-03-17T14:37:57	-66.30990	90.32623	1039	FLOAT	Station end	
PS141_63-1		2024-03-18T03:39:56	-65.27425	93.06400	592	SEIS	Station start	
PS141_63-1		2024-03-18T17:20:17	-64.49486	93.58603	2625	SEIS	Station end	
PS141_64-1		2024-03-19T06:22:27	-63.82970	98.03525	1880	MUC	max depth	
PS141_64-2		2024-03-19T08:28:09	-63.82944	98.03456	1880	GC	max depth	
PS141_64-3		2024-03-19T11:01:25	-63.82906	98.03587	1879	CTD-RO	max depth	

Event label	Optional label	Date/Time	Latitude	Longitude	Depth [m]	Gear	Action	Comment [*]
PS141_64-4		2024-03-19T12:03:19	-63.82901	98.03575	1879	MSN	Station start	
PS141_64-4		2024-03-19T12:29:39	-63.82877	98.03603	1879	MSN	Station end	
PS141_64-5		2024-03-19T12:30:08	-63.82876	98.03620	1878	MSN	Station start	
PS141_64-5		2024-03-19T13:51:40	-63.82924	98.03521	1879	MSN	Station end	
PS141_65-1		2024-03-19T13:52:00	-63.82923	98.03522	1879	PS	Station start	
PS141_65-1		2024-03-20T03:24:00	-64.17656	98.76938	406	PS	Station end	
PS141_65-2		2024-03-19T13:53:00	-63.82915	98.03531	1880	DS3	Station start	
PS141_65-2		2024-03-20T03:23:00	-64.17658	98.76932	406	DS3	Station end	
PS141_66-1		2024-03-20T03:46:23	-64.17691	98.76900	406	CTD-RO	max depth	
PS141_66-2		2024-03-20T04:46:36	-64.17695	98.76914	406	MUC	max depth	
PS141_66-3		2024-03-20T05:32:09	-64.17685	98.76843	406	GC	max depth	
PS141_67-1		2024-03-20T06:21:09	-64.19735	98.78398	406	GC	max depth	
PS141_68-1		2024-03-20T08:02:09	-64.12397	99.08978	529	GC	max depth	
PS141_68-2		2024-03-20T08:38:18	-64.12381	99.09020	529	MUC	max depth	
PS141_69-1		2024-03-20T10:24:18	-64.31297	99.11575	482	MUC	max depth	
PS141_69-2		2024-03-20T11:01:37	-64.31292	99.11556	481	GC	max depth	
PS141_70-2		2024-03-21T01:19:07	-65.70712	100.31061	372	PS	Station start	
PS141_70-2		2024-03-21T04:49:22	-65.73497	100.17374	510	PS	Station end	
PS141_70-1		2024-03-21T01:20:29	-65.70652	100.31077	368	DS3	Station start	
PS141_70-1		2024-03-21T04:48:49	-65.73645	100.17510	508	DS3	Station end	
PS141_71-1		2024-03-21T05:22:09	-65.71409	100.15302	540	MUC	max depth	
PS141_71-2		2024-03-21T06:07:18	-65.71414	100.15414	540	GC	max depth	
PS141_72-1		2024-03-21T07:35:45	-65.77804	100.21472	538	CTD-RO	max depth	
PS141_72-2		2024-03-21T08:28:45	-65.77827	100.21711	538	GC	max depth	
PS141_72-3		2024-03-21T09:14:23	-65.77833	100.21715	538	MUC	max depth	
PS141_73-1		2024-03-21T15:12:30	-65.18991	100.29427	488	PS	Station start	
PS141_73-1		2024-03-22T00:52:37	-65.10665	100.48821	446	PS	Station end	

Event label	Optional label	Date/Time	Latitude	Longitude	Depth [m]	Gear	Action	Comment [*]
PS141_73-2		2024-03-21T15:13:45	-65.18868	100.29641	490	DS3	Station start	
PS141_73-2		2024-03-22T00:51:54	-65.10622	100.48690	446	DS3	Station end	
PS141_74-1		2024-03-22T01:33:15	-65.10845	100.49625	446	MUC	max depth	
PS141_74-2		2024-03-22T02:14:13	-65.10864	100.49671	446	MUC	max depth	
PS141_74-3		2024-03-22T02:56:12	-65.10887	100.49701	446	GC	max depth	
PS141_75-1		2024-03-22T03:44:35	-65.06860	100.47381	456	FLOAT	Station start	
PS141_75-1		2024-03-22T03:47:49	-65.06588	100.47402	206	FLOAT	Station end	
PS141_76-1		2024-03-22T05:27:09	-64.88962	100.27782	452	GC	max depth	
PS141_77-1		2024-03-22T06:13:16	-64.88250	100.25755	465	GC	max depth	
PS141_77-2		2024-03-22T06:44:44	-64.88235	100.25710	466	MUC	max depth	
PS141_78-1		2024-03-22T10:45:16	-64.39113	99.80850	558	GC	max depth	
PS141_78-2		2024-03-22T11:20:18	-64.39124	99.80810	557	MUC	max depth	
PS141_79-1		2024-03-22T13:25:49	-64.24649	99.54600	504	MUC	max depth	
PS141_79-2		2024-03-22T14:10:58	-64.24644	99.54625	504	GC	max depth	
PS141_80-1		2024-03-22T14:47:56	-64.24435	99.56579	507	PS	Station start	
PS141_80-1		2024-03-23T02:13:00	-64.42332	99.62040	573	PS	Station end	
PS141_80-2		2024-03-22T14:48:36	-64.24339	99.56899	506	DS3	Station start	
PS141_80-2		2024-03-23T02:12:00	-64.42119	99.61682	574	DS3	Station end	
PS141_81-1		2024-03-23T02:36:18	-64.41958	99.61637	573	SEIS	Station start	
PS141_81-1		2024-03-23T16:26:33	-64.25763	98.87410	421	SEIS	Station end	
PS141_82-1		2024-03-24T02:51:29	-64.42833	102.68295	1771	SEIS	Station start	
PS141_82-1		2024-03-24T20:11:27	-64.34413	102.08324	2109	SEIS	Station end	
PS141_83-1		2024-03-25T01:48:21	-64.41873	101.77554	1121	MUC	max depth	
PS141_83-2		2024-03-25T02:18:50	-64.41865	101.77542	1122	GC	max depth	
PS141_84-1		2024-03-26T13:19:13	-63.75299	98.89917	1265	GC	max depth	
PS141_84-2		2024-03-26T15:22:54	-63.75281	98.89898	1463	MUC	max depth	
PS141_84-3		2024-03-26T17:05:45	-63.75119	98.90626	1458	CTD-RO	max depth	

Event label	Optional label	Date/Time	Latitude	Longitude	Depth [m]	Gear	Action	Comment [*]
PS141_85-1		2024-03-28T07:21:36	-65.89585	83.94335	413	MAG	Station start	
PS141_85-1		2024-03-28T08:15:15	-65.89516	83.94298	413	MAG	Station end	
PS141_86-1		2024-04-08T06:57:55	-42.12896	17.24182	4968	MAG	Station start	
PS141_86-1		2024-04-08T07:59:40	-42.12134	17.23846	5010	MAG	Station end	

** Comments are limited to 130 characters. See https://www.pangaea.de/expeditions/events/PS141 to show full comments in conjunction with the station (event) list for expedition PS141*

Abbreviation	Method/Device
ADCP	Acoustic Doppler Current Profiler
ARVORFL	ARVOR I Profiling Float (NKE Instrumentation)
CT	Underway cruise track measurements
CTD-RO	CTD/Rosette
DS3	Swath-mapping system Atlas Hydrosweep DS-3
FBOX	FerryBox
FLOAT	Floater
GC	Gravity corer
GRAV	Gravimetry
HN	Hand net
MAG	Magnetometer
MSN	Multiple opening/closing net
MUC	MultiCorer
MYON	DESY Myon Detector
NEUMON	Neutron monitor
PC	Piston corer
PS	ParaSound
SEIS	Seismic
SNDVELPR	Sound velocity probe
SWEAS	Ship Weather Station
TSG	Thermosalinograph
pCO2	pCO2 sensor

A.5 LIST OF SEISMIC PROFILES COLLECTED DURING PS141

Note: Profile AWI-20240101 was a test profile during which each GI-Gun was fired in sequence and the acquisition with the Uni Kiel streamer was tested over half an hour (from 04:30 to 05:00 UTC) on 20.02.24. The Uni Kiel streamer was then retrieved and the CSIRO streamer was deployed for acquisition of AWI-20240001. The data from AWI-20240101 are not archived.

Profile Number # AWI-…	Start/ End	Date	Time [UTC]	Latitude [S]	Longitude [E]	File No. [Number of shots]	Profile length [km]	GI-Gun config.	Streamer active length	Comments
20240001	Start	20.02.2024	11:42	64°55.74’	100°15.72’	1-6505	144.8	3 x 2.4 litre GI-Guns operated in true GI mode (40 ms G-I delay)	CSIRO (587.5 m)	
	End	21.02.2024	05:45	63°52.56’	098°47.73’	(6506)				
20240002	Start	21.02.2024	05:45	63°52.56’	098°47.73’	6506-8950	58.2			
	End	21.02.2024	12:34	63°48.73’	097°37.25’	(2445)				
20240003	Start	21.02.2024	12:34	63°48.73’	097°37.25’	8951-10938	45.0			
	End	21.02.2024	18:05	63°34.80’	097°42.01’	(1988)				
20240004	Start	21.02.2024	18:05	63°34.80’	097°42.01	10939-16476	130.7			
	End	22.02.2024	09:30	63°46.78’	095°06.09’	(5538)				
20240005	Start	22.02.2024	09:30	63°46.78’	095°06.09’	16477-21067	110.7			
	End	22.02.2024	22:18	64°28.66’	093°29.61’	(4591)				
20240006	Start	22.02.2024	22:18	64°28.66’	093°29.61’	21077-23912	66.9			
	End	23.02.2024	06:10	65°03.60’	093°48.37’	(2836)				
20240007	Start	23.02.2024	06:10	65°03.60’	093°48.37’	23913-31620	180.6			
	End	24.02.2024	03:38	65°47.84’	090°47.71’	(7708)				
20240008	Start	27.02.2024	09:20	65°10.42’	093°33.40’	32000-32636	15.5	1-2 x 2.4 litre GI-Guns operated in true GI mode (40 ms G-I delay)	CSIRO (587.5 m)	Technical problems with the GI guns due to extreme cold in the two days before deployment
	End	27.02.2024	11:07	65°02.26’	093°37.05’	(637)				

Profile Number # AWI-…	Start/ End	Date	Time [UTC]	Latitude [S]	Longitude [E]	File No. [Number of shots]	Profile length [km]	GI-Gun config.	Streamer active length	Comments
20240102	Start	01.03.2024	03:05	64°46.74’	100°15.22’	33000-34497	15.359	1 x 2.4 litre GI-Gun operated in true GI mode (40 ms G-I delay)	Uni Kiel (86 m)	
	End	01.03.2024	05:09	64°41.23’	100°00.31’	(1498)				
20240103	Start	01.03.2024	06:39	64°40.84’	100°07.55’	35577-37189	16.3			
	End	01.03.2024	08:53	64°56.58’	100°22.63’	(1613)				
20240104	Start	01.03.2024	08:53	64°56.58’	100°22.63’	37190-38647	14.3			
	End	01.03.2024	10:56	64°53.05’	100°12.60’	(1458)				
20240105	Start	01.03.2024	10:56	64°53.05’	100°12.60’	38648-38944	2.9			
	End	01.03.2024	11:21	64°54.24’	100°14.54’	(297)				
20240106	Start	01.03.2024	11:21	64°54.24’	100°14.54’	38945-40070	10.9			
	End	01.03.2024	12:56	64°50.76’	100°25.10’	(1126)				
20240107	Start	01.03.2024	12:56	64°50.76’	100°25.10’	40071-41380	12.247			
	End	01.03.2024	14:44	64°46.33’	100°14.10’	(1310)				
20240108	Start	01.03.2024	15:17	64°44.16’	100°11.79’	41781-42985	11.3			
	End	01.03.2024	16:58	64°39.23’	100°17.36	(1205)				
20240009	Start	05.03.2024	14:31	66°25.29’	108°38.89’	43008-52982	238.5	2-4 x 2.4 litre GI-Guns operated in true GI mode (40 ms G-I delay)	CSIRO (587.5 m)	
	End	06.03.2024	18:17	64°37.33’	106°29.65’	(9975)				
20240010	Start	06.03.2024	18:17	64°37.33’	106°29.65’	52983-58019	116.6			
	End	07.03.2024	08:17	65°37.45’	106°26.40’	(5037)				
20240011	Start	07.03.2024	08:17	65°37.45’	106°26.40’	58020-62550	115.4			
	End	07.03.2024	20:53	65°19.06’	108°42.46’	(4531)				
20240012	Start	07.03.2024	20:53	65°19.06’	108°42.46’	62551-64193	43.2			
	End	08.03.2024	01:28	65°41.66’	108°31.23’	(1643)				
20240109	Start	08.03.2024	04:45	65°41.47’	108°16.35’	65000-65494	4.7	1 x 2.4 litre GI-Gun operated in true GI mode (40 ms G-I delay)	Uni Kiel (86 m)	Streamer broken after end buoy caught in ice
	End	08.03.2024	05:42	65°40.08’	108°11.03’	(495)				

Profile Number # AWI-...	Start/ End	Date	Time [UTC]	Latitude [S]	Longitude [E]	File No. [Number of shots]	Profile length [km]	GI-Gun config.	Streamer active length	Comments
20240110	Start	08.03.2024	10:45	65°32.98'	108°05.95'	66000-67866	23.7	1 x 2.4 litre GI-Gun operated in true GI mode (40 ms G-I delay)	CSIRO (587.5 m)	
	End	08.03.2024	13:20	65°44.97'	108°11.34'	(1867)				
20240111	Start	08.03.2024	13:20	65°44.97'	108°11.34'	67867-70099	27.4			
	End	08.03.2024	16:26	65°34.53'	107°51.80'	(2233)				
20240112	Start	08.03.2024	16:26	65°34.53'	107°51.80'	70100-72738	32.0			
	End	08.03.2024	20:07	65°51.17'	107°55.99'	(2639)				
20240113	Start	08.03.2024	20:07	65°51.17'	107°55.99'	72739-76000	38.8			
	End	09.03.2024	00:39	65°38.84'	107°17.02'	(3262)				
20240114	Start	09.03.2024	00:39	65°38.84'	107°17.02'	76001-80660	57.7			
	End	09.03.2024	07:08	65°59.04'	108°07.25'	(4660)				
20240115	Start	09.03.2024	07:08	65°59.04'	108°07.25'	80661-82338	20.7			
	End	09.03.2024	09:28	65°51.15'	107°48.95'	(1678)				
20240116	Start	09.03.2024	09:28	65°51.15'	107°48.95'	82339-84180	32.0			
	End	09.03.2024	12:01	65°42.58'	108°08.86'	(1842)				
20240117	Start	09.03.2024	12:01	65°42.58'	108°08.86'	84181-86876	30.7			
	End	09.03.2024	15:47	65°26.27'	108°01.67'	(2696)				
20240118	Start	13.03.2024	09:12	66°26.69'	110°16.79'	87000-88142	12.5	1 x 2.4 litre GI-Gun operated in true GI mode (40 ms G-I delay)	Uni Kiel (73.4 m)	
	End	13.03.2024	10:46	66°32.91'	110°21.72'	(1143)				
20240119	Start	13.03.2024	10:53	66°33.48'	110°21.56'	88150-88679	5.8			
	End	13.03.2024	11:37	66°34.13'	110°14.75'	(530)				
20240120	Start	13.03.2024	11:37	66°34.13'	110°14.75'	88680-89787	10.6			
	End	13.03.2024	13:10	66°30.56'	110°24.87'	(1108)				
20240013	Start	18.03.2024	04:30	65°14.93'	093°09.00'	90000-94331	90.7	4 x 2.4 litre GI-Guns operated in true GI mode (40 ms G-I delay)	CSIRO (587.5 m)	
	End	18.03.2024	16:32	64°31.83'	093°33.01'	(4332)				

Profile Number # AWI-…	Start/ End	Date	Time [UTC]	Latitude [S]	Longitude [E]	File No. [Number of shots]	Profile length [km]	GI-Gun config.	Streamer active length	Comments
20240121	Start	23.03.2024	03:38	64°24.80’	099°29.46’	96000-97322	12.7	1 x 2.4 litre GI-Gun operated in true GI mode (40 ms G-I delay)	Uni Kiel (73.4 m)	Streamer section 4 missing 4 channels
	End	23.03.2024	05:42	64°17.76’	099°26.34’	(1323)				
20240122	Start	23.03.2024	06:28	64°17.04’	099°26.92’	98000-100191	22.3		Uni Kiel (60.9 m)	Damaged streamer section removed resulting in shorter active length
	End	23.03.2024	09:38	64°08.06’	099°14.91’	(2192)				
20240123	Start	23.03.2024	09:38	64°08.06’	099°14.91’	100192-101710	15.3			
	End	23.03.2024	11:44	64°14.14’	099°04.36’	(1519)				
20240124	Start	23.03.2024	11:44	64°14.14’	099°04.36’	101711-103359	16.3			
	End	23.03.2024	14:02	64°06.60’	098°54.98’	(1649)				
20240125	Start	23.03.2024	14:02	64°06.60’	098°54.98’	103360-104812	15.1			
	End	23.03.2024	16:04	64°14.16’	098°52.08’	(1453)				
20240014	Start	24.03.2024	03:40	64°27.45’	102°34.63’	105000-108063	78.0	4 x 2.4 litre GI-Guns operated in true GI mode (40 ms G-I delay)	CSIRO (587.5 m)	
	End	24.03.2024	12:15	64°50.48’	101°19.56’	(3064)				
20240015	Start	24.03.2024	12:15	64°50.48’	101°19.56’	108064-110612	64.5			
	End	24.03.2024	19:21	64°22.56’	102°00.59’	(2549)				

A.6 PARASOUND LOGS

Please find the A.6 Parasound Logs of expedition PS141 for February, March and April as a supplement.

A.7 PARASOUND PROFILES AND STATIONS

Please find the A.7 Parasound Profiles and Stations of expedition PS141 for February, March and April as a supplement.

A.8 VISUAL CORE DESCRIPTIONS

Please find following Visual Core Descriptions of expedition PS141 as a supplement:

- PS141_3-2
- PS141_5-5
- PS141_7-3
- PS141_23-2,
- PS141_37-1

A.9 LIST OF COORDINATES INFERRED BY RTK MEASUREMENTS AT GAUSSBERG (REFERENCE: WGS84)

The uncertainty can be assumed to be in the level of ±(1…2) cm for the horizontal coordinates (equals about $2 \cdot 10^{-7}$ in latitude and $5 \cdot 10^{-7}$ in longitude), and ±(2…4) cm for the height. –

- Dry-A to Dry-G2: identified mountain points of the Gaussberg survey.
- Cam1 to Cam4: Locations of time-laps cameras
- Cam-Sea: Time-laps camera looking towards northern bay
- GCP1 and GCP2: Ground control points for UAV-aided photogrammetry
- GAxx: Geologic sampling sites (see also Appendix A.11)

  Additional points of interest were measured. –
- GAP1: Top of antenna of the permanent GNSS site
- AUS296: Australian survey mark
- Dry-Stein: Large cairn erected by Drygalski expedition at lower moraine northwest to Kap Lewald
- Dry-Rest: Remnants of the Drygalski expedition

Location	Internal ID	Latitude South [°]	Longitude East [°]	Height [m]	Time stamp [UTC]
GAU1	RTCMRef	66.80276375	89.18188715	132.39	2024-03-08T10:16:26.75
GCP1	GPS0007	66.80311424	89.17802603	103.91	2024-03-08T10:46:00.49
Cam4	GPS0008	66.80302142	89.17773464	100.92	2024-03-08T10:49:16.03
Cam3	GPS0009	66.80287591	89.17798034	104.69	2024-03-08T10:52:20.03
Cam2	GPS0010	66.80273758	89.17812408	105.94	2024-03-08T10:55:30.81
Cam1	GPS0011	66.80252915	89.17829649	106.25	2024-03-08T10:57:56.94
GAP1	GPS0012	66.80247546	89.17860435	108.45	2024-03-08T10:59:35.39
AUS296	GPS0013	66.80234160	89.17859268	107.00	2024-03-08T11:02:38.03
GCP2	GPS0014	66.80112798	89.17617762	75.43	2024-03-08T11:08:02.07
Dry-A	GPS0015	66.80114959	89.17634522	76.71	2024-03-08T11:09:53.46
Cam-Sea	GPS0016	66.80083529	89.17816092	61.26	2024-03-08T11:15:35.10
Dry-B2	GPS0020	66.80489744	89.17540525	110.22	2024-03-10T04:35:48.28
Dry-B1	GPS0021	66.80493945	89.17518335	109.41	2024-03-10T04:41:30.69
Dry-Stein	GPS0024	66.80015087	89.17725687	22.85	2024-03-10T06:40:43.84
Dry-Rest	GPS0025	66.80022700	89.17829387	13.69	2024-03-10T06:51:52.19
Dry-N1	GPS0026	66.79958531	89.18859720	55.60	2024-03-10T07:43:03.68
Dry-N1a	GPS0027	66.79957415	89.18864608	55.49	2024-03-10T07:44:52.06
GA08A	GPS0029	66.79962379	89.18908552	55.91	2024-03-10T08:45:19.90
GA08B	GPS0030	66.79964943	89.18909969	55.80	2024-03-10T08:46:30.85
GA08C	GPS0031	66.79962930	89.18914641	55.85	2024-03-10T08:47:34.95
GA08D	GPS0032	66.79963964	89.18909927	55.77	2024-03-10T08:48:59.61
Cam4	GPS0033	66.80302106	89.17773364	100.94	2024-03-12T03:18:45.87
Cam3	GPS0035	66.80287556	89.17797951	104.72	2024-03-12T03:23:35.06

Location	Internal ID	Latitude South [°]	Longitude East [°]	Height [m]	Time stamp [UTC]
Cam2	GPS0036	66.80273743	89.17812306	105.96	2024-03-12T03:25:17.33
Cam1	GPS0037	66.80252840	89.17829514	106.27	2024-03-12T03:26:54.31
_vGCP_1.1	GPS0038	66.80253023	89.17819747	104.22	2024-03-12T03:32:57.16
_vGCP_1.2	GPS0039	66.80250726	89.17819382	103.93	2024-03-12T03:34:10.31
_vGCP_1.3	GPS0040	66.80252405	89.17818921	104.00	2024-03-12T03:35:40.56
_vGCP_1.4	GPS0041	66.80253163	89.17821930	104.59	2024-03-12T03:37:12.92
_vGCP_1.5	GPS0042	66.80250845	89.17821754	104.32	2024-03-12T03:40:00.42
_vGCP_2.1	GPS0043	66.80273387	89.17804451	104.08	2024-03-12T03:42:42.70
_vGCP_2.2	GPS0044	66.80273110	89.17796870	102.80	2024-03-12T03:44:14.93
_vGCP_2.3	GPS0045	66.80274450	89.17798615	103.17	2024-03-12T03:45:50.76
_vGCP_2.4	GPS0046	66.80272265	89.17804651	103.90	2024-03-12T03:47:19.54
_vGCP_2.5	GPS0047	66.80271493	89.17803189	103.58	2024-03-12T03:48:28.30
_vGCP_2.6	GPS0048	66.80270220	89.17796995	102.21	2024-03-12T03:50:11.71
_vGCP_3.1	GPS0049	66.80285500	89.17788348	102.10	2024-03-12T03:52:23.22
_vGCP_3.2	GPS0050	66.80280766	89.17781452	100.81	2024-03-12T03:53:55.50
_vGCP_3.3	GPS0051	66.80285380	89.17786452	101.76	2024-03-12T03:55:03.47
_vGCP_3.4	GPS0052	66.80287302	89.17782818	101.11	2024-03-12T03:55:56.98
_vGCP_3.5	GPS0053	66.80285540	89.17776061	99.78	2024-03-12T03:57:48.27
_vGCP_4.1	GPS0054	66.80297851	89.17759400	97.12	2024-03-12T04:02:03.30
_vGCP_4.2	GPS0055	66.80298100	89.17763935	97.91	2024-03-12T04:03:26.92
_vGCP_4.3	GPS0056	66.80298029	89.17766367	98.36	2024-03-12T04:04:39.70
_vGCP_4.4	GPS0057	66.80298545	89.17757043	96.64	2024-03-12T04:07:10.21
_vGCP_4.5	GPS0058	66.80297066	89.17757832	96.70	2024-03-12T04:09:14.55
_vGCP_4.6	GPS0059	66.80296005	89.17762124	97.58	2024-03-12T04:11:11.68
Dry-G2	GPS0062	66.80574435	89.19334355	375.83	2024-03-15T06:50:56.79
Dry-F	GPS0063	66.80601199	89.19459471	362.54	2024-03-15T06:58:47.78
Dry-G1	GPS0064	66.80548179	89.19157641	375.10	2024-03-15T07:02:52.18
GA09A	GPS0065	66.80551083	89.19264324	369.47	2024-03-15T07:08:02.57
GA09B	GPS0067	66.80551515	89.19261220	369.54	2024-03-15T07:09:41.32
GA09C	GPS0069	66.80548762	89.19257559	369.32	2024-03-15T07:12:09.52
GA09D	GPS0070	66.80554224	89.19250745	370.42	2024-03-15T07:13:05.64
GA09E	GPS0072	66.80554606	89.19264542	370.24	2024-03-15T07:14:46.16
Dry-C2	GPS0073	66.80627182	89.18904502	337.68	2024-03-15T07:27:44.19
Dry-C1	GPS0075	66.80596613	89.18765713	322.04	2024-03-15T07:33:26.01

A.10 UAV AND HELICOPTER FLIGHTS FOR PHOTOGRAMMETRIC DATA ACQUISITION

Flights 1 to 14 were performed using a DJI Phantom 4 RTK drone. Flights M1 and M2 were performed with a DJI Mavic 2 Pro drone, while flight M1 was used for a video acquisition. Flights Heli1 and Heli2 were accomplished on board the helicopter BK117. Areas – *glacier:* glacier to the west of Gaussberg; *camp:* field camp and adjacent area at the plateau; *northern bay:* ocean bay to the north of Gaussberg; *summit:* Gaussberg summit area.

Flight No.	Area	Date	Start Time [hh:mm]	End Time [hh:mm]	Duration [min]	Number of images	Status
1	glacier	28.02.24	10:58	11:02	04	40	cancelled due to increasing wind
2	glacier	07.03.24	06:03	06:20	17	355	completed
3	camp	07.03.24	07:34	07:55	21	453	completed
4	glacier	07.03.24	08:03	08:25	22	468	completed
5	northern bay	07.03.24	08:45	08:59	14	283	70% covered, stopped due to low battery
6	northern bay	07.03.24	09:02	09:10	08	123	continuation of flight #5, remaining 30% completed
7	glacier	08.03.24	08:19	08:40	21	468	completed
8	glacier	14.03.24.	09:37	09:58	21	474	completed
9	summit	15.03.24	06:51	07:11	20	435	completed
10	glacier	15.03.24	09:14	09:35	21	474	completed
11	northern bay	15.03.24	09:47	10:04	17	362	completed
12	camp	16.03.24	05:37	05:51	14	282	completed
13	northern bay	16.03.24	06:35	06:48	13	271	75% covered, stopped due to low battery
14	northern bay	16.03.24	06:50	06:55	05	94	continuation of flight #13, remaining 25% completed
M1	camp	27.02.24	10:30	10:43	13	video	completed
M2	camp	08.03.24	07:14	07:45	31	363	completed, with intermediate landing for battery change
Heli1	Gaussberg	27.02.24	00:40	00:50	10	380	completed
Heli2	Gaussberg	17.03.24	03:23	03.42	19	556	completed

A.11 GEOLOGICAL SAMPLES COLLECTED AT GAUSSBERG

Approximate coordinates were determined using a handheld GPS receiver (Garmin Montana 650 t); the uncertainty can be assumed to be not better than ± 2 m for the horizontal coordinates (equals about 0.00002° in latitude and 0.00005° in longitude), and up to ± 5 m for the height.

Sample	Date	Latitude South [°]	Longitude East [°]	Height [m]	Sample Type	Weight [kg]	Lithology
GA04A	28.02.24	66.80269	89.18142	120	Erratic	2.9	Granitic gneiss
GA04B	28.02.24	66.80267	89.18142	120	Erratic	0.6	Granitoid
GA04C	28.02.24	66.80269	89.18140	122	Erratic	1.3	Quartz veined granitic gneiss
GA04D	28.02.24	66.80271	89.18142	121	Erratic	3.7	Granitic gneiss
GA04E	28.02.24	66.80270	89.18143	115	In situ	1.4	Lamproite
GA05A	28.02.24	66.80096	89.17680	70	Erratic	1.2	Granitoid
GA05B	28.02.24	66.80097	89.17679	68	Erratic	2.1	Gneiss
GA05C	28.02.24	66.80095	89.17680	67	Erratic	4	Gneiss
GA05D	28.02.24	66.80096	89.17682	67	Erratic	2.1	Granitoid
GA05E	28.02.24	66.80097	89.17681	68	In situ	1	Lamproite
GA06A	29.02.24	66.80181	89.17784	86	Erratic	6	Quartz-feldspar gneiss
GA06B	29.02.24	66.80180	89.17787	85	Erratic	2	Garnet-quartz gneisss
GA06C	29.02.24	66.80180	89.17789	86	Erratic	6.5	Quartz-magnetite gneiss
GA06D	29.02.24	66.80182	89.17799	87	In situ	1.7	Lamproite
GA07A	07.03.24	66.80297	89.17857	101	Erratic	8.7	Gneiss
GA07B	07.03.24	66.80298	89.17860	103	Erratic	3.9	Quartz-feldspar granitoid
GA07C	07.03.24	66.80299	89.17861	100	Erratic	5.9	Gneiss
GA07D	07.03.24	66.80296	89.17864	102	In situ	1.3	Lamproite
GA08A	10.03.24	66.79964	89.18906	51	Erratic	1	Quartz-garnet gneiss
GA08B	10.03.24	66.79968	89.18911	56	Erratic	1.3	Quartz-feldspar granitoid
GA08C	10.03.24	66.79965	89.18907	50	Erratic	0.7	Quartz-gneiss
GA08D	10.03.24	66.79967	89.18907	50	Erratic	0.3	Quartz-gneiss
GA09A	15.03.24	66.80551	89.19257	358	Erratic	1.3	Quartzite
GA09B	15.03.24	66.80552	89.19256	368	Erratic	1.3	Quartz-feldspar-magnetite gneiss
GA09C	15.03.24	66.80551	89.19255	369	Erratic	1.6	Quartz-feldspar-magnetite gneiss
GA09D	15.03.24	66.80558	89.19253	371	Erratic	1.6	Granitoid
GA09E	15.03.24	66.80556	89.19263	370	In situ	1.1	Lamproite
GV01	27.02.24	66.80113	89.17635	67	In situ	2	Lamproite
GV02	28.02.24	66.80264	89.18126	127	In situ	8.3	Lamproite

Sample	Date	Latitude South [°]	Longitude East [°]	Height [m]	Sample Type	Weight [kg]	Lithology
GV03	01.03.24	66.80182	89.17799	87	In situ	1.9	Lamproite
GV04	01.03.24	66.80286	89.17816	115	In situ	3	Lamproite
GV05	06.03.24	66.80268	89.17890	101	In situ	4	Lamproite
GV06	07.03.24	66.80242	89.17932	100	In situ	1.6	Lamproite
GV07	10.03.24	66.80497	89.17528	104	In situ	3.2	Lamproite
GV08	10.03.24	66.79965	89.18868	51	In situ	2.5	Lamproite
GV09	11.03.24	66.80066	89.17832	37	In situ	0.4	Volcaniclastic
GV10	11.03.24	66.80066	89.17832	37	In situ	0.4	Lamproite glassy clasts
GV11	11.03.24	66.80066	89.17832	37	In situ	1.4	Volcaniclastic sandstone
GV12	11.03.24	66.80066	89.17832	37	In situ	0.6	Volcaniclastic sandstone
GV13	11.03.24	66.80066	89.17832	40	In situ	0.3	Lamproite
GV14	11.03.24	66.80066	89.17613	31	In situ	2.2	Lamproite
GV15	12.03.24	66.80267	89.17917	102	In situ	1.4	Lamproite
GV16	12.03.24	66.80276	89.17886	106	In situ	1.4	Lamproite
GV17	12.03.24	66.80269	89.17873	107	In situ	0.5	Lamproite
GV18	14.03.24	66.80292	89.18059	121	In situ	1.5	Lamproite
GV19	14.03.24	66.80281	89.18097	116	In situ	2.4	Lamproite
GV20	15.03.24	66.80539	89.19175	366	In situ	2.6	Lamproite
GV21	15.03.24	66.80527	89.19166	364	In situ	2.2	Lamproite
GX01	07.03.24	66.80244	89.17928	100	In situ	2.7	Quartzite or gneiss
GX02	08.03.24	66.80209	89.17893	94	In situ	1.6	Quartz gneiss
GX03	12.03.24	66.80276	89.17886	106	In situ	0.4	Quartz-magnetite gneiss
GX04	14.03.24	66.80219	89.17934	97	In situ	2	Quartz-feldspar-magnetite gneiss
GX05	14.03.24	66.80219	89.17934	97	In situ	1.4	Quartz-feldspar-magnetite gneiss
GX06	14.03.24	66.80219	89.17934	97	In situ	1.8	Quartz-feldspar-magnetite gneiss
GX07	14.03.24	66.80246	89.17964	101	In situ	0.8	Quartz-feldspar-magnetite gneiss
NMNS1	14.03.24	66.80281	89.18097	116	In situ	2.4	Lamproite
NMNS2	14.03.24	66.80281	89.18097	116	In situ	0.7	Lamproite
NMNS3	14.03.24	66.80254	89.18021	101	In situ	2.1	Lamproite
NMNS4	14.03.24	66.80254	89.18021	101	In situ	2.1	Lamproite
NMNS5	14.03.24	66.80254	89.18021	101	In situ	1.3	Lamproite
NMNS6	14.03.24	66.80254	89.18021	101	In situ	2.5	Lamproite
NMNS7	14.03.24	66.80254	89.18021	101	In situ	2	Lamproite
NMNS8	14.03.24	66.80254	89.18021	101	In situ	1.1	Lamproite
GM01	27.02.24	66.80081	89.17760	67	Erratic	2.3	Quartz-magnetite gneiss
GM02	16.03.24	66.80246	89.17964	101	Erratic	2.3	Quartz-magnetite-minor pyrite granitoid
GM03	16.03.24	66.80246	89.17964	101	Erratic	2.6	Quartz-magnetite-biotite granitoid

Sample	Date	Latitude South [°]	Longitude East [°]	Height [m]	Sample Type	Weight [kg]	Lithology
GM04	16.03.24	66.80246	89.17964	101	Erratic	3.9	K-feldpsar-magnetite granitic gneiss
GM05	16.03.24	66.80246	89.17964	101	Erratic	3.7	K-feldspar-magnetite granitoid
GM06	16.03.24	66.80246	89.17964	101	Erratic	4.5	Quartz veined quartz-magnetite gneiss
GM07	16.03.24	66.80246	89.17964	101	Erratic	1.7	Quartz-feldspar-magnetite granitic gneiss
GM08	16.03.24	66.80246	89.17964	101	Erratic	3.3	Quartz-feldspar-magnetite gneiss
GM09	16.03.24	66.80246	89.17964	101	Erratic	3.6	Quartz-magnetite gneiss
GM10	16.03.24	66.80246	89.17964	101	Erratic	2.3	Quartz-magnetite gneiss
GM11	16.03.24	66.80246	89.17964	101	Erratic	1.9	Quartz-magnetite (minor pyrite) gneiss
GM12	16.03.24	66.80246	89.17964	101	Erratic	2.3	Quartz-feldspar-magnetite granitic gneiss
GM13	16.03.24	66.80246	89.17964	101	Erratic	1.7	Ultra Mafic - magnetite-serpentine-hematite-arsenopyrite
GM14	16.03.24	66.80246	89.17964	101	Erratic	2.1	Quartz-magnetite-garnet gneiss
GM15	16.03.24	66.80246	89.17964	101	Erratic	2	Quartz -magnetite(?) gneiss
GM16	16.03.24	66.80246	89.17964	101	Erratic	1	Quartz-magnetite (minor pyrite) gneiss
GM17	16.03.24	66.80246	89.17964	101	Erratic	0.7	K-feldspar-magnetite-quartz granitoid
GM18	16.03.24	66.80246	89.17964	101	Erratic	1.4	Quarz-magnetite granodiorite (ish)
GM19	16.03.24	66.80246	89.17964	101	Erratic	1.8	Serpentinised pyroxenite, minor pyrite
GM20	16.03.24	66.80246	89.17964	101	Erratic	0.7	Garnet-pyroxene-pyrite gneiss

Die **Berichte zur Polar- und Meeresforschung** (ISSN 1866-3192) werden beginnend mit dem Band 569 (2008) als Open-Access-Publikation herausgegeben. Ein Verzeichnis aller Bände einschließlich der Druckausgaben (ISSN 1618-3193, Band 377-568, von 2000 bis 2008) sowie der früheren **Berichte zur Polarforschung** (ISSN 0176-5027, Band 1–376, von 1981 bis 2000) befindet sich im electronic Publication Information Center **(ePIC)** des Alfred-Wegener-Instituts, Helmholtz-Zentrum für Polar- und Meeresforschung (AWI); see https://epic.awi.de. Durch Auswahl "Reports on Polar- and Marine Research" (via "browse"/"type") wird eine Liste der Publikationen, sortiert nach Bandnummer, innerhalb der absteigenden chronologischen Reihenfolge der Jahrgänge mit Verweis auf das jeweilige pdf-Symbol zum Herunterladen angezeigt.

The **Reports on Polar and Marine Research** (ISSN 1866-3192) are available as open access publications since 2008. A table of all volumes including the printed issues (ISSN 1618-3193, Vol. 377-568, from 2000 until 2008), as well as the earlier **Reports on Polar Research** (ISSN 0176-5027, Vol. 1–376, from 1981 until 2000) is provided by the electronic Publication Information Center **(ePIC)** of the Alfred Wegener Institute, Helmholtz Centre for Polar and Marine Research (AWI); see URL https://epic.awi.de. To generate a list of all Reports, use the URL http://epic.awi.de and select "browse"/"type" to browse "Reports on Polar and Marine Research". A chronological list in declining order will be presented, and pdf-icons displayed for downloading.

Zuletzt erschienene Ausgaben: **Recently published issues:**

793 (2025) The Expedition PS141 of the Research Vessel POLARSTERN to the Davis Sea and Mawson Sea in 2024, edited by Sebastian Krastel with contributions of the participants

792 (2025) Climate Signals from Neumayer, coastal Dronning Maud Land, Antarctica: A 33-Year statistical Analysis of Snow Accumulation in a Stake Farm, by Valerie Reppert

791 (2025) TIDAL–HX01: Trialing Innovative Data Acquisition from a Platform of Opportunity – the HX Vessel MS FRIDTJOF NANSEN, edited by Andreas Herber, Laura Köhler, Verena Meraldi, Katja Metfies, Melf Paulsen, Daniel Pröfrock, Tobias Steinhoff and Hongyan Xi with contributions of the participants

790 (2024) The Expedition PS140 of the Research Vessel POLARSTERN to the Cooperation Sea and Davis Sea in 2023/2024, edited by Marcus Gutjahr and Oliver Esper with contributions of the participants

789 (2024) The Expedition PS142 of the Research Vessel POLARSTERN to the Atlantic Ocean in 2024, edited by Simon Dreutter with contributions of the participants

788 (2024) The Expedition PS138 of the Research Vessel POLARSTERN to the Arctic Ocean in 2024 edited by Antje Boetius and Christina Bienhold with contributions of the participants

787 (2024) Dynamic Poles and High Mountain Environments, 29th International Polar Conference Rauris, 16 – 20 September 2024, Austrian Polar Research Institute and German Society for Polar Research, edited by H. Kassens, B. Diekmann, F. Lisker, G. Heinemann, M. Horwarth, U. Karsten, F. Kruse, R. Lehmann, C. Lüdecke, B. Sattler, W. Schöner and C. Spiegel

786 (2024) The MOSES Sternfahrt Expeditions of the Research Vessels ALBIS, LITTORINA, LUDWIG PRANDTL and MYA II to the Elbe River, Elbe Estuary and German Bight in 2023 edited by Ingeborg Bussmann, Martin Krauss, Holger Brix, Norbert Kamjunke, Björn Raupers and Tina Sanders with contributions of the participants

ALFRED-WEGENER-INSTITUT
HELMHOLTZ-ZENTRUM FÜR POLAR-
UND MEERESFORSCHUNG

BREMERHAVEN

Am Handelshafen 12
27570 Bremerhaven
Telefon 0471 4831-0
Telefax 0471 4831-1149
www.awi.de

HELMHOLTZ